The Pennsylvania State University

The Graduate School

College of Engineering

COMBINED AIRFLOW AND ENERGY SIMULATION PROGRAM FOR BUILDING MECHANICAL SYSTEM DESIGN

A Thesis in

Architectural Engineering

by

Atila Novoselac

Submitted in Partial Fulfillment
of the Requirements
for the Degree of

Doctor of Philosophy

May 2005

The thesis of Atila Novoselac was reviewed and approved* by the following:

Jelena Srebric
Assistant Professor of Architectural Engineering
Thesis Adviser
Chair of Committee

Stanley A. Mumma
Professor of Architectural Engineering

William P. Bahnfleth
Associate Professor of Architectural Engineering

John Mahaffy
Associate Professor of Nuclear Engineering

Richard A. Behr
Professor of Architectural Engineering
Head of the Department of Architectural Engineering

*Signatures are on file in the Graduate School.

ABSTRACT

Energy and airflow programs are the main tools for designing energy efficient and healthy buildings. Therefore, the goal of this thesis is to develop new models and improve existing models for simulating energy and air flows in buildings.

Indoor airflow simulation programs calculate most of the parameters needed to evaluate thermal comfort and indoor air quality. However, it is necessary that airflow simulation programs have correct boundary conditions which can be provided by energy simulation (ES) programs. In order to develop simulation tools for precise evaluations of thermal comfort and indoor air quality in buildings, the existing Computation Fluid Dynamics (CFD) airflow program is improved by adding new models for the calculation of thermal boundary conditions. Subsequently, this program is coupled with the newly-developed ES program.

This thesis considers different methods for coupling ES and CFD programs with particular attention given to boundary conditions on enclosure surfaces which connect the modeling domains of these two programs. Three different coupling approaches were investigated with special consideration given to accuracy and computation time. The results show that the Integrated Coupling Method provides the optimum compromise between accuracy and computation time.

In order to improve the accuracy of the calculations of thermal boundary conditions on building internal surfaces, experiment-based convection correlations are implemented in the CFD program. In the process, new convection correlations are developed based on measurements conducted in a state-of-the-art experimental facility. Correlations for characteristic surfaces in rooms with: cooled ceiling panels, displacement ventilation, or high aspiration diffusers are developed.

Furthermore, additional experiments are performed to collect data so as to validate new models for calculating thermal boundary conditions. A comparison of numerical and experimental results shows that the new models for thermal boundary conditions calculation, implemented in CFD, perform substantially better than wall functions. A certain level of grid dependency of heat flux calculation with new models still exists. However it is much smaller than with wall functions.

Finally, this thesis provides examples, which demonstrate that the coupled ES and CFD program is an effective tool for the evaluation of energy consumption, thermal comfort, and air quality in buildings.

TABLE OF CONTENTS

LIST OF FIGURES

LIST OF TABLES

NOMENCLATURE

A - surface area
ACH - number of room air changes per hour
A_i - anisotropy index
A_L - effective air leakage
c_p - specific heat
D_h - hydraulic diameter of cooling surfaces
E - cooling coil effectiveness
F' - radiant panel efficiency factor
$F_{i,j}$ - view factors from surface $'i'$ to surface $'j'$
g - gravitational constant
g - gravity acceleration
Gr - Grashof number
h - surface convection coefficient
I_{DIR} - direct solar radiation
I_{DNR} - direct normal radiation
I_{GHR} - global horizontal radiation
J - radiosity
k - conductivity
k - turbulent kinetic energy
L - characteristic length
m - mass flow rate
Nu - Nusselt number
P - power
p - pressure
P_r - Prandl number
Q - heat flux
q - specific heat flux
R - conductive resistance
r - re-circulated air portion
Re - Reynolds number
S_c - Schmidt number
T - temperature
u - local velocity in the vicinity of the surface
U - wind speed
V - velocity
w - humidity ratio

ν - kinematic viscosity
σ_t - turbulent Prandtl number
α – absorptivity
μ - viscosity
Γ - effective diffusivity
δ - boundary layer thickness
θ - incident angle
ρ - density
- reflectance
$\psi_{i,j}$ - radiative heat exchange factors from surface $'i'$ to surface $'j'$

ΔT - temperature difference
Δx_p - distance from wall to the adjacent cell centre
$\Delta \tau$ - time step
β - thermal expansion coefficient or the surface slope
ε - contaminate removal effectives
- surface emissivity
- dissipation rate of turbulent energy
ε_a - air exchange efficiency
ϕ - general variable
μ_t - turbulent viscosity
τ - time

ABBREVIATIONS

ACA - Adaptive Convection Algorithm

ACH - Air Changes per Hour
AHU - Air Handling Unit
ASHRAE - American Society of Heating Refrigerating and Air-Conditioning Engineers
BES - Newly Developed Building Energy Simulation Software
CAV - Constant Air Volume
CFD - Computational Fluid Dynamics
CFD0 - Research CFD software
CPU - Central Processing Unit
DDC - Direct Digital Control
DNS - Direct Numerical Simulation
DOAS - Dedicated Outdoor Air System
DV - Displacement Ventilation
ES - Energy Simulation
ESP-r - Commercial Energy Simulation Software
FLUENT - Commercial CFD software
GUI - Graphical User Interface
HVAC - Heating Ventilating and Air-Conditioning
IAQ - Indoor Air Quality
IGU - Model for Insulated Glazing Units
LES - Large Eddy Simulation
MACA - Modified Adaptive Convection Algorithm
MIT - Massachusetts Institute of Technology
PHOENICS - Commercial CFD software
RANS - Raynold's Average Navier-Stokes equations
RNG - k-ε model based on Renormalization Group
SIMPLE - Semi-Implicit Method for the Pressure-Linked Equations
TMY2 - Typical Metrological Year Weather Database
VAV - Variable Air Volume

ACKNOWLEDGEMENTS

First, I would like to offer my gratitude to my thesis advisor, Professor Jelena Srebric for her support and guidance. She actively encouraged, motivated, and challenged me throughout the completion of this thesis. With her highly positive attitude she helped me to become more independent researcher.

Next, I would like to thank Ivana Veljkovic, Akhil Kamat, and Brendon Burley. They are students from the Pennsylvania State University, and they have been of a great help to me with this thesis. Ivana Veljkovic, a PhD student at the Computer Science and Engineering Department, developed the graphical user interface for software developed as a part of this thesis; Akhil Kamat, a student at Computer Science and Engineering Department, developed a 3D visualization tool for software result presentation; and Brendon Burley, a student at the Architectural Engineering Department, helped me with the experimental measurements that were conducted as a part of this thesis.

Last but not least, I would like to acknowledge the counseling and assistance given by my thesis committee members: Professor Stanley Mumma, Professor William Bahnfleth, and Professor John Mahaffy.

CHAPTER 1

INTRODUCTION

1.1 General Statement of Problem

People spend most of their time in buildings. Hence, issues related to the indoor environment, such as indoor air quality (IAQ) and thermal comfort, are of great public concern. Poor IAQ and inadequate thermal comfort in buildings adversely affect the health condition of occupants (NIOSH 2004). Furthermore, recent incidents related to bioterrorism (anthrax attacks) and the fast spread of infectious diseases (SARS), have triggered many concerns about the control of the indoor environment. Building heating, ventilating, and air-conditioning (HVAC) systems provide control of major parameters related to the indoor environment. To evaluate and improve IAQ and thermal comfort resulting from HVAC systems, airflow simulation programs are used. These are programs based on Computational Fluid Dynamics (CFD) or zonal modeling.

Improvements made to building HVAC systems can provide direct and indirect economic benefits. Direct benefits relate to the reduction of energy consumption, and indirect benefits are related to increased productivity and reduction of medical expenses. In addition, lower energy consumption in buildings can significantly reduce the emission of CO_2 because buildings use around 50% of the total energy consumption in developed countries (Harris and Eliot, 1997, DOE 2004) Therefore, any analysis of building HVAC system that can effectively reduce this consumption is highly valuable. In order to evaluate and reduce energy consumption in the design phase of building, energy simulation (ES) programs are used.

It is commonly believed that improvements made to indoor air quality must lead to an increase in energy consumption. This is the case when the air quality is improved by a simple increase of fresh air supply. With careful selection of an HVAC system, building materials, and air-distribution devices, IAQ can be improved and energy consumption can be reduced simultaneously. To achieve this worthy goal, air flow simulation and ES programs are used for energy consumption, thermal comfort and IAQ analyses. At present, most of these analyses are performed with separate ES and air flow programs. However, because of the interaction between building elements and air temperature distribution, a building's air and energy flows should be considered together by using combined ES and airflow programs.

Separate applications of ES and airflow programs usually provide acceptable results for certain types of analysis. However, many assumptions used in these programs decrease the accuracy these programs when they are used separately. For example, accuracy of an airflow program results is highly sensitive to the boundary conditions assumed (or eventually measured) by the user (Emmerich 1997, Xu and Chen 1998). The reason for this is that the flow inside the airflow simulation domain (i.e. a room) is driven by the boundary conditions. Also, the assumption in an ES program of uniform air temperature in the room can cause imprecise calculation of convective heat fluxes on room surfaces. This can lead to large inaccuracy in energy consumption calculations since different convection coefficients models can create difference in cooling load calculation up to 27% for the same test case (Lomas 1995). An integration of ES and airflow programs can eliminate many of these assumptions, since the information provided by ES and airflow programs are complementary related to boundary conditions (refer to Section 1.2). With coupling ES and air flow programs, increased accuracy in both programs is achieved.

The development of ES and air flow programs is connected to the development of computer technologies. The fast development of computing power has enabled the use of more complex models for air-flow and energy-flow simulations. In addition, the current speed of computing enables the combination of ES and air flow programs for specific analyses on a personal computer. Extensive research has been conducted in order to reach the point that air-flow and energy-flow systems are combined in the analysis of a single building. The next section describes only basic properties of these programs, while Chapter 2 provides a detailed literature review on the development of ES, air flow, and combined programs.

1.2 Basic Properties of Energy Simulation and Indoor Airflow Programs

Building Energy Simulation (ES) programs are tools used for the analysis of building energy consumption and the evaluation of architectural designs. These tools are used for modeling heating, cooling, and ventilating flows in a building. The modeling domain of the ES program (Figure 1.1) comprises of:

- Building envelope,
- Heating Ventilating and Air-Conditioning (HVAC) systems,
- External and internal parameters, such as weather conditions or occupancy level
- Indoor air represented as uniform thermal mass for a particular zone.

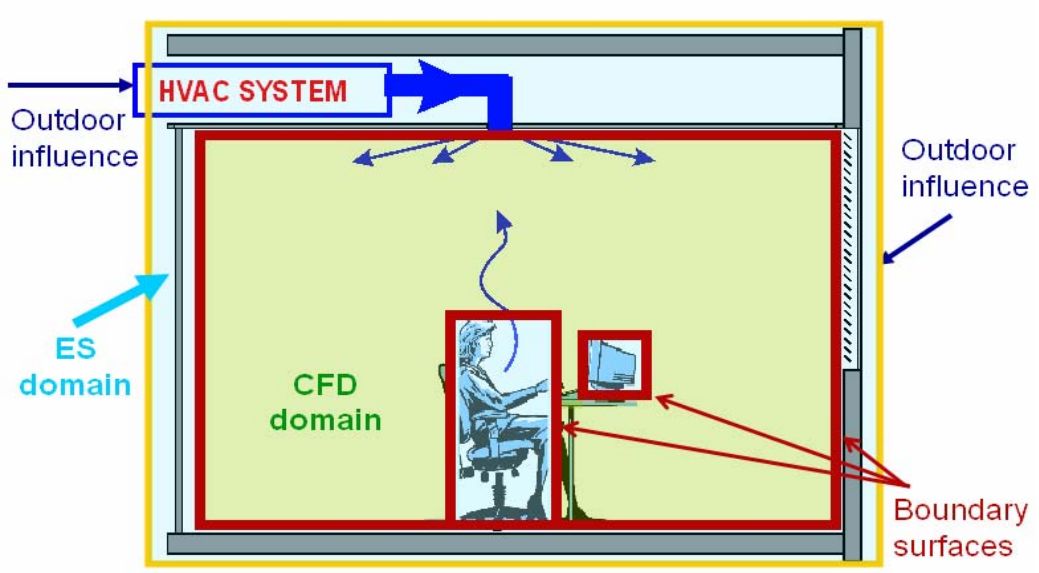

Figure 1.1 Modeling domains for Energy Simulation (ES) and Airflow (CFD) programs

Energy Simulation (ES) programs provide data related to energy consumption and general information about thermal comfort in a space for a period of analysis. These programs integrate a large number of analytical and numerical models. For example, analytical models are used for the calculation of solar radiation. When calculating heat transfer through the building envelope, numerical models for one dimensional heat transfer are typically used. Besides building geometry and material properties, input data in these programs are HVAC system properties and the hourly weather data related to the location of the building. Based on these input data, ES programs perform calculations of energy demand for heating, cooling and ventilating for a certain period of time with a span of an hour or less. ES can also provide general thermal comfort parameters, such as uniform air temperature, humidity, and enclosure temperature.

In this thesis, the airflow simulation programs are computer tools that use CFD to calculate the spatial distribution of temperature, velocity, and contaminant concentration. The modeling domain for the CFD program used for the evaluation of indoor airflows is the air in the space inside of building enclosures (refer to Figure 1.1).

With CFD, the studied space is divided into a finite number of volumes. For each volume, mass, momentum, and energy conservation laws are applied. This means that each volume is represented by several equations that are coupled to the equations of neighboring volumes. To solve this system of equations, numerical models are used. Beside these numerical

models, building airflow simulation programs use models that are based on experimental data. These experiment-based models are integrated into the CFD program code and used for the prediction of human responses to various air velocities and temperatures. Beside space geometry, input data in these airflow simulation programs are surface contaminant emission, surface thermal properties and properties of supplied air, such as volume flow rate, temperature and concentration. With these input data, the CFD numerical solver calculates temperature, velocity, and contaminant concentration for each finite volume of the analyzed space. These data enable detailed analyses of thermal comfort and air quality.

Coupling of ES and CFD programs occurs at boundary surfaces, which are the domains between these two programs. The ES calculates the temperature of the surfaces, which constitute input data for the CFD program. On the other side, the CFD program calculates convective heat fluxes based on velocity and temperature fields near the surfaces. These convective heat fluxes are defined by near- surface (local) air temperatures and by convective coefficients. To satisfy the energy balance, heat fluxes at all surfaces have to be the same when they are calculated for the ES and CFD program domains. Therefore, the CFD provides to the ES local air temperatures and convective coefficients which constitute input data for this program. Besides enclosure temperatures, the ES provides to the CFD program input data related to boundary conditions at thermal objects, such as occupants and computers, if any. Boundary conditions for thermal devices are defined by air velocity, temperature, and concentration for air supply thermal devices, or by surface temperature or heat flux for devices like radiant panels, baseboard heaters, and computers. By the consecutive exchange of information at the boundary domains between these two programs, increasingly accurate input data are provided for each program.

For the calculation of convective heat flux, the CFD can use wall functions or convection experimental-based expressions. Log-law wall functions, which are based on the correlation between velocity and temperature field in the boundary layer, are extensively used in CFD applications to calculate convective heat flux. However, wall functions are inaccurate for flow driven by natural convection which is a predominant type of flow on building surfaces. Therefore, this thesis is also focused on alternative methods for the calculation of heat flux. These methods include the application of convection correlations, which are based on experimental results.

1.3 Research Objective and Thesis Outline

The objective of this thesis is to enhance indoor air and energy flow modeling in the context of simulation of all building systems. Improvement of indoor air and energy flow modeling includes the following:

(1) ES and CFD programs coupling, with special attention given to the
-development of a method which satisfies the energy balance between two program domains and
-use of accurate surface heat transfer models;

(2) Further development of models for surface heat transfer calculations on buildings' internal surfaces;

(3) Development of new methods for simultaneous load calculations and HVAC performance simulation, that enables a modular approach for HVAC system modeling,

(4) Analysis of different indoor air quality parameters for their use in coupled ES and CFD programs.

In order to gather knowledge of existing models for ES and air flow simulations, a critical review of existing literature was conducted. The review of these models is presented in Chapter 2, with a special focus on integrated modeling approaches that were used as a basis for further developments in this thesis.

As a part of this thesis, a new ES program was developed and used as a platform for coupling with air flow programs. This ES program incorporates existing and newly developed building system simulation models. It also implements a new method for simultaneous load calculations and HVAC performance simulations. Details about the newly developed ES program are presented in Chapter 3 with a special focus on methods for simultaneous load calculations and HVAC performance simulations.

An existing CFD program (Srebric 2000) was used for coupling with the new ES program. This CFD program was further developed in order to implement models for accurate

boundary conditions calculations. Details about CFD models are provided in Chapter 4 with a focus on new models for thermal boundary conditions.

Chapter 5 contains details about three different methods for the coupling of ES and CFD programs. It contains comparative analyses of these methods, with a discussion about the respective advantages and disadvantages of each method.

To enable easy use of the coupled ES and CFD program a new graphical user interface (GUI) for this program was developed in collaboration with students mentioned in acknowledgments. Basic details about the new GUI and structure of the coupled program are provided in Chapter 6.

New convection correlations were developed as part of this thesis in order to improve the performance of experiment-based models for the calculation of thermal boundary conditions in CFD program. Chapter 7 contains the experimental results and details about these newly developed convection correlations.

In order to develop new convection correlations, full-scale laboratory experimental measurements were performed. Also, measurements for the validation of new models for thermal boundary conditions calculation in the CFD program and measurements for coupled code validations were conducted. Details about these measurements are presented in Chapter 8.

Chapter 9 presents application examples for the coupled program. It contains an analysis of thermal comfort and energy consumption of displacement ventilation systems, combined with cooling radiant panels. Also, this chapter contains an analysis of different IAQ parameters.

Finally, Chapter 10 summarizes the work presented in this thesis, and provides recommendations for further research.

CHAPTER 2

CURRENT DESIGN TOOLS FOR BUILDING ENERGY AND AIRFLOW SIMULATIONS

In this chapter, a critical overview of energy simulation and airflow programs is given. This overview focuses on their respective advantages and disadvantages when these programs are applied in analyses of buildings. In addition, other researchers' efforts of coupling these two types of programs are considered. Finally, the two most recently proposed models for the coupling of energy simulation and airflow programs are critically analyzed in detail to explore the respective advantages and disadvantages of both models.

2.1 Energy Simulation Programs

Until the mid 1960s, only simple manual methods were used to estimate energy usage in buildings. Two of the most widely used manual methods are the degree day method and the bin method. The simplest method is the degree day method, which is based on the averaging of outdoor weather influence over a long period of time (ASHRAE Fundamentals 2001). This method was successfully used for rough estimations of heating energy requirements. For more detailed heating and cooling analysis, the bin method was used. This method calculates energy over several intervals (bins) of temperature using a simplified quasi-steady-state approach (ASHRAE Fundamentals 1985). Besides very limited accuracy, these simple manual methods could not provide any information about thermal comfort such as enclosure temperature and air temperature when the heating/cooling system does not work.

More detailed energy simulation methods include sophisticated models of a building and its HVAC systems. These methods are computationally intensive and require extensive use of computers. Today, there is a larger variety of Energy Simulation (ES) programs with building system models of various complexities.

For building heating/cooling load calculation, ES programs may use the:

- Weighting factor method, or
- Energy balance method.

To integrate of HVAC models with heating/cooling load calculation models, ES programs may use the:

- integrated method, or
- Loads-System-Plant method.

Considering the complexity of HVAC models, ES programs may use the following three methods for HVAC system simulation and energy consumption calculations:

- psychometric chart zoning method,
- whole-building simulation method, or
- component-based simulations method.

2.1.1 Weighting Factor Method versus Energy Balance Method

In the calculation of the heating/cooling load, the thermal mass of the building has to be considered. Because of the thermal capacity, the heat gains and cooling loads in the analyzed building zone are different. Therefore, unsteady heat conduction needs to be solved for each element of the building enclosure. The weighting factor and the heat balance methods are the two approaches used for these calculations.

The weighting factor method estimates the ratio of convective heat transfer to the total incoming energy on a building element during a time period. Weighting factors depend on building material properties and they are usually pre-calculated for certain types of building elements. Based on the structure of a building element, the ES program selects an appropriate weighting factor and calculates the convective load. Programs based on the weighting factor method do not need extensive computations. They were, therefore, popular during the 1970's when the computer power was very limited. The ES programs that use weighting factors are: NESCAP (NASA 1975), DOE-1 (Diamond et al. 1977), DOE-2 (Birdsall et al. 1985), and VISUAL DOE-3 (Visual DOE 3.1 2003).

The energy balance method is based on the heat balance for zone air and enclosure elements. With this method, conductive, convective, and radiative heat fluxes are in balance for each surface. Equations for surface heat balance are usually linearized (radiation terms) and organized into a surface balance matrix. After the matrix is solved, the cooling load for the considered zone is determined. BLAST (Hittle 1979), ACCURACY (Chen et al. 1988), ESP-r (Clarke et al. 1985) and EnergyPlus (Crawley 2000) are ES programs based on the energy

balance method. Relative to the coupling of ES and airflow programs, the energy balance method has an advantage when compared to the weighting factor method. This is due to the fact that the room surface convective coefficient can vary across the enclosure and room air temperature can be non-uniform. Furthermore, energy balance method has advantages over weighting factor when thermal comfort and moisture transport is considered. Enclosure surface temperatures computed by the energy balance method can be used for thermal comfort evaluation and radiant heating and cooling systems analyses. Also, temperature distributions in building elements calculated by the energy balance method enable the study of moisture transport (Crawley et al. 2001).

Depending on how the conduction through building elements is solved, energy balance programs may use:

- discretization methods or
- conduction transfer functions.

Commonly used discretization methods are finite volume and finite difference methods, where the enclosure elements are discretized (one-dimensionally) into a finite number of nodes. Energy balance equations for building discretization nodes create a system of equations organized in a matrix which is numerically solved. The solution of this system provides the cooling/heating load, surface temperature, and temperatures inside each element of the building enclosure. ESP-r (Clarke 1985) uses this discretization method.

Programs that use conduction transfer functions calculate heat fluxes and surface temperatures based on the "history" of surface temperatures. The energy balance matrix for this method is simpler than the matrix with discretization methods because only surface nodes are considered. However, the stability limits of conduction transfer functions restrict this method to analyses where small time steps are used (EnergyPlus 2001). Programs that use conduction transfer functions are BLAST (Hittle 1979), ACCURACY (Chen et al. 1988), and EnergyPlus (Crawley 2000).

2.1.2 Integrated Method versus Loads-Systems-Plant Method

Earlier generations of energy simulation (ES) programs have not integrated models of HVAC systems into the cooling load calculation procedure. These programs use the Loads-

Systems-Plant (LSP) modeling strategy, which subdivides the simulation of the building into three sequential steps:

1) the building's heating and cooling loads are calculated for the analyzed period and assumed set of indoor environmental conditions. These loads are then imposed as inputs to the second step of the simulation.

2) the plant's air handling and energy distribution systems are modeled. This simulation step predicts the demands of the plant's energy conversion systems such as boilers, chillers and other related equipment.

3) the program calculates the energy required in the energy plant and estimates the costs of this energy.

The most popular programs which use this method are DOE-2 (Birdsall et al. 1985) and BLAST (Hittle 1979).

With the LSP approach, mass and energy balance equations which describe HVAC systems are solved without iterations. In this way, the LSP method reduces computing costs by using the values of key variables from the calculations in the previous time step. However, this method does not provide the feedback information from HVAC systems to the heating/cooling load calculation. The lack of the feedback has a potentially serious impact on the accuracy of temperature and comfort predictions. As an example, in reality, when a central plant cannot satisfy the demand for heating due to its limited capacity, temperatures in the zones will drop below the set point. However, the LSP method assumes that central plants always have a large enough capacity to maintain the temperature set point in the zone. Beside giving inaccurate thermal comfort predictions, this assumption may affect the calculation of the heating/cooling load because, in reality, temperature offsets from previous time steps affect the demand for heating/cooling load in next time step.

The disadvantages of the LSP method stimulated the development of a new generation of programs. These new programs employ simultaneous procedures for building load calculations and HVAC performance simulations. This integrated method is implemented into the ESP-r program (Clarke 1985) and EnergyPlus program (Crawley 2000). The integrated method requires more computational time and more complex equation solvers than the LSP method. However, the integrated solution technique with accurate predictions of space temperatures enables a more reliable analysis of HVAC system performance and occupant comfort. This integrated analysis

enables predictions of realistic system controls, moisture transfer in building elements, and performance of radiant heating and cooling systems.

2.1.3 HVAC System Models

HVAC system models use conservation of mass and energy to calculate the respective cooling, heating, and electric energy demands of various components of the system. These components include coils, pumps, fans, humidifiers, ducts, mixing boxes, chillers, boilers and other HVAC components. Depending on each application, ES programs use methods of various complexities for the required energy calculation.

Among available methods, psychometric chart zoning is the simplest. This method does not explicitly simulate any component of the HVAC system. Weather data in the psychometric chart are divided into several zones (Paassen 1986). Within each similar zone, the air handling process is assumed to be the same. The annual energy consumed by an HVAC component in each zone is equal to the energy required by an the component multiplied by the time of operation. Considering the integration of building and HVAC models, this method uses a simplified version of the LSP method, known as the Loads-Plant method. Psychometric chart zoning is not very accurate. However, it is very straightforward and easy to understand. ACCURACY (Chen et al. 1988) uses this method.

When simulating whole buildings, HVAC systems are preconfigured and program users are offered fixed menus of common HVAC system configuration settings. For example, a user can select the Variable Air Volume (VAV), Single Zone Variable Temperature or any other typical HVAC system with the appropriate central plant configuration settings. In more powerful versions of such simulations, the ES program user has the freedom to configure elements in air handling units or power plants. Typical whole-building ES programs are DOE-2 (Birdsall et al. 1985), VISUAL DOE 3 (Visual DOE 3.1 2003), BLAST (Hittle 1979), and Energy Plus (Crawley 2000). However, with this method, the number of HVAC system configurations is still limited.

The most powerful models for energy calculations have component-based models. With these programs, the user interconnects the models of HVAC components, freely creating his/her own HVAC configuration. These programs focus on the performance of the HVAC system. Therefore, they usually have less detailed building load models. Generally, component-based

programs have more accurate algorithms and, therefore, they are useful for detailed studies of special systems. These systems include control systems and active solar heating/cooling systems. Typical component-based programs are TRNSYS (Klein et al. 1994) and CLIMA 2000 (Gautier et al. 1991). These most powerful procedures for HVAC systems analysis demand considerable effort from the user for system modeling. They are also computationally expensive for buildings with many zones undergoing long periods of analysis such as one year or more.

The simplicity of the whole-building simulation method and the HVAC precision of the component-based method are complementary. Therefore, programs such as ESP-r (Clarke 1985) combine strong points of these two types of programs. However, considering thermal comfort and air quality, there is no significant difference between whole-building and component-based methods because improvements in HVAC system simulations have very low impact on these environmental parameters.

2.2 Airflow Simulations Programs

For indoor airflow simulations, the Multi-zone method and Computational Fluid Dynamic (CFD) method are used. Each method has certain advantages and disadvantages related to computation speed, accuracy, thermal comfort, and air quality prediction ability.

2.2.1 Multi-zone and Zonal Methods

Energy simulation (ES) programs and building airflow programs were developed at approximately the same time. The initial models for indoor airflow simulations are based on multi-zone methods. Jackman (1970) was one of the first researchers to use multi-zone network airflow models for the simulation of building infiltration and the airflow between spaces. This multi-zone method uses macroscopic models, which represent large air volumes such as rooms by single nodes, and calculate the flow through discrete paths such as doors and cracks. On the other hand, Lebrun (1970) used the related zonal method for room airflow simulations. The zonal method splits a room into different zones and characterizes the main driving flows in order to predict the spatial temperature distribution in the room. For both methods, multi-zone and zonal methods, the principles of calculation are the same. The considered space (building or room) is divided into sub-spaces (rooms or part of the rooms) in which only the conservations of mass and

energy are applied. The solution to this system of equations provides general information about the considered airflow.

When the multi-zone method is applied to the simulation of airflows in-between rooms, the program results include: infiltration rate, airflow between zones, and contaminant distribution. Programs which use this approach are CONTAM (Dols 2003) and COMIS (Feustel 1998). These programs require small computation time and are user-friendly in their operation. However, they provide only general information about air quality since each zone (room) is assumed to have uniform contaminant distribution. These programs do not provide any information about thermal comfort. Furthermore, this method requires the temperature distribution in the building as input data, which is difficult to know in advanced even for experienced program users. Many simulations simply use measured on-site data if available or assume set-point temperature for each building zone.

The zonal method used for room airflow simulations has been used in different studies related to building airflow (Inard et al. 1996 and Musy et al. 2001). With this method, the temperature distribution in the room is calculated. Therefore, this method provides more information about thermal comfort than the multi-zone models that simulate only airflow between zones (rooms). Similar to multi-zone models, zonal models also require small computing power. However, this performance is highly dependent on assumptions related to boundary conditions and experimental data. Therefore, the existing zonal models are limited only to general predictions of mean temperatures and mass flow rates in each zones of the room.

2.2.2 Computational Fluid Dynamic Methods

Computational Fluid Dynamic (CFD) methods have been successfully applied in the prediction of room airflow since the 1970's. Nielsen (1989), and Jones et al. (1992) provide a detailed reviews of CFD applications in building simulations. Due to high computational requirements, a CFD analysis is usually restricted to single rooms or several spaces within buildings. Typical outputs of a CFD simulation are three-dimensional spatial distributions of:

– air velocity for all three directional components,
– air temperature,
– relative humidity,

– turbulent intensity, and

– different contaminants concentration.

These CFD outputs enable considerably better air quality and thermal comfort analysis than any multi-zone or zonal model.

The largest challenge of CFD modeling is the prediction of turbulent flows. Turbulence can be characterized as a chaotic state of fluid motion. It is characterized in terms of irregularity, diffusivity, large Reynolds numbers, three-dimensional vorticity fluctuations, dissipation and continuum (Tennekes and Lumley 1972). Due to these features, it is difficult to establish whether airflow in a room is an artificially induced, transitional, or fully developed turbulent. It is also observed that very few room airflows are laminar.

Because all non-laminar room airflows can be defined as turbulent ones, the CFD program used for airflow prediction requires appropriate models for turbulence. Generally, turbulent flows are predicted by three approaches:

- Direct Numerical Simulation (DNS),
- Large Eddy Simulation (LES), and
- Turbulence transport models.

The DNS method requires very fine space discretization with cell size on the order of 10^{-3} m. In consideration of typical room sizes and computation power of today's computers, simulations of indoor airflows are not realistic with this method. The LES method was developed by Deardorff (1970) who hypothesized that the turbulent motion could be separated into large and small eddies and that the separation between these two does not have a significant effect on the evolution of large eddies. Because this method assumes that small eddies are independent of the flow geometry, the need for a very fine grid is eliminated. The main contribution to turbulent transport comes from the large-eddy motion and, therefore, this method provides better results than methods which are based on empirical turbulent transport models. Some successful applications of LES related to building simulation are: the flow around a building (Murakami et al. 1996, Jiang et al. 2003), jet flow (Voke et al. 1993), forced convection flow in a room (Davidson et al. 1996, Emmerich et al. 1998), natural ventilation flow in buildings (Jiang at al 2001), and particle dispersion in buildings (Jiang et al. 2002). However, this method requires large computer power and memory. Therefore, LES is still rarely applied for the simulation of

indoor airflows. Therefore, like DNS, LES requires computers that are more powerful than those typically available today to be effectively applicable to room airflow simulation.

Because of the difficulties involved in deterministic turbulence models, turbulence transport models are widely used in engineering applications. All the turbulence transport models solve the Reynolds statistically averaged Navier-Stokes (RANS) equations. These models can be generally divided into two categories:

- Reynolds stress models, and
- eddy-viscosity models.

Reynolds stress models use transport equations for the individual Reynolds stress, while the eddy-viscosity models use Boussinesq approximation that relates Reynolds stress to the rate of mean stream through an "eddy" viscosity (Wilcox 2000). Reynolds stress models are applied to predict room airflow patterns in a room with jets (Renz et al. 1990). The results indicate that the Reynolds stress model is superior to the standard k-ε model, which is eddy viscosity model, because anisotropic effects of turbulence are taken into account. However, Chen (1996) compared three Reynolds-stress models with the standard k-ε model for natural convection, forced convection, mixed convection, and impinging jet in a room. He concluded that the Reynolds-stress models are only slightly better than the k-ε model. Nevertheless, the Reynolds stress models require three to ten times more computing time than the eddy-viscosity models because of the greater algebraic complexity. With this increase of computing time and relatively small improvement in indoor airflow prediction, Reynolds stress models are still very rarely applied in building simulations.

Classic eddy-viscosity models include mixing-length models such as the zero equation, one equation, and two equations eddy-viscosity model (Rodi 1993). The two equation model, often referred to as the "standard" k-ε model, is the most widely-used turbulence model in engineering practice. Here, k presents the turbulence kinetic energy, while ε represents the dissipation rate of turbulence energy. There are several variations of k-ε model. Chen (1995) tested five different k-ε models for natural convection, forced convection, mixed convection, and impinging jet in a room. Chen found that it is very difficult to identify any other model superior to the standard k-ε model. Many studies confirmed applicability of the k-ε model for thermal comfort and indoor air quality analyses Nielsen (1998). However, there are many factors that

influence the results such as mesh generation, convergence procedure, and boundary condition implementation. Therefore, a more powerful computer and a skilful user are necessary for an effective and accurate simulation.

To decrease computational time, Chen and Xu (1998) developed a zero-equation model specifically developed for modeling room airflows and heat transfer. This model uses an algebraic equation to calculate the local eddy viscosity instead of differential equations for kinetic energy (k) and dissipation rate (ε). This substantially reduces the computation time compared to the more complex k-ε approaches. Chen and Xu (1998) tested this model on four airflow types: displacement ventilation, natural ventilation, forced convection, and mixed convection. They found good agreements between the zero-equation model predictions and the experimental data. In fact, in some cases the zero-equation model outperformed the k-ε model. Srebric et al. (1999) provided further validation of this approach by comparing the zero-equation model's predictions to experimental data for three additional cases of airflows in rooms. These included natural convection with infiltration, forced convection, and mixed convection with displacement ventilation. They found good agreement between the computed and measured air velocity and temperature profiles.

2.3 Integration of ES and CFD Models

When CFD models are used alone for the prediction of indoor airflows, the user, besides the enclosure geometry, provides the following boundary conditions:

- Convective heat flux or surface temperature at enclosure surfaces,
- Flow entering or leaving the room at enclosure openings.

These boundary conditions are based on known design data, measured data, and other assumptions. Usually, known design data are volume flow rate at enclosure openings, such as air volume flow at inlets and heat fluxes at certain surfaces such as computers or heaters. Other assumptions are surface temperatures and volume flow at openings created by infiltration or natural ventilation. The accuracy of airflow prediction is very sensitive to these assumed boundary conditions (Awbi 1998 and Xu et al. 1998) because the flow inside the CFD domain (room) is driven by the boundary conditions.

In the case where the building simulation program considers the whole building including the HVAC systems and indoor air distribution, the boundary conditions are placed at the exterior

surfaces of the building. Boundary conditions are then derived from exterior conditions such as temperature, solar radiation, wind velocity, humidity, and other relevant weather data. In this way, the overall influence of dynamic weather conditions on airflows and HVAC system is established. Considering this, CFD researchers have begun to integrate building models and inter-surface radiation models into CFD codes (Holmes et al. 1990, Chen et al. 1995, and Moser et al. 1995). This type of CFD programs solves convective, radiative, and conductive heat transfer simultaneously. This method is powerful, but it is also computationally very expensive (Chen et al. 1995) because CFD treats heat transfer though building elements as a three-dimensional unsteady conduction problem. Also, when CFD calculates the heat transfer in solid materials, the calculation becomes stiffer and the computing time goes up dramatically (Thompson 1988).

Chen (1988) is probably the first researcher who tried to couple an ES program with a CFD program. He showed that the coupling of ES and CFD programs can provide more accurate predictions of cooling loads, especially in the case of stratified flows. Nielsen et al. (1998) confirmed that an interconnection between these two programs would improve the energy consumption calculation including an improvement in the prediction of thermal comfort and air quality in a selected area of a building. Srebric et al. (2000) continued Chen's study (1988) by using coupling for dynamic heating/cooling load calculations. However, this coupling is a quasi-dynamic coupling, which with large time-steps (time discretization) do not enforce heat flux conservation in-between the CFD and ES calculation domains.

For the energy balance between the ES and CFD domains, a slightly better approach than that of Srebric (2000) was used by Clarke et al. (1995) and Negrao et al. (1995), whereby a CFD code was integrated into the ESP-r building simulation program. The two modeling domains exchange information on a time step basis. The overall energy balance is then achieved through an iterative procedure. This fully dynamic coupling increases accuracy, but the iterative procedure considerably increases the computation time.

Recent progress in the coupling of ES and CFD programs was provided by Beausoleil et al. (2000, 2001, 2003) and Zhai et al. (2001). Beausoleil continued Clarke's (1995) and Negrao's (1995) work by focusing on improving the convective heat flux calculation between the ES and CFD domains. Zhai at al (2001) continued Chen's (1988) and Srebric's (2000) work by implementing the CFD into EnergyPlus. In these studies, they focused on numerical stability of

coupling models and heat flux conservation in-between the two domains. Since these two research studies considered very important issues related to

- methods for accurate surface convective heat flux calculation and
- methods for coupling ES and CFD programs

which are complementary, the next two subsections present more details about these research studies.

2.3.1 Convective Heat Flux Problems

In the integrated modeling approach, the ES and CFD domains interact on surfaces (walls). However, in near-wall regions the CFD has difficulty performing accurate convective flux calculations. With the k-ε models, standard log-law wall-functions (Launder and Spalding 1974) are usually used for wall shear and surface convection calculations. These wall-functions only provide good results for a particular type of room airflow. Chen et al. (1990), Niu et al (1992), and Awbi (1998) showed that the logarithmic profile poorly approximates velocities, and especially surface convection, in the boundary layer for buoyancy-driven flows. This model is sensitive to the location of the near-wall grid points. In principle, the smaller the first grid size, the larger the calculated heat flux. Overall, log-law wall functions are valid only for forced convention in near-wall regions.

To solve the boundary condition problem, Beausoleil (2000, 2001) created the "Adaptive Convection Algorithm" and "Adaptive Conflation Controller". These procedures combine convection correlations and wall-functions models for the calculation of surface heat fluxes.

The adaptive convection algorithm calculates convection coefficients based on:

- Geometry, such as height of a wall and characteristic dimension of a room,
- Temperature of surface, supply air, and room air,
- Type and position of an HVAC device in a room (refer to Figure 2.1),
- Supplied air volume flow rates.

Based on these data, the adaptive convection algorithm dynamically assigns (for each surface) an appropriate convection model from 24 experiment-based convection correlations. Also, during the simulation, this algorithm monitors the operational state of the HVAC device

(on/off) to estimate the flow regime (forced or convective flow). This algorithm is used for convection calculation in both CFD and ES program domains.

Convection models that are implemented into the adaptive convection algorithm are based on the following research works:

- The Alamdari-Hammond correlations (Alamdari et al. 1983) for natural convection in a room,
- The Khalifa correlations (Kalifa et al. 1990) for surface convection in a room with baseboard heaters and fan devices,
- The Awbi-Hatton correlations (Awbi et al. 1999) for convection on heated room surfaces,
- The Fisher correlations (Fisher 1995) for forced convection with ceiling-jet and free horizontal-jet,
- ESP-r mixed flow correlations (Beausoleil 2000) for rooms with mixing diffuser and large surface-air temperature differences.

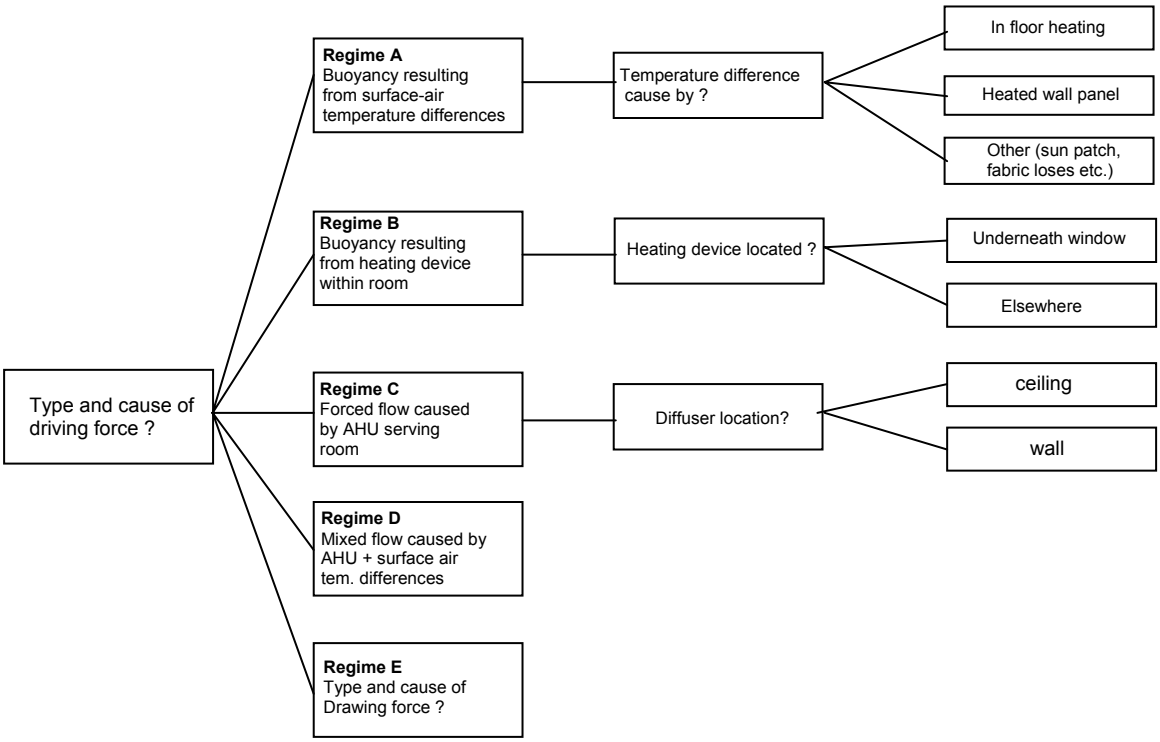

Figure 2.1 Influence an HVAC device type and position on the selection of a surface convection correlation (Beausoleil 2000)

The adaptive conflation controller makes a choice between two approaches to calculate the convective heat flux for each surface: (1) convection correlation models as mentioned above, and (2) wall functions models. The decision is based on the airflow regime in

the vicinity of considered surface. The ES and CFD programs operate independently, but exchange information on the internal surfaces at the beginning of each simulation time step. However, special boundary condition treatments were developed to improve surface conflation. For each time step, the adaptive conflation controller first performs an investigative CFD simulation to approximate the room's airflow and temperature field. Subsequently, the controller calculates dimensionless numbers (Re, Gr) that define the type of airflow on each surface. In this process, the controller selects a model for the boundary condition calculations on each surface. For example, the controller uses log-law wall functions for surfaces with only forced convection, Yuan's wall-functions (Yuan et al. 1993) for vertical surfaces with only natural convection, or adaptive convection algorithm to select the appropriate convection correlation for all other flow-types. Finally, with the new boundary conditions, the CFD calculates the final flow, temperature, and concentrations distributions.

In the boundary condition calculation, this method provides highly accurate results. However, the conflation controller requires a double run of the CFD calculation for each surface temperature distribution provided by the ES program. This double run of CFD is computationally expensive and requires a coupling method which does not provide the full coupling of the ES and CFD programs. As a result, this type of coupling is time step sensitive and the Beausoleil (2000) suggest a time step of 15 minutes or less.

Beausoleil's research (Beausoleil 2000 and 2001) considerably improved the coupling. However, he still did not completely resolve all the important issues. The adaptive conflation controller improves the boundary condition calculations, but it limits the coupling of the ES and CFD programs to one-directional coupling or quasy dynamic coupling. These two coupling methods have certain weaknesses related to accuracy and sensitivity to calculation time step, which are described in Chapter 5. Also, the adaptive convection algorithm needs additional models to calculate convection coefficients. Most of the 24 convection correlations are applicable to mixed air in a room. Surface convection models for stratified room airflows such as those with displacement ventilation or flows in a room with chilled ceiling panels are not included.

2.3.2 Numerical Stability and Heat Flux Conservation in-between Two Domains

Zhai et al. (2001) and Chen et al. (2002) focused their research on integrated coupling. They used the heat flux balance between two program domains for coupling in the ES and CFD programs. For several modifications of fully dynamic coupling, these two researchers analyzed

convergence and stability problems that may occur in the coupled program due to different mathematical and numerical models used in ES and CFD programs.

Considering information which describes the surface heat flux between two programs, four different "data-type methods" were analyzed:

(1) ES to CFD by T; CFD to ES by h and ΔT

(2) ES to CFD by T; CFD to ES by $h_{corrected}$

(3) ES to CFD by T; CFD to ES by q

(4) ES to CFD by q; CFD to ES by h and ΔT

where 'T' is the interior surface temperature; 'q' is convective heat flux on interior surfaces; 'h' is the convective heat transfer coefficient; $\Delta T=T_{local\ air}-T_{room\ air}$; and $h_{corrected}=q_{CFD}/(T_{room\_air}-T_{surface})$.

Zhai and Chen found that all four data-type methods can provide the energy balance in-between two program domains. However, the data-type method (1) has the best performance in terms of numerical stability, and iteration speed. Also, this research showed that the order of the numerical scheme in the CFD has little impact on the coupling of the ES and CFD programs. The researchers showed that lower order schemes (upwind and hybrid), which can be applied consistently throughout the enclosure, lead to lower accuracy of the results. On the other hand, more accurate higher order schemes, which require more nodes, are adjusted to lower order schemes in the vicinity of the surfaces due to the luck of sufficient nodes. This combination of different schemes creates inconsistency of surface flux for a node adjacent to the surface. As a result, a higher order schemes do not contribute to the accuracy of coupling.

This study considerably contributed to the literature on the coupling of the ES and CFD programs by introducing new coupling techniques. However, Zhai and Chen assumed that the wall functions in CFD can accurately predict boundary conditions. They used zero-equation turbulence model with simplified wall functions which provide grid dependent surface heat flux calculation, especially with a buoyancy-driven flow (Beausoleil 2000). Also, with fully dynamic coupling that was used in this analysis, the ES and CFD programs exchange information up to 10 times until a satisfactory energy balance is achieved. This might be computationally expensive even with the use of a fast zero equation models in the CFD program.

CHAPTER 3

DEVELOPMENT OF NEW ENERGY SIMULATION PROGRAM

3.1 Introduction

In this thesis, a new Building Energy Simulation (BES) program is developed to enable effective testing of research hypotheses for heat transfer in spaces with unconventional Heating, Ventilating and Air-Conditioning (HVAC) systems, which have a potential to save building energy consumption while simultaneously increasing indoor air quality. The program is designed for single room analyses with or without plenum and all-air, air-water, or all-water HVAC. The HVAC configuration models are implemented with a focus on integrating models for building load calculation and HVAC performance simulation. For load calculations, BES uses the energy balance method with a one-dimensional finite volume discretization for conduction computations. The grid size and time step can be changed arbitrarily, enabling grid dependency testing. Considering the heat balance in a zone, the BES program has up-to-date models that are used in the latest generation of ES programs such as ESP-r and EnergyPlus. These models are used for the calculation of external boundary conditions, conduction, fenestration, solar radiation distribution, lighting radiation distribution, internal radiation distribution, and heat transfer from adjacent zones. the BES program has simplified models for ground heat transfer and air infiltration.

This chapter describes the existing and newly developed models used in the BES program and presents validation results. Section 3.2 describes the heat transfer model for each of the energy subsystems of the simulation domain. In this section, the existing models are only briefly described to review fundamentals of new BES program features. Section 3.3 describes numerical methods used for solving systems of linear equations in the thermal domain. Readers not interested in building heat flux models and numerical methods implemented into BES can go to Section 3.4. Section 3.4 gives details about newly developed models for simultaneous load calculation and HVAC performance simulation. A validation of the BES program is provided in Section 3.5, and Section 3.6 contains the relevant discussion and closing remarks.

3.2 Heat Transfer Models for Energy Subsystems

Heat transfer models for energy subsystems include calculations of external boundary conditions based on weather data, heat and mass transfer models such as heat conduction through building elements, radiation through transparent surfaces, short and long wave radiation distribution, internal and external convection, infiltration, and heat gains distribution from internal objects. In this section these models are organized into 5 groups:

- Boundary Conditions at External Surfaces,
- Boundary Conditions at Internal Surfaces,
- Energy Equations for Building Systems,
- Inter-zone Airflow and Infiltration, and
- HVAC Models.

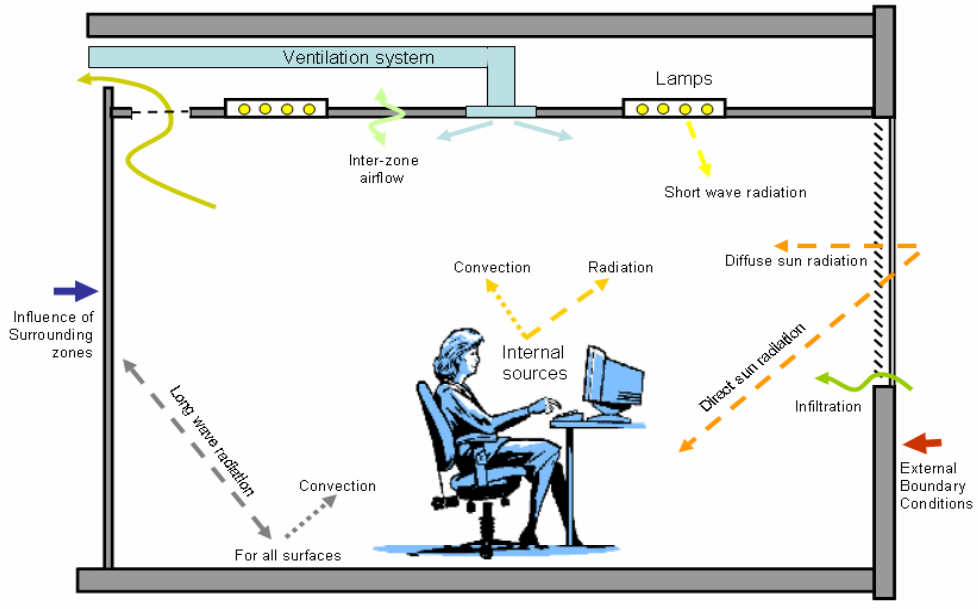

Figure 3.1 Building heat flow mechanisms implemented in a new building energy simulation (BES) program

3.2.1 Boundary Conditions at External Surfaces

External boundary conditions are the main causes of unsteady heat transfer through building elements, because the external boundaries are based on variable weather data. These weather data affect convective and radiative heat fluxes at building surfaces in the contact with the air and conductive heat flux at surfaces in contact with the soil. The BES program uses Typical Meteorological Year (TMY2) data base (Marion and Urban 1995) as the weather data source. In the next subsections the models for the following phenomena on external surfaces are

presented: (1) convective heat flux, (2) solar radiation, (3) shading, (4) external long wave radiation, and (5) conduction to the ground.

Convective heat flux

On external building surfaces the major factors that affect the convective heat transfer are wind speed and wind direction in relation to the geometry of the surface. Forced convection is dominant on external building surfaces due to the wind velocities which are typically above 1m/s. BES calculates external convective heat flux by a widely used empirical model for different building facades (Kimura 1977). This model uses wind speed (U) and wind direction on a facade surface to calculate the local velocity in the vicinity of the surface (u). For surfaces that are windward:

$$u = \begin{cases} 0.5 & \text{for } U < 2 \text{ m/s} \\ 0.25 \cdot U & \text{for } U > 2 \text{ m/s} \end{cases} \tag{3.1}$$

For surface that are leeward:

$$u = 0.3 + 0.05 \cdot U \tag{3.2}$$

The external convection coefficient *(h)* is modeled as:

$$h = 3.5 + 5.6 \cdot u \tag{3.3}$$

The coefficient *3.5* in Equation (3.3) represents the influence of natural convection in the case when wind speed is low and natural convection is dominant on the considered surface. For the calculation of h, BES uses wind speed and direction as input data from the weather database.

Solar radiation

Solar radiation is an important heat transfer mechanism, especially for buildings with large windows. Therefore, the BES program accurately calculates solar radiation components. The program accounts for the components of solar radiation based on the following input data:

- Direct Normal Radiation *(I_{DNR})* - solar radiation to a surface normal to a solar beam,
- Global Horizontal Radiation *(I_{GHR})* - solar radiation that hits a horizontal surface.

BES also calculates all the angles for tracking the position of the sun related to the considered surface. This position is based on building location as well as the period of the year and day. Appendix A contains calculation models and procedures for these solar angles.

Solar radiation that hits the considered external surfaces is divided into direct and diffuse components (Figure 3.2). Direct solar radiation (I_{DIR}) is directional and depends on the incident angle (θ):

$$I_{DIR} = I_{DNR} \cos\theta \tag{3.4}$$

Diffuse solar radiation encompasses sky-diffuse and ground-reflected (diffusely reflected) solar radiation (Figure 3.2). Diffuse solar radiation is assumed to be totally or partially isotropic depending on the applied model for sky-diffuse radiation.

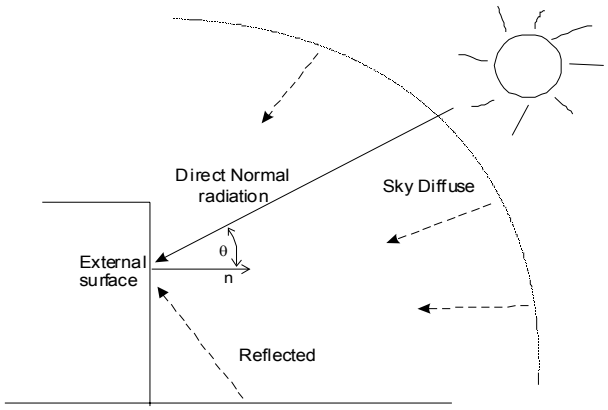

Figure 3.2 Solar radiation on the external surface of a building

Because calculation of building energy consumption is very sensitive to solar radiation calculation, three existing models for solar diffuse radiation are implemented into the BES program:

- Isotropic Diffuse Radiation Model
- HDKR Anisotropic Diffuse Radiation Model
- ASHRAE Anisotropic Diffuse Radiation Model

The *Isotropic Diffuse Radiation Model* uses the assumption of uniform sky diffuse radiation (Duffie and Beckman 1991). With this model, sky radiation is independent of the solar azimuth and it is only a function of the surface slope β (90° for vertical surface). The sky diffuse radiation component on the considered surface is calculated as follows:

$$I_{dif\_sky} = (I_{GHR} - I_{DNR} \sin\alpha) \cdot (1 + \cos\beta)/2 \tag{3.5}$$

where term $(I_{GHR} - I_{DIR} \sin\alpha)$ represents the diffuse solar radiation on a horizontal surface and term $(1+\cos\beta)/2$ represents the view factor of the sky to the considered surface. Diffuse solar radiation is calculated as the difference between Global Horizontal Radiation *(I_{GHR})* and

orthogonal component of Direct Normal Radiation *(I_{DIR})*. The angle α is solar altitude (see Appendix A).

The *HDKR Anisotropic Diffuse Radiation Model* (Hay, Davies, Klucher, and Reindl radiation model) is an anisotropic diffuse radiation model (Duffie and Beckman 1991). This model corrects the *Isotropic Diffuse Radiation Model* for circumsolar diffuse radiation and horizon brightening. The sky diffuse radiation component on a considered surface is calculated as follows:

$$I_{dif\_sky} = (I_{GHR} - I_{DIR}\sin\alpha)\cdot\left[(1-A_i)\cdot(1+\cos\beta)/2\cdot(1+f\sin^3(\beta/2)) + A_i R\right] \tag{3.6}$$

The equation terms (1-A_i) and (A_iR) are for the correction for circumsolar diffuse radiation. Coefficient R is the ratio between global radiation on considered surface and global horizontal radiation. Anisotropy index A_i is a function of atmosphere transmittance, which is calculated as a ratio between Direct Normal Radiation on the ground (I_{DIR_ground}) and Direct Normal Radiation on the outer layer of the atmosphere ($I_{DIR\_extraterrestrial}$):

$$A_i = I_{DIR\_ground} / I_{DIR\_extraterrestrial} \tag{3.7}$$

Term $(1+f\sin^3(\beta/2))$ is the correction for horizon brightening where f is function of the ratio between Direct Normal Radiation and Global Horizontal Radiation.

$$f = \sqrt{I_{DIR}/I_{GHR}} \tag{3.8}$$

The *Anisotropic Diffuse Radiation Model* presented by ASHRAE (ASHRAE Fundamentals 2001) introduces a simpler correction method of the *Isotropic Diffuse Radiation Model* that is valid only for vertical surfaces. Here, the sky diffuse radiation component on the considered surface is calculated as follows:

$$I_{dif\_sky} = (I_{GHR} - I_{DIR}\sin\alpha)\cdot Y \tag{3.9}$$

where coefficient Y represents the ratio of the sky diffuse radiation on a vertical surface to the sky diffuse radiation on a horizontal surface. This coefficient is calculated as follows:

$$\begin{aligned} Y &= 0.55 + 0.437\cdot\cos\theta + 0.313\cdot(\cos\theta)^2 \quad \text{for} \quad \cos\theta > 0.2 \\ Y &= 0.45 \qquad\qquad\qquad\qquad\qquad\qquad\quad \text{for} \quad \cos\theta < 0.2 \end{aligned} \tag{3.10}$$

All surfaces, except the vertical surface *Y*, are the same as $(1+\cos\beta)/2$. This is the view factor of sky to the considered surface (as depicted in Equation 3.5).

Ground reflected radiation is assumed to be isotropic because of the effect of surface roughness. Therefore, the ground reflected radiation component is given as:

$$I_{dif\_reflected} = I_{GHR} \cdot \rho_{ground} \cdot (1-\cos\beta)/2 \tag{3.11}$$

where ρ_{ground} is the ground solar radiation reflection coefficient and term $(1-\cos\beta)/2$ is the view factor of ground to the considered surface.

The total diffuse radiation on the considered surface is calculated as the sum of the sky diffuse radiation component and ground reflected radiation component as follows:

$$I_{dif} = I_{dif\_sky} + I_{dif\_reflected} \tag{3.12}$$

Shading

Building facades are rarely plane surfaces. Usually, there are architectural elements that block the direct solar radiation on the considered external surfaces. Because shaded surfaces receive only diffuse radiation, the reduction of received radiation might be significant. This is the case for a sunny day when the direct component is several times larger than the diffuse component. Therefore, the BES program calculates the shaded portion (A_{shaded}/A_{total}) of the considered surface (Figure 3.3) based on geometry data for the surface, geometry data for horizontal and vertical shading devices, sun azimuth and altitude, and surface azimuth (γ_S, α_S, γ see Appendix A).

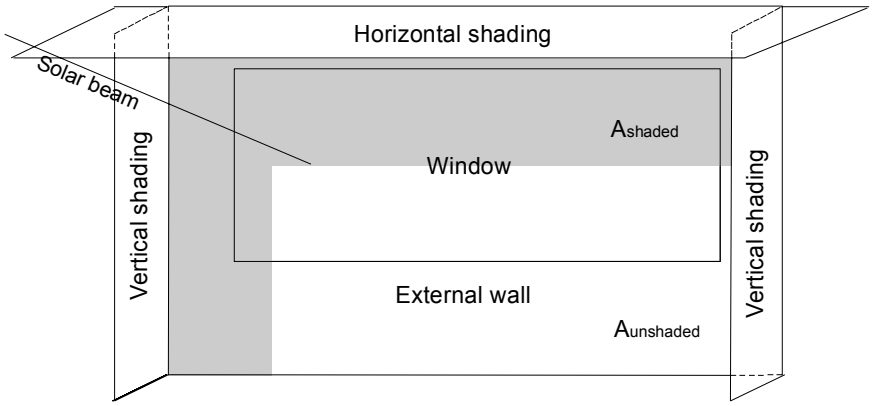

Figure 3.3 Geometry of a building facade used in the shading model for solar radiation calculation

Based on the shaded portion, diffuse (I_{dif}), and direct (I_{DIR}) components of solar radiation, program calculates absorbed and, in the case of windows, the transmitted portion of the solar radiation. For opaque surfaces, absorbed solar radiation is calculated as follows:

$$q_{absorbed\_S} = \alpha_{shortwave} \cdot \left[I_{DIR} \cdot (1 - A_{shaded} / A_{total}) + I_{dif} \right] \tag{3.13}$$

where $\alpha_{shortwave}$ represents the absorption coefficient for shortwave radiation.

For windows, the transmitted portion of diffuse and direct radiation is calculated separately because these two components of solar radiation are distributed inside the room in two different ways. The details about transmitted direct and diffuse solar radiation in the room are given in the following section that describes the distribution of short wave radiation in a room. Direct solar radiation transmitted through windows is given as:

$$q_{transm\_DIR} = \tau_{DIR} \cdot I_{DIR} \cdot (1 - A_{shaded} / A_{total}) \tag{3.14}$$

where τ_{DIR} is the window transmittance coefficient for direct solar radiation. This coefficient depends on the window structure and it is described in the following section that explains how window models work. Windows transmitted diffuse radiation is given as:

$$q_{transm\_dif} = \tau_{dif} \cdot I_{dif} \tag{3.15}$$

where τ_{dif} is the window transmittances coefficient for direct solar radiation. This coefficient is also described in the following section (Section 3.2.3).

External long wave radiation

External surfaces exchange energy with surrounding surfaces of different temperatures by long-wave radiation. In the model used in the BES program, external surfaces "radiate" energy to the sky and to the ground as illustrated in Figure 3.4.

External surface heat exchange with the ground is given as:

$$q_{surf\_ground} = (1 - \cos\beta)/2 \cdot \sigma \cdot \varepsilon_{surf} \cdot \varepsilon_{ground} (T_{surf}^{\ 4} - T_{ground}^{\ 4}) \tag{3.16}$$

where (1-cosβ)/2 is the view factor, σ is the black body radiation constant, and ε is the emissivity constant for the surface and ground. Because of the solution procedure, this radiative heat

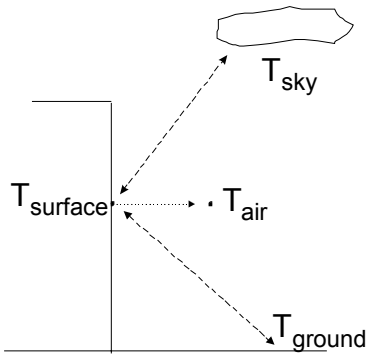

Figure 3.4 External surface convection and long wave radiation
on the external surfaces of buildings

exchange equation is linearized using temperature values from the previous time step to calculate the radiative convection coefficient h_{rad_ground}. The linearized equation is given as:

$$q_{surf\_ground} = h_{rad\_ground}(T_{surf} - T_{ground}) \tag{3.17}$$

The external surface heat exchange with the sky is given as:

$$q_{surf\_sky} = (1+\cos\beta)/2 \cdot \sigma \cdot \varepsilon_{surf} \cdot \varepsilon_{sky}(T_{surf}{}^4 - T_{sky}{}^4) \tag{3.18}$$

After linearization:

$$q_{surf\_sky} = h_{rad\_sky}(T_{surf} - T_{sky}) \tag{3.19}$$

The sky temperature (T_{sky}) is a "dummy" variable introduced to model surface radiation to the sky (Kimura 1977). It is calculated as:

$$T_{sky} = \left[Br(1 - Kc \cdot CC/10) + Kc \cdot CC/10\right]^{1/4} \cdot T_{air} \tag{3.20}$$

where influence of water vapor (Br) on this radiation is calculated as a function of the water vapor pressure in the air (p_{water_wapor} in mb):

$$Br = 0.51 + 0.066\sqrt{p_{water\_vapor}} \tag{3.21}$$

The influence of clouds is introduced through the coefficient $Kc = f(clouds\_height)$ and the portion of the sky covered by clouds CC (from 0 to 10). The sky temperature is calculated as a black body temperature and therefore $\varepsilon_{sky} = 1$.

To calculate external long wave radiation, the model implemented into BES program assumes that the ground surface temperature is equal to the air temperature. There is also an option that users define this temperature. The sky temperature is calculated based on meteorological data for cloud height, and the portion of the sky covered by clouds. Water vapor pressure needed for the sky temperature calculation (Equations 3.20 and 3.21) is calculated using relative humidity and the dry bulb temperature from weather data base.

Conduction to the ground

For an external surface that is in contact with the ground, the BES program uses the simplified model, which is given as:

$$q_{cond\_ground} = k_{ground} / L \cdot (T_S - T_{ground}) \tag{3.22}$$

Based on the location of the ground configuration, the user defines the ground temperature (T_{ground}) at distance (L) and ground conductivity (k_{ground}). The user may improve this model by providing the seasonal changes of ground temperatures.

3.2.2 Boundary Conditions at Internal Surfaces

In the next subsections the models for the following heat transfer mechanisms at internal surfaces are presented:

(1) convection,

(2) long wave radiation,

(3) short wave radiation.

Convection

Convection coefficients used in the BES program are calculated based on expressions for mixed convection provided by Beausoleil (2000). He created this correlation by combining the correlations for natural convection (Alamdari and Hammond 1983) and for forced convection where the air is supplied by a ceiling diffuser (Fisher 1995). For vertical surfaces, the program calculates convection coefficients for forced and natural convections (h_f and h_n). Depending on the air movement created by forced and natural convection (opposing or assisting), the BES program uses the appropriate model to combine these two heat transfer mechanisms (Table 3.1).

For horizontal surfaces, depending on the surface position (floor or ceiling) and type of natural convection (buoyant or stably stratified), the appropriate correlations for forced and natural convections are selected and combined. These correlations are primarily suitable for well-mixed airflows.

Table 3.1 Convection correlations for mixed, forced, and natural convection (Beausoleil 2000).

Vertical surfaces	assisting forces	$\alpha_n \left\{ \left[1.5 \cdot \left(\frac{\Delta T}{H} \right)^{1/4} \right]^6 + \left[1.23 \cdot \Delta T^{1/3} \right]^6 \right\}^{1/6}$ $\alpha_f = \left(\frac{T_s - T_f}{\Delta T} \right) \cdot \left[-0.199 + 0.19 (ACH)^{0.8} \right]$	$\alpha = \left(\alpha_n^3 + \alpha_f^3 \right)^{1/3}$
	opposing forces	$\alpha_n \left\{ \left[1.5 \cdot \left(\frac{\Delta T}{H} \right)^{1/4} \right]^6 + \left[1.23 \cdot \Delta T^{1/3} \right]^6 \right\}^{1/6}$ $\alpha_f = \left(\frac{T_s - T_f}{\Delta T} \right) \cdot \left[-0.199 + 0.19 (ACH)^{0.8} \right]$	$\alpha = \max \begin{Bmatrix} \left(\alpha_n^3 - \alpha_f^3 \right)^{1/3} \\ 0.8\alpha_n \\ 0.8\alpha_f \end{Bmatrix}$
Floor	buoyant	$\alpha_n \left\{ \left[1.4 \cdot \left(\frac{\Delta T}{D_h} \right)^{1/4} \right]^6 + \left[1.63 \cdot \Delta T^{1/3} \right]^6 \right\}^{1/6}$ $\alpha_f = \left(\frac{T_s - T_r}{\Delta T} \right) \cdot \left[-0.159 + 0.116 (ACH)^{0.8} \right]$	$\alpha = \left(\alpha_n^3 + \alpha_f^3 \right)^{1/3}$
	stabile stratified	$\alpha_n = 0.6 \cdot \left(\Delta T / D_h \right)^{1/5}$ $\alpha_f = \left(\frac{T_s - T_r}{\Delta T} \right) \cdot \left[-0.159 + 0.116 (ACH)^{0.8} \right]$	
Ceiling	buoyant	$\alpha_n \left\{ \left[1.4 \cdot \left(\frac{\Delta T}{D_h} \right)^{1/4} \right]^6 + \left[1.63 \cdot \Delta T^{1/3} \right]^6 \right\}^{1/6}$ $\alpha_f = \left(\frac{T_s - T_r}{\Delta T} \right) \cdot \left[-0.166 + 0.484 (ACH)^{0.8} \right]$	
	stabile stratified	$\alpha_n = 0.6 \cdot \left(\Delta T / D_h \right)^{1/5}$ $\alpha_f = \left(\frac{T_s - T_r}{\Delta T} \right) \cdot \left[-0.166 + 0.484 (ACH)^{0.8} \right]$	

$\Delta T = | T_{surface} - T_{room\_air} |$, ACH - room supply air changes per hour, T_s - supply air temperature, T_r - room air temperature, H - surface height, D_h -hydraulic diameter (4· Area / Perimeter)

Long wave radiation

Internal surfaces with different temperatures exchange energy through long wave radiation. To calculate the relevant radiative heat fluxes, view factors between all pairs of surfaces are required. The view factor of surface '*i*' to surface '*j*' is calculated by the following equation:

$$F_{ij} = \frac{1}{A_i} \int_{A_i} \int_{A_j} \frac{\cos\varphi_i \cdot \cos\varphi_j}{\pi s^2} dA_i dA_j \tag{3.23}$$

All internal surfaces used in the BES program are parallel or orthogonal to each other. Therefore, only two characteristic solutions of equation (3.23) are used in BES (F_{ij_parale} and $F_{ij\_ortogonal}$). Detailed expressions for the view factors are given in Appendix B. Using these expressions and room geometry, the program calculates view factors for all surfaces by creating a matrix [$n \times n$], where n is total number of surfaces. The room surfaces form a closed environment and therefore:

$$F_{i1} + F_{i2} + F_{i3} + ... + F_{in} = \sum_{j=1}^{n} F_{ij} = 1 \qquad i = 1,2,...,n \tag{3.24}$$

Long wave radiative heat flux at surface (q) may be determined by using the radiosity method (ASHRAE Fundamentals 2001). Radiosity (J) is the total energy that is emitted and reflected from a surface. It is calculated using the system of equations given by:

$$J_i = \varepsilon_i \sigma T_i^4 + (1 - \varepsilon_i) \sum_{j=1}^{n} F_{ij} J_i \qquad i = 1,2,...,n \tag{3.25}$$

The radiative heat flux that surface *'i'* receives is given as:

$$q_i = \frac{\sigma T_i^4 - J_i}{(1 - \varepsilon_i)/\varepsilon_i} \tag{3.26}$$

This radiosity method creates a system of equations dependent on fourth power of temperature. Combining of these equations with the linear temperature equations creates a system of linear and highly nonlinear equations that is difficult to solve. Therefore, instead of using the

radiosity method, the BES program uses a method based on the Radiative heat exchange factors. This method enables a linearization of equations that describe the radiative heat exchange.

Linearization of surface radiative heat exchange

Hoornstra (1986) presented a method that uses radiative heat exchange factors ($\psi_{i,j}$). According to this method, radiative heat exchange in-between surfaces *'i'* and *'j'* that include reflection from other surfaces is given as:

$$Q_{i,j} = \varepsilon_i \psi_{i,j} A_i \sigma \left(T_i^4 - T_j^4 \right) \tag{3.27}$$

Radiative heat exchange factor $\psi_{i,j}$ is the absorbed fraction (by surface *'i'*) of the emission from surface *'j'* that includes the reflection from other surfaces. Radiative heat exchange factor $\psi_{i,j}$ defined in this way considers multiple reflections of the radiative heat exchanges in the room.

If the view factor from surfaces *'i'* to *'k'* is $F_{i,k}$, then $F_{ik} A_i \sigma T_i^4$ is the radiation energy that the black body surface *'i'* radiates towards surface *'k'*. The reflected radiation from surface *'k'* is, therefore, given as, $(1-\alpha_k) F_{ik} A_i \sigma T_i^4$, where $(1-\alpha_k)$ represents reflection from the surface *'k'*. Part of this energy gets to the surface '*j*' by multiple reflections and the other part is absorbed by this surface. This is illustrated as $\psi_{k,j}(1-\alpha_k) F_{i,k} A_i \sigma T_i^4$. Finally, the total energy that get to surface *'j'* from surface *'i'* by multiple reflections from other surfaces is:

$$\sum_{k=1}^{n} \psi_{k,j} (1-\alpha_k) F_{i,k} A_i \sigma T_i^4 \tag{3.28}$$

The direct radiation from surface *'i'* absorbed by surface *'j'* is given as:

$$\alpha_j F_{i,j} A_i \sigma T_i^4 \tag{3.29}$$

where α_j is the absorptivity of surface '*j*'. For gray surfaces, the absorptivity is the same as the reflectivity ($\alpha = \varepsilon$). Taking into account the multiple reflections from all room surfaces, the total radiation from surface *'i'* absorbed by the surface *'j'* is given as:

$$\psi_{i,j} A_i \sigma T_i^4 = \alpha_j F_{i,j} A_i \sigma T_i^4 + \sum_{k=1}^{n} \psi_{k,j} (1 - \alpha_k) F_{i,k} A_i \sigma T_i^4 \tag{3.30}$$

Then, it follows that radiative heat exchange factors are calculated from the system of equations given by:

$$\psi_{i,j} = \varepsilon_j F_{i,j} + \sum_{k=1}^{n} \psi_{k,j} (1 - \varepsilon_k) F_{i,k} \quad , \quad i = 1,2,...,n \quad , \; j = 1,2,...,n \tag{3.31}$$

It is important to point out the difference between $F_{i,j}$ and $\psi_{i,j}$. The view factors define the room geometry while the radiative heat exchange factors define the geometry and surface conditions. For view factors, $F_{i,j} A_i = F_{j,i} A_j$, while for radiative heat exchange factors, $\psi_{i,j} A_i \neq \psi_{j,i} A_j$. On the other hand, similar to the view factors, $\sum_{j=1}^{n} \psi_{i,j} = 1$.

The linearization of surface radiative heat exchange using radiative heat exchange factors, which define radiative heat flux in-between two surfaces (Equation 3.27), is simpler than the radiosity method. This is illustrated as follows:

$$q_{i,j} = h_{ri,j} \left(T_i - T_j \right) \tag{3.32}$$

The radiation convection coefficient is calculated based on the temperature values from the previous time step. This is given as follows:

$$h_{ri,j} = \varepsilon_i \psi_{i,j} \sigma \left(T_i^2 + T_j^2 \right) \left(T_i + T_j \right) \tag{3.33}$$

Short wave radiation

Distribution of direct solar radiation

The distribution of direct radiation in the room is calculated using the BESTEST solar fractions method (Judkoff and Neymark 1995). This is an approximate method with the main assumption that direct solar radiation that enters the zone first hits the zone's floor. Part of the short wave solar radiation is absorbed by floor and the rest is diffusely reflected to the other zone surfaces (Figure 3.5). Each surface receives a part of this reflected energy according to the

position in the room and surface properties defined by view-factors and short wave absorption. This instantaneous reflection and absorption process, is repeated until all direct radiation is absorbed. The BESTEST solar fraction method considers three reflections and absorptions and the rest of the unabsorbed energy is distributed over each surface proportionally to its surface area.

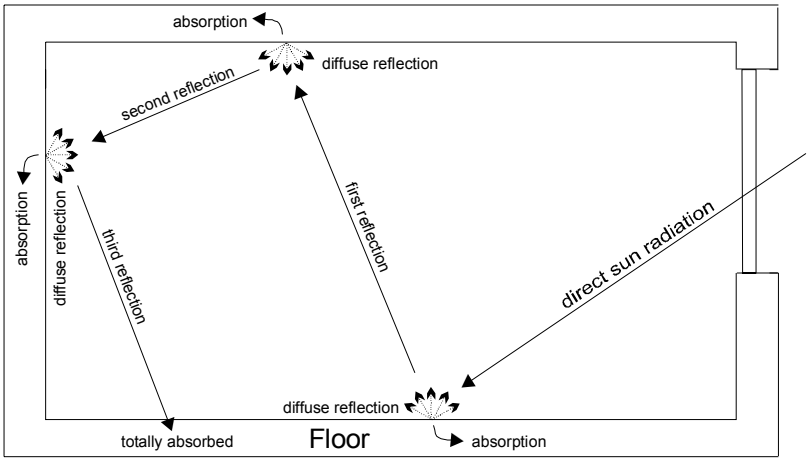

Figure 3.5 Distribution of direct solar radiation on internal room surfaces

The transmitted direct solar radiation that surface 'i' absorbs is given as:

$$SF_i = A1_i + A2_i + A3_i + AR_i \tag{3.34}$$

Fraction $A1_i$ is the absorbed energy at the first "strike" of the transmitted direct solar radiation. For the floor, this fraction is equal to the absorption coefficient where $A1_{floor} = \alpha_{floor}$ and for all other surfaces, $A1_{all\_other} = 0$. The fraction $A2_i$ describes the absorbed energy of surface 'i' at second "strike" that follows after first reflection (reflection from floor). For the floor, $A2_{floor-floor} = 0$, while for all other surfaces:

$$A2_{surfaces\_i-floor} = (1-\alpha_{floor}) \cdot F_{F,i} \cdot (\alpha_i + \tau_i) \tag{3.35}$$

where $F_{F,i}$ is the view factor of the floor to surface 'i', and τ is the transmittance coefficient that is 0 for all surfaces except the transparent ones (windows). The absorbed portion of the direct solar radiation that is transmitted by surface 'i' at third "strike" (after reflection from all surfaces) defines fraction $A3_i$:

$$A3_{surface\_i-all\_other\_surfaces} = (1-\alpha_{floor} - \sum_{k=1}^{n} A2_k) \cdot (Area_i / Area_{total}) \cdot (\alpha_i + \tau_i) \tag{3.36}$$

This fraction defines distribution of the remaining non-absorbed radiation $(1-\alpha_{floor}-\sum A2_k)$ over each surface, proportionally to its area-absorptance-transmittance product $(Area_i / Area_{total})\cdot(\alpha_i+\tau_i)$. The last fraction AR_i describes the distribution of all remaining (after third "strike") non-absorbed energy based on the distribution of fractions from the calculations for $A3_i$. This is given as:

$$AR_{surface\_i} = (1-\alpha_{floor} - \sum_{k=1}^{n} A2_k - \sum_{k=1}^{n} A3_k)\cdot(A3_i / \sum_{k=1}^{n} A3_k) \tag{3.37}$$

The conservation of energy requires that the sum of these four fractions for all surfaces is equal to 1. This is illustrated as:

$$\sum_{i}^{n}(A1_i + A2_i + A3_i + AR_i) = 1 \tag{3.38}$$

Distribution of diffuse solar radiation and shortwave radiation from lighting fixtures

Similar to the distribution of direct solar radiation, diffuse solar radiation is distributed in the room using diffuse solar fractions. The major difference from the distribution of direct radiation is that diffuse solar radiation is not directional. Therefore in the BES program, the window is modeled as the diffuse source of short wave radiation with an intensity that is equal to the transmitted diffuse solar radiation (refer to Figure 3.6). This means that the diffuse solar radiation is distributed according to the view factors between the window and surrounding surfaces.

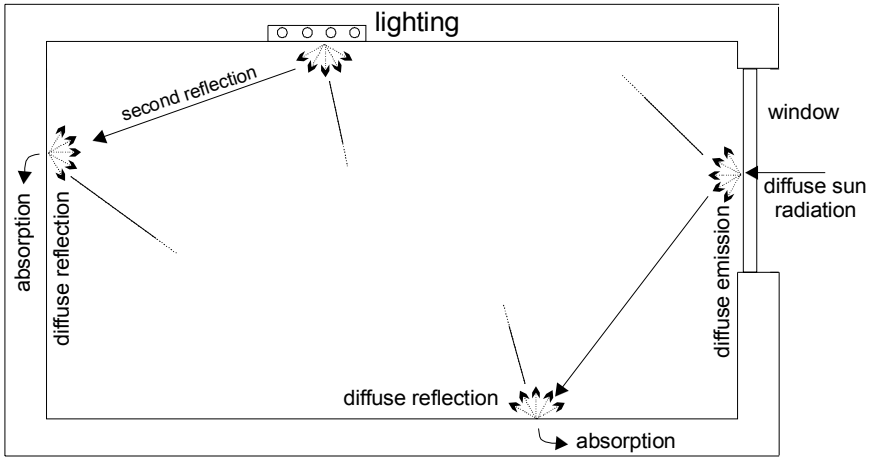

Figure 3.6 Distribution of diffuse solar radiation and shortwave radiation from lights on internal room surfaces

Similar to the distribution of direct solar radiation, three reflections and absorptions are considered for the distribution of diffuse solar radiation. The portion of transmitted diffuse solar radiation that is absorbed by surface 'i' is given as:

$$SF_i = A1_i + A2_i + A3_i + AR_i \tag{3.39}$$

Fraction $A1_i$ represents the absorbed energy diffusely emitted (transmitted) from the window surface, $A2_i$, the absorbed energy after first reflection, $A3_i$ after second reflection and the AR distribution of all the remaining non-absorbed energy.

Table 3.2 Fractions for diffuse radiation distributions

Fraction	Equation
$A1_i$	$(\alpha_i + \tau_i) \cdot F_{window,i}$
$A2_i$	$\sum_{p=1}^{n} \left[(1 - \alpha_p - \tau_p) \cdot F_{windows,p} \cdot F_{p,i} \right] \cdot (\alpha_i + \tau_i)$
$A3_i$	$(1 - \sum_{k=1}^{n} A1_k - \sum_{k=1}^{n} A2_k) \cdot (Area_i / Area_{total}) \cdot (\alpha_i + \tau_i)$
AR_i	$(1 - \sum_{k=1}^{n} A1_k - \sum_{k=1}^{n} A2_k - \sum_{k=1}^{n} A3_k) \cdot (A3_i / \sum_{k=1}^{n} A3_k)$

Because of the different distributions of incident transmitted radiation, the equations for the calculation of these fractions are different from the equations 3.34 - 3.37. These equations are presented in Table 3.2.

Building lighting systems are also sources of short wave radiation. Approximately 10 to 20% of electric power that lights use is radiated into the space as visible light (Kimura 1977, ASHRAE Fundamentals 2001). This portion of energy is not taken into account in the surface radiative heat exchange and, therefore, in the BES program, this energy is treated as a diffuse source of short wave radiation. Similar to the diffuse radiation transmitted through the window, this radiation from ceiling luminaries is distributed in the room using the same fractions as those in Table 3.2. The only difference is that instead of the window surface lighting surface is used (refer to Figure 3.6).

3.2.3 Energy Equations for Building Systems

In the following subsections energy equations for specific building components are described. These are equations (models) for: (1) energy balance for building elements, (2) energy balance for air, (3) energy equations for the window, (4) internal heat sources, and (5) energy equations for lamps.

Energy balance for building elements

For conductive heat transfer through building elements, the BES program assumes a one-dimensional heat flux. This assumption is justified by a considerably larger width and height (length) than thickness of building elements such as walls, floor, ceiling, and windows. This assumption is also justified by extensive successful use in other energy simulation programs described in Chapter 2. The one-dimensional convductive heat transfer is described with a partial differential equation as follows:

$$\frac{\partial(\rho c_p T)}{\partial \tau} = -\lambda\left(\frac{\partial^2 T}{\partial x^2}\right) + q_{source} \tag{3.40}$$

where the first term presents the transient term, second diffusion, and third internal source. the BES program uses a numerical discretization method to solve this equation. The solution method is described in Section 3.3.

Energy balance for air

BES program treats the room air as having homogeneous temperature (T_{air}) and other physical properties (density- ρ, specific capacity - c_p). The energy balance equation for room air is:

$$\frac{\partial(V_{room}\rho c_p T_{air})}{\partial \tau} = \sum_{i=1}^{n} h_i A_i \left(T_{S,i} - T_{air}\right) + \sum_{i=1}^{n} mc_{p\,i}\left(T_{ext\_air,i} - T_{air}\right) + \sum Q_{sources} \tag{3.41}$$

The left hand term of the equation is the transient term that describes the accumulated energy in the room air. The first term on the right hand side is the convective heat flux from the room surfaces. The second term is the heat transfer due to supplied air, infiltration, and/or inter-zone air mixing. The last term is the sum of convective heat sources in the room.

Energy equations for the window

Heat transfer through the window structure is a complex process. For multiple glazing windows, this process involves conduction, convection, and long wave radiation. Also, through window surfaces, short wave solar radiation gets into the room. This transmitted solar radiation is usually the major source of unsteady heat transfer in building elements. Therefore, a detailed window model is developed for the BES program.

A portion of the absorbed *(α),* transmitted *(τ),* and reflected *(ρ)* direct solar radiation that hits the window glazing is a function of the incident angle θ (refer to Figure 3.7). The parameters *α, τ,* and *ρ* are also functions of window glazing properties. However, *α, τ,* and *ρ* values for diffuse solar radiation only depends on surface glazing properties. Therefore, these coefficients are defined separately for direct and diffuse solar radiation.

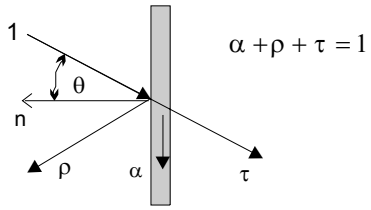

Figure 3.7 Transmission, absorption, and reflection on internal surfaces

For the calculation of the absorption *(α)* and transmission *(τ)* coefficients for diffuse *(I_{dif})* and direct *(I_{DIR})* solar radiation, the window model uses following expressions:

$$\tau_{DIR} = \sum_{i=0}^{5} ts_i \cos^i \theta\,, \quad \tau_{dif} = 2\sum_{i=0}^{5} ts_i /(i+2), \quad \alpha_{DIR} = \sum_{i=0}^{5} as_i \cos^i \theta\,, \quad \alpha_{dif} = 2\sum_{i=0}^{5} as_i /(i+2) \qquad (3.42)$$

The coefficients ts_i and as_i are constants which define glazing properties. In the BES program the coefficients for "one-eighth-inch, clear double-strength glass" (ASHRAE 2001) are used as the default.

For the double glazed window (refer to Figure 3.8), the overall transitivity and absorbtivity for each layer needs to be calculated. Figure 3.8-a shows the multiple repetitions of transmission, absorption and reflection. These repetitions can be expressed as a sum of an infinite series to calculate the overall transitivity (Kimura 1977) as follows:

$$\tau_{12} = \tau_1\tau_2 + \tau_1\tau_2\rho_1\rho_2 + \tau_1\tau_2\rho_1^2\rho_2^2 + \ldots = \frac{\tau_1\tau_2}{1-\rho_1\rho_2} \qquad (3.43)$$

The same approach is used for the calculation of the overall absorption coefficient of external ($\alpha_{1\_overall}$) and internal ($\alpha_{2\_overall}$) glazing units as follows:

$$\alpha_{1\_overall} = \alpha_1\left(1+\frac{\tau_1\rho_2}{1-\rho_1\rho_2}\right), \quad \alpha_{2\_overall} = \frac{\tau_1\alpha_2}{1-\rho_1\rho_2} \tag{3.44}$$

The conductive heat flux for a single glazed window is described with equation (3.40), where the absorbed solar radiation presents the source term. For the double glazed window, the calculation of conductive heat flux includes conduction through glazing units, convection in windows cavity and long wave radiation in-between glazing surfaces (Figure 3.8).

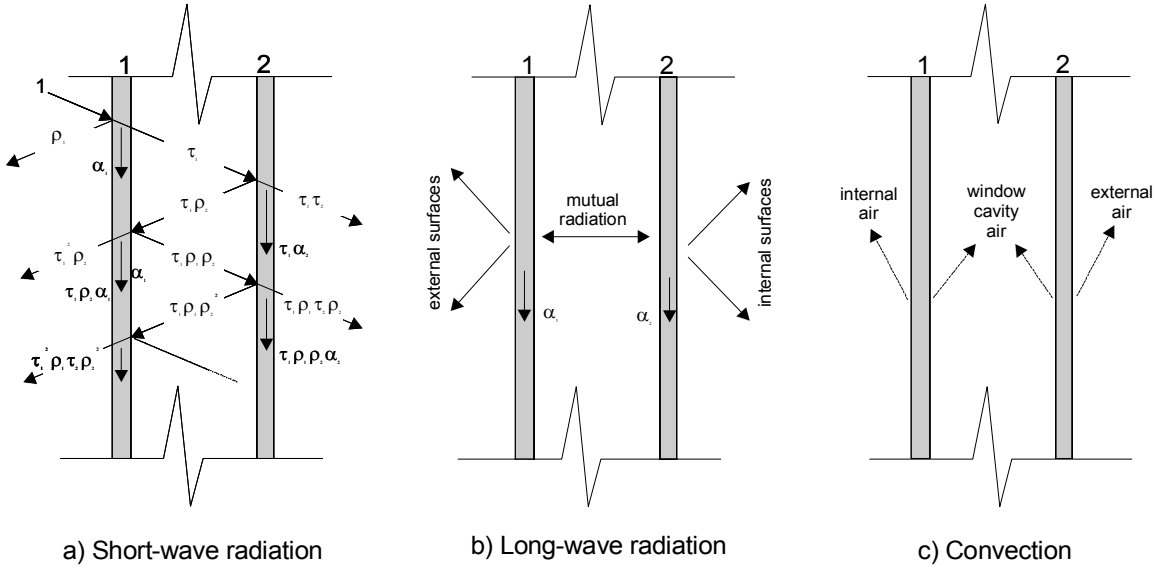

Figure 3.8 Heat transfer for a double glazed window implemented into the BES program

To predict the temperature of glazing surfaces, air-cavity convection and long-wave radiation heat fluxes need to be calculated. Radiative heat flux is calculated using a linearized radiation convection coefficient (Equation 3.32). The convective heat flux is calculated by convective model for Insulated Glazing Units (IGU) developed by Yin (Curcija 1992) as follows:

$$q_{IGU} = Nu\frac{k_{cavity\_air}}{l_{IGU}}\Delta t \tag{3.45}$$

The Nusselt number *(Nu)* is calculated based on the Grashof number *(Gr),* window cavity height (h), and thickness of the cavity (l_{IGU}) as follows:

$$Nu = 0.21\cdot Gr^{0.269}(h/l_{IGU})^{-0.131} \tag{3.46}$$

Internal heat sources

In the BES program, internal heat sources that are not part of the room enclosure are defined as elements with heat flux at their surfaces. For example, occupants, computers, machines, and lighting devices are internal heart sources which release energy by convection and radiation. Precise calculation of convective and radiative heat flux based on the surface temperature of the heat source is impractical because the exact position and surface temperature of these sources is unknown. Therefore, the convection/radiation portions for internal heat sources are input data in the BES program. Data for these portions that are based on experimental measurements can be found in existing literature (ASHRAE 2001, Kimura 1977).

The convective parts of internal heat sources ($Q_{source\_convection}$) directly affect the room air temperature and, therefore, it is the source term in equation (3.41). The radiative part of internal heat sources ($Q_{source\_radiation}$) is distributed over each room surface proportionally to its area-absorptance product ($Area_i \cdot \alpha_i / \sum(Area_i \cdot \alpha_i)$) as follows:

$$q_{source\ i} = 1/Area_i \cdot \left[Area_i \cdot \alpha_i / \sum(Area_i \cdot \alpha_i)\right] \cdot Q_{source\_radiation} \tag{3.47}$$

Energy equations for lamps

Besides transmitted solar radiation, lamps are among the largest heat sources in a typical building. Therefore, several energy balance models for lamps were developed and implemented into the BES program. The first model is used for lamps with covers that are integrated into the room surfaces. With these lamps, the total power *(P_{lamp})* is divided into radiative short-wave ($Q_{short\text{-}wave}$), long-wave, and convective heat flux. The distribution of short-wave radiative heat flux that is transmitted though the lamp's cover is given in Table 3.2. The remaining energy

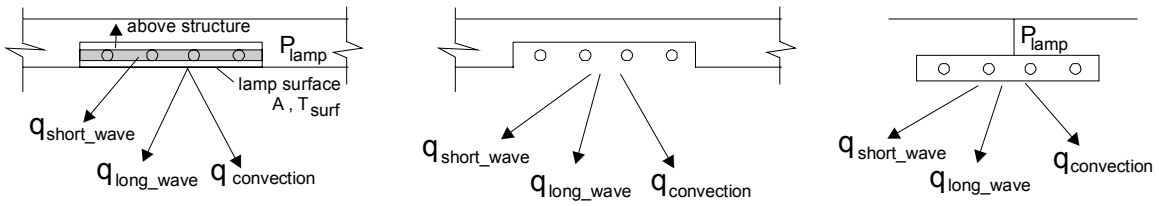

(a) (b) (c)

Figure 3.9 Different models for lamp heat flow for (a) lamps with cover, (b) lamps without cover, and (c) free hanging lamps

(P_{lamp}-$Q_{short\text{-}wave}$) is added to the lamp layer that represents lamp tubes as a heat source term (Figure 3.9a). Based on the ceiling structure above the lamp and conditions on the lamp surface, the program calculates the distribution of this remaining energy towards the surface or the plenum above the lamp as one-dimensional conduction. In this way, the temperature of the lamp surface is obtained.

For lamps integrated into the surfaces without covers, another model can be used (Figure 3.9b). This model uses radiative short-wave, long-wave, and convective heat flux as input data. Convective heat flux is added to the air equation as a source term, while short-wave and long-wave radiative heat fluxes are distributed at surfaces using a fraction method similar to the solar fraction method described in the previous section (refer to Table 3.2). This model should be used carefully because the program does not calculate the surface temperature at these lamp surfaces. This means that there is no "active" convective heat exchange with the air. The convection flux is one-directional (from surface to air) and constant regardless of the air temperature. The same is applicable to long-wave radiation towards the surrounding surfaces.

The third model is for lamps that are not part of the room surfaces (Figure 3.9c). These lamps behave like internal heat sources and the model is described in the previous section (refer to Equation 3.47).

3.2.4 Inter-zone Airflow and Infiltration

In the following two subsections short discussions about (1) inter-zone airflow and (2) infiltration models for ES programs are provided.

Inter-zone airflow

The current version of the BES program can simulate two zones. The first zone is the room and the second zone is the plenum above the room. In the case of the exhaust through the un-ducted plenum, all the air from the room passes through the plenum. In the case of ducted exhaust, the inter-zone airflow is defined by the user. More detailed inter-zone models that consider airflow through the whole building, such as CONTAM (Dols and Walton 2003) or COMIS (Feustel 1998), can be coupled with the BES program. However, the current version of the BES program is not coupled with an inter-zone airflow program because it considers only two zones.

Infiltration

The infiltration of outdoor air depends on the geometry of the whole building and on the inter-zone airflow. Therefore, the infiltration in large buildings should be calculated using multu-zone airflow programs. Because the BES program considers only one room with or without plenum, the current version of the program offers the choice to the user to define the constant infiltration rate or to select a simple model for infiltration in residential buildings (ASHRAE 2001).

This infiltration model considers buildings as a single zone and uses a superposition of wind and stack effects. The infiltration mass flow rate is given as:

$$m = \rho_{air} \frac{A_L}{1000} \sqrt{C_S \Delta t + C_w U^2} \tag{3.48}$$

where A_L is the effective air leakage area in cm^2, C_s is stack coefficient, Δt is temperature difference between the room and outdoor air, C_w is the wind coefficient, and U is the wind speed. The stack and wind coefficients are provided by the user based on building height and shelter class information (ASHRAE 2001). For wind speeds and external temperatures, the BES program uses meteorological data for each time step, while effective leakage area is a property of the openings and it is defined as input data.

3.2.5 HVAC Models

The current version of the BES program has models for several HVAC configurations. The primary purpose of integrated HVAC models is to demonstrate the performance of developed methods for simultaneous load calculation and HVAC performance simulation. The selection of integrated HVAC models is performed in such a way that all characteristic types of control systems are present:

1) HVAC systems that control the room temperature, using the flow rate of supply air (V_{supply}), are represented by the Variable Air Volume (VAV) system for a single zone.
2) HVAC systems that use variable supply air temperature (T_{supply}) for control are represented by the Constant Air Volume (CAV) system.
3) Systems that use HVAC device surface temperature ($T_{surface}$) to control the environment temperature are presented by the radiant panel system.

4) Pure convective HVAC systems, which have negligible radiative heat exchange with room surfaces and exchange energy with air directly by convection ($Q_{convective}$), are represented by fan-coil and baseboard heater systems.

Surface temperature ($T_{surface}$) and convective heat flux ($Q_{convective}$) of HVAC device are regulated by temperature of fluid that circulates through the device. However, for linking of the HVAC model with the building load calculation model, $T_{surface}$ and $Q_{convective}$ are used. Details about this linking are given in Section 3.4. The circulating-fluid temperature that is needed for providing certain values of $T_{surface}$ or $Q_{convective}$ is calculated in HVAC models.

Models of the HVAC system implemented into the BES program were developed for steady state condition. Energy accumulation in HVAC components is not considered because it is significantly smaller than energy accumulation in the building structure. The implemented HVAC components are: radiant panels, fan coils, baseboard heaters and elements of simple air handling units.

All-Air systems

The configurations of the Air Handling Unit (AHU) for VAV and CAV systems are the same (Figure 3.10). The reason is that only single zones are analyzed and, therefore, there are neither zone reheaters nor VAV boxes. The only difference lies in the control parameter. For VAV, it is the supply air volume flow rate, while for CAV, it is the supply air temperature.

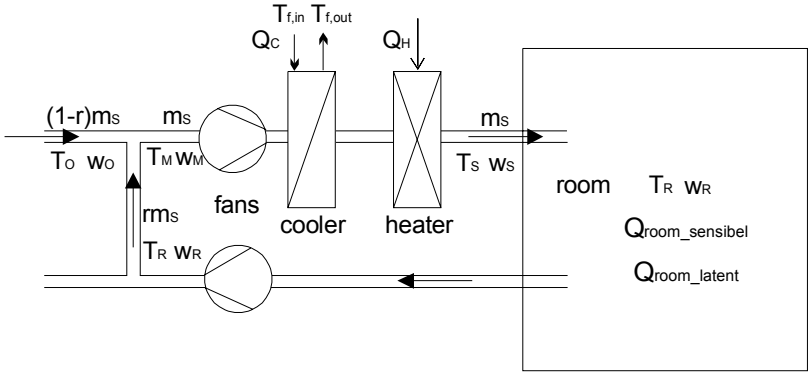

Figure 3.10 Schematic for a model of a simple air handling unit

The VAV and CAV are modeled with equations that describe energy, air-mass, and air-humidity balances for each component of the air handling units. In this model, the cooling load is

divided into a sensible ($Q_{room\_sensible}$) and latent part (Q_{room_latent}). The energy balance for the room is given as:

$$Q_{room\_sensible} = m_S c_p \left(T_R - T_S\right) \tag{3.49}$$

where m_S is the supply air mass flow rate c_p - specific capacity for air, T_R is the room temperature and T_S is the supply air temperature. The air-humidity balance for room is given as:

$$Q_{room\_latent} = m_S \left(w_R - w_S\right) \cdot i_{phase\_change} \tag{3.50}$$

where w_R and w_S are room and supply humidity ratios respectively and i_{phase_change} is the energy for phase change of water into vapor. The energy balance for the mixing box is:

$$T_M = (1-r) \cdot T_O + r \cdot T_R \tag{3.51}$$

where *'r'* is the recirculated air fraction, T_O is the outdoor air temperature, and T_M is the temperature of the air after the mixing box. The air-humidity balance for the mixing box is:

$$w_M = (1-r) \cdot w_O + r \cdot w_R \tag{3.52}$$

where w_O is the outdoor air humidity ratio and w_M is the humidity ratio after the mixing box. The energy balance for the heating coil is:

$$Q_H = m_S c_p (T_S - T_M) \tag{3.53}$$

The energy balance for the cooling coil is:

$$Q_C = m_S c_p (T_S - T_M) + m_S \left(w_S - w_M\right) \cdot i_{phase\_change} \tag{3.54}$$

For the VAV system, supply air temperature (T_S) is provided as input data while sensible cooling/heating load in the room ($Q_{room\_sensible}$) is calculated by equations that define the energy balance in the room for certain air temperatures (T_R). The supply air flow rate (m_S) is calculated by equation (3.49). For a situation whereby cooling is needed, the humidity ratio of supply air

(w_S) is calculated based on the given Q_{room_latent} and w_R (equation 3.50). With knowledge of values T_S, T_R, m_S, w_S, w_R, and r, the energy of the cooling coil (Q_C) or heating coil (Q_H) is calculated using equations (3.49-3.54).

For the CAV system, the supply air flow rate (m_S) is provided as input data and supply air temperature (T_S) is calculated based on the cooling/heating load in the room ($Q_{room\_sensible}$). For the situation in which cooling is needed, the humidity ratio of supply air (w_S) is calculated from equation (3.50). Then Q_C or Q_H are calculated in the same way as for the VAV system.

To enable coupling of this air handling unit model with the chiller model, the cooling coil needs to be modeled. This coupling requires a relationship between the supply temperature (T_{f_in}) and return temperature (T_{f_out}) of the circulating fluid for a given mass flow rate (m_f) of this fluid thorough the cooling coil (refer to Figure 3.10). The current model uses cooling coil effectiveness (E) to describe this relationship. This is given as follows:

$$T_{f\_out} = T_{f\_in} + (m_S c_p)/(m_f c_{p,f}) \cdot E \cdot (T_M - T_{f\_in}) \tag{3.55}$$

Cooling coil effectiveness (E) is a function of T_M,,w_M, T_{f_in}, $m_s c_p$ and $m_f c_{p,f}$. In addition, it depends on the cooling coil geometry and type of circulating fluid (water or refrigerant). In the current version of the AHU model, E is not modeled but is provided by the user as an input value.

Radiant panel system

The radiant panel is a system from which 35-65% of the total flux is exchanged by radiation with room surfaces (Novoselac and Srebric 2001). Therefore, it is crucial to consider this system as a HVAC device with $T_{surface}$ as a control parameter. Furthermore, the surface temperature is a function of the supply temperature and the volume flow rate of the fluid (water) in radiant panel tubes (refer to Figure 3.11). The radiant panel system is usually combined with the air supply system. Because the air supply system has a constant volume flow rate and supply air temperature, it is included in the air balance equation (3.41) in the same way as inter-zone air flow described in Section 3.2.4.

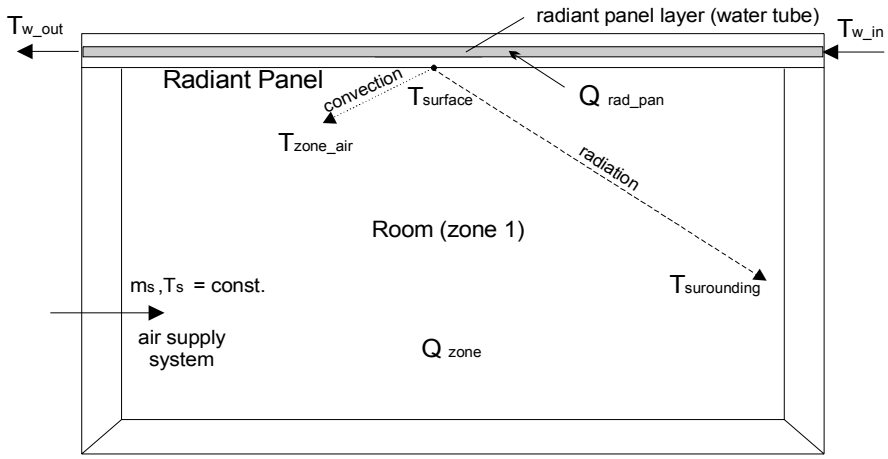

Figure 3.11 Schematic for a radiant panel heat transfer model

When modeling radiant panels in the BES program, the model for a solar collector is adapted (Duffie and Beckman 1991). The total cooling/heating load in the room (Q_{zone}) is divided into energy extracted/added by the air system (Q_{air}) and by the radiant panel (Q_{rad_pan}):

$$Q_{zone} = Q_{rad\_pan} + Q_{air} \tag{3.56}$$

The energy extracted/added by the radiant panel is the sum of the radiative and convective parts as follows:

$$Q_{rad\_pan} = Q_{radiation} + Q_{conv} \tag{3.57}$$

Also, the radiant panel energy is given as:

$$Q_{rad\_pan} = mc_{pw}(T_{w\_out} - T_{w\_in}) \tag{3.58}$$

where m is the water flow rate, T_{w_in} and T_{w_out} are temperatures of the water at the inlet and outlet of the radiant panel. The change of water temperature in radiant panel is given as:

$$\frac{(T_{w\_in} - T_{zone\_air})Ah_{room} + (T_{w\_in} - T_{above\_air})Au_{above} - Q_{radiation}}{(T_{w\_out} - T_{zone\_air})Ah_{room} + (T_{w\_out} - T_{above\_air})Au_{above} - Q_{radiation}} = \exp\left(\frac{Au_{total}}{mc_{pw}}F'\right) \tag{3.59}$$

where A is the panel area, h_{rom} is the convection coefficient on room side, u_{above} is the loss coefficient to the air above the radiant panel (T_{above_air}), and u_{total} is total loss coefficient which

encompasses the convection on the room side and the loss above the radiant panel. It is calculated as $u_{total} = h_{room} + c \cdot u_{above}$, where c is a correction for unequal T_{above_air} and T_{zone_air}. It can be approximated as $c = (T_{w\_in} + T_{w\_out} - 2 \cdot T_{above\_air}) / (T_{w\_in} + T_{w\_out} - 2 \cdot T_{zone\_air})$. The coefficient F' is the efficiency factor of radiant panel (collector) defined by geometry and construction of the radiant panel (Duffie and Beckman 1991).

The system of equations (3.56-3.59) is a closed system which enables the calculation of water inlet (T_{w_in}) and outlet temperature (T_{w_out}) using known values of $Q_{radiation}$ and Q_{conv}. Heat fluxes $Q_{radiation}$ and Q_{conv} are solved by the energy balance equations of the room together with room temperature (T_{zone_air}) and temperature of the air above the panel (T_{above_air}). For a given mass flow rate of water '*m'*, this model provides the relationship between the inlet T_{w_in} and outlet T_{w_out} water temperatures. This enables further coupling of the radiant panel system with the chiller model.

Pure convective system

The heating load (Q_{room}) for pure convective devices such as baseboard heaters or fan coil systems in a heating regime is equal to the load of the heating plant (Q_H) that is reduced by the amount of energy lost in the pipe system. This is defined by the heating distribution system efficiency ($\eta_{distribut\_system}$) as follows:

$$Q_{room} = Q_H \cdot \eta_{distribut\_system} \tag{3.60}$$

For fan coil systems in cooling regime, condensation may appear on the fan-coil heat exchanger. This primarily depends on surface temperature of the fan coil heat exchanger ($T_{FC\_surface}$) and room dew-point temperature (T_{dp}). In the model implemented in the BES program, it is assumed that $T_{FC\_surface} > T_{dp}$. This means that the water supply temperature for the fan coil is controlled in order to avoid condensation. Therefore, it follows that:

$$Q_{room} = mc_p(T_{w\_out} - T_{w\_in}) \tag{3.61}$$

where m is the water flow rate, T_{w_in} is the inlet and T_{w_out} the outlet water temperatures. The relationship between inlet T_{w_in} and outlet T_{w_out} water temperatures enables further coupling of the fan coil system with the chiller.

3.3 Numerical Models for ES Equations

The partial differential equation (3.40) has an analytical solution only for simple geometry, and this solution is highly non-linear. Analytical solution is, therefore, impractical for the calculation of energy flows in a complex system such as a building zone. Hence, this equation needs to be discretized and solved numerically.

3.3.1 Discretization

Discretization of building elements that form a closed space is presented in Figure 3.12. Each surface of the element is represented by internal and external surface nodes. All internal surface nodes are connected to one another by radiation, to the air node by convection, and to the adjacent element-inner node by conduction. The elements' inner nodes are connected to their neighboring nodes by conduction. External surface nodes are connected to adjacent element-inner node by conduction, to external surfaces by radiation, and to external air by convection.

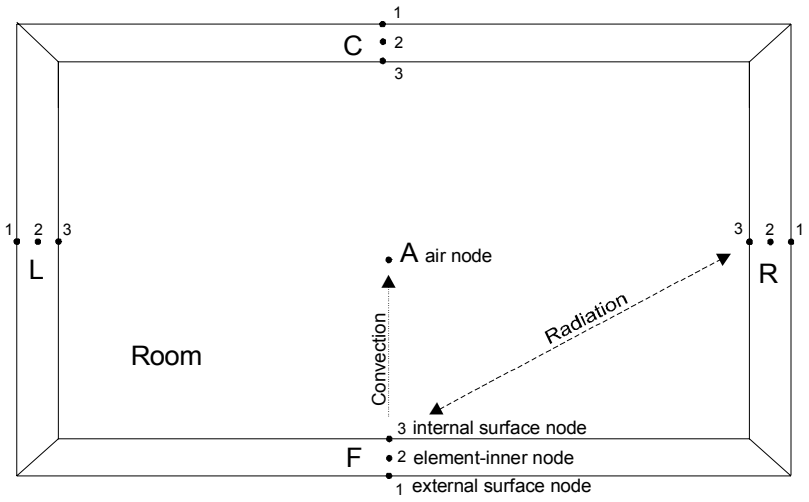

Figure 3.12 Discretization of a building zone in the BES program

Discretization of building element is based on the finite volume method (Patankar 1980). For complex building elements that are built from several homogeneous layers, such as an external wall as presented in Figure 3.13, a certain number of nodes is distributed in each homogeneous layer. For each layer, the user defines the number of nodes that are uniformly distributed in that layer.

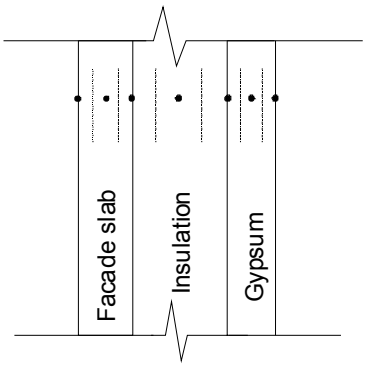

Figure 3.13 Discretization of a non-homogeneous zone element in the BES program

Inner node

Figure 3.14 presents three inner nodes for the building element with unit width and height (length). The dotted lines represent the faces of the control volume for the central node "I". The control volume of the element is $\Delta x_I \times 1 \times 1$. Integration of equation (3.40) over this control volume and over the time interval from τ to $\tau+\Delta\tau$ gives the following expression:

$$\rho_I c_{pI} \int_{I-\Delta X_I/2}^{I+\Delta X_I/2} \int_{\tau}^{\tau+\Delta\tau} \frac{\partial T}{\partial \tau} d\tau dx = \int_{\tau}^{\tau+\Delta\tau} \int_{I-\Delta X_I/2}^{I+\Delta X_I/2} k\left(\frac{\partial^2 T}{\partial x^2}\right) dx d\tau + \int_{\tau}^{\tau+\Delta\tau} \int_{I-\Delta X_I/2}^{I+\Delta X_I/2} \dot{q}' dx d\tau \tag{3.61}$$

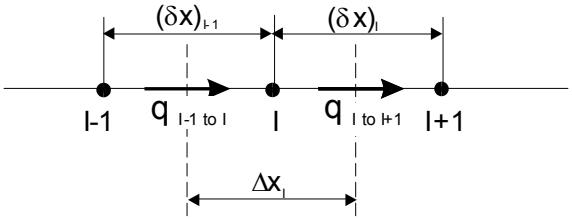

Figure 3.14 Energy balance of an element-inner node

Assuming that the temperature is constant over the control volume, the transient term on the left-hand-side of the equation is approximated as:

$$\int_{I-\Delta X_I/2}^{I+\Delta X_I/2} \int_{\tau}^{\tau+\Delta\tau} \frac{\partial T}{\partial \tau} d\tau dx = \Delta x_I \left(T_I^{\tau+\Delta\tau} - T_I^{\tau}\right) \tag{3.62}$$

Integration over the control volume of the diffusion term on right-hand-side of the equation gives the following expression:

$$\int_{I-\Delta X_I/2}^{I+\Delta X_I/2} k\left(\frac{\partial^2 T}{\partial x^2}\right) = \int_{I-\Delta X_I/2}^{I+\Delta X_I/2} \frac{\partial}{\partial x}\left(k\frac{\partial T}{\partial x}\right) = \left(k\frac{dT}{dx}\right)_{I+\Delta X_I/2} - \left(k\frac{dT}{dx}\right)_{I-\Delta X_I/2} = \frac{k_I\left(T_{I+1}-T_i\right)}{\left(\delta x\right)_I} - \frac{k_{I-1}\left(T_I-T_{I-1}\right)}{\left(\delta x\right)_{I-1}} \quad (3.63)$$

where "I-1" and "I+1" are neighboring nodes (Figure 3.14). Here, it is assumed that there is a linear profile of temperature in-between two nodes. Integration of the diffusion term over the control volume and over the time interval, gives the following expression:

$$\int_{\tau}^{\tau+\Delta\tau}\int_{I-\Delta X_I/2}^{I+\Delta X_I/2} k\left(\frac{\partial^2 T}{\partial x^2}\right)dx\,d\tau = \int_{\tau}^{\tau+\Delta\tau}\left[\frac{k_I\left(T_{I+1}-T_I\right)}{\left(\delta x\right)_I} - \frac{k_{I-1}\left(T_I-T_{I-1}\right)}{\left(\delta x\right)_{I-1}}\right]d\tau \quad (3.64)$$

Substituting (3.62) and (3.64) into (3.61) and integrating the source term gives the following expression:

$$\Delta x_I\left(T_I^{\tau+\Delta\tau}-T_I^{\tau}\right) = \frac{1}{\rho_I c_I}\int_{\tau}^{\tau+\Delta\tau}\left[\frac{k_I\left(T_{I+1}-T_I\right)}{\left(\delta x\right)_I} - \frac{k_{I-1}\left(T_I-T_{I-1}\right)}{\left(\delta x\right)_{I-1}}\right]d\tau + q\Delta x_I \quad (3.65)$$

Depending on time step values that are used for T_I, T_{I-1}, and T_{I+1} on right-hand-side of the equation, explicit (values for time step τ), implicit (values for time step $\tau+\Delta\tau$), or the Crank-Nicolson (values for in-between time step) scheme is applied. In the BES program, the general method is used. This is given as follows:

$$\int_{\tau}^{\tau+\Delta\tau} T_I\,dt = \left[f\cdot T_I^{\tau+\Delta\tau} + \left(1-f\right)\cdot T_I^{\tau}\right]\Delta\tau \quad (3.66)$$

With this method, the user can define the value f which determines the method. The default value in the BES program is f=1 which is the fully implicit method. Using equation (3.66), equation (3.65) becomes:

$$\begin{aligned}\frac{\rho_I c_I \Delta x_I}{\Delta\tau}\left(T_I^{\tau+\Delta\tau}-T_I^{\tau}\right) = {} & f\left[\frac{k_I\left(T_{I+1}^{\tau+\Delta\tau}-T_I^{\tau+\Delta\tau}\right)}{\left(\delta x\right)_I} - \frac{k_{I-1}\left(T_I^{\tau+\Delta\tau}-T_{I-1}^{\tau+\Delta\tau}\right)}{\left(\delta x\right)_{I-1}} + q^{\tau+\Delta\tau}\right] + \\ & \left(1-f\right)\left[\frac{k_I\left(T_{I+1}^{\tau}-T_I^{\tau}\right)}{\left(\delta x\right)_I} - \frac{k_{I-1}\left(T_I^{\tau}-T_{I-1}^{\tau}\right)}{\left(\delta x\right)_{I-1}} + q^{\tau}\right]\end{aligned} \quad (3.67)$$

By grouping elements according the time step and space, the next equation is derived:

$$T_I^{\tau+\Delta\tau}\left[\frac{\rho_I c_I}{\Delta\tau}+f\frac{k_{I-1}}{(\delta x)_{I-1}\Delta x_I}+f\frac{k_I}{(\delta x)_I\Delta x_I}\right]-T_{I-1}^{\tau+\Delta\tau}\left[f\frac{k_{I-1}}{(\delta x)_{I-1}\Delta x_I}\right]-T_{I+1}^{\tau+\Delta\tau}\left[f\frac{k_{I+1}}{(\delta x)_{I+1}\Delta x_I}\right]-f\,q^{\tau+\Delta\tau}=$$
$$T_I^{\tau}\left[\frac{\rho_I c_I}{\Delta\tau}-(1-f)\frac{k_{I-1}}{(\delta x)_{I-1}\Delta x_I}-(1-f)\frac{k_I}{(\delta x)_I\Delta x_I}\right]+T_{I-1}^{\tau}\left[(1-f)\frac{k_{I-1}}{(\delta x)_{I-1}\Delta x_I}\right]+T_{I+1}^{\tau}\left[(1-f)\frac{k_{I+1}}{(\delta x)_{I+1}\Delta x_I}\right]+(1-f)q^{\tau} \quad (3.68)$$

Temperatures from the previous time step (τ) are known, while temperatures for the considered time step (τ+Δτ) are unknown. Therefore, these system need to be solved simultaneously. The general equation is obtained for each inner node in the building elements:

$$A\cdot T_{I-1}^{\tau+\Delta\tau}+B\cdot T_I^{\tau+\Delta\tau}+C\cdot T_{I+1}^{\tau+\Delta\tau}=F \quad (3.69)$$

The equation coefficients A, B, C, and F are given in Appendix C.

Surface node

Figure 3.15 shows the typical surface node. Surface node "I" is connected to the adjacent element-inner node "I-1" by convection, to external surfaces "S_I" by radiation, and to the air node "A" by convection. Also, node "I" receives outer radiative heat fluxes *(q_{or})* such as solar radiation.

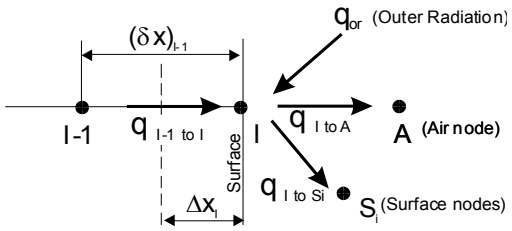

Figure 3.15 Energy balance for an element's surface node

Using equation (3.68) for the inner grid node and replacing the conductive flux from node "I+1" to "I" ($k_I(T_{I+1}-T_I)/(\delta x)_I$) with the sum of: convective ($h_C(T_A-T_I)$), radiative ($\sum_{i=1}^{n}h_R(T_{Si}-T_I)$), and outer (q_{or}) heat fluxes, the equation for the surface node is obtained. This is given as follows:

$$T_I^{\tau+\Delta\tau}\left[\frac{\rho_I c_I}{\Delta\tau}+f\frac{k_{I-1}}{(\delta x)_{I-1}\Delta x_I}+f\frac{h_C^{\tau+\Delta\tau}}{\Delta x_I}+f\frac{\sum_{i=1}^{n}h_{R,i}^{\tau+\Delta\tau}}{\Delta x_I}\right]-T_{I-1}^{\tau+\Delta\tau}\left[f\frac{k_{I-1}}{(\delta x)_{I-1}\Delta x_I}\right]-T_A^{\tau+\Delta\tau}\left[f\frac{h_C^{\tau+\Delta\tau}}{\Delta x_I}\right]-$$
$$f\frac{\sum_{i=1}^{n}h_{R,i}^{\tau+\Delta\tau}\cdot T_{Si}^{\tau+\Delta\tau}}{\Delta x_I}-f\,q_{or}^{\tau+\Delta\tau}=T_I^{\tau}\left[\frac{\rho_I c_I}{\Delta\tau}-(1-f)\frac{k_{I-1}}{(\delta x)_{I-1}\Delta x_I}-(1-f)\frac{h_C^{\tau}}{\Delta x_I}-(1-f)\frac{\sum_{i=1}^{n}h_{R,i}^{\tau}}{\Delta x_I}\right]+ \tag{3.70}$$
$$T_{I-1}^{\tau}\left[(1-f)\frac{k_{I-1}}{(\delta x)_{I-1}\Delta x_I}\right]+T_A^{\tau}\left[(1-f)\frac{h_C^{\tau}}{\Delta x_I}\right]+(1-f)\frac{\sum_{i=1}^{n}h_{R,i}^{\tau}\cdot T_{S,i}^{\tau}}{\Delta x_I}+(1-f)q_{or}^{\tau}$$

This equation can be written in a general form for each internal surface node as:

$$A\cdot T_{I-1}^{\tau+\Delta\tau}+B\cdot T_I^{\tau+\Delta\tau}+R\cdot T_A^{\tau+\Delta\tau}+\sum_{i=1}^{n}S\cdot T_{S,i}^{\tau+\Delta\tau}=F \tag{3.71}$$

For external surface nodes, the general equation is written in a different form because these surfaces exchange the energy with elements that have known temperatures (or the temperatures are calculated based on input data for a considered time step). These elements are external air, sky, and ground, or soil for surfaces in contact with the ground. Because the temperatures of these elementals are independent of surface temperature (T_I), they are moved to the right-hand-side of the equation to be a part of the free coefficient (F). The general form of equation for external surface is given as:

$$B\cdot T_I^{\tau+\Delta\tau}+C\cdot T_{I+1}^{\tau+\Delta\tau}=F \tag{3.72}$$

Coefficients *A, B, C, R, S*, and *F* for internal and external surface nodes are given in Appendix C.

Air node

Room air in the BES program is represented with a single node (refer to Figure 3.12). This air node is connected to each surface node by convection, to external air by the mass flow rate of infiltration air, and to the HVAC supply system by mass flow rate of supply air. Also, air node "A" receives energy from other internal heat sources (Q_{is}), which includes the convective source from occupants, for instance.

Integrating the energy conservation equation for air (3.41) over the room volume (V_{room}) and over the time interval $\Delta\tau$, the following equation is obtained:

$$T_A^{\tau+\Delta\tau}\left[\frac{\rho_I c_{p,I}}{\Delta\tau}+f\frac{\sum_{i=1}^{n}(h_C^{\tau+\Delta\tau}A_i)}{V_{room}}+f\frac{\sum_{j=1}^{m}mc_{p,j}^{\tau+\Delta\tau}}{V_{room}}\right]-f\frac{\sum_{i=1}^{n}(h_C^{\tau+\Delta\tau}A_i\cdot T_{S,i}^{\tau+\Delta\tau})}{V_{room}}-$$
$$f\frac{\sum_{j=1}^{m}(mc_{p,j}^{\tau+\Delta\tau}\cdot T_{E,j}^{\tau+\Delta\tau})}{V_{room}}-f\frac{Q_{is}^{\tau+\Delta\tau}}{V_{room}}=T_A^{\tau}\left[\frac{\rho_I c_{p,I}}{\Delta\tau}-(1-f)\frac{\sum_{i=1}^{n}(h_C^{\tau}A_i)}{V_{room}}-(1-f)\frac{\sum_{j=1}^{m}mc_{p,j}^{\tau}}{V_{room}}\right]+ \tag{3.73}$$
$$(1-f)\frac{\sum_{i=1}^{n}(h_C^{\tau}A_i\cdot T_{S,i}^{\tau})}{V_{room}}+(1-f)\frac{\sum_{j=1}^{m}(mc_{p,j}^{\tau}\cdot T_{E,j}^{\tau})}{V_{room}}+(1-f)\frac{Q_{is}^{\tau}}{V_{room}}$$

The general form of air node equation is given as:

$$D\cdot T_A^{\tau+\Delta\tau}+\sum_{i=1}^{n}E\cdot T_{S,i}^{\tau+\Delta\tau}+\sum_{j=1}^{m}I\cdot T_{E,j}^{\tau+\Delta\tau}=F \tag{3.74}$$

where coefficients *D, E, I*, and *F* are given in Appendix C.

3.3.2 System of Equations

The energy conservation equations for each element-inner (equations 3.68) and surface nodes (equations 3.70) together with the air node (equation 3.73) form a system of linear equations. In the case of a fully implicit scheme, this system solves temperatures of all building elements for a time step ($\tau+\Delta\tau$) based on boundary conditions for that time step, and temperatures of all building elements for the previous time step (τ). In the case of the Crank-Nicolson scheme (*f=0.5*), boundary conditions from the previous time step are also used. With the explicit scheme, solving the simultaneous equations is unnecessary because the temperature distribution for the considered time step ($\tau+\Delta\tau$) is explicitly obtainable from the temperatures of previous time step. In the BES program, an explicit scheme is possible but completely impractical because of the numerical stability problem. To obtain a numerically stable system with an explicit scheme (Patankar 1980), a selected time step ($\Delta\tau$) should satisfy:

$$\Delta\tau < \rho c_p(\Delta x)^2/(2k) \tag{3.75}$$

for each node of the building zone. This means that for conductivity (k), density (ρ) and specific capacity (c_p) of building materials and typical discretization, where Δx is in range of 0.001 to 0.1 m, the selected time step ($\Delta\tau$) should be less than a second. Therefore, in the BES program the system of equations is solved simultaneously (using implicit schemes).

Energy flow by heat transfer mechanisms such as radiation, convection, and inter-zone air flow are described by non-linear equations. Linearization of these phenomena is described in Section 3.2.2. In the solution procedure, radiative heat exchange coefficients (h_r) are calculated using the temperature distribution from the previous time step. Surface convection coefficient (h) or inter-zone air mass flow (m_i) are obtained in the same manner. Because these coefficients are based on temperature values from the previous time step, it is very important to have a realistic initial temperature distribution. This problem is solved by using a "warming" calculation procedure which defines the initial temperatures. This "warming" procedure is described in detail in Chapter 6.

The equation's right-hand-side coefficient (F) is updated for each time step based on the calculated temperature distribution in the previous time step. Also, for surface nodes, this term defines the "outer" radiative heat flux (q_{or}) which is completely independent of the surface temperature. For internal surfaces, the outer radiative heat flux contains absorbed direct and diffuse solar radiation, lighting short wave radiation, and radiation from internal sources. For external surfaces, "outer" radiative heat flux contains absorbed diffuse and direct solar radiation. For the air node, coefficient (F) contains a term which defines internal convective heat flux (Q_{is}) which is also independent of temperature distribution. These heat fluxes are also updated for each calculation step based on input data such as weather condition or the power and the working period of a lighting system.

For all surface nodes, the coefficients A, R, and S in equation (3.71) and C in equation (3.72) are updated for each time step because of the change of the radiative heat exchange coefficients (h_r) and surface convection coefficient (h) at internal and external surfaces. For the same reason, all air node coefficients (D, E, I, and F) are updated in each time step. Only for internal nodes (equation 3.69), coefficients A, B, and C do not change during the calculation procedure because temperature independent conduction coefficients (k) are assumed.

The system of linear equations (3.69, 3.71, 3.72, and 3.74) is organized into a matrix called a zone-matrix. To explain the structure of this zone-matrix, a simplified two-dimensional model of a room presented in Figure 3.16 is used. This model has 13 nodes. In this example three nodes are used for each zone element (F-floor, C- ceiling, L-left wall, and R-right wall) and one node is for the air (node A).

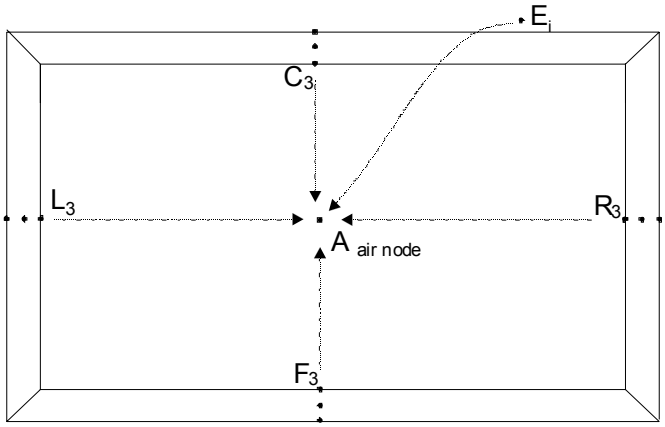

Figure 3.16 Two-dimensional model of a room discretization

The energy balance equations form a system of 13 equations with 13 unknowns. The corresponding zone matrix is shown in Figure 3.17. The node coefficients are marked in a way to show the type of coefficient, building element, and node in building element. For example, the matrix coefficient $b_{C,2}$ is a type B coefficient (from equation 3.69) and it belongs to the node 2 (middle node) of zone element C (Figure 3.16). Coefficients marked as "s" represent the internal-surface-coupling nodes (S in equation 3.71). For example, $s_{C,F}$ presents a coefficient that couples surface of element C with surface of element F (by radiation). Coefficients marked as "r" are coupling coefficients to the air point (R in equation 3.71). For example, r_C is a coupling coefficient of element C with the air point (by convection). The coefficient marked with "e" is the coupling coefficient of the air with the appropriate surface (E in equation 3.74). Temperatures (T) and elements of free vector (f) are also marked according to the corresponding node in the respective elements. Finally, coefficient "d" represents coefficient D in the air node equation (3.74).

Solution of the zone-matrix system (Figure 3.17) provides the temperature distributions in building elements D, E, I, and F together with air temperature. This temperature distribution is for the boundary conditions (such as: external temperature, solar radiation, and internal heat sources), where the system is not controlled (free floating temperatures). Usually in buildings, air temperature is controlled by the building's HVAC system. To provide a certain air temperature

defined by the set point temperature, the HVAC system provides (or removes) certain energy to the zone (cooling/heating load). To solve the cooling/heating load zone matrix, Figure 3.17 needs to be modified.

$$
\begin{vmatrix}
b_{C,1} & c_{C,1} & & & & & & & & & & & & \\
a_{C,2} & b_{C,2} & c_{C,2} & & & & & & & & & & & \\
 & a_{C,3} & \mathbf{b_{C,3}}+s_{C,C} & & & s_{C,F} & & & s_{C,L} & & & s_{C,R} & \mathbf{r_C} & \\
 & & & b_{F,1} & c_{F,1} & & & & & & & & & \\
 & & & a_{F,2} & b_{F,2} & c_{F,2} & & & & & & & & \\
 & & s_{F,C} & & a_{F,3} & \mathbf{b_{F,3}}+s_{F,F} & & & s_{F,L} & & & a_{F,R} & \mathbf{r_F} & \\
 & & & & & & b_{L,1} & c_{L,1} & & & & & & \\
 & & & & & & a_{L,2} & b_{L,2} & c_{L,2} & & & & & \\
 & & s_{L,C} & & & s_{L,F} & & a_{L,3} & \mathbf{b_{L,3}}+s_{L,L} & & & s_{L,R} & \mathbf{r_L} & \\
 & & & & & & & & & b_{R,1} & c_{R,1} & & & \\
 & & & & & & & & & a_{R,2} & b_{R,12} & c_{R,2} & & \\
 & & s_{R,C} & & & s_{R,F} & & & s_{R,L} & & a_{R,3} & \mathbf{b_{R,13}}+s_{R,R} & \mathbf{r_R} & \\
 & & \mathbf{e_C} & & & \mathbf{e_F} & & & \mathbf{e_L} & & & \mathbf{e_R} & \mathbf{d} &
\end{vmatrix}
\times
\begin{vmatrix} T_{C1} \\ T_{C2} \\ T_{C3} \\ T_{F1} \\ T_{F2} \\ T_{F3} \\ T_{L1} \\ T_{L2} \\ T_{L3} \\ T_{R1} \\ T_{R2} \\ T_{R3} \\ T_A \end{vmatrix}
=
\begin{vmatrix} f_{C1} \\ f_{C2} \\ \mathbf{f_{C3}} \\ f_{F1} \\ f_{F2} \\ \mathbf{f_{F3}} \\ f_{L1} \\ f_{L2} \\ \mathbf{f_{L3}} \\ f_{R1} \\ f_{R2} \\ \mathbf{f_{R3}} \\ \mathbf{f_A} \end{vmatrix}
$$

Figure 3.17 The example zone matrix for a two-dimensional model presented in Figure 3.16

Figure 3.18 shows the case where the cooling/heating load is added to the system as an internal source of the building element (node 2 in ceiling element C). For example, element C can represent the cooling or heating panel which controls the room temperature directly by convective heat flux from its surface, and indirectly by radiation to the other surfaces.

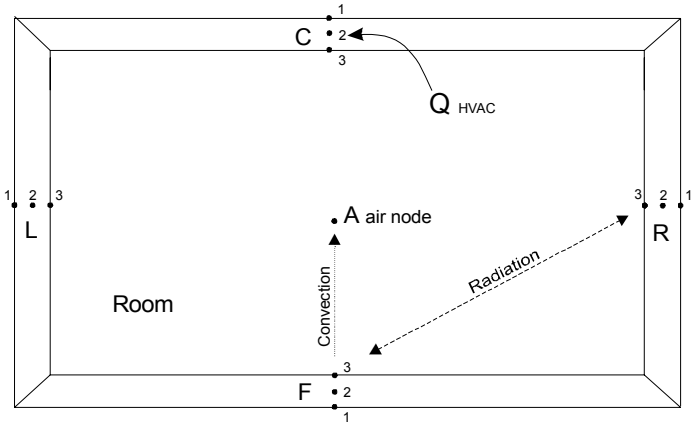

Figure 3.18 Two-dimensional model of a room with a controlled source of energy (Q_{HVAC})

The zone matrix for this case is presented in Figure 3.19. This system has a cooling/heating load as an additional unknown (Q_{HVAC}) and the same number of equations (14 unknowns and 13 equations). The actual number of unknowns is 13 because in the case where the HVAC system works, the air temperature (T_A) is known and equal to the set point temperature. In

the case where the HVAC system does not work, T_A is unknown, but the cooling/heating load is equal to zero ($Q_{HVAC}=0$). This general form of the zone matrix (Figure 3.19) is developed in order to use the same zone matrix solver for the case where the HVAC system is ON or OFF.

$$
\begin{vmatrix}
b_{C,1} & c_{C,1} & & & & & & & & & & & & \\
a_{C,2} & b_{C,2} & c_{C,2} & & & & & & & & & & & \\
 & a_{C,3} & b_{C,3}+s_{C,C} & & s_{C,F} & & & s_{C,L} & & & s_{C,R} & r_C & & \\
 & & & b_{F,1} & c_{F,1} & & & & & & & & & \\
 & & & a_{F,2} & b_{F,2} & c_{F,2} & & & & & & & & \\
 & & s_{F,C} & & a_{F,3} & b_{F,3}+s_{F,F} & & & s_{F,L} & & & a_{F,R} & r_F & \\
 & & & & & & b_{L,1} & c_{L,1} & & & & & & \\
 & & & & & & a_{L,2} & b_{L,2} & c_{L,2} & & & & & \\
 & & s_{L,C} & & & s_{L,F} & & a_{L,3} & b_{L,3}+s_{L,L} & & & s_{L,R} & r_L & \\
 & & & & & & & & & b_{R,1} & c_{R,1} & & & \\
 & & & & & & & & & a_{R,2} & b_{R,12} & c_{R,2} & & \\
 & & s_{R,C} & & & s_{R,F} & & & s_{R,L} & & a_{R,3} & b_{R,13}+s_{R,R} & r_R & \\
 & & e_C & & & e_F & & & e_L & & & e_R & d &
\end{vmatrix}
\times
\begin{vmatrix} T_{C1} \\ T_{C2} \\ T_{C3} \\ T_{F1} \\ T_{F2} \\ T_{F3} \\ T_{L1} \\ T_{L2} \\ T_{L3} \\ T_{R1} \\ T_{R2} \\ T_{R3} \\ T_A \\ Q_{HVAC} \end{vmatrix}
=
\begin{vmatrix} f_{C1} \\ f_{C2} \\ f_{C3} \\ f_{F1} \\ f_{F2} \\ f_{F3} \\ f_{L1} \\ f_{L2} \\ f_{L3} \\ f_{R1} \\ f_{R2} \\ f_{R3} \\ f_A \end{vmatrix}
$$

Figure 3.19 Zone matrixes for a room (zone) with a controlled source of energy (Q_{HVAC})

The general matrix solver used for the zone matrix is given by Clarke (2001). This is a direct method which uses a sub-partitioning to break this sparse matrix into a system of smaller matrices. The solution procedure is adjusted for use in the BES program, and it enables the solution of the temperature distribution when the HVAC system is ON and OFF. A detailed solution procedure is given in Appendix D.

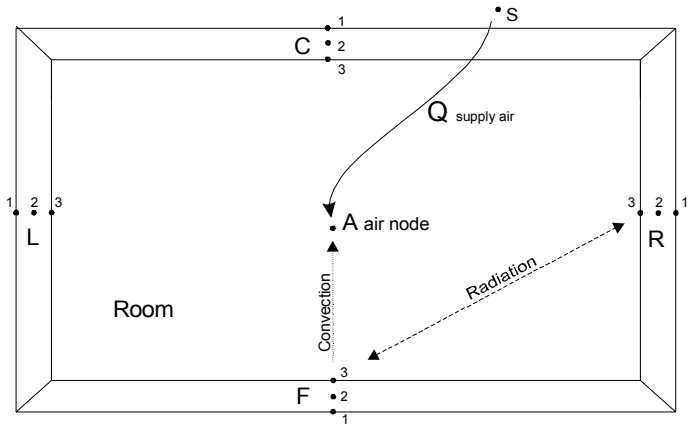

Figure 3.20 Two-dimensional model of a room with controlled supply air (Q_{supply_air})

In the case where the HVAC system controls the air temperature by supply air, the zone matrix has a slightly different form. With the air system, the energy of supply air (Q_{supply_aur}) is directly added to (or extracted from) the room air (Figure 3.20). If the air system with Variable Air Volume (VAV) is used, the supply air volume flow rate (m_S) is unknown. If the Constant Air Volume (CAV) system with variable air temperature is used the supply air temperature (T_S) is unknown. The zone matrix for this case is presented in Figure 3.21. The coefficient "k" in the air equation (last row) depends on which variable is used (m_S or T_S). In the solution procedure, the matrix solver presented in Appendix D is used where the second and last rows of the zone matrix are switched.

$$
\begin{vmatrix}
b_{C,1} & c_{C,1} & & & & & & & & & & & & \\
a_{C,2} & b_{C,2} & c_{C,2} & & & & & & & & & & & \\
 & a_{C,3} & b_{C,3}+s_{C,C} & & & s_{C,F} & & & s_{C,L} & & & s_{C,R} & r_C & \\
 & & & b_{F,1} & c_{F,1} & & & & & & & & & \\
 & & & a_{F,2} & b_{F,2} & c_{F,2} & & & & & & & & \\
 & & s_{F,C} & & a_{F,3} & b_{F,3}+s_{F,F} & & & s_{F,L} & & & a_{F,R} & r_F & \\
 & & & & & & b_{L,1} & c_{L,1} & & & & & & \\
 & & & & & & a_{L,2} & b_{L,2} & c_{L,2} & & & & & \\
 & & s_{L,C} & & & s_{L,F} & & a_{L,3} & b_{L,3}+s_{L,L} & & & s_{L,R} & r_L & \\
 & & & & & & & & & b_{R,1} & c_{R,1} & & & \\
 & & & & & & & & & a_{R,2} & b_{R,12} & c_{R,2} & & \\
 & & s_{R,C} & & & s_{R,F} & & & s_{R,L} & & a_{R,3} & b_{R,13}+s_{R,R} & r_R & \\
 & & e_C & & & e_F & & & e_L & & & e_R & d & k
\end{vmatrix}
\times
\begin{vmatrix}
T_{C1} \\ T_{C2} \\ T_{C3} \\ T_{F1} \\ T_{F2} \\ T_{F3} \\ T_{L1} \\ T_{L2} \\ T_{L3} \\ T_{R1} \\ T_{R2} \\ T_{R3} \\ T_A \\ T_S \text{ or } m_S
\end{vmatrix}
=
\begin{vmatrix}
f_{C1} \\ f_{C2} \\ f_{C3} \\ f_{F1} \\ f_{F2} \\ f_{F3} \\ f_{L1} \\ f_{L2} \\ f_{L3} \\ f_{R1} \\ f_{R2} \\ f_{R3} \\ f_A
\end{vmatrix}
$$

Figure 3.21 Zone matrix for a room (zone) with HVAC system that control supply air

In the case of the room with plenum (two zones), the plenum temperature is added into the system as an unknown. Also, the number of nodes is increased because additional nodes of the elements that form the plenum zone are added into the zone matrix (Figure 3.22). In the new matrix, additional equations for the element (P) and equation for the air in the plenum are present (Figure 3.23). Coefficients marked with *"k"* are coupling coefficients of elements with the plenum air point. Coefficients *"pa"* and *"ap"* define inter-zone airflow in-between the plenum and room air. The problem with multiple air nodes (multiple zones) is that some surfaces are coupled from both sides to the unknown air nodes. For example, surface C has two internal surfaces. Node C1 is coupled to the plenum air and node C3 to the room air. The coupling coefficient of node C1 to the plenum air is presented by letter X in the matrix (Figure 3.23). Also C1 is coupled with P3 by radiation and this is presented by coefficient Y in the zone matrix. With

these coefficients (X and Y) sub-partitioning of the zone matrix (described in Appendix D) cannot be used and the matrix solution procedure becomes complex. As a solution, the temperature for node C1 (T_{C1}) from the previous time step is used for the calculation of heat fluxes from surface C1 to the plenum air and surface P3. This solution moves coefficients X and Y into the free vector (F) and the matrix solver described earlier is used.

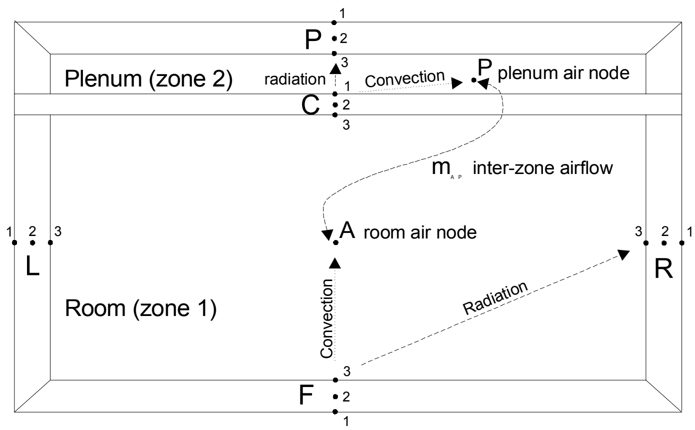

Figure 3.22 An example model of a room with two zones:
(1) room and (2) plenum zones

$$
\left|\begin{array}{ccccccccccccccccc}
b_{C,1} & c_{C,1} & & & & & & & & & & & & & \mathbf{Y} & \mathbf{X} & \\
a_{C,2} & b_{C,2} & c_{C,2} & & & & & & & & & & & & & & \\
 & a_{C,3} & b_{C,3}+s_{C,C} & & & s_{C,F} & & & s_{C,L} & & & s_{C,R} & & & & k_C & r_C \\
 & & & b_{F,1} & c_{F,1} & & & & & & & & & & & & \\
 & & & a_{F,2} & b_{F,2} & c_{F,2} & & & & & & & & & & & \\
 & & s_{F,C} & & a_{F,3} & b_{F,3}+s_{F,F} & & & a_{F,L} & & & a_{F,R} & & & & k_F & r_F \\
 & & & & & & b_{L,1} & c_{L,1} & & & & & & & & & \\
 & & & & & & a_{L,2} & b_{L,2} & c_{L,2} & & & & & & & & \\
 & & a_{L,C} & & & a_{L,F} & & a_{L,3} & b_{L,3}+s_{L,L} & & & a_{L,R} & & & & k_L & r_L \\
 & & & & & & & & & b_{R,1} & c_{R,1} & & & & & & \\
 & & & & & & & & & a_{R,2} & b_{R,12} & c_{R,2} & & & & & \\
 & & a_{R,C} & & & a_{R,F} & & & a_{R,L} & & a_{R,3} & b_{R,13}+s_{R,R} & & & & k_R & r_R \\
 & & & & & & & & & & & & b_{P,1} & c_{P,1} & & & \\
 & & & & & & & & & & & & a_{P,2} & b_{P,12} & c_{P,2} & & \\
 & & & & & & & & & & & & & a_{P,3} & b_{P,13}+s_{R,R} & k_P & r_P \\
 & & p_C & & & p_F & & & p_L & & & p_R & & & p_P & pp & pa \\
 & & e_C & & & e_F & & & e_L & & & e_R & & & e_P & ap & aa
\end{array}\right|
\times
\left|\begin{array}{c}
T_{C1} \\ T_{C2} \\ T_{C3} \\ T_{F1} \\ T_{F2} \\ T_{F3} \\ T_{L1} \\ T_{L2} \\ T_{L3} \\ T_{R1} \\ T_{R2} \\ T_{R3} \\ T_{P1} \\ T_{P2} \\ T_{P3} \\ T_P \\ T_A
\end{array}\right|
=
\left|\begin{array}{c}
f_{C1} \\ f_{C2} \\ f_{C3} \\ f_{F1} \\ f_{F2} \\ f_{F3} \\ f_{L1} \\ f_{L2} \\ f_{L3} \\ f_{R1} \\ f_{R2} \\ f_{R3} \\ f_{P1} \\ f_{P2} \\ f_{P3} \\ f_P \\ f_A
\end{array}\right|
$$

Figure 3.23 A zone matrix for room and plenum zones

Equations for the HVAC model described in Section 3.2.6 are not included into the described system of linear equations. Only the "link" in-between the zone matrix, which describes the energy balance in the zone, and the equations for the HVAC model are included. This "link" is defined by:

1) Cooling/heating load Q_{load} and surface temperature $T_{surface}$ - for HVAC systems that use $T_{surface}$ as the control parameter as described in Section 3.2.6,
2) Cooling/heating load Q_{load} and supply air temperature T_{supply} - for VAV systems,
3) Cooling/heating load Q_{load} and supply air mass flow rate m_S - for VAT systems,
4) Cooling/heatin load Q_{load} - for pure convective systems.

Based on information in this "link", the model that couples zone matrix equations with equations of HVAC systems is developed for the BES program. This model enables simultaneous load calculation and HVAC performance simulation.

3.4 Model for Simultaneous Load Calculation and HVAC Performance Simulation

This section gives details about newly developed models for simultaneous load calculation and HVAC performance simulation. It provides details about coupling approaches of Load and HVAC models and Constraints Control Algorithm (CCA).

3.4.1 Coupled versus Not-Coupled Load and HVAC Calculation

Section 2.1.2 describes two basic methods, used in other energy simulation programs, for the calculation of total energy consumption in building's HVAC systems:

- A method with separated models for calculation of load and HVAC performance and
- A method with integrated load and HVAC models.

In the newly developed BES program, a method with an integrated model is used. The integration of the building zone and HVAC models is necessary in order to accurately calculate energy consumption and thermal conditions in the room.

The effect of load and HVAC model integration on thermal conditions in the room is illustrated in Figure 3.24. In this example the temperature of the room is controlled at a set point temperature of 24°C during working hours (8 am - 6 pm) for a period of three days. The room temperature (T_{air}) is controlled by the surface temperature of cooling radiant panels (T_{pnSurf}). In the case with separate models, T_{air} is always equal to set point temperature because of the assumption that the HVAC systems always keeps the air temperature at set point. As a consequence, the surface temperature of cooling panels is higher than set point temperature in

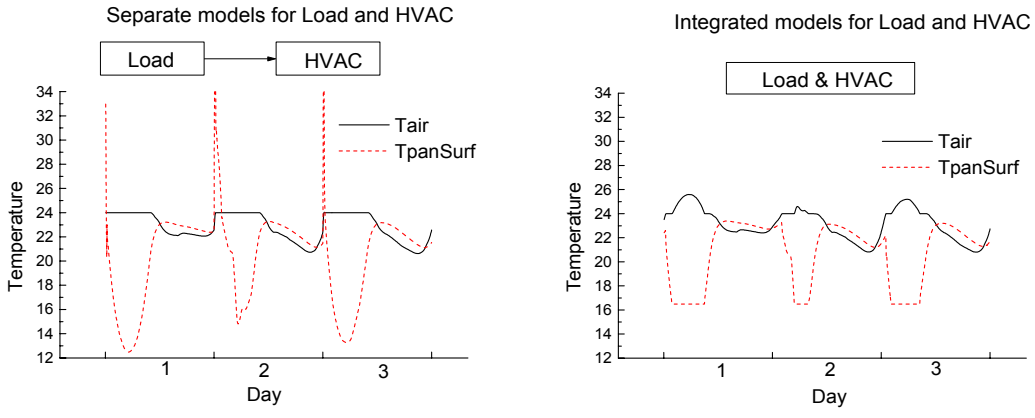

Figure 3.24 Air and radiant panel temperatures in a room when
(a) separate and (b) integrated Load and HVAC models are used

early hours of the morning (refer to Figure 3.24a) because heating is needed to maintain the set point temperature. In the case with integrated models, limitations of HVAC systems are considered and realistic temperatures are calculated (refer to Figure 3.24b). The air temperature during the day is different because of two reasons. First, in the morning hours, there is no heating and room temperature is lower than the set point temperature. Second, constraints related to the minimum dew-point temperature of the panel surface (that prevent condensation) limit the surface minimum temperature to 16°C (Figure 3.24b). As a consequence, air temperatures in the afternoon hours are higher than the set point temperature.

Also, the energy consumption (energy extracted by radiant panel) calculated by separate and integrated models can be considerably different. In this example, the energy consumption calculated by integrated models is approximately 30% smaller than the energy consumption calculated using separate models. There are two reasons for this large difference. First, in a realistic case (integrated model), the radiant panel extracts less energy than in the case where the limitation of HVAC is not considered because of constraints related to minimum value for $T_{panSurf}$. Second, heating in early hours of the morning (which is present in calculation with separate models) increases the accumulated energy in the building elements and increases the cooling energy consumption in afternoon hours.

Generally, this example shows that integrated load and HVAC models provide more relalistic results related to energy consumption and thermal comfort evaluation. This is especially the case with HVAC systems that include radiant panels. Therefore, in view of its advantages, the BES program uses integrated load and HVAC models.

3.4.2 Coupling Approaches of Load and HVAC Models

Section 2.1.2 shows that ESP-r (Clarke 1985) and EnergyPlus (Crawley 2001) programs have integrated HVAC models into the cooling load calculation procedure. However, these two programs have considerably different approaches for the integration procedure.

In ESP-r, HVAC equations are integrated into the zone matrix (Figure 3.25). In this way, all equations are solved directly using solvers for sparse linear systems. The HVAC system of equations, like the zone system, creates a sparse matrix. However, coefficients are not regularly distributed as in the building zone matrix in Figure 3.17. Also, depending on the HVAC system

configuration, each HVAC matrix is connected in different way to the zone matrix by coefficients (matrix elements), which create "irregularity" in the zone-HVAC matrix (Figure 3.25). This "irregularity" precludes the simple matrix partitioning used in the zone matrix solver (refer to Appendix D). Therefore, the solution procedure is mathematically more complex and more time consuming. Also, with this method, all HVAC models have to be linearized. This is an even larger problem than solving the matrix. For example, the radiant panel model contains an exponential function (Equation 3.59), which is very difficult to linearize.

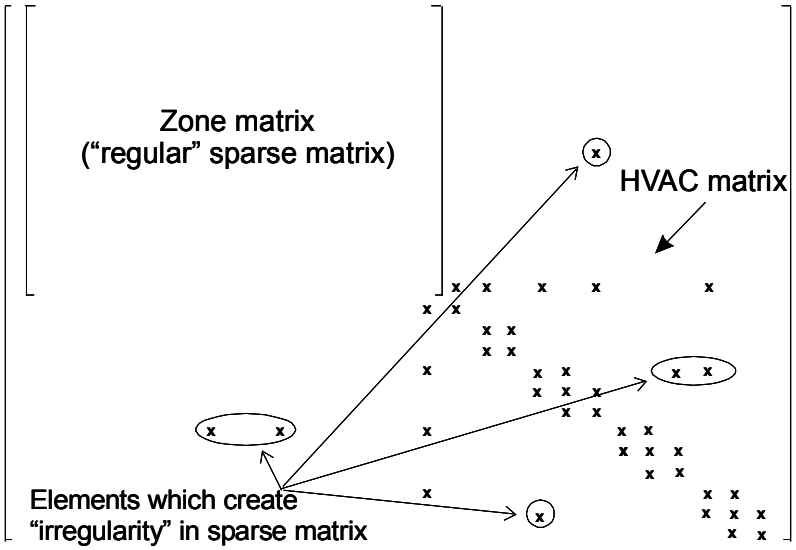

Figure 3.25 Structure of a zone and HVAC matrix
where HVAC models are integrated into the zone matrix

Because of linearization and matrix solution problems, the BES program uses iterative solution procedures for HVAC models. This method enables the implementation of various HVAC system models organized in modules. To integrate the load (zone matrix) and HVAC models, the two models exchange information several times during the calculation procedure (refer to Figure 3.26). This procedure is similar to the procedure used in the EnergyPlus program. The simultaneous solution scheme of EnergyPlus is further developed for use in the zone matrix and different control schemes.

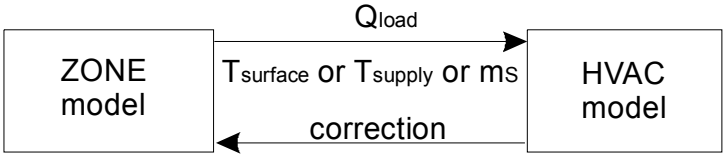

Figure 3.26 Schematic of a simultaneous solution scheme
Implemented into the BES program

The EnergyPlus program uses the "predictor-corrector" method for integrating the HVAC system and heating/cooling load models (EnergyPlus 2001). This method is used for the correction of zone air temperatures in cases where the central plant cannot satisfy heating/cooling load requirements (Figure 3.26). However, the predictor-corrector scheme used in the EnergyPlus program corrects only air temperature. The enclosure temperatures and temperatures in building elements that define thermal energy stored in building are not corrected because the EnergyPlus program uses conduction transfer functions (EnergyPlus 2001). With the simultaneous solution scheme developed for the BES program, the relevant correction is returned to the zone matrix which enables the correction of temperatures in the whole energy simulation domain.

The simultaneous solution scheme used in the BES program consists of the following steps:

(1) For air temperature set point (T_{AIR}): thermal device surface temperature (T_{HVAC}) and required heating/cooling load (Q_{HVAC}) are calculated.

(2) Based on these two parameters and outdoor weather data, HVAC models determine if a thermal plant has the required capacity.

(3) If a thermal plant capacity is not sufficient, the actual capacity (Q_{HVAC}) is returned to the zone matrix (refer to Figure 3.26). After reorganizing the zone matrix, a completely new temperature distribution in all building elements is calculated.

This simultaneous solution scheme checks only if the power plant has enough cooling/heating capacity (Q_{HVAC}). However, there is a limitation of the HVAC system related to thermal comfort, air quality, and designed capacity constraints. These constraints are related to control parameters (T_{supply}, $T_{surface}$, and m_{supply}) which are described in Section 3.2.6. For example, VAV's power plant has enough cooling capacity but its maximum flow rate ($m_{supply\ max}$) is smaller than the one needed to provide the set point temperature in the room. Otherwise, thermal comfort may limit the minimum supply temperature with a displacements diffuser. As part of the solution scheme, the Constraints Control Algorithm was developed and implemented into the BES program.

3.4.3 Constraints Control Algorithm

The Constraints Control Algorithm is a solution procedure whereby the zone matrix solver and HVAC modules (HVAC equations solver) exchange information several times for a

considered time step. Depending on the HVAC system configuration, the algorithm makes a selection from six different procedures that are implemented (Figure 3.27):

Procedure I In the case where only a cooling/heating load calculation is required, the matrix solver calculates the required cooling/heating load for a given set point temperature (Figure 3.27).

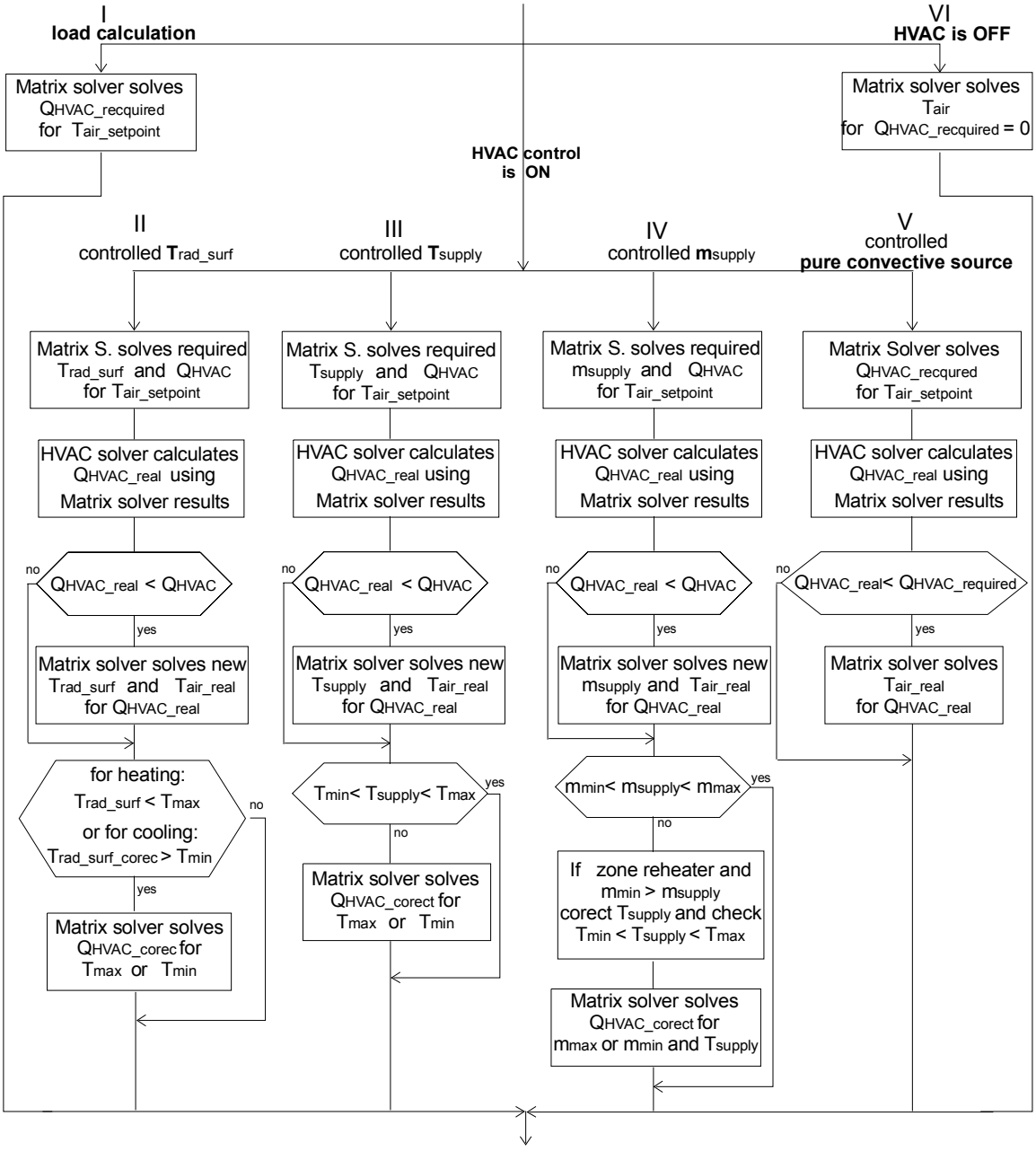

Figure 3.27 Constraints control algorithm implemented into the BES program

Procedure II With the HVAC system where a control parameter is $T_{surface}$, the matrix solver calculates the cooling/heating load (Q_{HVAC}), required $T_{surface}$ to keep set point temperature, and all other temperatures of building elements. Then the program delivers Q_{HVAC} to the HVAC module which checks if the cooling/heating plant has enough capacity to satisfy cooling/heating load. This check is based on output data from the matrix solver such as $T_{surface}$, convective and radiative heat flux on the controlled surface. If the cooling/heating plant does not have enough capacity, the matrix solver solves the new temperature distribution in building elements for a given cooling/heating capacity. Then, the program performs an additional "check" related to the limitations of $T_{surface}$. If $T_{surface}$ is not within the limit, the matrix solver performs another computation in order to calculate Q_{HVAC} for a new $T_{surface}$.

Procedure III In the case with HVAC system, where a control parameter is T_{supply}, the algorithm is similar to $T_{surface}$. The only difference lies in constraint conditions for T_{supply}.

Procedure IV In the case with HVAC system, where a control agent is m_{supply}, the algorithm is more complex because this HVAC system is a typical VAV system which may or may not have zone reheaters depending on its configuration. The program first checks if the mass flow rate is within the relevant range. If the mass flow rate is below the minimum required and zone reheaters are used, the program corrects the temperature accordingly. Also, a "check" for new temperatures is performed (refer to Figure 3.27).

Procedure V In case with pure convective HVAC systems, the HVAC module checks if cooling/heating plant has enough capacity to satisfy cooling/heating load.

Procedure VI In the case where the HVAC system is turned off, the program calculates the air temperature and all other temperatures for building elements when $Q_{HVAC}=0$.

3.5 Validation

Validation of BES was performed in two stages:

1. Validation of program components during code development, and
2. Validation of BES after all program components (models) had been implemented.

3.5.1 Validation of Program Components

During the program code development phase, different models, organized in program modules, were validated by comparing results obtained with these models with existing and well-established results. For example, temperature distributions for steady-state and unsteady-state heat transfer in building elements were first calculated by numerical models implemented in the BES program. These were then compared to the respective temperature distributions obtained by existing analytical models. In the same manner, solar angles were calculated by models implemented in the BES program and compared to solutions provided in ASHRAE Fundamentals (2001). Also, the view-factor program module was tested using view factor properties (Equation 3.24), symmetrical geometry, and manually calculated solutions.

This section only presents some of the validation tests performed for components of the BES program. Exact view factors for geometry of the test-building, obtained by the view-factor program module, are presented in Appendix E. This appendix also contains solar fractions for transmitted direct and diffuse solar radiation distributions on internal surfaces, which were calculated by models presented in Section 3.2.2. The presented results (Tables E1-E4) demonstrate energy conservation, since equations (3.24) and (3.38) are satisfied.

Figure 3.28 shows a comparison between numerical and analytical solutions for unsteady heat conduction (Equation 3.40). At a certain time step, when the temperature of the wall is uniform (T_o), the surface temperature at both sides is decreased (T_S). Change of dimensionless temperature (T-T_S/T_o-T_S) during the time at center of the homogeneous wall is plotted for the exact (analytical) solution and compared with results obtained by the numerical model implemented into the BES program. Numerical results for different time and space discretization show the sensitivity of the applied numerical model to this discretization. In the case where the change in air temperature causes a change of the surface temperature and where the surface heat

flux is defined by Dirichlet boundary conditions ($h_{surface}$, T_{air}), the change of T-T_{air}/T_o-T_{air} is less sensitive to time and space discretization compared to change of T-T_S/T_o-T_S. Clarke (2001)

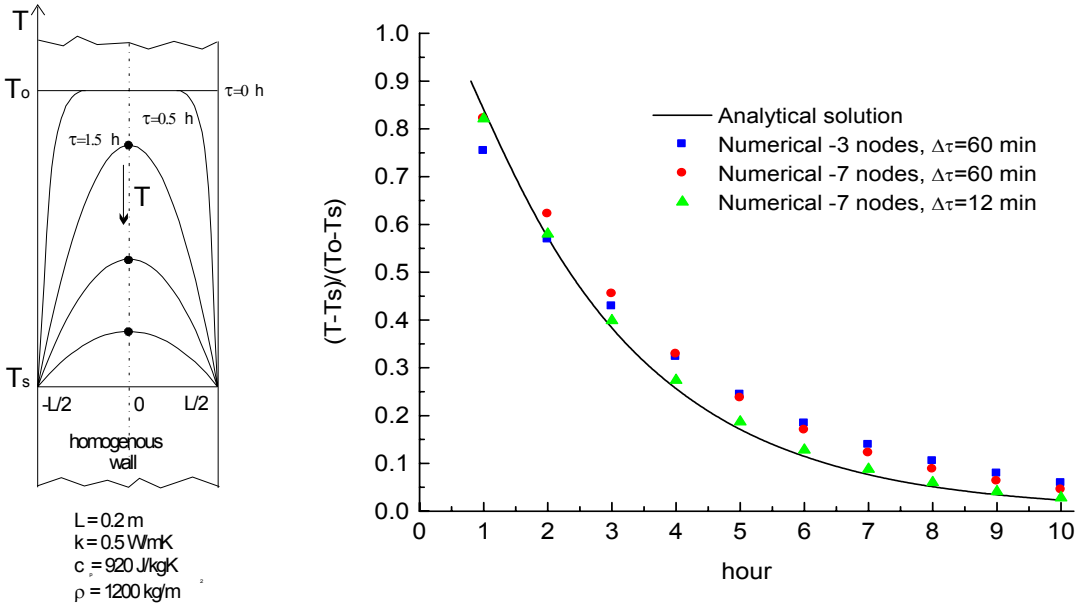

Figure 3.28 A comparison of analytical end numerical solution for the temperature distribution with unsteady heat transfer in a homogeneous wall

provided detailed analyses of the effects of space and time discretization on temperature distribution in building elements with realistic ranges of boundary conditions such as solar radiation, convection coefficients, and surface and air temperatures.

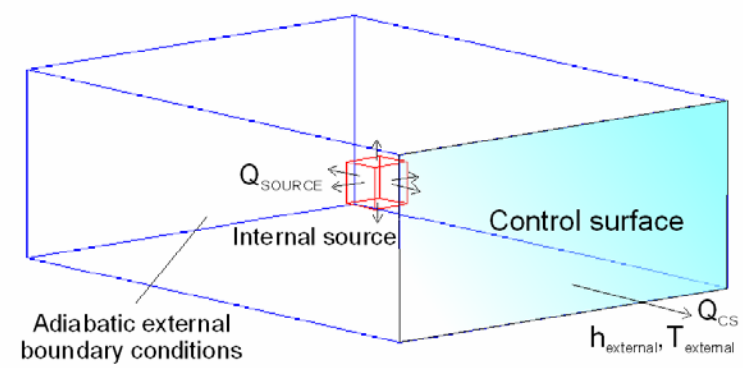

Figure 3.29 Room geometry for energy conservation tests

A second type of the program components validation was achieved by performing energy balance tests for various building configurations. In these tests, input and output energy for both steady state and unsteady state cases were compared. Figure 3.29 presents one of these tests.

External boundary conditions of the test building (single space) were set to be adiabatic for all surfaces except one control surface. At this surface heat flux was "monitored" (calculated for each time step). In the room, internal sources were set to Q=400W (200 W radiative and 200 W convective heat flux). To calculate the steady state, total heat flux on the control surface was 400 W, which means that program satisfied energy conservation for steady state calculation. For the unsteady state test, where the heat source was active for 24 hours, the building structure accumulated energy and then released through the control surface over a longer period of time. The change of this heat flux on the control surface is presented in Figure 3.30. Since areas (integrals) below lines which represent $Q_{\text{internal sources}}$ and $Q_{\text{at control surface}}$ are the same (9600 Wh), the program satisfies the energy conservation condition for an unsteady state type of calculation as well.

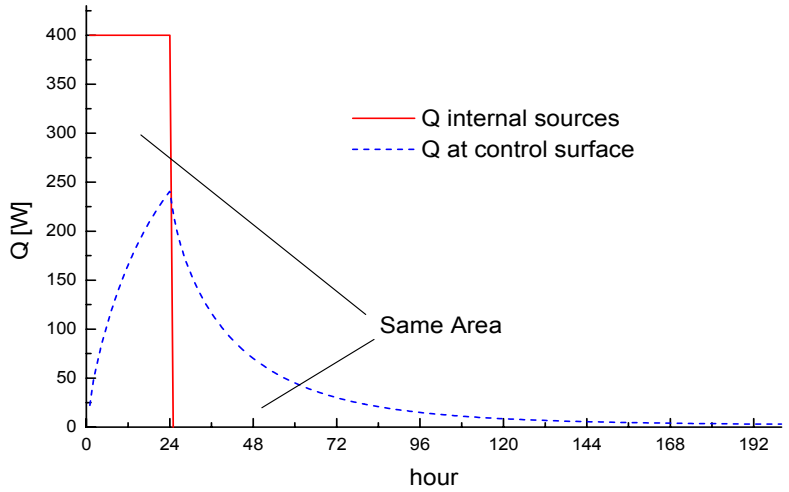

Figure 3.30 Energy conservation tests for unsteady heat transfer

3.5.2 Verification of New ES program Using BESTEST

After all models were implemented, the accuracy of the BES program was evaluated by a set of Building Energy Simulation Test (BESTEST) procedures. BESTEST is set of comparison tests in which, for specific input data, the program results of the tested program are compared to results of several well-tested and widely used energy simulation programs such as: ESP, BLAST, DOE2, TRNSYS, S3PAS, TASE, CLIMA 2000, and SERIRES (U.S. version SRES/SUN and British version SRES-BRE). Details about performed BESTEST procedures for each of these programs are provided by Judkoff and Neymark (1995).

The BESTEST primarily evaluates the ability of the tested program to model the dynamics of building's envelope by comparing:

- Annual energy consumption for cooling and heating, and
- Maximum heating and cooling load along with the time at which they occurred in the year.

As input data, building thermal and physical characteristics for a simple single zone building are provided along with weather data organized in the TMY whether database format. The geometry of test building is given in Figure E1 (in Appendix E) while building thermal and physical characteristics are given in Tables F1 and F2 (in Appendix F).

Test cases are designed to isolate particular aspects of energy flow in buildings and test the effects of these aspects on the annual energy consumption and maximum cooling load. These aspects are thermal mass, solar energy gain, windows, window-shading devices, internal heat sources, infiltration, sunspaces, earth coupling, and dead-band and setback thermostat control. BESTEST tests are divided into two groups: qualification tests and diagnostic tests. The qualification tests start with the basic building structure and then manipulate it by: moving the windows, adding exterior shading devices, changing the wall constructions, and surface radiative properties. When qualifications tests fail, (annual energy consumption and/or cooling/heating load is out of range defined by range of solutions obtained by reference programs) diagnostic tests are used for more specific and detailed problem detection.

The total number of BESTEST cases is 36 and the BES program was tested for most of them (24 cases). The testing did not include tests for sunspaces, earth coupling and setback thermostat control. These tests were excluded because of simplified simulation models implemented in the BES program, such as model for earth coupling; or because of the limitations of the BES program. An example of a limitation is where a single room model cannot be used for a sunspace test, because this test requires a two-room model. Some of the test results related to annual energy consumption are presented in Figures 3.31-3.36. In addition, Table 3.3 contains some of the comparison results for annual peak cooling and heating load.

Before any qualification or diagnostic tests were performed, the BES program was tested for annual incident and transmitted solar radiation. Results of the tests related to the annual incident solar radiation are presented in Figure 3.31. In these tests, the BES program module for solar radiation distribution (with the model described in Section 3.2.1) was verified. The Isotropic

Diffuse Sky Radiation model (Equation 3.5) was used in the BES program to calculate solar diffuse radiation. Figure 3.32 shows the results for transmitted solar radiations through the windows. The test for an unshaded window (Figure 3.32) verifies the model for diffuse and direct solar transmittance of the window (presented in Section 3.23). Pertaining to the test for the shaded window, a horizontal shading device was installed above the window. Good agreement between results obtained by the BES program (new ES program) and the other program verifies the shading model described in Section 3.2.1.

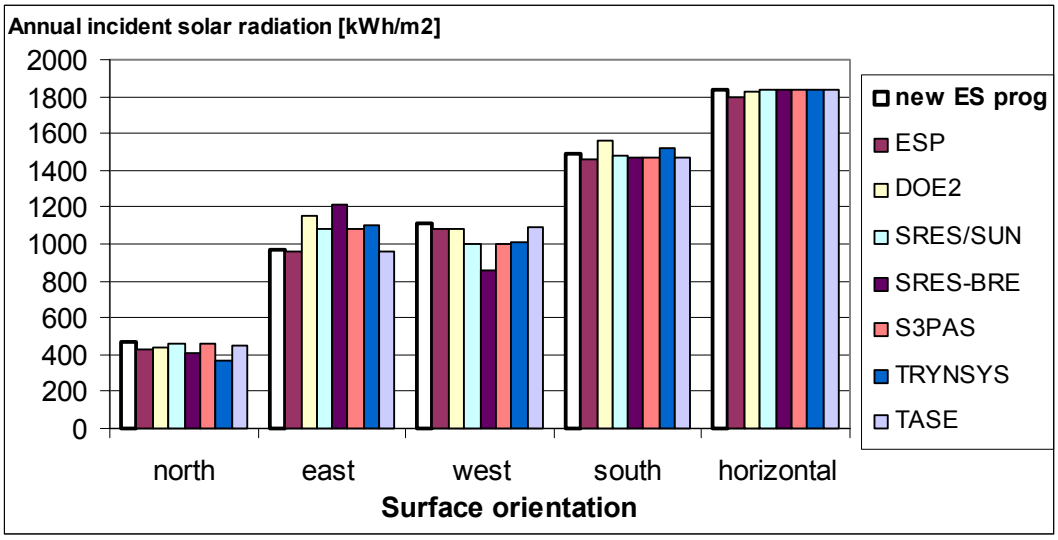

Figure 3.31 BESTEST comparison results for annual diffuse and direct incident solar radiation at different surface orientations

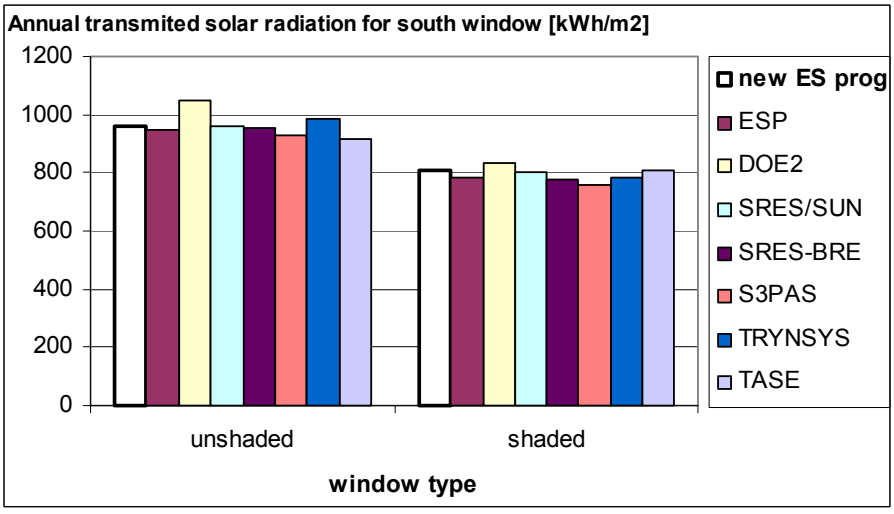

Figure 3.32 BESTEST comparison results for annual transmitted diffuse and direct solar radiation through a south oriented window with and without window shading overhang

Figures 3.33 and 3.34 present the comparison results for several diagnostic test cases. Test case 195 tests convection models in energy simulation programs. The test building in this case did not have windows. Therefore, effects of solar and internal radiation were excluded by setting the external and internal emissivity to 0.1. Case 200 tests window conductivity. It is the same as case 195 except that windows that are completely opaque were added to the test building model (refer to Figure G1). Case 220 test the long-wave radiative heat exchange models for external surfaces by setting external emissivity to 0.9 and shot-wave to 0.1. Case 230 tests the effect of infiltration. In this case infiltration for the test building model was set to 1 ACH. Case 240 tests the internal heat sources models by adding internal heat source of 200 W (40% by

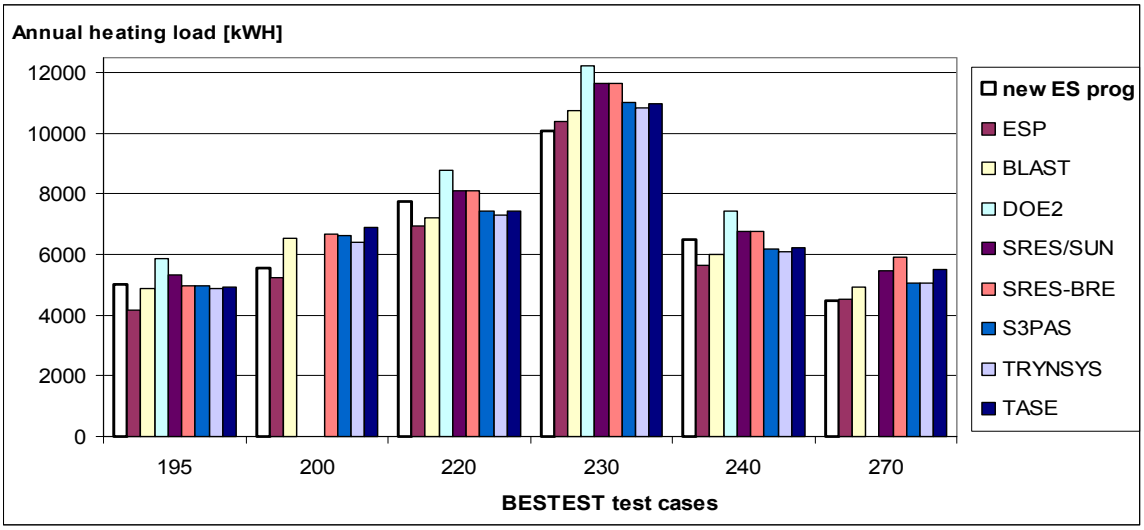

Figure 3.33 BESTEST comparison results for diagnostic test cases - heating

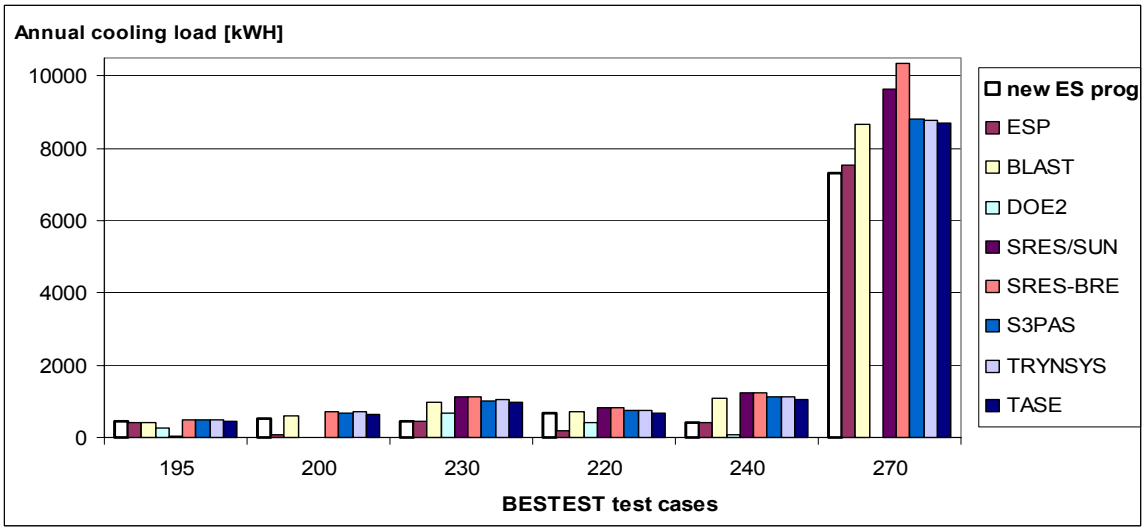

Figure 3.34 BESTEST comparison results of for diagnostic test cases - cooling

convection and 60% by radiation). Finally, case 270 has a building model with transparent windows. It tests the distribution of incident solar radiation. To ensure that certain tests emphasize the effect of tested parameter (phenomenon) on energy consumption, all these diagnostic tests enforce strict cooling/heating set-point temperature of 20°C. As seen in Figures 3.33 and 3.34, there are variations in annual energy consumptions calculated by different programs. The reason for these variations is difference in models for surface boundary condition calculation, which are discussed at the end of this section. Considering the new ES program, it provides results that are comparable to the result of other programs included in BESTEST.

More realistic test building models (cases) are used for qualification test cases. For these qualification tests, dead-band thermostat control is used (20°C for heating and 27°C for cooling).

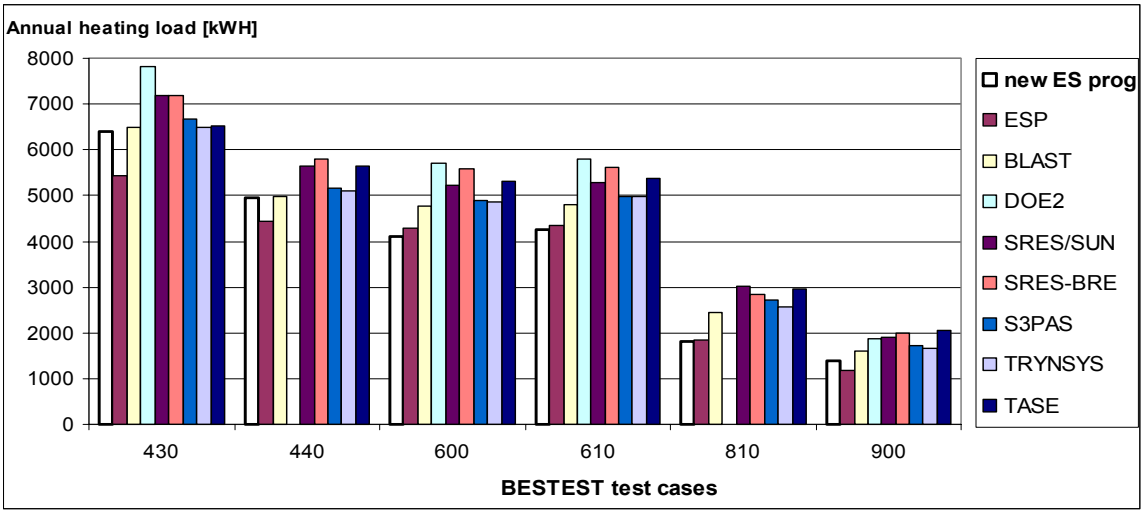

Figure 3.35 BESTEST comparison results for qualification test cases - heating

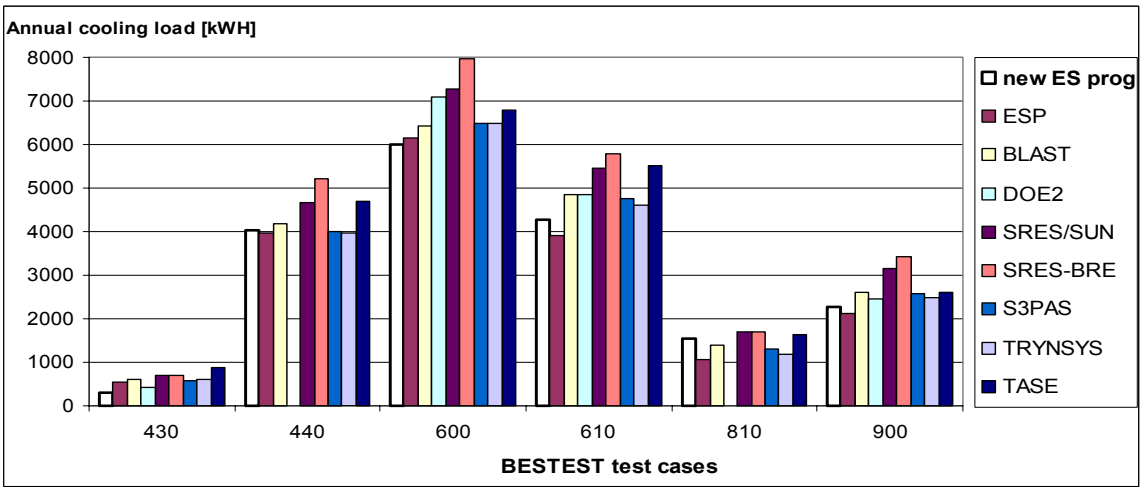

Figure 3.36 BESTEST comparison results for qualification test cases -cooling

The test results for these cases are presented in Figures 3.35 and 3.36. Case 430 tests the exterior solar absorptance and incident solar radiation. Case 440 tests the interior solar absorptance. Case 600 verifies the solar transmission thought the window, while case 610 verifies the south window shading device. Cases 810 and 900 verify the building thermal mass interaction with solar absorptance. As seen in Figures 3.35 and 3.36, the results for the new ES program are within ranges of the BESTEST qualification tests.

For each test case, the peak cooling and heating loads calculated by the new ES program were also compared with results from the other programs. Table 3.3 contains some of these comparisons along with the corresponding date and hour when the peak load appeared. Case 600 and 900 are completely similar, except for building mass. Case 600 has lightweight building construction, while case 900 has heavyweight (refer to Appendix F).

Through BESTEST testing of the new ES program, several program "bugs" were detected and corrected. Bugs that were corrected are related to use of improper models, errors in implementation, and errors in programming such as memory leaks and allocation issues. Some

Table 3.3 Annual peak cooling and heating loads

Test case	600						900					
	heating			cooling			heating			cooling		
	kW	date	hour	kW	date	hour	kW	date	hour	kW	date	hour
New ES prog.	3818	4-Jan	7	6094	16-Oct	14	3224	4-Jan	7	3092	17-Oct	15
ESP	3437	4-Jan	5	6194	17-Oct	13	2850	4-Jan	7	2888	17-Oct	14
BLAST	3940	4-Jan	5	5965	16-Oct	14	3453	4-Jan	7	3155	6-Oct	15
DOE2	4045	4-Jan	2	6656	16-Oct	13	3557	4-Jan	7	3458	17-Oct	14
SRES/SUN	4258	4-Jan	2	6827	16-Oct	14	3760	4-Jan	7	3871	17-Oct	14
SRES-BRE	4307	4-Jan	2	7551	16-Oct	13	4081	4-Jan	7	4901	17-Oct	14
S3PAS	4037	4-Jan	5	6286	25-Nov	x	3608	4-Jan	8	3334	17-Oct	x
TRYNSYS	3931	4-Jan	6	6486	16-Oct	14	3517	4-Jan	7	3567	17-Oct	15
TASE	4354	4-Jan	2	6812	17-Oct	14	3797	4-Jan	7	3457	17-Oct	15

examples include: (1) the substitution of an improper model for calculation of convective heat transfer in a window air cavity gap with a more appropriate model as presented by Equation 3.46; (2) correction of errors in the implementation of models for surface azimuth calculation and internal radiative heat exchange; and (3) remedy of programming errors related to limitations of the maximum number of internal nodes in the homogeneous wall layer and related to processing data from weather database. Furthermore, some additional models were added to the BES program in order to enable BESTEST procedures. For example: (1) the procedure for reading and

processing the TMY format of the weather database was added to the existing procedures for reading and processing TMY2 weather data; (2) the model for density correction with elevation of the building site are implemented into the BES program and (3) the dead bend control model is added to the constraint control model presented in Figure 3.27.

The differences in annual energy consumption and peak cooling/heating load calculated by different programs in BESTEST are primarily due to different models for internal and external convective heat flux calculation. The BES program, like the ESP program, uses convection correlations which generally provide smaller convection coefficients than coefficients used in other programs used in BESTEST. Most programs in BESTEST use yearly averaged constant convection coefficients that included effects of natural and forced convection. On the other hand, the BES program uses convection correlation for only natural convection because the test building model has no air supply system. Also, the model for external convection, presented in Section 3.2.1 for wind velocities from TMY weather database, provides on average lower convection coefficients than the constant value suggested by BESTEST authors. The reason for this is that the model presented in Section 3.2.1 treats surfaces that are windward and leeward differently. Related to radiative heat flux calculation at external surface, different programs used in BESTEST implement different models to calculate the radiative heat exchange between the surface and the atmosphere (sky). This also leads to differences among the results.

3.6 Summary

This chapter has described physical and numerical models that have been implemented into the newly developed BES program. Using these models, the BES program is capable of precisely calculating heat flow within a room with or without a plenum above it. The primary reason for the development of BES was to couple it with the airflow program. Therefore, during the BES program development, the focus was on the implementation of heat transfer models which enable accurate calculations of internal surface temperatures that are necessary for coupling.

This chapter has also described a new method for simultaneous load calculation and HVAC system simulation that was developed as part of the BES program. This new method has certain advantages over procedures used in the ESP-r and EnergyPlus programs. This method enables modular organization of HVAC system models because HVAC equations are NOT integrated into the zone matrix. On the other hand, this method calculates enclosure temperatures and energy stored in building elements because it uses a "predictor-corrector" method to correct all temperatures in the energy simulation domain. In this way, the new method enables better prediction of thermal comfort and HVAC system performance. This is especially so in the case with systems where building thermal storage has a large influence on energy flow, such as heating/cooling slabs and systems with radiant panels.

Finally, this chapter has described extensive validation procedures that were performed during the program code development. The good validation obtained results showed that the BES program can be coupled with the airflow program. Furthermore, BESTEST results demonstrate that the BES program can be used in various analyses related to energy consumption in buildings. Also, good validation results of the current version of BES demonstrate that the program is ready for further development. This can be done by: (1) adding procedures that will increase the number of rooms that can be analyzed (multizone building); (2) adding different HVAC system models that use the proposed coupling method for simultaneous load calculation and HVAC system simulation.

CHAPTER 4

AIR FLOW PROGRAM - BOUNDARY CONDITIONS

4.1 Introduction

As described in Chapter 2, Computation Fluid Dynamics (CFD) programs have been successfully used as indoor air flow programs. They provide detailed information about air velocity, temperature, and contaminant concentration in buildings. Hence, a CFD program was selected as the airflow simulation tool for coupling with the building energy simulation (BES) program. The CFD programs are used in a wide range of scientific and engineering fields. Therefore, there is a large number of well-established research and commercial CFD software packages.

The BES program has been coupled with a CFD program called CFD0, which was developed for research purposes at the Massachusetts Institute of Technology (MIT) (Srebric 2000). This program was extensively validated by the developer (Srebric 2000). Because of the necessity to modify the CFD source code for effective coupling with the BES program, priority was given to this CFD program over the other commercial codes that had larger variety of implemented turbulence models and more extensive validation, but provided none or very limited access to their respective source codes. The CFD0 program has certain limitations (these will be described later) and therefore for the particular analysis in this thesis, the PHOENICS commercial CFD package (CHAM 2004) is used in addition to the existing program.

Chapter 1 pointed out that the coupling of the ES and CFD programs takes place at the surfaces of simulation domains. Therefore, it is critical that CFD models accurately calculate the convective heat transfer on the envelope surfaces. Consequently, the focus of this chapter, besides the coupling interface, is the modification of the CFD0 program by implementation of newly developed convection correlations. The aim of this undertaking was to accurately calculate the surface convective heat flux. An understanding of the CFD's theoretical fundamentals is necessary in order to explore these issues. Therefore, Section 4.2 provides the conceptual basis of CFD programs, used numerical models, and the relevant equation solver. Readers interested only in new models for thermal boundary condition calculations in the CFD program can directly go to Section 3.4. This section provides information about the implementation of experiment-based convection correlations in CFD. Section 4.5 shows the validation of these new models for thermal boundaries in CFD. Finally, Section 4.6 concludes the chapter with a discussion and summary.

4.2 Fundamentals of CFD Programs

Indoor airflow is a nearly incompressible turbulent flow of Newtonian fluids. The Navier-Stokes equations (continuity and momentum) and energy and concentration transport equations describe this airflow. Detailed forms of these equations can be found in the literature (Versteeg and Malalaskera 1995). As described in Chapter 2, the modeling of turbulent indoor air flow by Reynolds Averaged Navier-Stokes (RANS) equations is still a necessary alternative to the computationally expensive Direct Numerical Simulation (DNS) of the Navier-Stokes equations. Therefore, this section describes the solution procedures of the RANS equations in CFD programs.

4.2.1 RANS Equations, Turbulent Models, and Boundary Conditions

By decomposing instantaneous variables ($\tilde{\phi} = \phi + \phi'$) to their mean ($\phi$) and fluctuating ($\phi'$) components in the governing Navier-Stokes equations and time averaging of these equations, the next forms of the RANS equations are obtained for the conservation of:

Continuity:

$$\frac{\partial \rho u_i}{\partial x_i} = 0 \tag{4.1}$$

Momentum:

$$\frac{\partial \rho u_i}{\partial \tau} + \frac{\partial \rho u_i u_j}{\partial x_j} = \frac{\partial p}{\partial x_i} + \frac{\partial}{\partial x_j}\left[\mu\left(\frac{\partial u_i}{\partial x_j} + \frac{\partial u_j}{\partial x_i}\right) - \rho\,\overline{u_i' u_j'}\right] + \rho\beta(T_0 - T)g_i \tag{4.2}$$

Energy:

$$\frac{\partial \rho\, T}{\partial \tau} + \frac{\partial \rho u_j T}{\partial x_j} = \frac{\partial}{\partial x_j}\left[\frac{\mu}{\mathrm{Pr}}\frac{\partial T}{\partial x_j} - \rho\,\overline{u_j' T'}\right] + S_t \tag{4.3}$$

Concentration:

$$\frac{\partial \rho\, c}{\partial \tau} + \frac{\partial \rho u_j c}{\partial x_j} = \frac{\partial}{\partial x_j}\left[\frac{\mu}{Sc}\frac{\partial c}{\partial x_j} - \rho\,\overline{u_j' c'}\right] + S \tag{4.4}$$

These equations determine the mean values of pressure (p), component velocity (u_i i =1, 2, 3), temperature (T), and concentration (c) using air density (ρ), air viscosity (μ), Prandtl number (Pr), Schmidt number (Sc), and specific capacity (c_p). The term $\rho\beta(T_0 - T)g_i$ is the Boussinesq

model for the effect of thermal buoyancy on momentum. The coefficient β is the thermal expansion coefficient of air, 'g' is the gravitational acceleration, and 'T_0' is the reference temperature. The source terms for energy and concentration are S_t and S respectively.

Terms such as Reynolds stresses ($\rho\ \overline{u_i' u_j'}$) and scalar fluxes ($\rho\ \overline{u_j' t'}$, $\rho\ \overline{u_j' c'}$) are modeled using the Eddy Viscosity Hypothesis (Rodi 1993). This hypothesis assumes that Reynolds stresses are proportional to the mean strain-rate, and the coefficient of proportionality is the turbulent (eddy) viscosity (μ_t). This is expressed as follows:

$$-\rho\ \overline{u_i' u_j'} = \mu_t \left(\frac{\partial u_i}{\partial x_j} + \frac{\partial u_j}{\partial x_i} \right) - \frac{2}{3} \delta_{ij} \rho k \tag{4.5}$$

The coefficient δ_{ij} is the Kronecker delta and 'k' is the turbulent kinetic energy: $k = (\overline{u_i u_i} / 2)$.

The scalar fluxes, such as turbulent heat and concentration fluxes are approximated as additional diffusion caused by turbulence (eddy-diffusivity). This is given as follows:

$$-\rho\ \overline{u_i' T'} = \Gamma_{temp,t} \frac{\partial t}{\partial x_j} \tag{4.6}$$

$$-\rho\ \overline{u_i' c'} = \Gamma_{con,t} \frac{\partial c}{\partial x_j} \tag{4.7}$$

$\Gamma_{temp,t} = \mu_t / \mathrm{Pr}_t$ and $\Gamma_{con,t} = \mu_t / Sc_t$ are the turbulent diffusion coefficients for heat and mass respectively. The parameter Pr_t is the turbulent Prandtl number, and Sc_t is the turbulent Schmidt number.

Substituting (4.5), (4.6), and (4.7) into (4.2), (4.3), and (4.4), the final forms of the RANS equations are obtained:

- Continuity:

$$\frac{\partial \rho u_i}{\partial x_i} = 0 \tag{4.8}$$

- Momentum:

$$\frac{\partial \rho u_i}{\partial \tau} + \frac{\partial \rho u_i u_j}{\partial x_j} = \frac{\partial p}{\partial x_i} + \frac{\partial}{\partial x_j}\left[\mu_{eff}\left(\frac{\partial u_i}{\partial x_j} + \frac{\partial u_j}{\partial x_i}\right)\right] + \rho\beta(T_0 - T)g_i \tag{4.9}$$

- Energy:

$$\frac{\partial \rho\ T}{\partial \tau} + \frac{\partial \rho u_j T}{\partial x_j} = \frac{\partial}{\partial x_j}\left[\Gamma_{temp,eff}\ \frac{\partial T}{\partial x_j}\right] + \frac{q}{c_p} \tag{4.10}$$

- Concentration:

$$\frac{\partial \rho\ c}{\partial \tau} + \frac{\partial \rho u_j c}{\partial x_j} = \frac{\partial}{\partial x_j}\left[\Gamma_{con,eff}\ \frac{\partial c}{\partial x_j}\right] + \rho C_s \tag{4.11}$$

The influence of turbulence is integrated into the effective viscosity as the sum of the turbulent and laminar viscosity $\mu_{eff} = \mu_t + \mu$. The effective diffusion coefficient for heat (temperature) is proportional to the effective viscosity $\Gamma_{temp,eff} = \mu_{eff} / \mathrm{Pr}_{eff}$ since the eddy mixing is a source of turbulent diffusivity ($\Gamma_{temp,eff} = \mu / \mathrm{Pr} + \mu_t / \mathrm{Pr}_t$). The same relation holds for the effective diffusion coefficient for mass (concentration). This is given as: $\Gamma_{con,eff} = \mu_{eff} / Sc_{eff} = \mu / Sc + \mu_t / Sc_t$.

Zero Equation Turbulence Model

The zero-equation turbulence models are eddy viscosity models in which the turbulent viscosity is represented by an algebraic equation. These models use a fixed value for the eddy viscosity or relate it to the mean-velocity distribution. In 1925, Prandtl (Rodi 1993) provided the basis for zero-equation models by introducing the mixing-length hypothesis. Forming an analogy with the molecular transport of momentum, Prandtl postulated the mixing-length hypothesis in the following form:

$$\mu_t = \rho \cdot l_{mix}^2 \left|\frac{du}{dy}\right| \tag{4.12}$$

where l_{mix} is the mixing length, ρ is the fluid density, and u is the average velocity.

The mixing length is a characteristic property of the flow field. The product of the mixing length and the velocity gradient is called the mixing velocity. This is also a property of turbulent flows. Prandtl (Rodi 1993) assumed that the mixing length near solid surfaces is proportional to the distance from the surface. This approximation gives good results for a certain class of

turbulent boundary layers such as free shear flows. However, calibration of the mixing length is always needed for complex flows (Wilcox 1993).

Considerable effort has been made to extend the applicability of the mixing length model (Rodi 1993). An example is a research project conducted by Chen and Xu (1998) who developed zero equation models for room airflows which are primarily buoyancy-driven flows. As the basis for this new model, they used the Prandtl-Kolmogorov assumption, which states that the turbulent viscosity is the product of turbulent kinetic energy (*k*) and length scale for turbulence interactions (l). This is given as follows:

$$\mu_t = C_v \cdot \rho \cdot k^{1/2} l \tag{4.13}$$

The coefficient $C_v = 0.5478$ is an empirical constant. Chen and Xu (1998) introduced additional assumptions related to turbulent kinetic energy using the relation between kinetic energy turbulence intensity T_i and mean airflow velocity *'u'*. This is given as:

$$T_i = \frac{\sqrt{\overline{u_i^2}}}{u} = \frac{\sqrt{2k}}{u} \tag{4.14}$$

Chen and Xu assumed a uniform turbulence intensity and derived an algebraic function to express the turbulent viscosity as a function of the local mean velocity (U) and length scale (l). This is given as follows:

$$\mu_t = 0.5487 \rho \frac{T_i u}{\sqrt{2}} l \tag{4.15}$$

Substituting $T_i = 0.1$, the final form of the new empirical zero equation model is obtained:

$$\mu_t = 0.03874 \rho u l \tag{4.16}$$

The empirical constant (0.03874) is a universal value for different room airflows. The length scale *(l)* is the distance to the closest surface of the enclosure and *u* is the local velocity.

The assumption, that the turbulence intensity for indoor airflow is uniform is a good estimate for the occupied zone and mixing ventilation. However, this assumption can differ considerably from reality in the jet region. To evaluate model performance, Chen and Xu (1998) presented simulation results for four room airflows with mostly two dimensional airflows. The

results showed good agreements between the zero-equation model predictions and the experimental data. Srebric et al. (1999) provided further validation of this turbulent model for three dimensional cases. They compared the zero-equation model's predictions to experimental data for three cases of room airflow: natural convection with infiltration, forced convection, and mixed convection with displacement ventilation. This second validation study found good agreements between the calculated and measured values for air velocity and temperature distribution.

k-ε turbulence model

Another approach to model turbulent viscosity is the use of two additional transport equations that model *turbulence kinetic energy (k*) and the *dissipation rate of turbulence energy* (ε). With this model, the turbulent viscosity is evaluated without assumptions regarding length scale. This is given as follows:

$$\mu_t = \rho C_\mu \frac{k^2}{\varepsilon} \tag{4.17}$$

The coefficient $C_\mu = 0.09$ is an empirical constant.

The equations that calculate local distributions of k and ε are derived from the Navier-Stokes equations (Rodi 1993). The following are equations for kinetic and turbulence energy:

Turbulence kinetic energy:

$$\frac{\partial \rho k}{\partial \tau} + \frac{\partial \rho u_i k}{\partial x_j} = \frac{\partial}{\partial x_j}\left(\mu_{eff} \frac{\partial k}{\partial x_j}\right) + \mu_t \frac{\partial u_i}{\partial x_j} \cdot \left(\frac{\partial u_i}{\partial x_j} + \frac{\partial u_j}{\partial x_i}\right) - \rho\varepsilon - g\beta \frac{\mu_t}{\mathrm{Pr}_t} \frac{\partial T}{\partial x_i} \tag{4.18}$$

Dissipation rate of turbulence energy:

$$\frac{\partial \rho \varepsilon}{\partial \tau} + \frac{\partial \rho u_i \varepsilon}{\partial x_j} = \frac{\partial}{\partial x_j}\left(\mu_{eff} \frac{\partial \varepsilon}{\partial x_j}\right) + C_1 \frac{\varepsilon}{k} \mu_t \frac{\partial u_i}{\partial x_j} \cdot \left(\frac{\partial u_i}{\partial x_j} + \frac{\partial u_j}{\partial x_i}\right) - C_2 \rho \frac{\varepsilon^2}{k} - C_1 \frac{\varepsilon}{k} g\beta \frac{\mu_t}{\mathrm{Pr}_t} \frac{\partial T}{\partial x_i} \tag{4.19}$$

Empirical constants σ_k, σ_ε, C_1, and C_2 are experimentally determined for certain types of flow.

There are many variations of the k - ε model depending on the values of the empirical constants and modifications of terms in equations (4.18) and (4.19). Chen (1995) evaluated the performance of five k-ε models: the standard k-ε model (Launder and Spalding 1974), a low-Reynolds-number k-ε model, a two-layer k-ε model, a two-scale k-ε model, and a renormalization

group (RNG) k-ε model. The results from the RNG k-ε model were slightly better than the other k-ε model. Therefore, this particular modification of the k-ε model is used in this thesis for certain analyses.

The RNG k-ε model is used in analyses related to contaminant dispersion. These results are presented in Chapter 9. In these analyses, the PHOENICS CFD software is used because the current version of the CFD0 program has concentration models that have not been validated at the present time. However, for the development of the coupled ES and CFD programs, concentration is not needed because the concentration equation (4.11) is decoupled from the rest of the RANS equations. Therefore, the CFD0 program with the zero equation turbulence model, is used in new boundary conditions development and coupling analyses. The zero equation turbulence model (4.16) considerably reduces the calculation time when compared to the RNG k-ε model because equations (4.18) and (4.19) are not solved (Srebric 2000).

Table 4.1 Variables constants and sources for the general transport equation (4.20)

ϕ	Γ_ϕ	S_ϕ
1	0	0
u_i	$\mu + \mu_t$	$-\partial p / \partial x_i - \rho g_i \beta (T - T_0)$
k	$\mu + \mu_t / \sigma_k$	$G - \rho\varepsilon - G_b$
ε	$\mu + \mu_t / \sigma_\varepsilon$	$(C_{\varepsilon 1} G - C_{\varepsilon 2}\rho\varepsilon - C_{\varepsilon 3} G_b)\varepsilon / k + R$
t	$\mu / \mathrm{Pr} + \mu_t / \mathrm{Pr}_\varepsilon$	S_t
c	$\mu / Sc + \mu_t / Sc_\varepsilon$	S_c

μ - Laminar viscosity

$\mu_t = \rho C_\mu \frac{k^2}{\varepsilon}$ -Turbulent viscosity

$G = \mu_t \frac{\partial u_i}{\partial x_j}\left(\frac{\partial u_i}{\partial x_j} + \frac{\partial u_j}{\partial x_i}\right)$ - Turbulent production

$G_B = -g_i \beta \frac{\mu_t}{\mathrm{Pr}_t}\frac{\partial T}{\partial x_i}$ - Turbulent production due to buoyancy

$R = \frac{C_\mu \eta^3 (1 - \eta/\eta_0)}{1 + \beta\eta^3}\frac{\varepsilon^2}{k}$ - Source term from renormalization (only with RNG model)

$\eta = S\frac{k}{\varepsilon}$, $\mathrm{S} = (2\mathrm{S_{ij}}\,\mathrm{S_{ij}})^{1/2}$, $S_{ij} = \frac{1}{2}\left(\frac{\partial u_i}{\partial x_j} + \frac{\partial u_j}{\partial x_i}\right)$, $\eta_0 = 4.38$, $\beta = 0.012$

$\mathrm{C}_\mu = 0.0845$, $\mathrm{C}_{\varepsilon 1} = 1.42$, $\mathrm{C}_{\varepsilon 2} = 1.68$, $\mathrm{C}_{\varepsilon 3} = 1$ -Model constants

$\mathrm{Pr} = 0.71$, $\mathrm{Pr}_t = 0.9$, $\sigma_\mathrm{k} = 0.7194$, $\sigma_\varepsilon = 0.7194$, $Sc = 1$, $Sc_t = 1$ - Prandtl and Schmidt

The transport equations (4.8-4.11, 4.18, and 4.19) can be written in a general form using a general variable (ϕ) as follows:

$$\frac{\partial}{\partial \tau}(\rho\phi) + \frac{\partial}{\partial x_j}(\rho u_j \phi) = \frac{\partial}{\partial x_j}(\Gamma_\phi \frac{\partial \phi}{\partial x_j}) + S_\phi \tag{4.20}$$

This general transport equation has transient, advection, diffusion and source terms. Table 4.1 shows the variables, constants and sources. In the case of the zero equation model, the equations for k and ε are not used and the turbulent viscosity is solved by equation (4.16).

Boundary Conditions

Inlet boundary conditions are defined by inlet velocity, temperature, concentration, and 'k' and 'ε' in the case of the two equation turbulent model. Outlet boundary conditions are defined by outlet pressure and by zero gradients to the outlet surface for all other variables. The no-slip condition is applied for the velocity components on solid surfaces. The velocity in the vicinity of the surface is defined by components parallel to the surfaces. Considering the momentum equation along the wall, the shear force at the wall is given by:

$$F_{wall} = A_{wall} \cdot \tau_{wall} \tag{4.21}$$

where τ_{wall} presents shear stress:

$$\tau_{wall} = \mu_{eff} \frac{\partial u_P}{\partial y_P} \tag{4.22}$$

For the zero equation turbulence model, Chen and Xu (1998) provided simplified boundary conditions. For shear stress, they used the form that describes a linear sub layer (Figure 4.1) that is used for laminar flow. The only difference is that instead laminar viscosity, this model uses turbulent viscosity which is defined by the zero equation model.

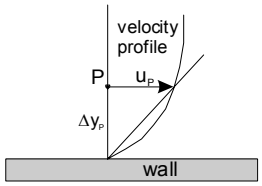

Figure 4.1 Velocity distribution on a surface

Convective heat transfer is defined by the temperature difference between the air in the vicinity of the surface (T_P) and surface temperature (T_{wall}) as follows:

$$q_{wall} = h(T_P - T_{wall}) \tag{4.23}$$

The local convection coefficient (h) is defined by effective diffusivity ($\Gamma_{temp,eff}$) as follows:

$$h = \Gamma_{temp,eff} \frac{c_p}{\Delta y_P} \tag{4.24}$$

These simplified boundary conditions are grid dependent and, therefore, inaccurate, especially for buoyancy-driven flows (Beausoleil 2000). The reason for the good agreement between experimental and numerical results during the validation of the zero equation models by Srebric et al. (1999) is that convective heat fluxes (q_{wall}) on surfaces are provided based on experimental measurements.

Boundary conditions models that use log-low wall functions have slightly better accuracy. This model is typically used with k-ε models. The previously described RNG k-ε model is valid for high Reynolds number turbulent flows. Therefore, wall functions are needed for the region near walls where the Reynolds number is low. The wall functions asume a velocity distribution near a solid wall. This velocity profile is usually described by dimensionless velocity (u^+) and dimensionless distance from the wall (y^+) for several regions of the boundary layer. These are given as follows:

- Laminar sub-layer: $u^+ = y^+$ for $0 < y+ \leq 5$ (4.25)

- Log-law layer: $u^+ = 1/\kappa \cdot \ln(Ey^+)$ for $30 < y+ \leq 500$ (4.26)

The $\kappa = 0.41$ is the Karman constant and $E = 9.8$ is an integration constant. The layer closest to the wall (laminar sub-layer) has dominant viscous forces, while the log-law layer are dominant turbulent forces. In-between these, lies the buffer zone where viscous forces and Reynolds stresses have the same order of magnitude. Depending on the position of first grid cell (adjacent to the wall) in boundary layer, the wall function algorithm selects an appropriate equation and

calculates τ_{wall} and q_{wall} based on local velocity, temperature, and kinetic energy. Details about the calculation of τ_{wall} and q_{wall} are provided in the literature (Versteeg and Malalaskera 1995).

Similar to simplified boundary conditions, log-law wall functions are grid-dependent (Chen and Jiang 1992). Generally, the log-law wall functions under-predict the heat flux on building surfaces. Depending on grid size in the vicinity of the surface convective heat flux might be several times smaller/larger. Log-law wall functions are good for boundary condition calculations only on surfaces where the Grashof-Reynolds ratio $Gr/Re^2 \ll 1$ and the turbulent-laminar viscosity ratio: $\mu_t/\mu > 30$ (Beausoleil 2000). This means that the log-law wall functions are applicable only on surfaces of the room that are in the vicinity of the supply diffuser, where the air velocity is large. Therefore, in this thesis neither simplified boundary conditions (used with new zero equation model) nor log-law wall functions are used for the calculation of thermal boundary conditions. Instead, experiment-based convection correlations are used. Details about these correlations are provided in Section 4.3.

4.2.2 Numerical Discretization

The RANS equations (4.1-4.4) create a non-linear system of equations. The diffusion term in the general transport equation (4.20) is a non-linear term. Also, the RANS equations are connected because of three reasons. First, each momentum equation contains all three velocity components; second, temperature appears in the momentum equation; and third, the energy equation contains the velocity components. Therefore, these equations can be solved analytically only for simple problems.

In order to use the numerical method, room air, which is the simulation domain of CFD program, needs to be discretized. Discretization transforms the partial differential equations into a system of algebraic equations which describe conservations of mass, momentum, energy, concentration, kinetic energy, and dissipation for each cell of discretized space. Using the *finite volume* method, the room is divided into a finite number of volumes using a grid system (Figure 4.2). Variables are calculated at discrete points located at the centers of these finite volumes, with the exception of velocities that are solved at volume surfaces in order to solve the problems related to linking the pressure and velocity solutions (Versteeg and Malalasekera 1995).

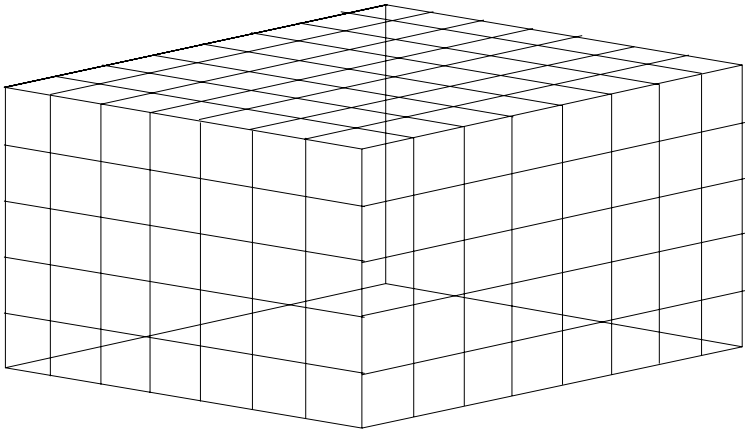

Figure 4.2 Finite-volume discretization of a room

Figure 4.3 shows finite volume P and its surrounding volumes (E, W, N, S, H, and L). The capital letters indicate solution points located at the centers of the finite volumes, while lower-case letters are used to mark the variable condition at the faces of the finite volume. In the case of an unsteady simulation, the variable value from a previous time stem ($P^{\tau-\Delta\tau}$) has an influence on the variable value in the considered time step (P^{τ}).

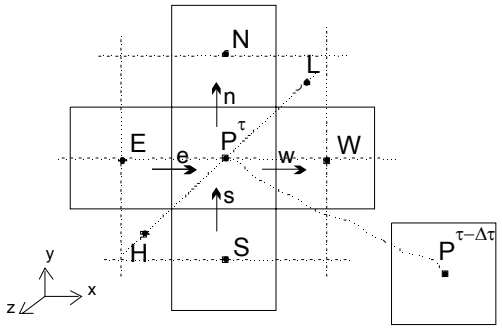

Figure 4.3 Finite volume discretization for upwind scheme

Integrating the general transport equation (4.20) over a control volume (cell) gives the following:

$$\int_V \frac{\partial}{\partial \tau}(\rho\phi)\ dV + \int_V \frac{\partial}{\partial x_j}(\rho u_j \phi)\ dV = \int_V \frac{\partial}{\partial x_j}(\Gamma_\phi \frac{\partial \phi}{\partial x_j})\ dV + \int_V S_\phi\ dV \qquad (4.27)$$

Each term in equation (4.27) is integrated separately:

Integrating the transient term expresses an accumulation of variable ϕ in finite volume V_P during the time period $\Delta\tau$ gives the following:

$$\int_V \frac{\partial}{\partial \tau}(\rho\phi)\ dV = \rho\frac{\phi_P^{\tau} - \phi_P^{\tau-\Delta\tau}}{\Delta\tau}V_P \tag{4.28}$$

To integrate the non-linear advection term, Gauss' theorem is used for the transformation of the volume integral into a surface integral (4.29). To simplify the solution procedure of the non-linear system of equations, linearization of term $\rho u_j \phi$ is performed. Here, in the considered iteration step, the value for u_j is provided from the previous iteration step. More details about the iteration procedure and equation solver are provided in the next section.

$$\int_V \frac{\partial}{\partial x_j}(\rho u_j \phi)\ dV = \int_A [(\rho u\phi)_e - (\rho u\phi)_w]dydz + \int_A [(\rho v\phi)_n - (\rho v\phi)_s]dxdz + \int_A [(\rho w\phi)_h - (\rho w\phi)_l]dxdy = \tag{4.29}$$
$$(\rho u\phi A)_e - (\rho u\phi A)_w + (\rho v\phi A)_n - (\rho v\phi A)_s + (\rho w\phi A)_h - (\rho w\phi A)_l = F_e\phi_e - F_w\phi_w + F_n\phi_n - F_s\phi_s + F_h\phi_h - F_l\phi_l$$

Integrating the diffusion terms results in the equation (4.30) where D is the diffusive coefficient defined on cell surfaces.

$$\int_V \frac{\partial}{\partial x_j}(\Gamma_\phi \frac{\partial\phi}{\partial x_j})\ dV = \int_A \left[(\Gamma_\phi \frac{\partial\phi}{\partial x})_e - (\Gamma_\phi \frac{\partial\phi}{\partial x})_w\right]dydz + \int_A \left[(\Gamma_\phi \frac{\partial\phi}{\partial y})_n - (\Gamma_\phi \frac{\partial\phi}{\partial y})_s\right]dxdz + \int_A \left[(\Gamma_\phi \frac{\partial\phi}{\partial z})_h - (\Gamma_\phi \frac{\partial\phi}{\partial z})_l\right]dxdy \tag{4.30}$$
$$= D_e(\phi_E - \phi_P) - D_w(\phi_P - \phi_W) + D_n(\phi_N - \phi_P) - D_s(\phi_P - \phi_S) + D_h(\phi_H - \phi_P) - D_l(\phi_P - \phi_L)$$

Integrating the source term produces the source coefficient that is associated with the value of the considered variable (S_P) and free coefficient (S_C) as follows:

$$\int_V S_\phi\ dV = S_\phi = S_C + S_P\phi_P \tag{4.31}$$

Linearizing the equation for finite volume P results in the following algebraic expression:

$$\begin{aligned} a_P\phi_P &= a_E\phi_E + a_W\phi_W + a_N\phi_N + a_S\phi_S + a_H\phi_H + a_L\phi_L + S_C \\ a_P &= a_E + a_W + a_N + a_S + a_H + a_L + S_P \end{aligned} \tag{4.32}$$

Detailed expressions for the coefficients: a_P, a_E, a_N, a_S, a_H, and a_L are provided in Appendix G.

Solver

Discretization and linearization transform the complex linear and non-linear governing differential equations into a set of simple algebraic relations. The next step is to solve this algebraic system of equations. The iterative solution of the non-linear advection term (4.29) mentioned previously, requires an iterative procedure. Also, the pressure field does not have a general transport equation. Therefore the pressure source term in the momentum equations (refer to Table 4.1) must be calculated indirectly. The pressure is calculated by connecting the continuity equation with the momentum equations and creating a system of four equations with four unknowns. The buoyant source term that connects temperature with the momentum equations is calculated based on temperature values from the previous iteration step.

The calculation procedure used in the CFD0 and Phoenics programs uses a variation of the Semi-Implicit Method for the Pressure-Linked Equations (SIMPLE) algorithm (Patankar and Spalding 1972). This method is a variation of the predictor-corrector iterative procedures for calculating the pressure field. The solution procedure starts with an initial estimate for pressure, velocities, turbulent parameters, temperature and concentration. Then, the estimated pressure (p^*) is used to calculate velocity components (u^*) from the momentum equations. Next, the pressure is corrected in such a way that the velocities satisfy the continuity equation. The correct pressure, (p) is linked to the pressure correction term (p'). This is illustrated as follows:

$$p' = p - p^* \tag{4.33}$$

Since the velocity field is calculated using estimated pressures, a velocity-correction term is given as:

$$u' = u - u^* \quad , \quad v' = v - v^* \quad , \quad w' = w - w^* \tag{4.34}$$

Using the assumption related to the SIMPLER modification of the SIMPLE algorithm (Versteeg and Malalasekera 1995), the relation between the velocity and pressure is given as:

$$u'_e = \frac{A_e}{a_P - \sum a_{nb}} (p_P - p_e) \tag{4.35}$$

where a_P is given by equation (4.32) and $\sum a_{nb}$ is the sum of neighboring coefficients.

Substituting the velocity correction into the mass continuity equation gives the pressure correction equation in the same form as the general transport equation. This is given as follows:

$$a_P p'_P = \sum a_{nb} p'_{nb} + S_C \tag{4.36}$$

The coefficient S_C is the source term and represents the continuity imbalance because of the incorrect velocity field ($S_C = m_e - m_w + m_n - m_s + m_h - m_l$ where 'm' is the mass flow in mass continuity equation).

Knowing the pressure correction p', values for the corrected pressure field p are calculated. Then, the velocity corrections (equation 4.34) and velocity components are solved accordingly. Finally, based on pressure and velocity fields, other scalar variables are calculated for the considered iteration step.

Iterative solution procedures can be unstable because of the non-linearity of advection terms in the transport equations (4.20). To control the rate of change for considered variables, linear and false-time step relaxation methods are used. Both relaxation methods control the change of variables during the iteration procedure. In this way, numerical instability is reduced.

The linear relaxation is based on a modification of the calculated variable (ϕ^n) by the value of the variable calculated in previous iteration step (ϕ^{n-1}). This is illustrated as follows:

$$\phi^{new} = f \cdot \phi^n + (1 - f)\phi^{n-1} \tag{4.37}$$

The coefficient f is the linear relaxation factor (value in-between 0 and 1) and ϕ^{new} is the value of variable that is used in next calculation step.

The false time step relaxation has the same form as the transient term given by Equation (4.28):

$$\rho \frac{\phi^n - \phi^{n-1}}{\Delta \tau_F} V_{cell} \tag{4.38}$$

The coefficient $\Delta \tau_F$ is the false time step relaxation factor. This term is added to both sides of the general transport equation as the source term. In this way, the false time step relaxation does not affect the final solution. Small values for $\Delta \tau_F$ increase the term as illustrated in equation (4.38). This "ballast" on left and right side of general transport equation slows down the solution procedure, but prevents the propagation of the instability caused by large variations of the calculated variables during the iteration procedure. Large values for $\Delta \tau_F$ speed up the calculation procedure but increase instability of the iterative solution procedure.

The SIMPLE method and its variations are not the only methods for solving coupled non-linear equations (RANS equations). There is another solution method which uses sparse linear system solvers like the one that the BES program uses, instead of the iterative procedure. With this method, the equations (4.8-4.11, 4.18, and 4.19) are structured for a Newton iterative method. After calculating the underlying Jacobian matrix, the appropriate linear sparse system solver is used. This method became more popular recently. However, available CFD programs (CFD0, PHOENICS, and FLUENT) use semi-implicit methods (SIMPLE). Therefore, these methods are considered in this thesis.

4.3 Improvement of CFD Program for Indoor Air-flow Calculation

As discussed previously, wall functions cannot accurately predict thermal boundary conditions on surfaces in buildings, with the exception of cases involving forced convection. Therefore, this section describes a new method for the calculation of thermal boundary conditions in CFD and provides a validation of this method.

4.3.1 Modification of Adaptive Convection Algorithm

Since wall functions cannot accurately calculate convective heat fluxes at surfaces in buildings, calculation of these fluxes by experiment-based correlations is still more reliable than by the wall functions. This section will discuss in detail the implementation of experimental models for the calculation of convective heat transfer in CFD programs. Chapter 2 discussed details about previous research in this direction, while this section presents the modifications and further developments of existing experiment-based convection models used in CFD programs.

The "Adaptive Convection Algorithm" (ACA) and Adaptive Conflation Controller (ACC), that were developed by Beausoleil (2000, 2001), use both experimental convection correlations and wall-function models to calculate surface heat fluxes. In this thesis, ACA is further developed to be used for the calculation of surface heat fluxes in the CFD domain, based solely on experiment-based convection correlations. This Modified Adaptive Convection Algorithm (MACA) operates in the near-wall region using reference air temperature, Dirichlet boundary conditions, and a system of experiment-based convection correlations.

MACA selects an appropriate convection correlation model based on room geometry, type of airflow, position of the HVAC device in the room, and condition of the HVAC device (i.e. on/off). The convection coefficient (h) is calculated based on characteristic length, surface temperature and reference air temperature. Depending on which convection correlation is selected, the reference air temperature can be local air temperature, room air temperature, supply temperature, or exhaust temperature (refer to Figure 4.4). Precise definition of the reference temperature is important because it is used in the CFD program for calculation of convective heat fluxes at the surfaces.

4.3.2 Calculation of Reference Temperatures

Depending on the air mixing in the room, temperatures of the room differ more or less from exhaust temperatures. Only in the case of perfect mixing, these two temperatures are the same. The room air temperature is defined as the temperature in the central part of the room that is usually the occupied part of that space. In MACA, room air temperature ($T_{room\ air}$) is calculated as mass-averaged air temperature of the space, excluding zones near surfaces. More precisely, the finite volumes (cells) in zones 0.1 m from surfaces are excluded to prevent that the local air temperatures in boundary layers (and near them) affect the calculation of room air temperature defined as the temperature in central part of the room.

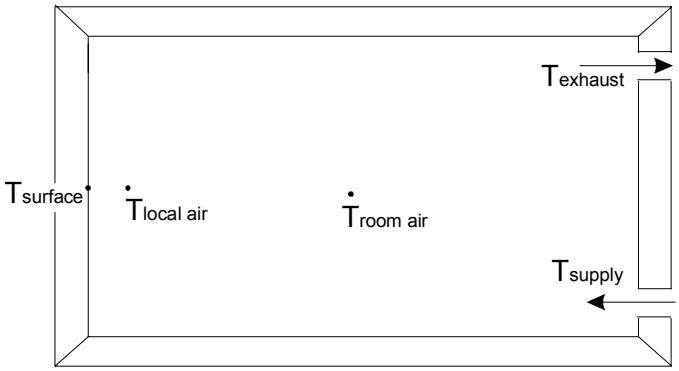

Figure 4.4 Reference temperatures used in MACA for convective heat flux calculations in a CFD program

Local air temperature is defined as temperature in the vicinity of the surface, but outside the surface boundary layer. Inside the boundary layer, temperature and velocity profiles change dramatically and therefore local temperature is defined as temperature on the outer side of boundary layer. In order to calculate the local air temperature, the thickness of the boundary layer (δ) should be defined. Boundary layer thickness is always larger with natural convection than with forced convection. Therefore, this thickness is used to determine the air layer that defines the local air temperature. For vertical surfaces, the temperature profile in the boundary layer is based on the velocity profile (refer to Figure 4.5).

Using Karman's method (Luikov 1980), the ratio between boundary layer thickness (δ) and surface height (z) can be approximated as:

$$\frac{\delta}{z} = 3.93 \cdot \mathrm{Pr}^{-0.5} \cdot (0.925 + \mathrm{Pr})^{0.25} \cdot (Gr_Z)^{-0.25} \tag{4.39}$$

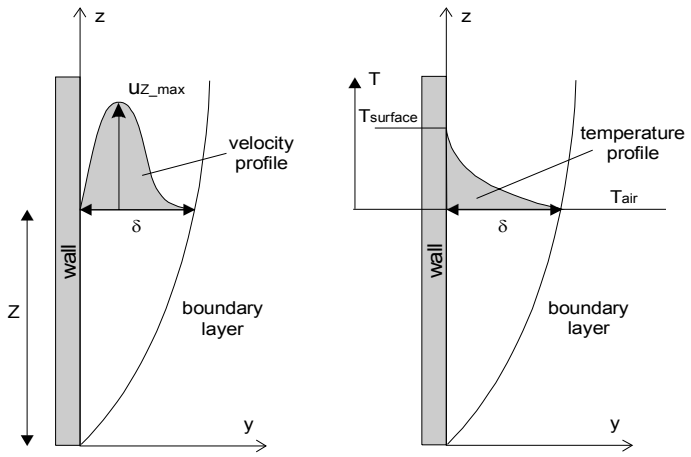

Figure 4.5 Velocity and temperature distributions in the boundary layer on a vertical room surfaces

where Prandtl *(Pr)* and Grashof *(Gr)* numbers are defined for temperatures of the surface and the air outside the boundary layer. As the difference between these temperatures *(ΔT)* increases, δ decreases because a larger velocity "brings" the boundary layer closer to the wall. For a standard room height of 2.5 m and ΔT =2 °C, the corresponding boundary layer thickness is 0.05 m. For an extreme height of 5 m and very small ΔT = 0.3 °C, the corresponding thickness is 0.09 m. Therefore, the boundary layer for vertical surfaces in rooms is rarely thicker than 0.1 m. Based on this, MACA defines the local air temperature for horizontal surfaces as the mass-averaged temperature for the parallel air layer that is 0.1 m away from the surface and has a thickness of 0.1 m (refer to Figure 4.6).

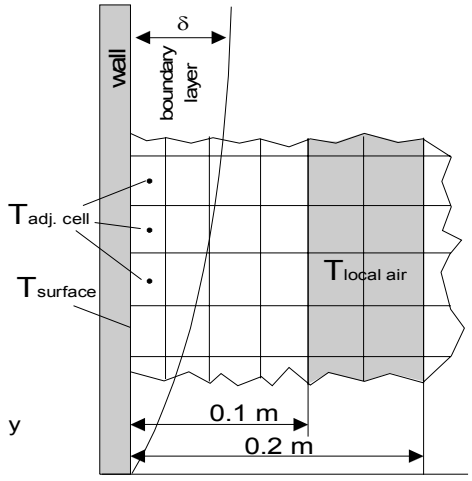

Figure 4.6 Local temperature calculations for vertical surfaces

For horizontal surfaces, the thickness of the boundary layer is not precisely defined. It depends on the type of flow that is usually either buoyant or stably stratified (Figure 4.7). With

buoyant boundary airflow, warm fluids have a tendency to go upward, thus leaving space for incoming cold fluids. With stably stratified flow, the fluid is gravitationally stable and vertical air movement is more dominant than horizontal.

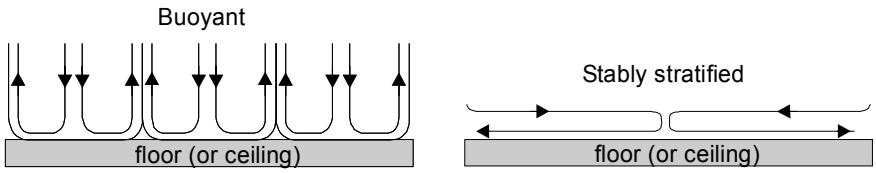

Figure 4.7 Boundary layers for horizontal room surfaces

Using equations similar to the ones for vertical surfaces (Luikov 1980), boundary layer thickness for horizontal surfaces is, in most cases, less than 0.1 m. Therefore, for horizontal surfaces, MACA calculates the local air temperature using a similar approach to that for vertical surfaces (Figure 4.6). Validity of application of these local temperatures in convection correlations at horizontal surfaces depends on the vertical temperature distribution. Local temperatures are defined by the reference temperature selection procedure.

The reference temperature is selected based on the convection correlation development method. For example, if the correlation is developed based on dimensionless analysis, the reference temperature is the local air temperature. For correlations where researchers, who developed a certain correlation, used a temperature sensor in the occupied zone to measure the air temperature, the reference temperature is the average temperature in the room. For correlations developed based on jet supply temperature, the reference temperature is the air supply temperature.

Selecting the reference temperature for horizontal surfaces requires a comparison between surface ($T_{surface}$) ,local air (T_{local_air}), and room air (T_{room_air}) temperatures. In the case where the air is totally stratified (Figure 4.8a), the temperature profile near floor surfaces is $T_{surface}<T_{local\_air}<T_{room\_air}$ (or for ceiling surfaces $T_{surface}>T_{local\_air}>T_{room\_air}$). For this totally stratified temperature distribution, the reference temperature is the room air temperature. Room air motion caused by downdraft, displacement ventilation, or hot surface thermal plume creates a "locally stratified" temperature distribution in the room. This slow air motion usually does not create forced convection but affects the local air temperature. In this case, temperature distribution is $T_{local\_air}<T_{surface}<T_{room\_air}$ (or $T_{local\_air}>T_{surface}>T_{room\_air}$) and heat transfer calculated based on $T_{surface}$ and T_{room_air} predicts inaccurately and often changes the direction of

heat flux (Figure 4.8b). Therefore, in cases with locally stratified temperature distributions, the reference temperature is the local air temperature.

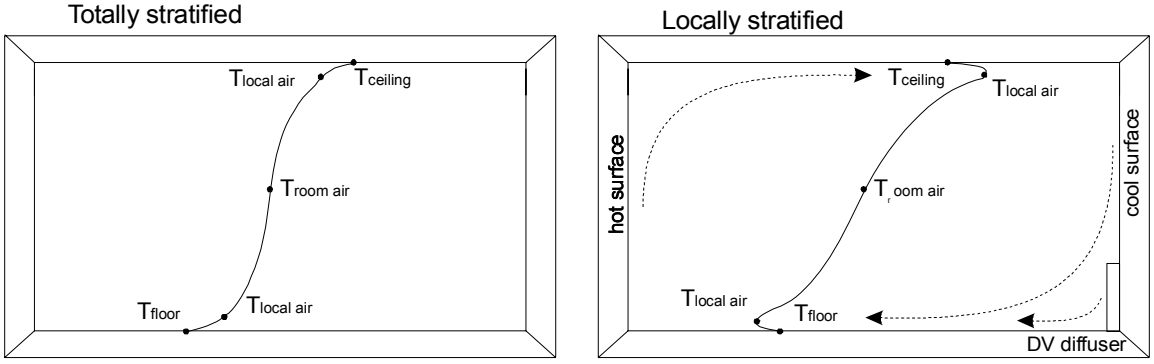

(a) (b)

Figure 4.8 Temperature profile for (a) totally and (b) locally strafed room air

4.3.3 Implementation of MACA into CFD

The Modified Adaptive Convection Algorithm (MACA) operates inside a CFD program during the iteration procedure. After each iteration step, MACA calculates reference temperatures based on the temperature distribution for the respective iteration step. Following this, the algorithm calculates convection coefficients (h_{MACA}) for all surfaces based on surface temperature and the appropriate reference temperatures. Finally, these new convection coefficients are used to provide the Dirichlet boundary conditions in the next iteration step.

CFD programs implement boundary conditions onto adjacent cells to the wall (Figure 4.6). Therefore, convection coefficients calculated by the MACA (h_{MACA}), which are based on reference temperatures ($T_{reference}$), need to be recalculated for use with the temperature of the adjacent cell layer ($T_{adj.cell}$). Taking into account the conservation of surface heat flux ($q_{surface}$):

$$q_{surface} = h_{MACA} \cdot (T_{surface} - T_{reference}) = h_{adj.cell} \cdot (T_{surface} - T_{adj.cell}) \tag{4.40}$$

the surface convection coefficient for adjacent cell layer ($h_{adj.cell}$) is calculated from the following expression:

$$h_{adj.cell} = \frac{h_{MACA} \cdot (T_{surface} - T_{reference})}{(T_{surface} - T_{adj.cell})} \tag{4.41}$$

This convection coefficient is the average value for the entire surface under consideration because the temperature of the adjacent cell layer ($T_{adj.cell}$) is obtained as the mass-average temperature of cells adjacent to the surface. The average surface convection coefficient $h_{adj.cell}$ is applied to each cell locally. Thus, non-uniform convective heat flux is obtained at surface because of use of Dirichlet boundary conditions that employ the local temperatures in these cells.

Convective heat fluxes calculated by MACA can be implemented into a CFD program using Neumann boundary conditions. This method is simpler than the Dirichlet method previously described because with Neumann boundary conditions $q_{surface}$ (Equation 4.40) is directly implemented into the source term of adjacent cells. However, method that employs the Neumann boundary condition is not used in MACA because it creates a constant average heat flux across the surface (Figure 4.9). With the used Dirichlet boundary conditions, local (for certain cell) heat flux is proportional to the local temperature difference, which is a better approximation of conditions in reality.

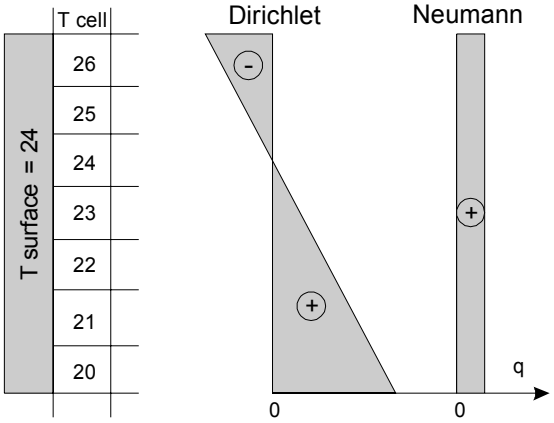

Figure 4.9 Surface heat flux distribution with Dirichlet and Neumann boundary conditions

4.3.4 Convection Correlations Implemented into MACA

The aim of convection correlations implemented into MACA is to encompass a wide range of room airflow regimes. All used correlations have a simple form where the convection coefficient is expressed as a function of temperature difference, characteristic length, and supply air flow rate. These correlations were developed by researchers using different methods. Therefore, besides the equation expressions, additional details are given for each group of correlations in order to provide information that is necessary to use them correctly. More elaborate analyses about many correlations used in MACA is provided by Beausoleil (2000).

Convection correlations developed by Alamdari and Hammond (1983) are based on collected experimental data (from different researchers) for isolated surfaces (surfaces which are not part of the room). Correlations are applicable for purely buoyant flows where the buoyancy is caused by a temperature difference between a surface and the surrounding room air. They are not good in cases where buoyancy is created by thermal devices such as a radiator, baseboard heater, or fan-coil. These correlations have laminar and turbulent terms and therefore are applicable to both laminar and turbulent flow regimes. They also cover the full range of temperatures and dimensions that appear in buildings.

Table 4.2 Alamdari and Hammond convection correlations

Surface type	Ventilation regime	Equation	h_c
Vertical	Natural convection (system is off)	1	$\left\{ \left[1.5 \cdot (\Delta T/H)^{1/4} \right]^6 + \left[1.23 \cdot (\Delta T)^{1/3} \right]^6 \right\}^{1/6}$
Floor ($T_{surface} > T_{air}$)		2	$\left\{ \left[1.4 \cdot (\Delta T/D_h)^{1/4} \right]^6 + \left[1.63 \cdot (\Delta T)^{1/3} \right]^6 \right\}^{1/6}$
Ceiling ($T_{surface} < T_{air}$)			
Floor ($T_{surface} < T_{air}$)		3	$0.6 \cdot (\Delta T/D_h)^{1/5}$
Ceiling ($T_{surface} > T_{air}$)			

Since these correlations are developed for isolated surfaces, local air temperatures should be used as reference temperatures for vertical and horizontal surfaces. These correlations are primarily used in MACA for calculating the convective heat fluxes when the ventilation system and/or terminal devices do not work.

Convection correlations developed by Khalifa (1989) are based on measurements in an experimental chamber with room sizes. These correlations are suitable for rooms with a strong buoyant flow created by radiators, baseboard heaters, warm walls, warm floors, and forced flow by circulating fan heaters. Two thermal-device placements are considered: on cold external walls and elsewhere. Convection correlations for vertical surfaces are defined for surfaces in the vicinity of a terminal device and for other surfaces.

Khalifa et al. (1989) used average room temperature as the reference temperature. Therefore, MACA uses room air temperature as the reference temperature when these correlations are selected.

Table 4.3 Khalifa convection correlations

Surface type	Ventilation regime	Equation	h_c
Vertical in the vicinity of terminal device	Buoyant with heater on internal surfaces	4	$1.98 \cdot \Delta T^{0.32}$
Vertical	Buoyant with heater on external surface	5	$2.3 \cdot \Delta T^{0.24}$
Vertical in the vicinity of terminal device	Forced by internal fan	6	$2.92 \cdot \Delta T^{0.25}$
Vertical (not in the vicinity of term. dev.)	Buoyant with heater on internal surfaces	7	$2.07 \cdot \Delta T^{0.23}$
	Forced by internal fan		
Ceiling	Buoyant with heater on external surface	8	$3.1 \cdot \Delta T^{0.17}$
Ceiling	Buoyant with heater on internal surfaces	9	$2.72 \cdot \Delta T^{0.13}$
	Forced by internal fan		

Convection correlations developed by Fisher (1995) are suitable for forced convection where the convection coefficients depend primarily on velocity in the vicinity of the surfaces. Therefore, these correlations are expressed as a function of supply air volume flow rate that affects the movement of the air in the vicinity of the room surfaces. Supply air volume flow rate is presented as Air Changes of supply air per Hour (ACH). These correlations are valid for a typical range of volume flow rates (3-12 ACH) where the air is supplied by wall diffusers. These correlations are primarily developed for cases where the supply temperature is lower than the room temperature (cooling). Fisher (1995) used supply air temperature for convection correlation development: $q_{surface}=h\cdot[T_{surface}-T_{supply}]$. Therefore, MACA, with these correlations, uses the supply air temperature as the reference temperature.

Table 4.4 Fisher convection correlations

Surface type	Ventilation regime	Equation	h_c
Vertical	Forced convection with wall diffuser (free jet)	10	$-0.11+0.132\cdot(ACH)^{0.8}$
Floor		11	$-0.704+0.168\cdot(ACH)^{0.8}$
Ceiling		12	$-0.064+0.0044\cdot(ACH)^{2.8}/\Delta T$

Convection correlations developed by Fisher and Pedersen (1997) are applicable to forced convection and work in similar conditions as the correlations developed by Fisher (1995). The main difference is the position of diffuser. These correlations are applicable in rooms with ceiling diffusers where the diffuser jet is attached to the ceiling surfaces. As with previous correlations, supply air temperature is used as the reference temperature.

Table 4.5 Fisher and Pedersen convection correlations

Surface type	Ventilation regime	Equation	h_c
Vertical	Forced convection with ceiling diffuser	13	$0.19 \cdot (ACH)^{0.8}$
Floor		14	$0.13 \cdot (ACH)^{0.8}$
Ceiling		15	$0.49 \cdot (ACH)^{0.8}$

Convection correlations developed by Awbi and Hatton (1999) are applicable to heated surfaces. The researchers performed experiments in two experimental chambers; first with a typical room size and second with a size that is considerably smaller. Therefore, these correlations are also a function of characteristic length. Since these correlations are developed for measured air temperatures at 0.1 m from the surfaces, MACA, with these correlations, uses local air temperature as the reference temperature.

Table 4.6 Awbi and Hatton convection correlations

Surface type	Ventilation regime	Equation	h_c
Walls	Buoyant with hated surface	16	$1.823 \cdot \Delta T^{0.293} / D_h^{0.121}$
Floor		17	$2.175 \cdot \Delta T^{0.308} / D_h^{0.076}$
Ceiling		18	$0.704 \cdot \Delta T^{0.133} / D_h^{0.601}$

Mixed convection - For the rooms with supply diffusers, natural and forced convection are very often present on the room surfaces at the same time. It is very difficult to predict whether natural or forced convection is predominant. Therefore, there is a need for mixed convection correlations. Mixing convection correlations developed by Beausoleil (2000) are implemented into MACA. These correlations are based on the Fisher and Pedersen correlations for forced convection and Alamdari and Hammond correlations for natural convection. These correlations

are used in the BES program and corresponding expressions are presented in Table 3.1 (refer to Section 3.2.2).

New convection correlations

The convection correlations presented above do not describe surface convection models for room airflow with displacement ventilation systems, radiant cooling panels, or high aspiration diffusers. Therefore, as a part of this thesis, convection correlations for specific surfaces with these ventilation systems were developed. The detailed development procedure and corresponding results are presented in Chapters 7 and 8. Tables 4.7 and 4.8 contain only expressions for these correlations.

The displacement ventilation diffuser creates specific air flow in the vicinity of the floor by creating low velocity jest attached to the floor. Therefore, new convection correlations are developed for floor surfaces (Equations 24 and 25 in Table 4.7). These correlations combine natural and forced convection. Correlations for natural convection are combined with newly developed terms for forced convection. For vertical surfaces and ceiling surfaces with a stable and stratified temperature distribution ($T_{surface} > T_{air}$) the existing correlations Awbi and Hatton are used (Equations 16 and 18 in Table 4.6). For ceiling surface with buoyant boundary conditions ($T_{surface} < T_{air}$) a new correlation is developed (Equation 28 in Table 4.7). This new convection correlation is primarily developed for the cooling radiant panel surfaces. In addition, it is also valid for any other ceiling surface with buoyant boundary conditions.

Table 4.7 Correlations for ventilation with displacement ventilation diffuser

Surface type	Equation	h_c
Floor ($T_{surface} > T_{air}$)	24	$\left[\left(2.175\cdot\Delta T^{0.308}/D_h^{0.076}\right)^6+\left(\frac{\lvert T_s-T_{supply}\rvert}{\Delta T}\cdot 0.48\cdot ACH^{0.8}\right)^6\right]^{1/6}$
Floor ($T_{surface} < T_{air}$)	25	$\left[\left(0.704\cdot\Delta T^{0.133}/D_h^{0.601}\right)^6+\left(\frac{\lvert T_s-T_{supply}\rvert}{\Delta T}\cdot 0.48\cdot ACH^{0.8}\right)^6\right]^{1/6}$
Vertical surfaces	26	$1.823\cdot\Delta T^{0.293}/D_h^{0.121}$
Ceiling ($T_{surface} > T_{air}$)	27	$0.704\cdot\Delta T^{0.133}/D_h^{0.601}$
Ceiling ($T_{surface} < T_{air}$)	28	$2.12\cdot\Delta T^{0.33}$

A high aspiration diffuser creates a considerably larger jet momentum of supply air than the standard ceiling and wall diffusers that were investigated by Fisher and Pedersen (1995 and 1997). Therefore, convection correlations from Tables 4.4 and 4.5 cannot be used with these diffusers. Newly developed convection correlations for these high aspiration diffusers are presented in Table 4.8. These new forced convection correlations are combined with existing and newly developed convection correlations for natural convection to get universal equations for mixed convection.

Table 4.8 Correlations for ventilation with high aspiration diffuser

Surface type	Equation	h_c
Floor ($T_{surface} > T_{air}$)	29	$\left[(2.175 \cdot \Delta T^{0.308} / D_h^{0.076})^3 + (0.96 \cdot ACH^{0.8})^3\right]^{1/3}$
Floor ($T_{surface} < T_{air}$)	30	$\left[(0.704 \cdot \Delta T^{0.133} / D_h^{0.601})^3 + (0.96 \cdot ACH^{0.8})^3\right]^{1/3}$
Vertical surfaces	31	$\left[(1.823 \cdot \Delta T^{0.293} / D_h^{0.121})^3 + (1.31 \cdot ACH^{0.8})^3\right]^{1/3}$
Ceiling ($T_{surface} > T_{air}$)	32	$\left[(2.12 \cdot \Delta T^{0.33})^3 + (1.19 \cdot ACH^{0.8})^3\right]^{1/3}$
Ceiling ($T_{surface} < T_{air}$)	33	$\left[(0.704 \cdot \Delta T^{0.133} / D_h^{0.601})^3 + (1.19 \cdot ACH^{0.8})^3\right]^{1/3}$

Newly developed convection in Table 4.7 and 4.8 use local air temperature as the reference temperature.

4.3.5 MACA Algorithm

A major purpose of MACA is to calculate the surface convection coefficient of the adjacent cell layer ($h_{adj.cell}$) for each surface in each iteration step. This calculation is based on surface temperature ($T_{surface}$), reference air temperature ($T_{reference}$), characteristic surface length (H or D_h), and/or supply air flow rate (ACH). The crucial facet is of the algorithm is the selection of the appropriate convection correlation for each surface. Based on parameters such as ventilation regime, system condition (on/off), and surface type, MACA selects an appropriate equation from 33 equations integrated into this algorithm (Figure 4.10). Type of airflow regime needs to be defined as input data by the user during the problem definition, while other two parameters are selected automatically during the CFD calculation procedure.

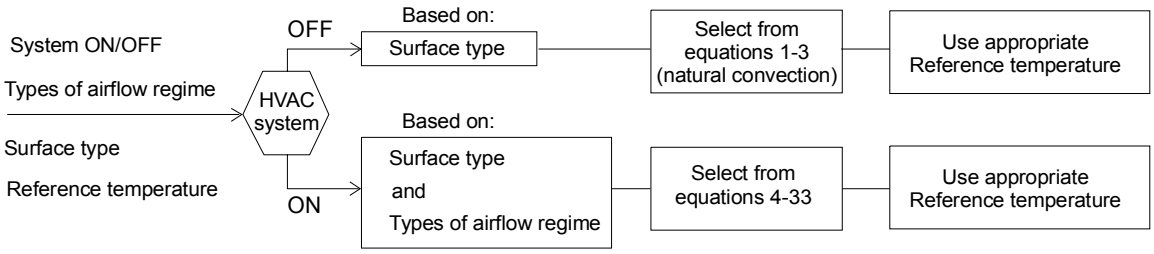

Figure 4.10 MACA algorithm

A ventilation regime describes the general airflow pattern that is expected in the room. It is strongly related to the HVAC system installed in the room. Therefore, this parameter is defined by the user when selecting the HVAC system. Based on the selected HVAC system and position of the terminal device (radiator, baseboard heater, fan coil, cooled radiant panels, and diffuser), the user select one of nine types of airflow regimes presented in Table 4.9. Short guidelines for this selection are also provided in this table. Based on the ventilation regime, MACA makes an appropriate selection from different convection correlations presented in Tables 4.2-4.8.

Table 4.9 Types of airflow regime

1 Forced convection with ceiling diffuser	Standard ceiling diffusers which attach a jet to ceiling surface. For rooms with large flow rate of supply air.
2 Forced convection with wall diffuser	Diffusers which provide free jet. For rooms with large flow rate of supply air.
3 Buoyant with hater on external surface	Heater is: radiator, baseboard heater, or any device attached to the external wall surface and creates strong buoyancy.
4 Buoyant with heater on internal surfaces	Heater is: radiator, baseboard heater, or any device attached to any internal wall and creates strong buoyancy.
5 Forced by internal fan	Terminal device that create air circulation - floor standing fan-coil unit or similar device.
6 Buoyant with heated surface	Heater is: panel attached to any internal surface and creates strong buoyancy. Also, god for sun patches.
8 Displacement ventilation diffuser	Diffuser that supply air at floor level at low velocity.
7 High Aspiration diffuser	Diffusers which provide high momentum with low flow rate. Diffuser attaches to ceiling and combines with cooling panels.
9 All natural convection	For rooms with natural ventilation without supply diffusers or internal fans.

System conditions define working conditions of the HVAC system. If the HVAC system is turned OFF, only natural convection is present in the room. In this case, equations for natural convection are used (Table 4.2). In the case where the HVAC system is turned ON, MACA selects a correlation based on the type of airflow regime. The parameter that defines the system condition is introduced primarily for an unsteady type of simulation when the system is turned ON or OFF. This is dependent on the working period of the system. This parameter is provided to MACA automatically by CDF0 program.

Surface type defines the position of the surface related to room geometry (wall, floor, or ceiling) and related to terminal device. This parameter primarily defines which correlation will be used in group of correlations selected by ventilation regime type. It is defined automatically based on room geometry data. Surface types implemented into MACA are provided in Table 4.10.

Table 4.10 Surface types

1 Vertical	All wall surfaces except surfaces on wall with terminal device
3 Floor	All surfaces on floor
5 Ceiling	All ceiling surfaces except cooling radiant panel surface
2 Vertical in the vicinity of terminal device	Surfaces on the wall adjacent to terminal device

Reference temperatures used in MACA are supply air temperature, local air temperature, and room air temperature. For each convection correlation, MACA uses the appropriate reference temperature that is determined based on the air temperature used in the correlation development procedure. To calculate convection correlations of horizontal surfaces that use room air temperature as a reference temperature, MACA automatically checks if stratification is total or local (Figure 4.8). In the case where stratification is local, the local air temperature is used as the reference temperature even if room air temperature is associated with an applied convection correlation.

4.4 Validation of MACA

Numerical results obtained by CFD simulations in which MACA was used for thermal boundary conditions calculation were compared with experimental results. Temperature distributions and convective heat fluxes at characteristic surfaces were compared for several complex indoor airflows. Measured surface temperatures were used as boundary conditions for the CFD program. In order to create a challenging airflow for CFD simulations, a Displacement Ventilation (DV) system was used as an air supply system in all validation experiments. This system created a non-uniform temperature distribution with strong stratification (Figure 4.11).

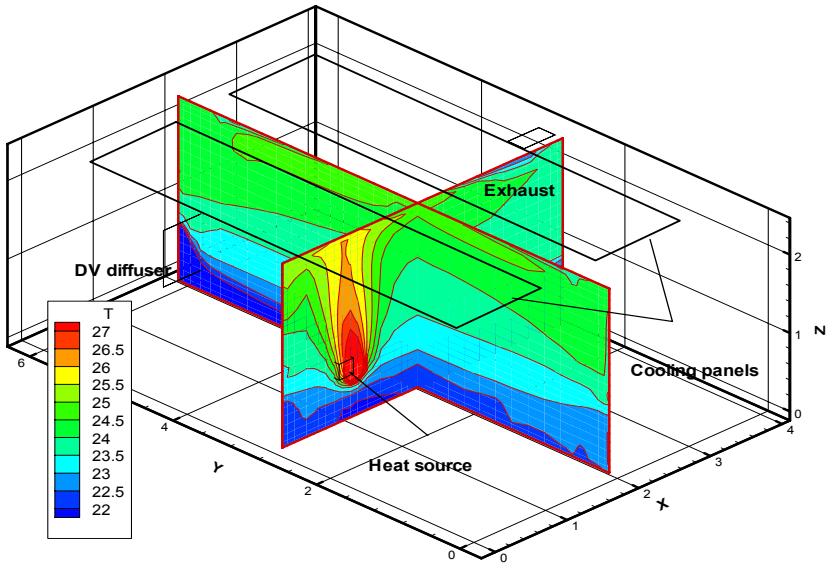

Figure 4.11 Temperature stratification in a room with cooled ceiling and displacement ventilation

MACA was validated for three different validation cases (experiments). Depending on the validation case, cooled ceiling panels, heating panels and/or convective sources were used as heat sources/sinks.

1. Case 1 had a sun patch on the floor. This was a major heat source which created complex heat transfers on this and other floor surfaces due to stratified temperatures.
2. Case 2 had cooling panels and convective heat source (refer to Figure 4.11) which created complex airflows by a collision of an upward air-stream from the heat source and a downward buoyant air-stream from cooling panels.
3. Case 3 combined low airflow rate with strong buoyant airflow on a hot window surface asymmetrically positioned to the main stream of the displacements ventilation flow.

This section considers the validation results and Chapter 8 (Section 8.4) contains details about the measurements.

For measured surface temperatures in the room, heat fluxes and corresponding temperature distributions were calculated, by the use of both MACA and two types of wall functions, in all three validation cases. Surface heat fluxes were calculated by three models: (1) the MACA model used in the CFD0 program with zero equation turbulence model, (2) the simplified thermal boundary conditions model provided by Chen and Xu (1998) for the CFD0 program, and (3) the log-law wall functions used in the PHOENICS program with the k-ε turbulent model. For the wall function in the PHOENICS program, the RNG k-ε turbulent model was selected because it produced slightly better results for thermal boundary calculations compared to other turbulence models (Chen 1995). For all three simulation models (MACA, simple wall function, and log-law wall function with k-ε turbulent model) the same grid resolution (37×32×22 cells) was used with identical grid distribution near surfaces. Table 4.11 contains the results of measurements and calculations. This table shows heat fluxes at surfaces with the largest convective heat fluxes and heat fluxes at some other characteristic surfaces.

Table 4.11 Comparison of convective heat flux calculated by MACA and wall functions

Characteristic surfaces	Area [m^2]	Q_C measured		Q_C calculated [W]			Diff. related to measured [%]		
		Qc [W]	Qc/A [W/m^2]	MACA	simple wall funct.	log-law wall fun.	MACA	simple wall funct.	log-law wall fun.
Case1 : Sun patch at floor, all air system -3.8 ACH									
Sun patch at floor	6.3	427	67.7	392	496	153	8	16	64
All walls	46.6	118	2.5	144	249	343	22	111	190
Whole floor	23.5	645	27.4	573	669	496	11	4	21
Case2 : Convective heat, air system combined with cooled ceiling -1.7 ACH									
Cooled ceil panels	12.0	-284	-23.7	-245	-136	-221	14	34	22
All walls	46.6	-139	-3.0	-124	-169	-222	11	22	60
Whole floor	23.5	-22	-0.9	-39	-2	19	77	90	177
Case3 : Hot window surface, all air system -1.8 ACH									
Hot window surf.	4.8	165	34.4	180	509	88	9	208	47
Whole floor	23.5	223	9.5	163	111	133	27	55	40

In simulation Case 1, floor and wall surfaces have higher temperatures than the local air. In contrast, these temperatures are similar at the ceiling surfaces. The largest heat flux is on the

sun patch surface. On this surface, heat flux calculated by MACA differs by 8% from the measured value (Table 4.11). With the simple wall functions this difference is slightly larger (16%), while the log-law wall functions predicted a considerably smaller heat flux on this surface (64%). At walls in the Case 1, MACA also predicts heat fluxes considerably better than other tow models. In Case 2, MACA's prediction of heat flux on cooled panels is more precise than with other two models. Heat flux predicted by MACA is almost in the range of the uncertainty of hear flux measurements (which is 13%). Same is for wall surfaces. At floor, the difference in-between MACA predicted and measured heat fluxes is large (77%). This large difference at floor surface is due to very small temperature difference in-between surface and local air. At this floor surface specific heat flux (Qc/Area) is very small and total convective heat flux (Q_C) is negligible compare to the fluxes at other surfaces. Also, accuracy of measurements with this small specific heat flux is low. In Case 3, MACA provides far beater prediction of heat fluxes than other two models at all surfaces.

Overall, MACA gave heat fluxes that were in good agreement with measured fluxes at all surfaces in all three cases excluding floor surface in Case 2, which had negligible effect on overall heat transfer in the room. On the other hand, simple wall functions and log-law wall functions provided only occasionally good agreement with experimental results.

Surface temperatures with applied thermal boundary conditions models in the CFD program define total heat flux which is delivered to the air. This heat flux is equal to the sum of convective fluxes on surfaces and internal objects. Smaller/larger calculated total heat flux than real one generally results in lower/higher predicted room air temperature. The effects of local and total heat fluxes on temperature distribution is shown in Figures 4.13-4.15 in which measured temperatures are compared with those calculated by MACA and by log-law wall functions. These figures show temperature profiles for 6 positions in the room (refer to Figure 4.12).

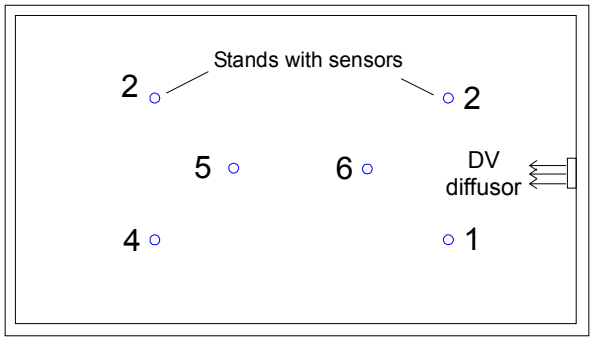

Figure 4.12 Stand positions (1 to 6) for temperature measurements

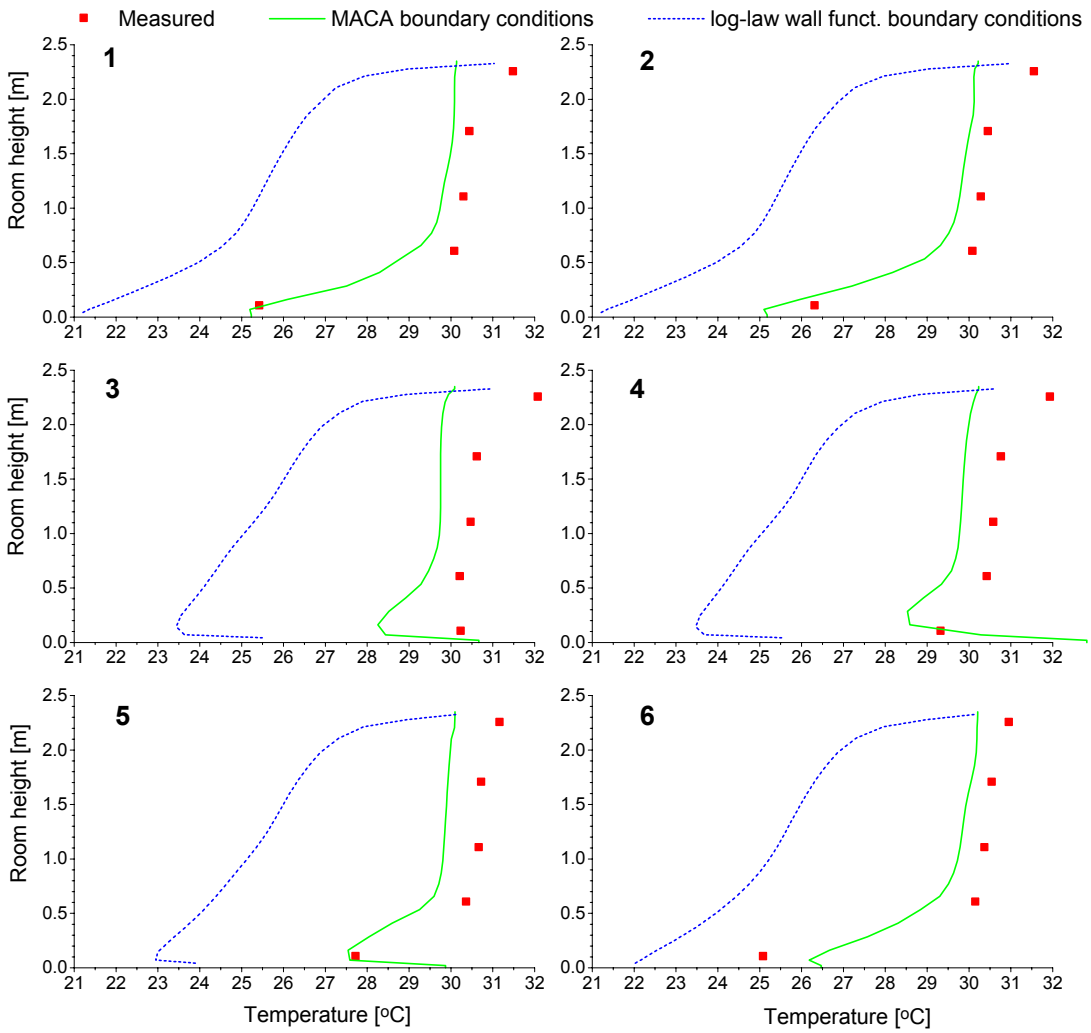

Figure 4.13 A comparison of measured and calculated temperature profiles for Case1: Sun patch at floor, all air system - 3.8 ACH

When comparing the temperature distribution predicted using MACA with the measured distribution, one can see that MACA predicts slightly lower temperatures at all 6 stand positions in Case 1. This is due to the lower calculated heat fluxes at floor and ceiling surfaces, which causes a smaller total heat flux and lower exhaust temperature. On the other hand, considerable under-prediction of floor heat fluxes and over-prediction of wall heat fluxes with calculations by log-law wall functions (refer to Table 4.11) creates considerably different temperature distributions (refer to Figure 4.13). In Case 2, the temperatures calculated by MACA are generally larger than those measured although the calculated and measured total heat fluxes are largely similar. Beside small differences in-between measured and calculated values for local heat fluxes (refer to Table 4.11), the possible reason for higher temperatures calculated by MACA is

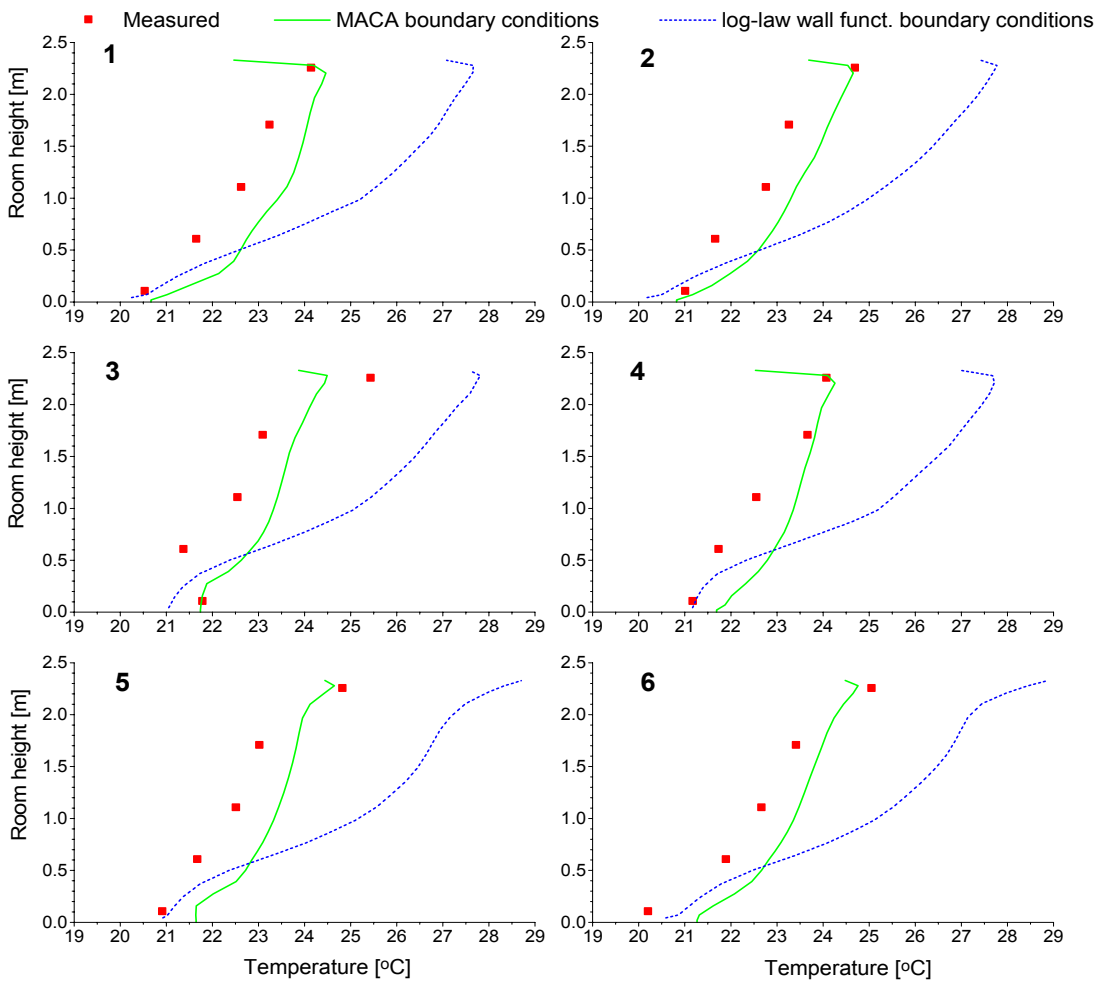

Figure 4.14 A comparison of measured and calculated temperature profiles for Case2: Convective heat source, air system combined by cooled ceiling - 1.7 ACH

the performance of the zero equation turbulence model with strong upward and downward buoyant air-streams (Figure 4.11). Nevertheless, with log-law wall functions, CFD predicts considerable lower heat flux at the cooling panels which creates larger temperature gradient in upper part of the room (Figure 4.14). In Case 3, the measured temperature profile overlaps with the temperature profiles obtained by use of MACA in most parts of the room. In the same case, CFD with log-law wall functions under predicts room temperature because of lower calculated heat flux at the floor surface.

Overall, for all three validation cases the CFD program that uses MACA predicts better temperature profile than the CFD program that uses log-wall functions. This is the consequence of more precise calculation of surface thermal boundary conditions with MACA compared to log-law wall functions.

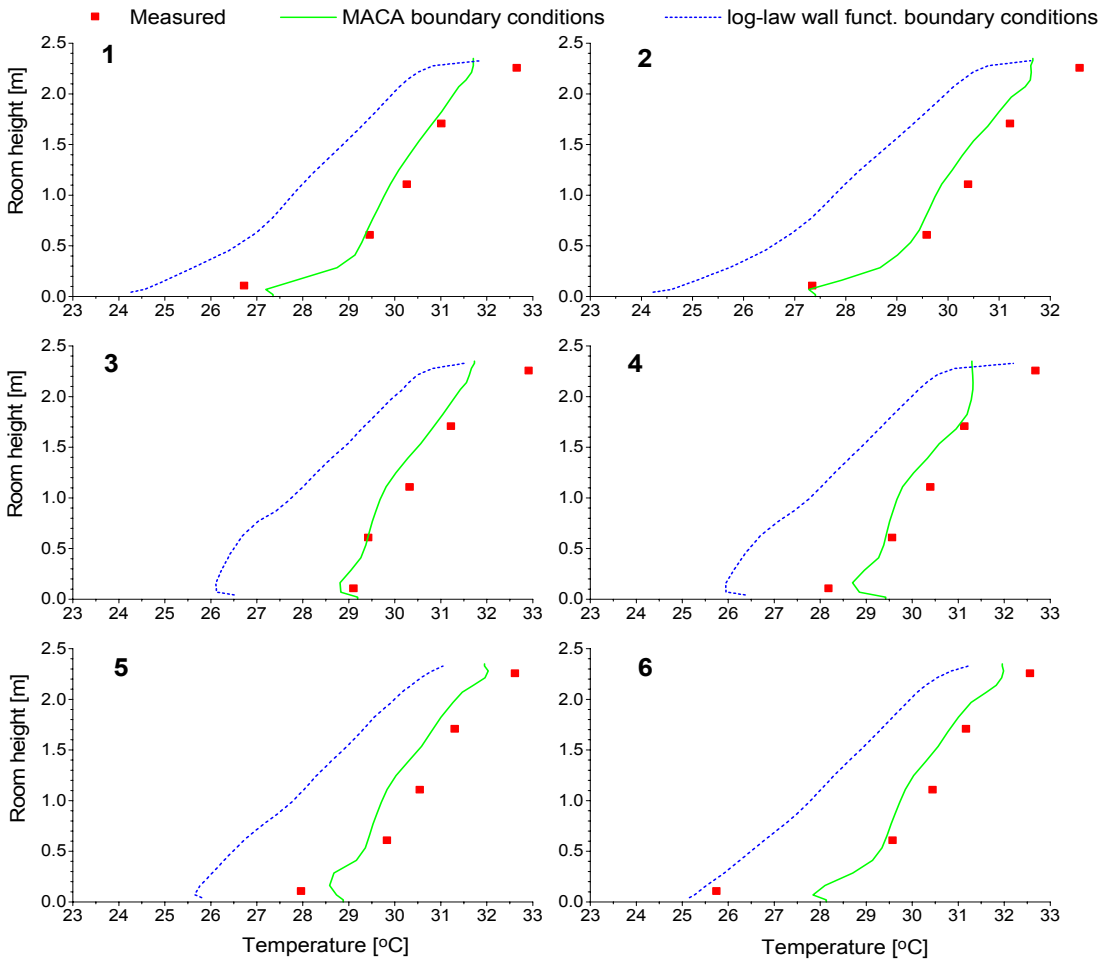

Figure 4.15 A comparison of measured and calculated temperature profiles for Case3: Heated wall, all air system - 1.8 ACH

Generally, for the analyzed cases, MACA performed considerably better than simple and log-law wall functions for all three types of surfaces (floor, walls, and ceiling). However, the accuracy of MACA depends very much on selecting the appropriate convection correlations from correlations provided in Tables 4.2-4.8. Therefore, for good accuracy with the MACA model, it is important that the user of the CFD program specifies the appropriate ventilation regime (Table 4.9) based on the installed ventilation system.

Grid dependency

Considering the grid dependency of the heat flux calculation, MACA also performs considerably better than simple and log-law wall functions used for thermal boundary condition calculations. Section 4.2.1 provides information about previous research that report large grid dependencies where wall functions are used for heat flux calculation. In order to investigate this

issue with MACA, this section compares heat fluxes calculated by MACA when different discretizations are used in the vicinity of the surfaces. The results calculated by wall functions are also provided for comparison.

Figure 4.16 shows the calculated heat fluxes on a hot window surface in validation Case 3 (Table 4.11). The grid resolution on these surfaces is varied from 1 cell to 3 cells in the air layer 0.1 m from wall (Figure 4.16). This represents the number of grid points in the air-layer between the surface and the layer of local air. In MACA, the local air temperature is calculated based on the temperature in cells 0.1-0.2 m from the wall (refer to Figure 4.6). Variation of calculated heat fluxes, by MACA, for analyzed grid variation is in range of 10% (Figure 4.16). For the same local air temperature, MACA should not provide grid dependent results because it uses a recalculation of the local convection coefficient as calculated by the convection correlation to the coefficient for adjacent cells (Equation 4.41). However, discretization in region near the wall affects the velocity field calculation, which further affects the temperature in the local air layer. Therefore, a certain grid dependency with the calculation of thermal boundary conditions still exists. However, this grid dependency is much smaller than the dependency observed when using simplified and log-law wall functions with typical discretization in the vicinity of the surfaces for indoor airflow simulations (Figure 4.16).

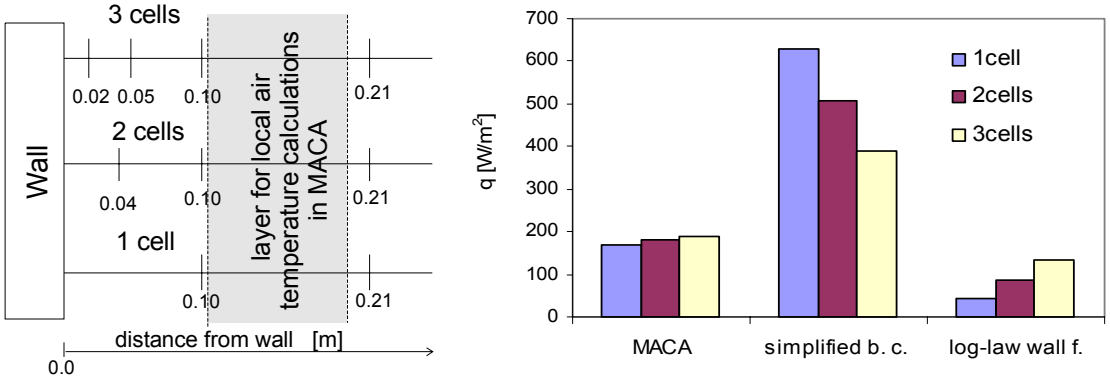

Figure 4.16 Grid dependency for MACA and wall functions for three different grid resolutions in the vicinity of a surface

Considering the effect of discretization in the vicinity of the surfaces on the convergence of CFD results when MACA is used, a general recommendation is that users should define at least 1 cell layer in the air layer 0.1m from the surfaces. Coarser meshes may create problems in the convergence procedure due to the oscillation of surface heat fluxes in the iteration procedure as described in Section 4.2.2. Generally, 2-3 cells layers provide good results and good convergence rates.

4.5 Discussion and Summary

The previous section illustrates that MACA provides more accurate calculations of heat fluxes on building surfaces than wall functions in the cases where the air flow type in the room is described with convection correlations implemented in MACA. By adding more correlations for specific air flows, the performance of this algorithm with various indoor airflow types can be further improved.

Compared to the previous model, which uses experiment-based convection correlations developed by Beausoleil (2000), MACA is simpler and less computationally expensive. The previous model that uses the "Adaptive Convection Algorithm" (ACA) in combination with "Adaptive Conflation Controller" (ACC) requires a double run of the CFD program (refer to Section 2.3.1). With this model, adaptive convection algorithm (ACA) defines the convection coefficients in-between two runs of CFD program. With MACA, convection coefficients are calculated in the convergence procedure which considerably speeds up the calculation. Also, by use of local temperatures, the performance of MACA is improved compared to ACA which use temperatures in the adjacent (first) cells. On the other hand, the use of the Adaptive Conflation Controller and second run of CFD in Beausoleil's model increase the accuracy of heat flux calculation on surfaces where experiment-based convection correlations are not suitable. These are surfaces with local effects such as surfaces in the vicinity of the diffusers where experiment-based convection correlations developed for average temperatures are not suitable. Generally, MACA is faster and more flexible when it comes to the coupling with the energy simulation program, while Beausoleil's models (ACA and ACC) are more flexible when dealing with an application with different airflow regimes.

CHAPTER 5

COUPLING OF ENERGY SIMULATION AND AIR FLOW PROGRAMS

5.1 Introduction

Pertaining to the accuracy of results obtained by the coupled program, the most important boundary conditions are convective heat transfer rates at the enclosure surfaces which connect modeling domains of Energy Simulation (ES) and Computational Fluid Dynamics (CFD) programs. Other than accuracy, numerical stability and computational time are also important and they strongly depend on the coupling method. This chapter presents specific coupling procedures and resulting simulation accuracy. Section 5.2 describes these procedures and discusses three different coupling methods. Section 5.3 compares the results of the coupled program for four selected coupling procedures. A comparison with experimental measurements is provided in Section 5.4. Finally, discussion and recommendations are provided in Section 5.5.

5.2 ES and CFD Programs Coupling Methods

For the coupling of ES and CFD programs, specific procedures are required due to the different physical models and numerical schemes of these two programs. Discontinuity of heat transfer rates in the ES and CFD domains as well as the differences in computational time are the main reasons to keep the existing numerical schemes of the ES and CFD programs separate.

Discontinuity of heat transfer rates in the ES and CFD domains implies that characteristic time-scales for heat transfer are very different. This difference requires different discretizations in time ($\Delta\tau$) for unsteady-state calculations. The scale analysis of transient conductive energy flow, provided by Bejan (1995), shows that the time needed to reach a steady state condition in a standard building wall structure is measured in hours or days. On the other hand, the time needed to reach a steady state air temperature distribution with transient air flow in a room (with constant boundary conditions) is measured in minutes. This indicates that several orders of magnitude different time steps ($\Delta\tau$) are needed to simulate the transient energy flow in building structures and transient air flow in rooms. Because of the large accumulation of thermal energy in building

elements (walls, floor, and ceiling), the time discretization in the coupled program is defined by a time step that provides satisfactory accuracy for transient energy flow in the domain of the ES program. This gives a relatively large time step ($\Delta\tau_{ES}$ ~ hour). Putting this large $\Delta\tau_{ES}$ in the general transport equation for the CFD domain (Equation 4.27), the transient term (Equation 4.28) becomes much smaller than the advection and convection terms, for all variables calculated in the CFD domain. Therefore, in the CFD transport equation, the transient term is neglected. This means that in coupled program, the ES program provides the solution to transient heat transfer through building elements, while the CFD program provides the solution to the steady state temperature and velocity distribution for the considered time step.

An approximation of the steady state CFD calculations does not affect the result of an air flow distribution as long as $\Delta\tau$ is large enough (larger than few minutes), and thus the transient term is negligible for CFD. Unsteady CFD application of airflow in buildings are required only when fast phenomena are considered and the required time step is small enough (less than minute) to cause that air parameters from the previous time step influence the calculation in the present time step. However, in most of the typical building airflow simulation cases, CFD and ES do not require coupling with small time steps. Only different kind of emergency situations with fast release of thermal energy, such as fire, might require unsteady CFD application, which is not the topic of this thesis.

5.2.1 One-Directional Coupling Method

The coupling of CFD and ES programs can be one-directional or two-directional. Figure 5.1 shows the schematic of one-directional coupling. With a one-directional coupling method, the ES program calculates room surface temperatures ($T_{surfaces}$) and heat fluxes ($Q_{surfaces}$) based on assumption of uniform air temperature. These data are used in the CFD program as boundary conditions. Depending on the thermal boundary conditions model in the CFD program, surface temperature or heat fluxes are used. The CFD program with MACA provides better accuracy of surface heat fluxes than standard CFD with wall functions as described in the previous chapter. Therefore for a CFD program with MACA surface temperature should be used. On the other hand, heat fluxes based on ES (assuming uniform temperature) are in most of the cases more accurate than heat fluxes calculated by CFD with log-law wall functions. Therefore, specifying heat fluxes based on the ES program results, and this way avoiding log-law wall functions, in many cases improves the accuracy of the CFD simulations of indoor airflow.

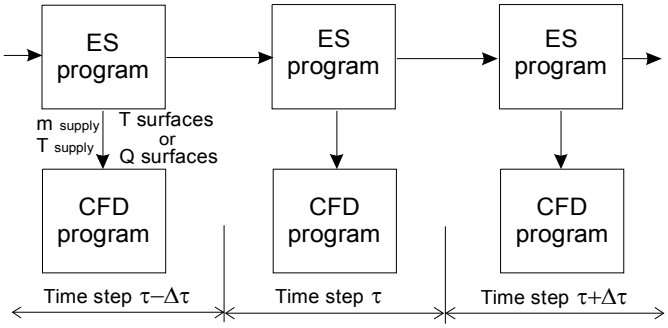

Figure 5.1 One-directional coupling of ES and CFD programs

With one-directional coupling there is no feedback information from CFD to ES, and the ES calculation does not depend on the CFD results. In the case of two-directional coupling, the information about air temperature distribution, which affects local convection coefficients, is retuned to the ES program. This two-directional coupling is more accurate than one-directional and this type of coupling is recommended for users of coupled programs.

5.2.2 Two-Directional Coupling Methods

As mentioned in Chapter 1, the coupling of ES and CFD programs takes place on enclosure surfaces which connect the simulation domains of these two programs. With the assumption that the air temperature distribution is uniform, the ES program calculates the temperature of the surfaces ($T_{surface}$). Using Modified Adaptive Convection Algorithm (MACA), the CFD program calculates surface convective heat fluxes based on the spatial air temperature distribution by using these enclosure temperatures as input data. To satisfy the condition for energy conservation, heat fluxes on boundary surfaces have to be the same for both the ES and CFD domains (Figure 5.2). Therefore, the CFD program returns data about surface heat fluxes to the ES program. In this way, ES and CFD are coupled by the two-directional coupling method. Consecutive exchange of data on boundary conditions increases accuracy of the input data for both programs.

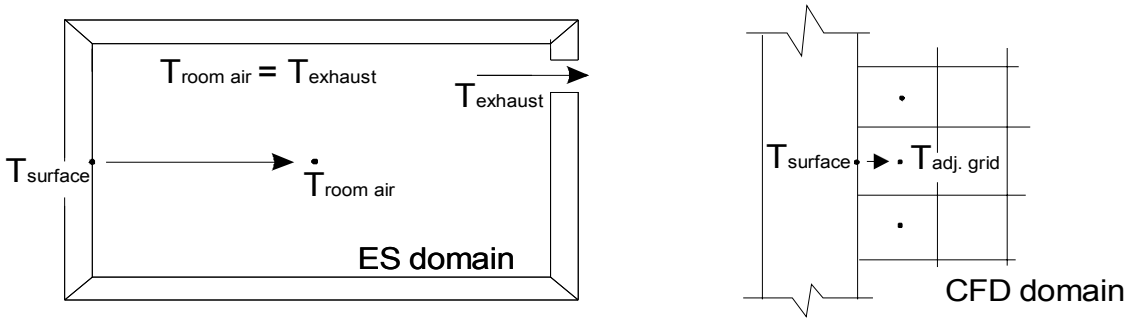

Figure 5.2 Heat flux on surfaces in the ES and CFD domains

Besides enclosure temperatures, the ES program provides the CFD program with input data related to boundary conditions at thermal units, if any. Boundary conditions for thermal units are defined by air velocity, temperature and concentration for air supply thermal units, or by surface temperature or heat flux for units such as radiant panels, baseboard heaters, or computers. On the other hand, the CFD program provides the ES program with surface heat fluxes and in some cases, local temperature at the control point. Surface heat flux is defined by air temperatures in cells-layers adjacent to the surfaces ($T_{adj.cell}$) and corresponding convective coefficients ($h_{adj.cell}$).

In the ES program, the temperature of the air is equal to the exhaust temperature ($T_{room\_air}=T_{exhaust}$), because the ES program considers air as a single node assuming perfect mixing. To implement locally defined boundary conditions from CFD into ES, the method described by Chen (1988) is adjusted to be used with the ES program solver as described in Chapter 3. This method is derived from the heat flux equation used in the CFD program:

$$q = h_{adj.cell} \cdot (T_{surface} - T_{adj.cell}) \tag{5.1}$$

Equation (5.1) is adjusted into the form where uniform room temperature is equal to the exhaust air temperature:

$$q = h_{adj.cell} \cdot (T_{surface} - T_{exhaust}) - h_{adj.cell} \cdot (T_{adj.cell} - T_{exhaust}) \tag{5.2}$$

The first term in equation (5.2) is the same as the equation which describes convective heat in the uncoupled ES program. Therefore, this term does not change the zone matrix solution procedure in the ES program (Figure 3.17). The difference lies in the surface convection coefficients ($h_{adj.grid}$) which modify the coefficients in the energy balance matrix (coefficients which are bolded in the zone matrix as shown in Figure 3.17). This coefficient is based on temperature in adjacent cell layer ($T_{adj.cell}$), and in zone matrix it is used with uniform room temperate ($T_{exhaust}$). Therefore, correction that includes temperature difference ($T_{adj.cell}$ -$T_{exhaust}$) should be introduced in zone matrix. This is done by second term on the right-hand-side of Equation (5.2), which is introduced in the ES matrix solution procedure by correcting the free vector (Figure 3.17). Each element of the free vector that describes surface convection (bolded coefficients in free vector as shown in Figure 3.17) is corrected by adding this term.

Depending on the technique and dynamics of information exchange between the unsteady state energy simulation and steady state airflow programs, three two-directional coupling methods

are possible. They are: (1) quasi dynamic coupling, (2) fully dynamic coupling, and (3) integrated coupling methods.

Quasi Dynamic Coupling

Through a quasi dynamic coupling, energy and air flow programs run in sequence where the ES program uses the results of the CFD program from the previous time step to calculate its own boundary conditions for the next time step calculation (Figure 5.3). The two programs operate independently, but exchange information before the beginning of each calculation step. This type of coupling is also called "ping pong" (Hensen 1999). The quasi dynamic coupling approach is time step sensitive because the heat fluxes between ES and CFD domains for any individual time step are based on air velocity and temperature distribution from the previous time step. Therefore, this method does not strictly satisfy energy conservation between the two domains. Differences in heat fluxes on the boundary surfaces of the two domains (Figure 5.1) depend on the time step and intensity of the change of the boundary conditions. For large and rapid change of boundary conditions in the ES program domain, such as the start of the HVAC system or sudden increase of sun radiation, this coupling method requires an appropriately small time step. Details about time steps sensitivity are provided in Section 5.3.

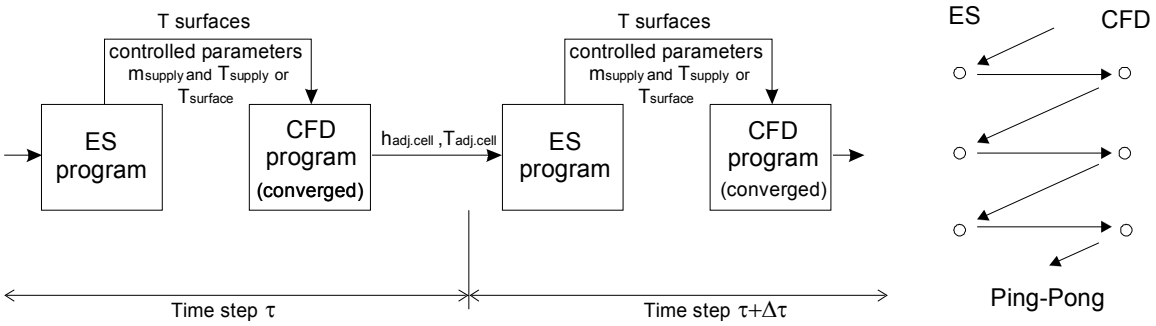

Figure 5.3 Quasi Dynamic Coupling of ES and CFD programs

Fully Dynamic Coupling

With a fully dynamic coupling, there are several consecutive runs of the ES and CFD programs for each time step (Figure 5.4). The two programs work consecutively for certain time steps, exchanging boundary conditions information, until the surface heat fluxes defined by the ES and CFD programs are in balance. This balance is established when satisfactorily small difference (error) of surface heat fluxes defined in the two domains is achieved. Fully dynamic coupling is also called "onion" coupling. This coupling is time step independent with respect to the energy balance on surfaces between two domains. However, the total computational time

needed for one time step with the fully dynamic coupling is considerably larger than with the quasi dynamic coupling. Details are provided in Section 5.3.

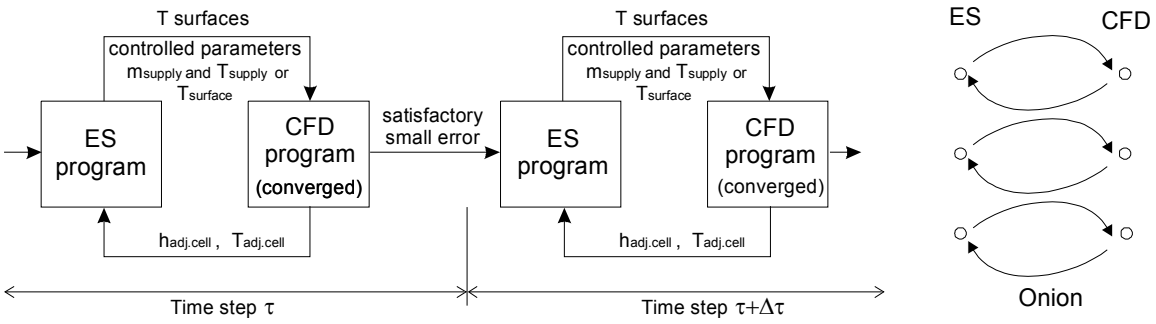

Figure 5.4 Fully Dynamic Coupling of ES and CFD programs

Integrated Coupling

With an integrated coupling, ES and CFD programs exchange information during the convergence process of the CFD program (Figure 5.5). The ES program, which has a calculation time that is several orders of magnitude smaller than that of the CFD program, periodically updates boundary conditions, while the CFD program converges towards the final solution. In addition, for each update, the ES program uses new boundary conditions based on results from CFD program that are not completely converged. In this way, both programs progress towards the final solution. When convergence in the CFD program is achieved, the calculated convective heat fluxes present the final solutions that satisfy the energy balance between the two domains. CFD and ES cooperatively calculate the energy transfer with support from the modified adaptive convection algorithm (MACA). This coupling method has a smaller computational time requirement than the fully dynamic coupling, which is described in the next section.

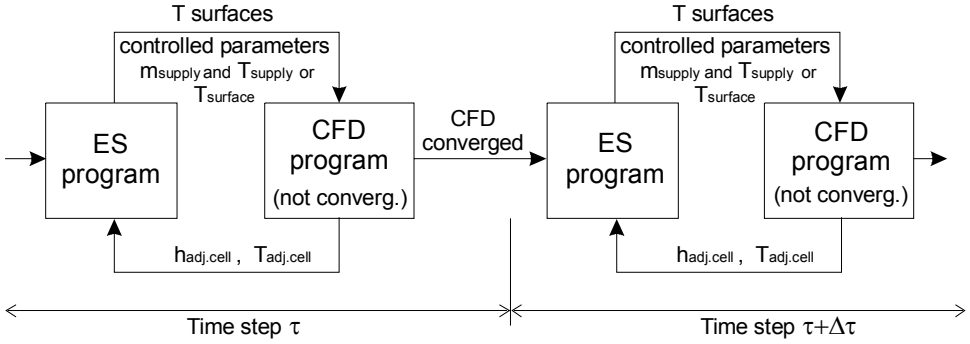

Figure 5.5 Integrated Coupling of ES and CFD programs

5.3 Comparison of Different Coupling Methods

This section provides analysis of coupling procedures considering accuracy, computation time, and numerical stability. Performance of one-directional coupling method and all three two-directional coupling methods are compared for a representative test case.

5.3.1 Definition of a Numerical Test Case

Figure 5.6 shows the geometry of the room for the test case. This room is 4.5m long, 3.5m wide and 2.4 m high with two internal heat sources. It has one external wall with a window oriented to the south. Displacement ventilation is selected as the HVAC system because it creates a nonuniform (stratified) temperature distribution in the room that requires use of the coupled ES and CFD program. Details about the HVAC systems and heat sources are provided in Table 5.1.

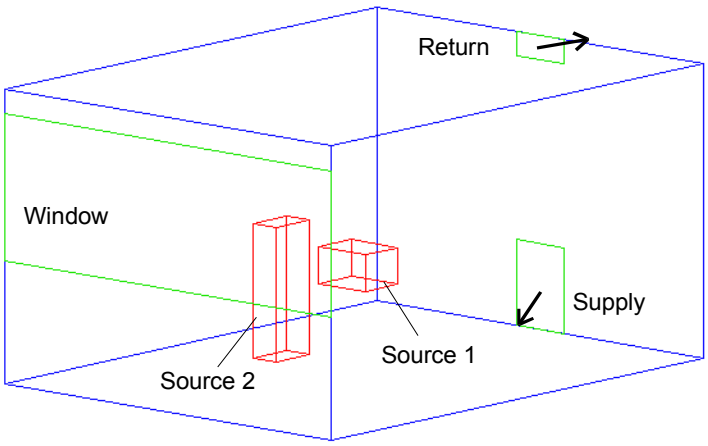

Figure 5.6 Geometry of the test room for comparison of different coupling methods (source 1 – computer simulator, source 2 – humans simulator)

Table 5.1 Properties of heat sources and the HVAC system for the test room

Heat sources and HVAC system	Q_{total} [W]	Q_{conv}/Q_{total}	Active period
Internal Source 1	120	0.5	continuous
Internal Source 2	300	0.5	18-20 h
Solar gain though south shaded window	depends on day period		5-19 h
Conduction through external wall an widow	depends on day period		continuous
HVAC system -displacement ventilation	Figure 5.7	1.0	9-21 h

The active periods of internal sources and the displacement ventilation system were selected to create a dynamic change of: (1) room temperature, by turning HVAC system ON and OFF, and (2) cooling load, by turning internal sources ON and OFF. Dynamic change of cooling load and temperature in the room were selected to create the situations where advantages and disadvantages of different coupling methods can be tested. These situations are the start of an HVAC system and sudden increase/decrease of cooling loads. Figure 5.7 shows the daily change of cooling loads and room temperature for the test case calculated by ES program only. Considering just ES, time a step of $\Delta\tau$ = 30 min provides a time step independent solution for this test case. Therefore, in the analyses related to coupling methods, a time step of 30 min is used, except in analyses related to time step selection with quasi-dynamic coupling. In the CFD program, MACA was used for thermal boundary condition calculations. For simple room geometry and displacement air flow used in the test case, grid resolution of 20×19×17 cells is applied since it requires relatively small computation time and provides grid independent solution.

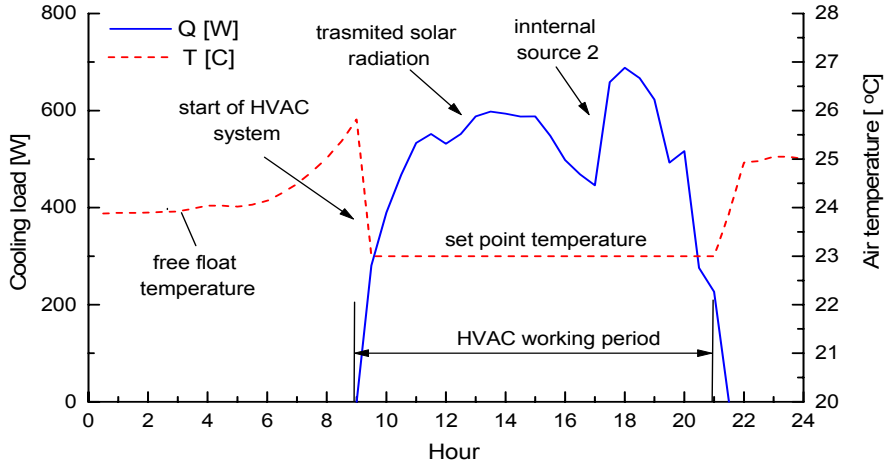

Figure 5.7 Temperature and cooling load for the test case used for coupling methods comparison

5.3.2 Performance of the Fully-Dynamic Coupling for the Numerical Test Case

Because *fully-dynamic coupling* provides time step independent results with respect to the energy balance on surfaces between the ES and CFD domains, it is the first of the four methods to be tested. By use of this coupling method and time step of 30 minutes, which provides time step independent results in the ES domain, time step independent coupling is achieved for this test case. The major issue with fully-dynamic coupling is how to define the moment when the energy balance on surfaces between the two domains is established with a satisfactorily small difference ("error" in Figure 5.4). In the developed coupling procedures, two criteria were used.

The first criterion uses the relative difference between total surface heat fluxes calculated in the ES and CFD domains. The second criterion uses the relative difference of heat fluxes calculated in two domains at surface with maximum heat flux. When both of these differences are smaller than some predetermined value, the coupled program proceeds to the calculations of next time step. The same relative tolerance is used for both criteria. With these criteria, surfaces with small heat fluxes that have minor effect on the overall heat and air flows in the room are excluded from influencing the duration of the calculation. On the other hand, the second criterion prevents the situation when total surface heat flux calculations in the ES and CFD domains overlap by a chance.

To find an optimal criterion for termination of consecutive runs of the ES and CFD programs for a certain time step, several criteria which involve relative difference (error) of heat fluxes in two domains were tested. Figure 5.8 shows the cooling loads calculated by the fully-dynamic coupling method when relative difference tolerance of 1% or 5% is used. Figure 5.8 shows that the difference in calculated cooling loads by use of these two different tolerances is very small, which is also the case for temperature and airflow distributions in the CFD domain. However, the 1% criterion (tolerance) requires many more consecutive runs of two programs than the 5% criterion (Figure 5.8). The number of consecutive runs varies for different calculation time steps because it depends on the intensity of the change of the cooling loads in the room. This change of cooling loads affects the change in boundary conditions at the surfaces and with more intense change more consecutive runs are needed. For example, in the period from 12 to 16 hours cooling load changes gradually and 2 iterations are needed to achieve 5% accuracy. On the other

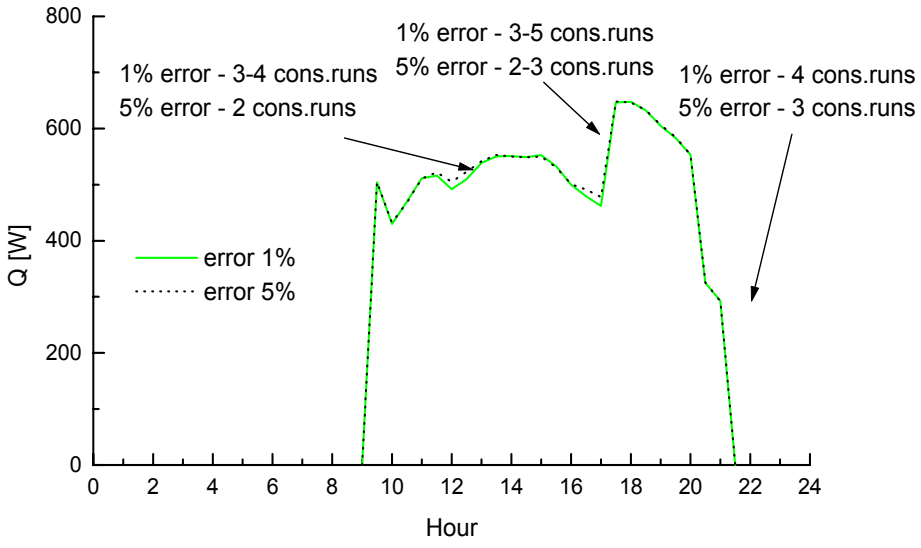

Figure 5.8 Cooling loads for the test case calculated using the fully-dynamic coupling method

hand, when the system shuts down (hour 19), the number of consecutive runs for the same accuracy is 3. With decrease of tolerance from 5% to 1% error, total number of consecutive ruins (indicator of computation time) for analyzed case increases significantly, while the accuracy of calculated cooling load, temperature, and airflow distributions improves only slightly.

5.3.3 Performance of the Quasi-Dynamic Coupling for the Numerical Test Case

Quasi-dynamic coupling requires only one run for each analyzed time step, which reduces the calculation time compared to fully-dynamic coupling. However, quasi-dynamic coupling is time step sensitive and for large time steps certain inaccuracies appear, especially with large changes of the boundary conditions as illustrated in Figure 5.9. The figure shows the effect of different time step ($\Delta\tau$) on cooling load calculations. Also, cooling loads calculated by time step independent fully-dynamic coupling is presented on this figure for comparison.

Results show that with gradual change of cooling load in the period from 12 to 16 hours, all analyzed time steps (10, 30, and 60 minutes) provide results similar to results obtained by the fully dynamic coupling (Figure 5.9). However, with sudden change of boundary conditions inaccuracy is not negligible. For example at hour10, the quasi-dynamic coupling with $\Delta\tau$= 60 minutes calculates 30% lower cooling loads than fully dynamic coupling. In fact, with the quasi dynamic coupling, local convection coefficients and local temperature distribution from the previous time step ($h_{adj.cell}$ and $\Delta T = T_{adj.cell} - T_{exhaust}$ in Equation 5.2) are transferred to the next

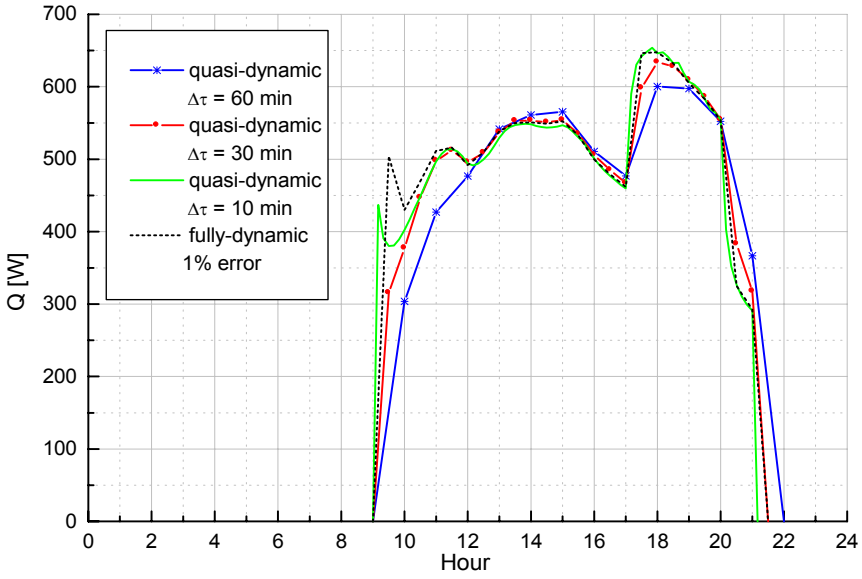

Figure 5.9 Cooling load calculations for different time steps with the quasi-dynamic coupling

time step calculation. At hour 9 in test case, the HVAC system is OFF and temperature is uniform. Hence the calculated ΔT and $h_{adj.cell}$ for this hour is small. Use of these ΔT and $h_{adj.cell}$ in the next calculation time step at hour 10, when HVAC system is ON and temperature distribution is different, creates previously mentioned error in cooling load calculation. Time step sensitivity also affects the calculation of air temperature and velocity distributions in the CFD domain. Generally, with decrease of time step, this inaccuracy decreases and for considered test case, the quasi-dynamic coupling method with $\Delta\tau$ = 10 minute provides almost the same result as the fully-dynamic coupling method for the whole analyzed period (Figure 5.9).

5.3.4 Performance of the Integrated Coupling for the Numerical Test Case

Considering coupling methodology, the *integrated coupling* is the same as the quasi-dynamic coupling except that the CFD program does not converge fully before the ES program updates boundary conditions. This type of coupling requires well defined convergence criterion for CFD, which can be defined in different ways (CHAM 2004 and Fluent NEWS 2004). In the CFD0 program, total residuals, defined as sums of absolute values of imbalance in each cell, for mass, velocities, and energy are calculated. As a criterion for termination of iterative process, the mass residual is normalized by (1) supply air volume flow rate and (2) bulk flow in the room. If one of these two values is smaller than the preset residual tolerance, CFD0 terminates the calculation. Bulk flow is used as additional scaling factor because the supply flow rate is zero when HVAC system is OFF. Using convergence criterion of $\varepsilon_{residual\_supply}<10^{-2}$ when supply flow rate is used as scaling factor or $\varepsilon_{residual\_bulk}<10^{-7}$ when bulk flow in the room is used as scaling factor, good convergence for temperature field is achieved. However, even if this criterion is not satisfied, the ES program can update boundary conditions using temperature field of not fully

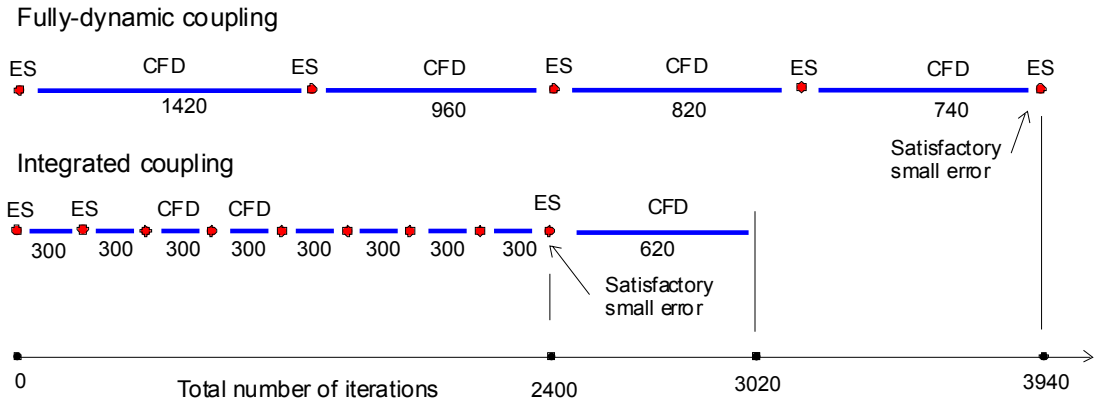

Figure 5.10 Comparison of computation time for the fully-dynamic and integrated coupling

converged CFD result, where convergence is defined by $\varepsilon_{residual\_supply}$ and $\varepsilon_{residual\_bulk}$. For successful update of boundary conditions, CFD needs to converge only to a certain level. Hence, with fewer number of iteration than needed for the full convergence, satisfactory accurate temperature distribution can be obtained. For example, in the moment after a shutdown of HVAC system in the test case (hour 21 in Figure 5.8), temperature field is defined to the level needed for successful update of boundary conditions after several hundred iterations, while much more iterations are needed to achieve the full convergence. This is illustrated in Figure 5.10.

With the fully-dynamic coupling, 4 consecutive run of the ES and CFD programs are needed (with the total iteration number of 3940) to achieve satisfactory small error of 1% (Figure 5.10). For the same case with the integrated coupling and the same error tolerance of 1%, the same surface heat fluxes as with the fully-dynamic coupling are obtained after 8 consecutive run of CFD and ES program. Total number of CFD iterations that is needed to reach this result is 2400 and it is considerably smaller than with the fully-dynamic coupling. To achieve the fully converged airflow result with the integrated coupling, an additional run of the CFD program is needed (Figure 5.10). This additional CFD run increases the total number of iterations to 3020, which is still considerably less than with the fully dynamic coupling.

In some simulations, the integrated coupling may create divergence of results calculated by the coupled program. Sometimes, not fully converged CFD results that are processed by the ES program may create unrealistic boundary conditions for the ES domain and lead to divergence. This may happen after the first consecutive run of the programs for certain calculation time step when the initial values for temperature field are far from the converged result values. To avoid this, the number of CFD iterations in the first consecutive run should be carefully selected.

5.3.5 Performance of the One-Directional Coupling for the Numerical Test Case

One-directional coupling is the simplest method that calculates up to 30% different cooling loads than the fully dynamic coupling for the considered test case (Figures 5.7 and 5.8). Considering temperature distributions calculated by the CFD program that uses MACA, the temperature calculated by one-directional coupling is by 0.5°C to 1°C off when compared to temperatures calculated by the fully dynamic coupling. The reason for this is a different surface temperature distribution obtained by the two way coupling. In general, the one-directional coupling is suitable for manual coupling of any ES and CFD program.

5.4 Summary

This section defined four ES and CFD coupling methodologies and analyzed performance of different coupling techniques. All three two-directional coupling methods can provide the same result. The quasi-dynamic coupling method is suitable for simulations with gradual change of cooling loads or in simulations that require small time steps measured in minutes such as analyses that incorporate control system models. Fully-dynamic coupling provides time step independent solution because of default energy balance on surfaces between the ES and CFD calculation domains. This method has the disadvantage of being computationally expensive since it requires several consecutive runs of the ES and CFD programs. The number of consecutive runs depends on the criterion for advancing into the next time step. An analysis showed that a criterion of 5% heat flux difference provides good accuracy and relatively small computation time. The integrated coupling also satisfies the energy balance on surfaces and needs a much smaller computational time than the fully dynamic coupling. However, with this type of coupling, the period for boundary condition updates should be carefully selected.

CHAPTER 6

ORGANIZATION AND GRAPHICAL USER INTERFACE OF COUPLED PROGRAM

6.1 Introduction

In the coupling of Energy Simulation (ES) and Computational Fluid Dynamics (CFD) programs, as presented in Chapters 3, 4, and 5, a specific organization of data flow between these two programs is needed. Both programs require a large amount of input data organized in formats readable by these programs. In addition, output results represent a large amount of data that need to be organized in easily understandable ways such as charts and graphics. Therefore, during the development of a coupled program, considerable effort was made to organize these data. As a result, a new Graphical User Interfaces (GUI) for (1) input data organization and (2) result presentation were developed.

In the following sections, basic data about the source code of Building Energy Simulation (BES) program and CFD program (CDF0) are presented followed by details about the structure of the coupled program (Section 6.2). Newly developed GUI for input data is presented in Section 6.3, while the GUI for output result presentation is presented in Section 6.4. At the end of this Chapter (Section 6.4), a short summary is provided.

6.2 Data Flow in the Coupled ES and CFD Program

Coupling models implemented into BES and CFD0 programs were selected and developed to provide optimal accuracy for energy and airflow simulations in buildings. Organizing these two programs into coupled program provides flexibility in addition to accuracy. A data flow between the two programs is organized to enable different types of coupling, as described in Chapter 5, without changing the programs' solver procedures, as described in Chapters 3 and 4. The data-flow procedures exchange information between two programs, which have their source codes written in different programming languages.

The CFD0 source code is written in FORTRAN programming language. As mentioned in Chapter 4, this code was initially developed at MIT (Srebric et al. 2000). As part of this thesis, the CFD0 program was further developed by adding functions to calculate thermal boundary conditions by convection correlations based on experimental measurements (Section 4.3). Input

data for this program such as: geometry, boundary conditions, iteration control, fluid properties, and discretization (mesh) data are organized in ASCII format (txt). Output data, such as spatial values for pressure, velocity, temperature, and output data related to coupling such as data for surface convection boundary conditions (Section 5.2) are also organized in ASCII formats (Figure 6.1).

The newly developed BES program is written in 'C' program language. Besides models for simulation of energy flow in buildings, as described in Chapter 3, this program contains procedures that control the coupling of the two programs. Since the BES program solves unsteady heat flow and CFD0 solves steady state air flow (Section 5.2), it controls the calculation progress for the analyzed period of time. Therefore, BES contains functions that "guide" the process of coupling depending on the type of coupling (Section 5.2). The BES program creates the input for the CFD0 program in each calculation time step. Communication between BES and CFD0 programs occurs through ASCII files (see "Solver" in Figure 6.1). At the beginning of each hour of the calculation period, the BES program reads a TMY2 weather file to calculate the external boundary conditions (Figure 6.1). TMY2 files contain hourly values of weather data for different locations. Therefore, for analyses where finer discretization in time is used

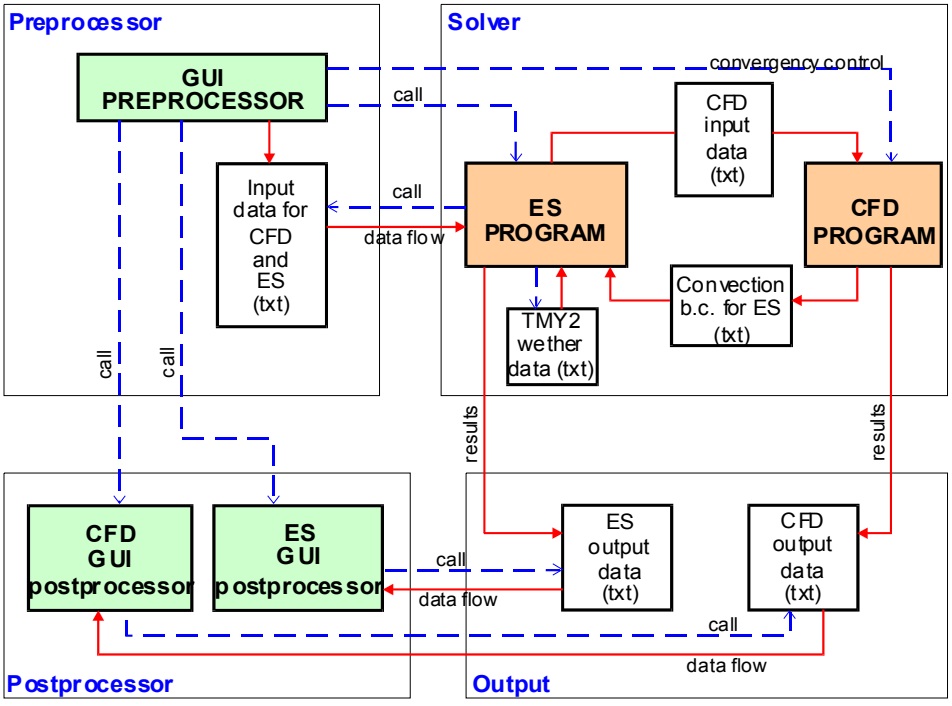

Figure 6.1 Data flow diagram for the coupled program

($\Delta\tau$<60 min), the BES program uses linear interpolation of hourly weather data. In order to define temperature distribution in buildings' elements for initial calculation time step, the BES program uses a "warming" procedure. In this procedure, the BES program sets back the calculation date for 7 days and uses a uniform temperature of 20^{o}C as initial guess. During this warming period, the temperature distribution in building elements is established considering daily and weekly schedule of operation of HVAC and other building systems. Output from the BES program is also organized in an ASCII file. More details about this file are provided in Section 6.4.

Besides the major data flow in the solver of the coupled program, Figure 6.1 shows the data flow among the preprocessor, solver, output and postprocessor. The preprocessor is the GUI for the coupled program, which is described in detail in the next section. The postprocessor contains GUIs that graphically present the output results from both programs. These GUIs are presented in Section 6.4. The user of the coupled program provides all input data and controls the entire process through the preprocessor GUI. After creating the building model, the user initiates the solver and the BES program proceeds with the calculation. Throughout the GUI, the user may affect the convergence process in the CFD0 program by changing relaxation factors. When the calculation is completed, the user may call the postprocessor GUI to create graphical interpretations of the results (Figure 6.1).

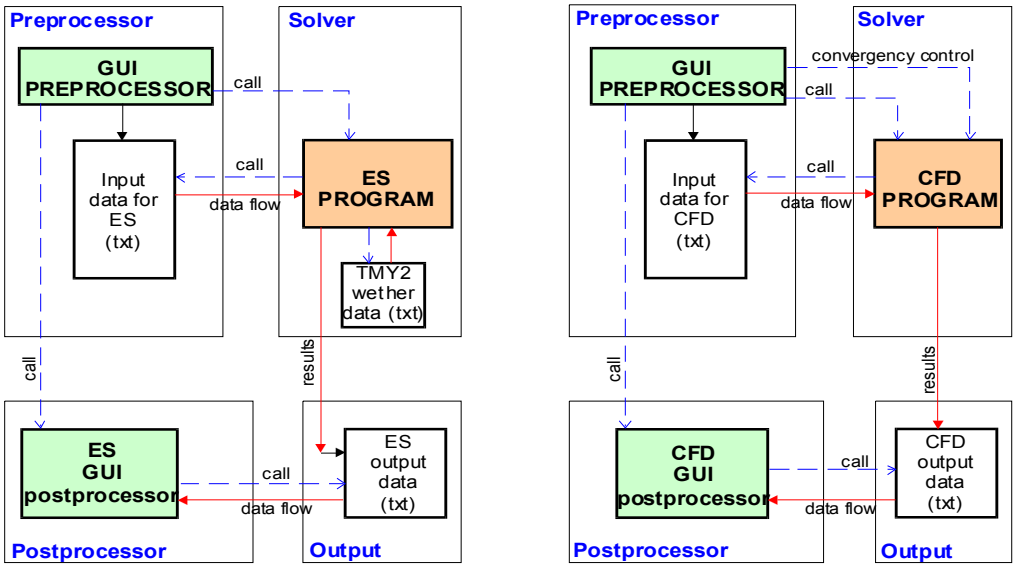

Figure 6.2 Data flow diagrams for cases whre the coupled program is used for only a) energy or b) airflow simulation

The coupled program can be used for separate energy or airflow simulations. When the user is only interested in energy consumption, the preprocessor is used to provide only the data needed for the BES program. The data flow diagram in this case is provided in Figure 6.2a. In the case where only indoor air flow analysis is performed, the user provides surface boundary conditions for the CFD0 program based on measurements or experience. In this case, the BES program is not used and the preprocessor GUI creates the input file for the CFD0 program directly (Figure 6.2b). In this type of analysis, the CFD0 output file contains spatial distribution of analyzed parameters for only one considered time step.

6.3 GUI Preprocessor

The amount of time needed to create a building model varies considerably depending on the user's skill and quality of used GUI. For a steady state CFD analysis of air flow in a building zone, the amount of time needed for setting up building zone models is similar to the amount of time needed for calculations. Furthermore, when the annual energy consumption analysis is performed by the BES program, modeling of a building is more time consuming than calculation that takes less than a few minutes. Therefore, in recent research, program developers put significant effort in developing user-friendly GUIs for their programs. In fact, the quality of the GUI often determines the popularity of different programs. Many powerful simulation tools for energy and air flow simulations have a small number of users just because of poor, inefficient, or the complete lack of a graphical user interface system. In view of this, a GUI for the coupled BES and CFD0 program was developed. Its primary purpose was to speed up the manipulation of large amounts of input/output data as presented in this thesis. In addition, the user-friendliness of this GUI enables the easy use of coupled programs by other users.

The source code for the newly developed GUI was produced by students at the computer science department of Pennsylvania State University, as mentioned in the Acknowledgments section of this thesis. The author of this thesis was involved in the GUI's development by designing and organizating GUI's window forms and testing the program. The source code was written in C++. For a graphical presentation of space geometry (Figure 6.3), an OpenGL library is used. As mentioned in the previous section, this GUI is used for data input and initialization of different processes in the coupled program such as the start of the solver or result analysis. Data input is organized in 36 windows forms, which group together similar types of input data. This interface provides robustness to the coupled program by setting default values for most input

parameters. Besides giving reference data for beginner users, the default values for variables that rarely change speed up the process of building the model.

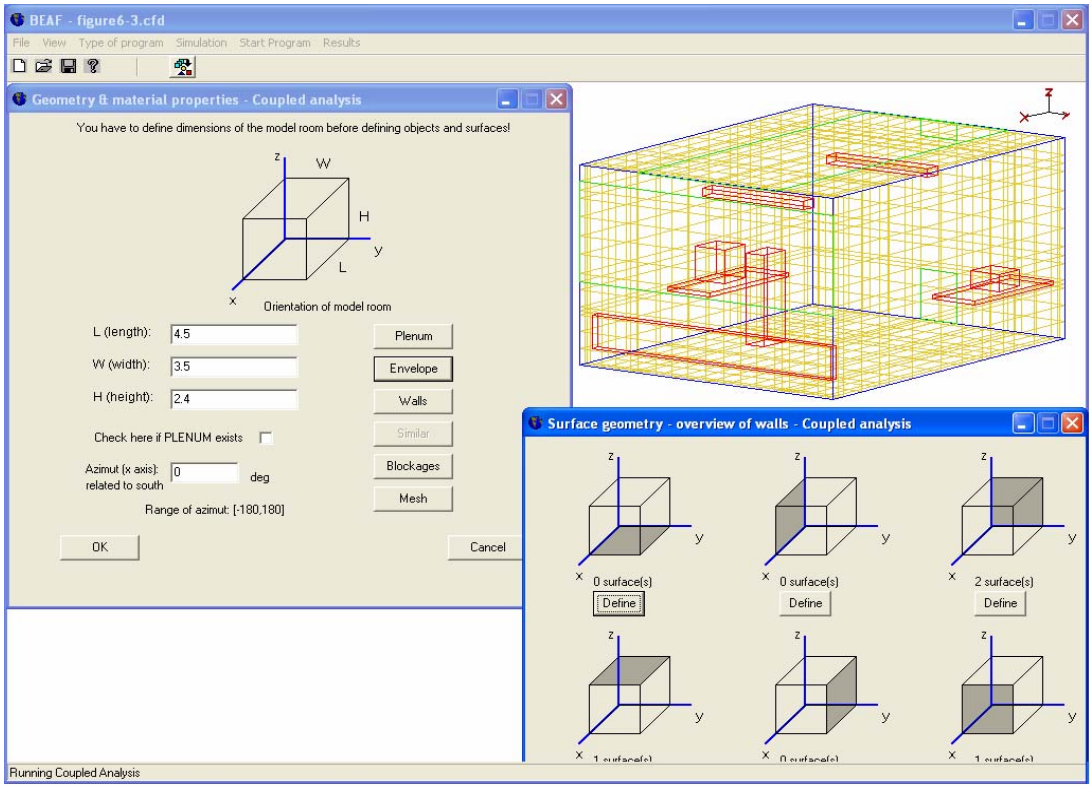

Figure 6.3 GUI of the coupled program representing model geometry, and two basic window forms

The GUI window forms are connected in a way that leads and assists the user though the process of building the model. In the next few paragraphs and figures, the key GUI window forms are briefly described to present the structure and capabilities of this new interface.

The first step in data input is to define the simulation type. The user selects the variables among energy simulation, airflow simulation, or coupled analysis (Figure 6.4a). This selection activates certain windows forms for the input data which are needed for selected type of analysis. Afterwards, the user defines the simulation parameters in the order defined in the "Simulation" form. Most of the simulation parameters are presented in Figure 6.4b.

The first group of input data that the user needs to define is related to geometry and material properties. Geometry data are needed in all three types of simulations and the window

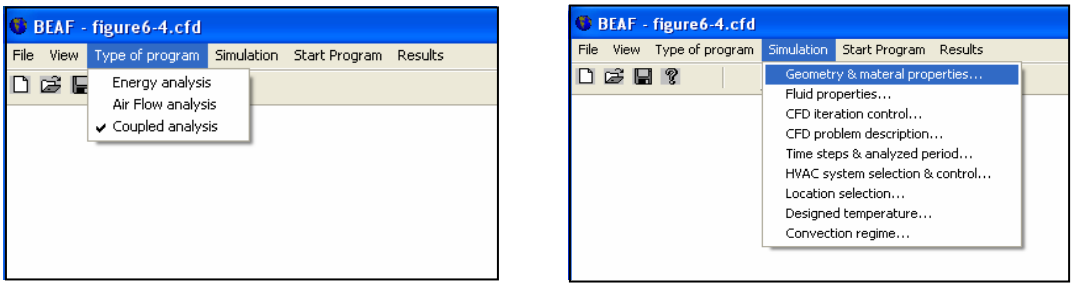

(a) (b)

Figure 6.4 The toolbar of coupled programs for the selection of the simulation
(a) type, (b) parameters

form is presented in Figure 6.3. In this form, the user provides input data for "Envelope" and "Walls". When the option "Envelope" is selected, the user provides the data for room envelope surfaces, structure layers for the BES or coupled program, which are part of the whole wall area (Figure 6.5a). When the option "Walls" is selected, the user provides data for the wall surface (or structure layers), which contains the remaining wall area when the envelope surfaces are excluded (surface 3 in Figure 6.5a). Without the "Walls" option, the user would have to divide the wall surface 3 (Figure 6.5a) into 7 rectangular surfaces (Figure 6.5b) and define the surface properties for each of them. Therefore, with the data input organized in this way, a large amount of time is saved. However, this organization of data input requires additional procedures that are related to the calculation of the view factors and coupling of the programs.

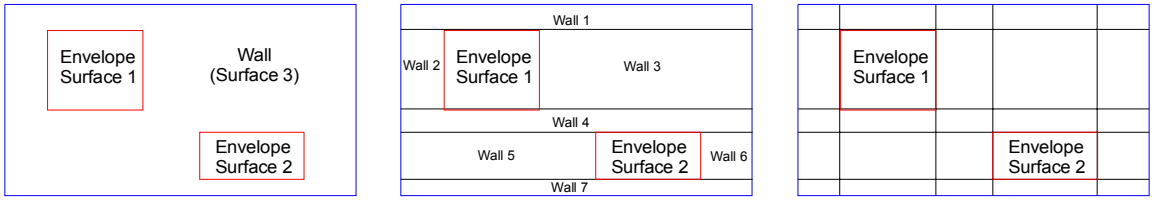

a) b) c)

Figure 6.5 Different types of surface definitions (a) surface definition in GUI,
(b) surface definition in typical CFD and ES programs, (c) internal GUI surface definition

To calculate view factors for surface 3 in Figure 6.5a (the surface with "holes"), the BES program module for view factors uses set of functions that are developed for this type of surfaces based on view factor properties presented in Section 3.2.2. Also, for the coupling of BES and CFD0 programs, surface 3 is automatically divided (by an internal procedure in the BES program) into a set of rectangular surfaces as illustrated in Figure 6.5c. The reason for this discretization of surfaces is the input format for the CFD0 program, which uses rectangular surfaces without "holes".

Figure 6.6 illustrates the widow form in which the position of the surface object(s) is defined. In this form, the user selects the type of surface object such as temperature wall, heat flux surface, adiabatic surface, window, supply, exhaust, radiant panel, and lighting. By selecting the option "Give more details", a window form for characteristic data input will open. This form is different for each of surface object. In the case that surface with similar properties is previously defined, the user just needs to select the option "Copy surface" and select the appropriate surface. Subsequently, the properties of selected surface object are assigned to the new surface object.

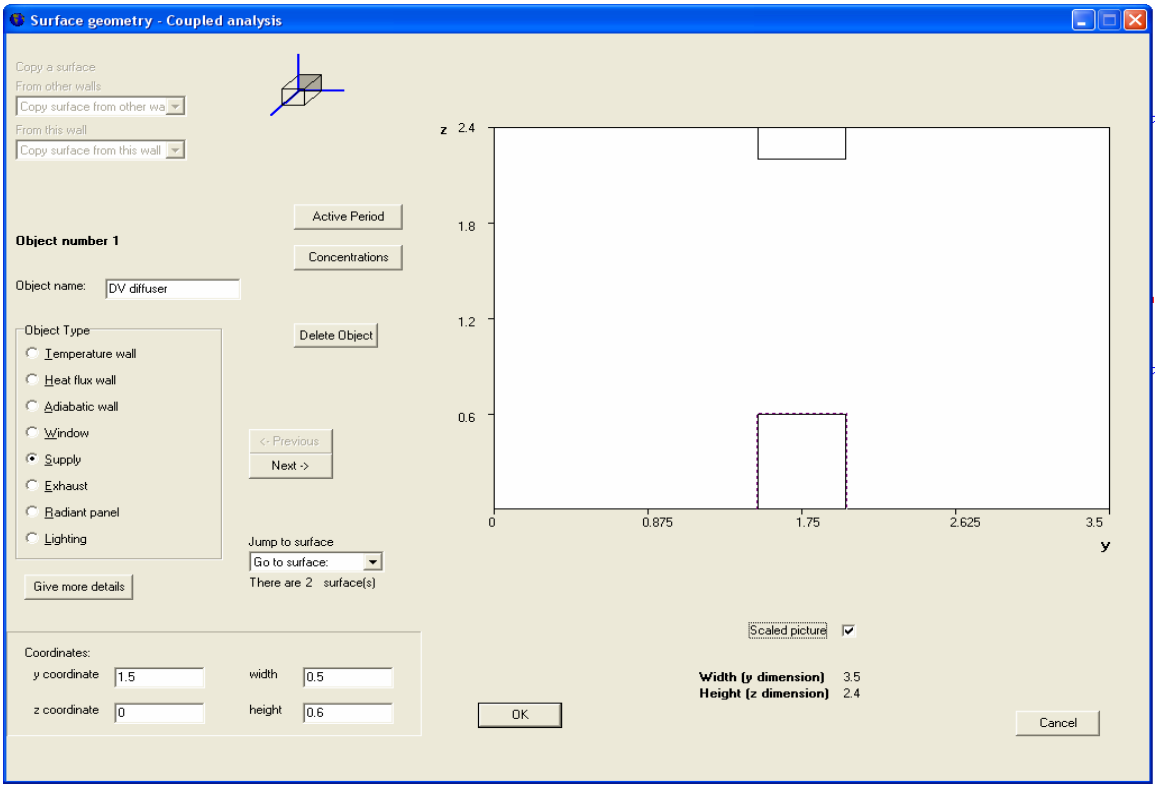

Figure 6.6 Surface positioning and type selection (temperature wall, heat flux surface, adiabatic surface, window, supply, exhaust, radiant panel, and lighting)

Figure 6.7 shows an example of a characteristic data input when object type "Temperature wall" is selected. The user defines the surface as internal or external, and its corresponding surface properties, number of homogeneous layer, material properties for each layer, and number of grid points for each layer (discretization). In the case where only CFD analysis is performed, the user defines only surface temperatures instead of the previously described input data. Forms for other surface objects are organized in a similar way.

For internal objects, called “Blockages”, the user provides data by using windows forms organized in a similar way to the above described forms for surface elements on the wall. The internal object can be defined as: 1) adiabatic surfaces such as furniture, 2) object with constant heat flux at surfaces such as lamps, or 3) controlled thermal devises such as baseboard heaters or fan coils.

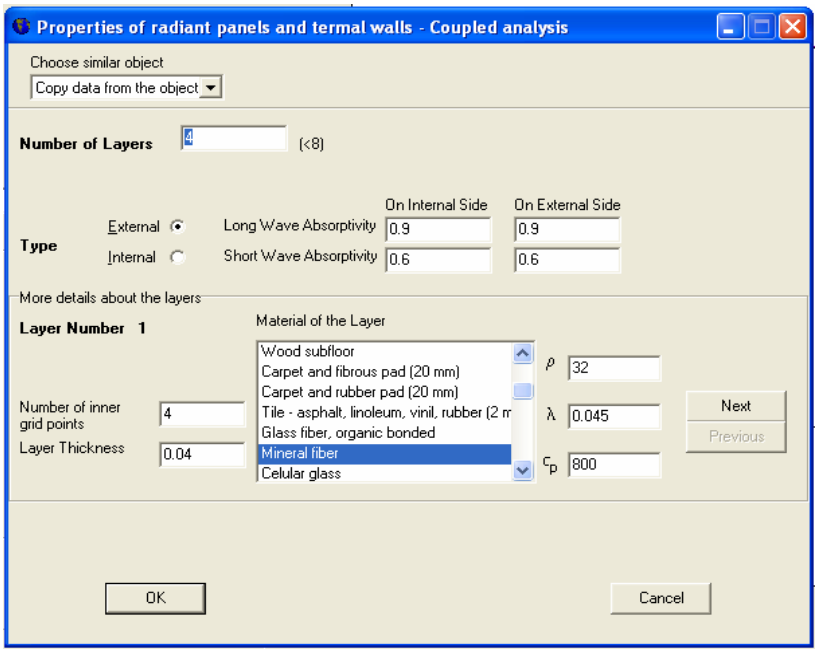

Figure 6.7 Windows form for specification of surface object properties

Mesh generating functions, implemented in the GUI, create a three dimensional grid system. The window for mesh generation in the GUI is shown in Figure 6.8. Depending on the position of the surface object and internal blockages, the internal space is automatically divided into regions, which overlap with edges of these objects and blockages. Following this procedure, the grid between these objects is defined. This is done in one of three ways: 1) automatically by equally spaced grid where the user defines the number of grid points in certain direction (x, y, or z) of a region, 2) automatically by using exponential functions for nonuniform mesh generation in the region, or 3) manually where the user selects and splits the region arbitrarily, creating finer or coarser mesh.

After providing geometry and material property data, and generating the mesh, the user can select other options under the menu “Simulation” (Figure 6.4b), where each option opens a corresponding window form. Depending on which of the three types of simulation is selected, the number of available options changes. For example, when the user selects only the energy flow analysis, options that are related to the CFD iteration control are inactive.

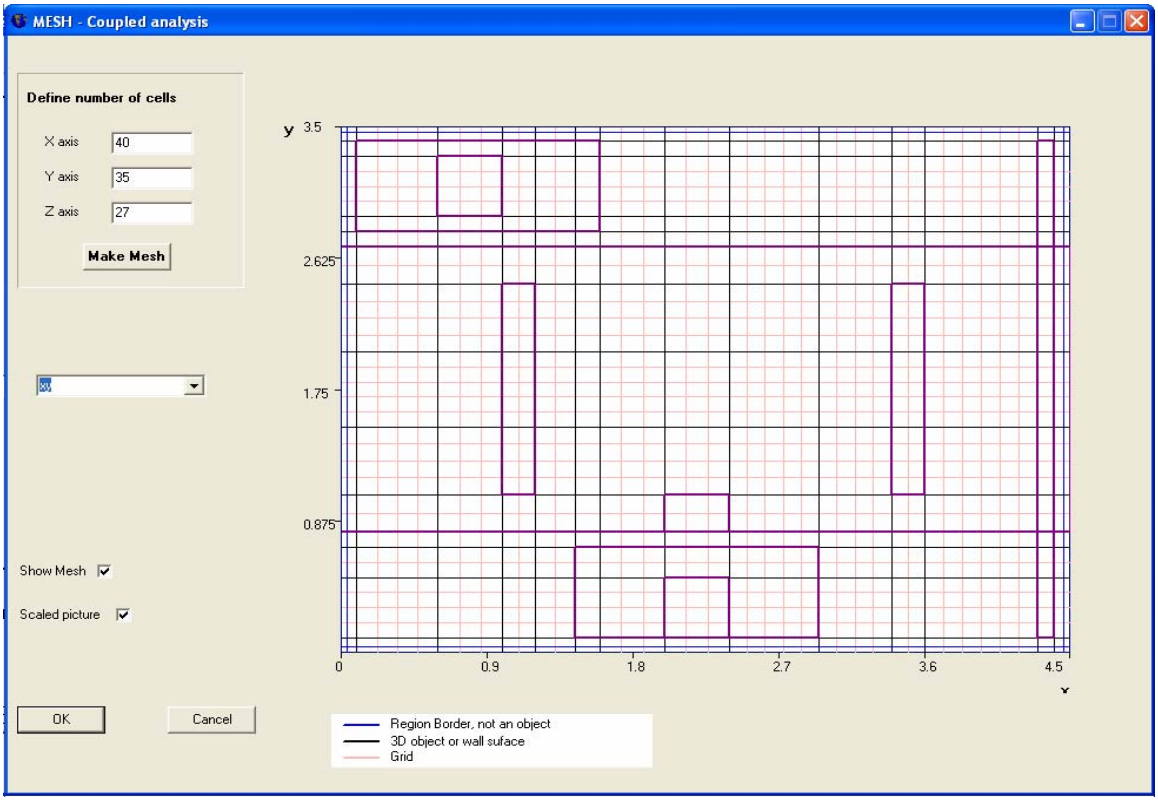

Figure 6.8 Windows form for mesh generation presenting room geometry and regions defined by internal room objects

During the GUI development, special attention was dedicated to organizing the control data needed for different HVAC systems. Figure 6.9 illustrates the windows which allow the user to specify HVAC parameters. These parameters are characteristic for specific HVAC systems, and are input data for constrains control algorithm as described in Figure 3.27.

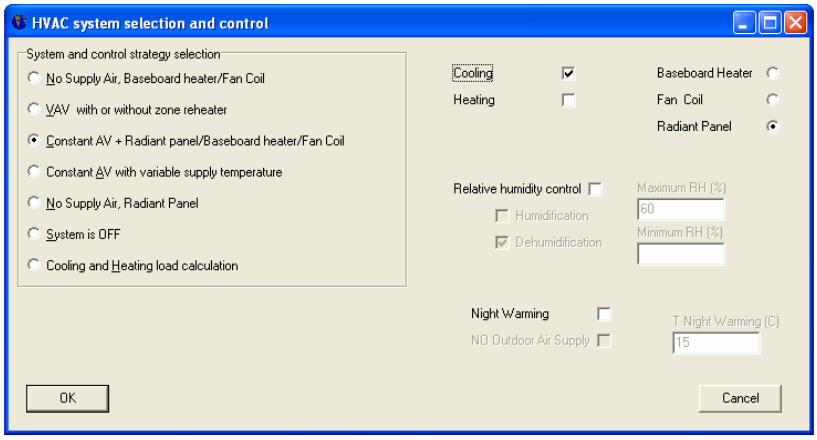

Figure 6.9 Windows form for HVAC system selection
(variations of: all-air, all-water, or combined water air system)

For each type of simulation where the BES program is used, the user specifies the design set point temperatures and location selection of the modeled building. The form for location selection is shown in Figure 6.10. Based on this data, BES selects the appropriate file from TMY2 database.

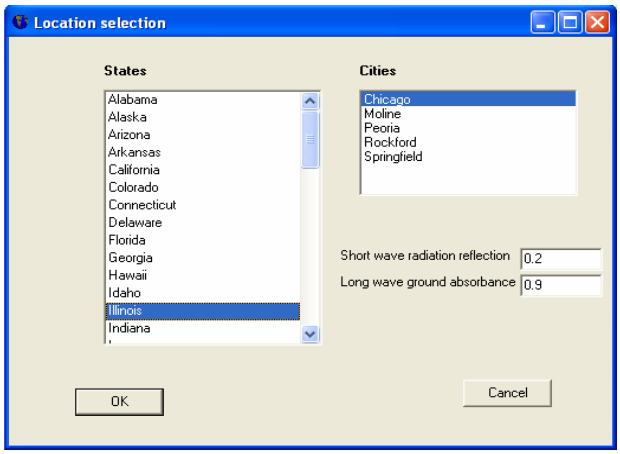

Figure 6.10 Location selection and surface properties of ground or surrounding objects

6.4 GUI Postprocessors

When coupled energy and airflow analysis is performed, the coupled program creates two major output files (Figure 6.1). Each of the coupled programs creates its own output files organized in ASCII format. These files contain large amounts of data. A graphical representation is usually used to analyze these results. A graphical representation is provided by the GUI for result analysis (Figure 6.1).

For the representation of BES output results, any spreadsheet program such as Excel, Origin, and Grapher can be used. The ASCII output file is organized in a chart format and is easily readable by any spreadsheet program. The data are organized in columns where temperatures for each node of all elements of the building are presented for each analyzed time step (Figure 6.11). Besides the temperature distribution in elements, this output file contains basic weather conditions such as external temperature and data which define solar radiation. Also, the file contains data about energy consumption such as cooling/heating energy used in different components of the selected HVAC system. The simplicity of the output file from the BES program enables easy manipulation of data such as representation by graphical charts, calculation of annual energy consumption, or peak cooling load detection. Since almost each computer has

installed at least one of the above spreadsheet programs, the coupled program package does not include any.

Month	Day	Hour	T(1,1)	T(1,2)	T(8,13)	Tair	Text	DNR	DHR	QCload	QHload
5	21	23	19.77	19.96	9.65	20	10.7	0	0	0	724.1
5	21	24	19.35	19.55	7.5	20	8.9	0	0	0	906.7
5	22	1	19.08	19.25	7.43	20	8.9	0	0	0	1004.5
5	22	2	18.89	19.02	7.42	20	8.9	0	0	0	1058.4
5	22	3	18.76	18.86	7.57	20	8.9	0	0	0	1084.9
5	22	4	18.62	18.71	6.35	20	7.6	0	0	0	1175.1
5	22	5	18.47	18.56	5.1	20	6.3	0	0.6	0	1281.9
5	22	6	18.62	18.63	4.51	20	5	132.5	81.7	0	1239.8
5	22	7	19	18.92	7.86	20	8.1	537.5	276.7	0	907.8
5	22	8	19.54	19.38	11.85	20	11.3	746.1	485	0	494.6
5	22	9	20.57	20.25	17.47	20	14.4	845.3	677.5	-122.9	0
5	22	10	21.79	21.35	21.63	20	16.3	864.4	816.4	-852.4	0
5	22	11	23.11	22.59	24.82	20	18.1	862.5	901.9	-1597.5	0
5	22	12	24.15	23.65	27.65	20	20	842.8	933.9	-2184.3	0
5	22	13	24.35	24.07	24.95	20	18.5	514.2	748.1	-2215.1	0
5	22	14	24.11	24.03	21.99	20	17.1	161.4	534.4	-1998.8	0
5	22	15	23.34	23.48	19.35	20	15.6	36.7	319.4	-1500.6	0
5	22	16	22.75	22.94	18.13	20	15.2	33.1	260.8	-1142.4	0
5	22	17	22.13	22.36	16.85	20	14.8	24.7	186.4	-788	0

Figure 6.11 A segment of output files of the BES program

Representation of results from the CFD0 program is more complex than representation of those from the BES program because of the amount and structure of output data from the former program. The output file of the CFD0 program contains solution data that describe the vector and scalar fields in the room for a certain time step or over a certain time period, depending on which type of analysis was selected (air-flow or coupled). Also, this output file contains the room dimensions, positions of the objects in the room, positions of the surfaces on the walls, and data about the grid imposed onto the room. To compile all these data into a graphical interpretation, the GUI for result presentation is almost always used. Graphical programs for 3D visualization such as TECPLOT are suitable for this type of representation. However, these types of programs are specialized programs, and, therefore, not as common as spreadsheet programs. Therefore, a new 3D visualization program is developed and added to couple the program package. The author of this thesis was involved in development of the 3D visualization tools as a program planer and tester, while the source code was developed by the students mentioned in Acknowledgments of this thesis.

The name of the new 3D visualization program is ArchTech. A screen shot is shown in Figure 6.12. The program is written in Visual C++. For the graphical representation of room geometry as well as scalar and vector fields of the results, OpenGL library is used. ArchTech is capable of visualizing both scalar fields (such as pressure, temperature, concentration, intensity of velocity, thermal comfort, and air quality parameters) and vector fields (such as air velocity) in

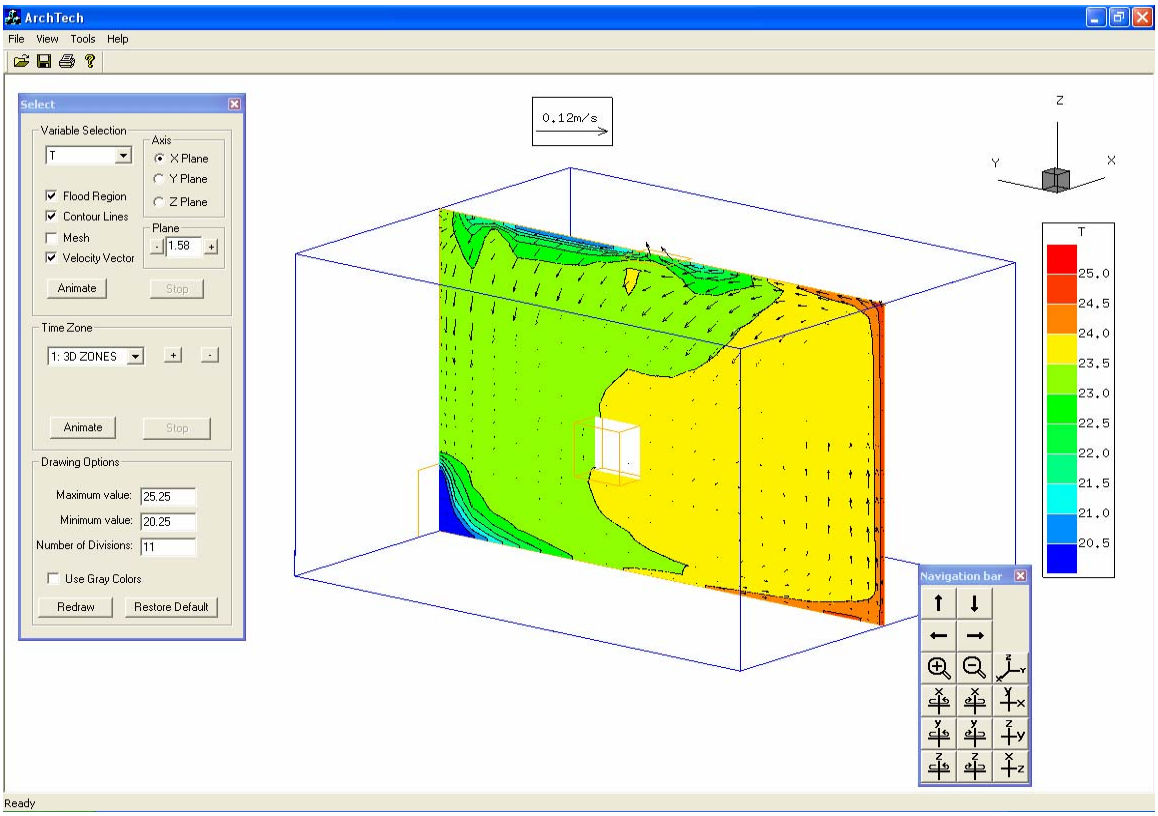

Figure 6.12 New 3D visualization tools developed for presentation of results obtained from CFD0 or coupled program

any given coordinate plane. The program is also capable of presenting the results in the whole space using animation. In this animation, for a specific time step, the coordinate plane (X, Y, or Z) is moving through the space showing the distribution of the specified scalar or vector variables. Also, the program is capable of doing animation in terms of time. In this animation, the change in the scalar or vector variable is presented at a specific coordinate plane for the period of analysis.

Using the "Select" bar (Figure 6.12), the user of ArchTech selects the scalar variable, position of coordinate plane, and time step (zone). The user is also able to change the default spectrum of colors for visualization and choose the size and color map of the vector field. Using the "Navigation" bar (Figure 6.12) the user can manipulate the graphical presentation. This manipulation includes zooming in and out, rotating, and translating. Also, in the window form "Preferences," the user sets up different graphical parameters of the program (Figure 6.13).

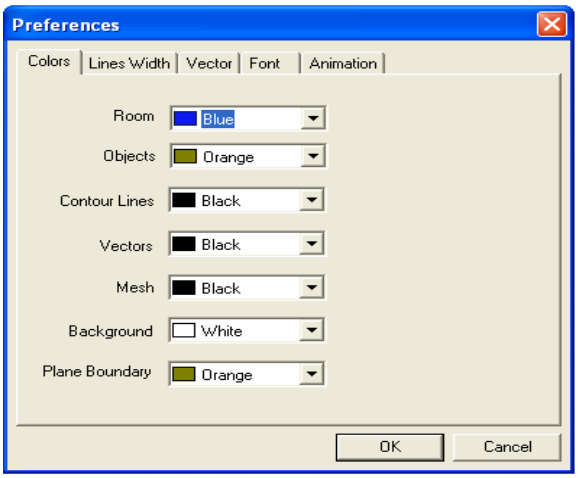

Figure 6.13 Windows form of new 3D visualization tools for the set up of graphical parameters

6.5 Summary

This chapter has presented the structure of the coupled program that provides successful integration of BES and CFD0 programs. Data flow between the preprocessor, BES, and CFD0 programs by ASCII files, used in coupled program, does not occur at optimum speed because a certain amount of CPU time is needed for writing and reading these files. The communication would be faster in the case where these components of the coupled program communicate directly through memory registers. However, the overall reduction of computational time with the direct communication approach, instead of the used method, is negligible. The reason is that the computation time of the CFD0 program (measured in minutes) is very large compared to time used for reading the ASCII file (measured in milliseconds). On the other hand, the applied communication method enables control of the program execution since the user can open the ASCII files and check the parameters in any phase of the calculation. Also, communication by ASCII files enables replacement of certain components of the coupled program. For example, the CFD0 program code can be replaced by some other commercial CFD source code with cretin adjustment in the input and output files.

The newly developed GUI is specialized to provide input data for ES and CFD when they are used specifically for simulation of energy and airflow in buildings. Therefore, it enables users, with little training in numerical simulation code, to apply the coupled program for different energy consumption, air quality, and thermal quality analysis. Finally, the new 3D visualization tool, ArchTech, enables easy analysis of program results.

CHAPTER 7

DEVELOPMENT OF NEW CONVECTION CORRELATIONS

7.1 Introduction

Ventilation systems that use displacement ventilation or high aspiration diffusers, with or without radiant cooling panels, are relatively new and not widely used in building mechanical systems. As a consequence, convection correlations for surface heat transfer in rooms with these ventilation systems are still not developed. Until now, convection correlations used with these types of flow have been based on convection correlations developed for: isolated surfaces, free edge heated plates, or standard ventilation systems. These convection correlations are used in various analyses of these two ventilation systems without any explicit experimental validation. Nevertheless, both displacement and high aspiration diffusers have recently attracted significant attention of design community due to their performance characteristics; therefore, validated correlations are needed.

This chapter presents newly developed convection correlations for displacement ventilation and ventilation with high aspiration diffusers combined with cooled ceiling panels. First, validity of the existing correlations for considered airflow regimes is investigated. Afterwards, new convection correlations are developed for surface types and airflow regimes where validation for the existing correlations fails. These additional convection correlations for calculation of heat fluxes at internal surfaces are needed to improve performance of MACA described in Section 4.3. In addition, these correlations can be used with other simulation tools or in design procedures.

In the next section (Section 7.2) of this chapter, basic details about convection correlation development are presented. The following sections (Sections 7.3, 7.4, and 7.5) provide results for newly developed correlations. The final section (Section 7.6) contains general discussion about these correlations. Detailed reports about the experimental facility, conducted experiments, and result processing are provided in Chapter 8, together with other details of measurements conducted as a part of this thesis.

7.2 Convection Correlations Development

Experimental measurements for the validation of existing and the development of new convection correlations were conducted in experimental chambers with typical room size and typical positions of diffusers and radiant panels. For the correlations developed with a displacement ventilation system, air was supplied by displacement diffusers as shown in Figure 7.1. For the forced convection correlations with mixing ventilation systems, a high aspiration diffuser, located at the ceiling, discharged jets along the long side of the radiant panels. Cooling panels occupied 50% of ceiling space and they were integrated into the suspended ceiling structure.

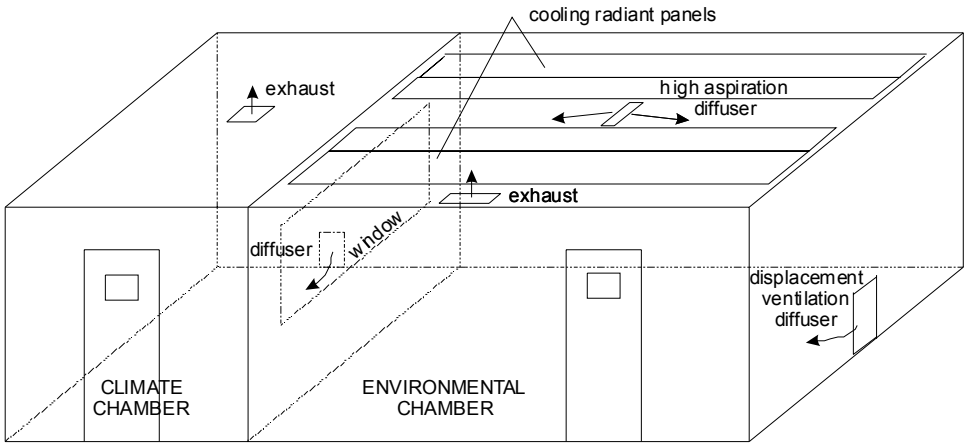

Figure 7.1 An experimental facility for the development of convection correlations

Most of the measurements were conducted in the environmental chamber. Adjacent to the environmental chamber is climate chamber (Figure 7.1). The climate chamber which was used to simulate external conditions is separated from the environmental chamber by a partition wall with a window. This climate chamber is also used for development of convection correlation with displacement ventilation diffusers. Experimental set-up for the validation of existing and development of new convection correlations was adjusted to be as close as possible to realistic situations in building. For example, room geometry, surface and supply temperatures, supply air volume flow rates were selected to be in a range that appears in real buildings.

Convection correlations were developed for steady state conditions, based on measured specific surface heat fluxes (q_{conv}), surface temperatures (T_{surf}), and air temperature (T_{air}). Using a basic equation for convective heat transfer, the convection coefficient was calculated as:

$$h = \left| \frac{q_{conv}}{T_{surf} - T_{air}} \right| \tag{7.1}$$

Convective heat transfer at internal surfaces was not measured directly, but rather calculated from the temperature measurements. This was accomplished using a heat balance at internal surfaces (Figure 7.2):

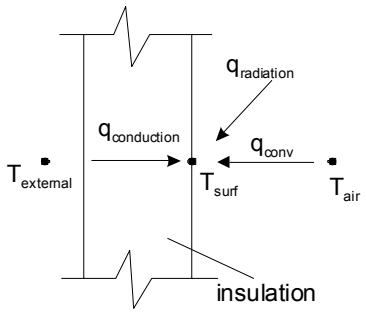

Figure 7.2 Energy balance on internal surfaces of an experimental facility

Heat balance equation:

$$q_{conv} = -q_{radiation} - q_{conduction} \tag{7.2}$$

Conductive heat flux ($q_{conduction}$) was calculated based on insulation resistance and temperature difference between internal surface and external air temperature. For windows and partition walls that do not have thick insulation the conductive heat flux was directly measured using a system of heat flux meters. Radiative heat flux ($q_{radiation}$) at surface *'i'* is calculated by using the radiative heat exchange factor $\psi_{i,j}$ described in Section 3.2.2:

$$q_{radiation,i} = \sum_{j=1}^{n} \varepsilon_i \psi_{i,j} \sigma_o \left(T_i^4 - T_j^4 \right) \tag{7.3}$$

For this method long wave emissivity *(ε)* and temperatures (*T*) are needed for all surfaces of the enclosure. To precisely calculate radiative heat fluxes, the enclosure was divided into 38 surfaces and more than 50 temperature sensors were attached to these surfaces.

Air temperature was measured in the vicinity of each surface (0.1 m from surface) and at different positions in the central part of the room. Overall, air temperature was measured at more than 45 positions in the room including supply and exhaust air temperatures. Using this

temperature distribution, natural convection correlations at surfaces were calculated for local air temperature. For surfaces with dominant forced convection, the correlation was expressed as a function of number of Air Changes per Hour in the room *(ACH)* using the local air temperature as the reference temperature.

Convection correlations developed as a part of this thesis are presented in a simplified form. General relationships between Nusselt numbers *(Nu)*, Prandtl numbers *(Pr)*, and Grashof numbers *(Gr)* are defined differently for laminar and turbulent flows (ASHRAE 2001). These equations are:

For laminar flow: $$Nu = C_L (Gr \cdot \mathrm{Pr})^{1/4} \tag{7.4}$$

For turbulent flow: $$Nu = C_T (Gr \cdot \mathrm{Pr})^{1/3} \tag{7.5}$$

By substituting values for constant *Pr* for air, and other air constants in the expressions for *Nu* and *Gr* numbers, simplified forms for convection correlations are obtained:

$$h_{c\_laminar} = a(\Delta T / L)^{1/4} \tag{7.6}$$

$$h_{c\_turbulent} = b(\Delta T)^{1/3} \tag{7.7}$$

The Rayleigh number ($Ra = Gr\,Pr$) is used as a criterion to define if the flow is laminar or turbulent.

For forced convection and turbulent flow:

$$Nu = C_T \,\mathrm{Re}^{4/5}\,\mathrm{Pr}^{1/3} \tag{7.8}$$

Nusselt and Reynolds numbers can be expressed as functions of room volume (V_{room}) and air supply volume flow rate ($\dot{V}_{supply}$):

$$Nu = \frac{h V_{room}^{1/3}}{k_{air}} \tag{7.9}$$

$$Re = \frac{\dot{V}_{supply}}{\nu_{air} V_{room}^{1/3}} \tag{7.10}$$

Substituting Equations (7.9) and (7.10) into expression (7.8) and substituting values for constant Prandtl number *(Pr)*, air conductivity *(k_{air})* and dynamic viscosity *(v_{air})*, the following expression is obtained:

$$h_{c\_forced} = C\left(\dot{V}_{supply} / V_{room}^{3/4}\right)^{4/5} = C \cdot V_{room}^{1/5} ACH^{4/5} \tag{7.11}$$

Very often the influence of space volume ($V_{room}^{1/5}$) is omitted and forced convection at surfaces is presented as a function of volume flow rate (Fisher 1995, Fisher and Pedersen 1997):

$$h_{c\_forced} = c \cdot ACH^{4/5} \tag{7.12}$$

where each type of surface (floor, ceiling, or walls) has a different coefficient '*c*'.

To combine effects of: (1) laminar and turbulent flow in natural convection correlations or (2) natural convection with forced convection, the following equation is used (Churchill and Usagi 1972):

$$h_{combined} = (h_1^n + h_2^n)^{1/n} \tag{7.13}$$

This equation favors a dominant term (h_1 or h_2), and exponent coefficient '*n*' determines the value for $h_{combined}$ when both terms have the same order of values (Figure 7.3).

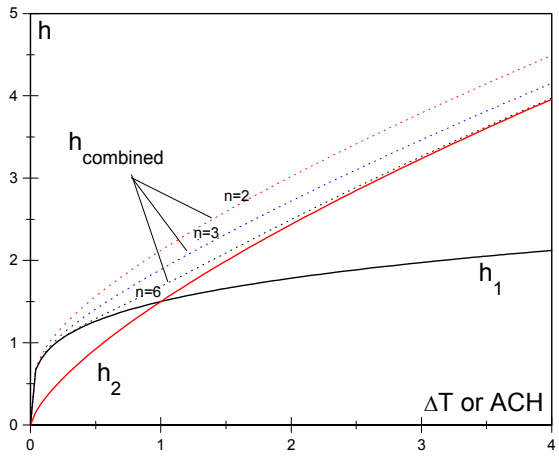

Figure 7.3 Combined convection coefficients for natural and forced convections

7.3 Convection Correlation at Cooled Ceiling Panels

A precise convective heat-flux calculation at cooling panels is essential for evaluation of cooled ceiling systems. Therefore, in this section new convection correlations for cooled ceiling surfaces are presented. Currently used convection correlations for natural convection at cooled ceiling surfaces (Alamdari 1983, Awbi and Hatton 1999, and Min 1956) are not based on measurements at cooled surfaces. Instead of these measurements, convection correlations for heated floor surfaces are applied at cooled ceilings using an analogy to assume that the equation for a heated floor is valid for cooled ceiling surfaces. The analogy between convective heat transfer for cooled ceiling surfaces and for heated floor surfaces is valid in the boundary layers. Therefore, the convection correlations for these surfaces are represented with the same equation. However, temperature stratification in the room, combined with reference temperature selection, limits the use of the same convection correlation for calculation of convective heat flux at cooled ceiling and heated floor surfaces.

Figure 7.4 shows the temperature profiles near the heated floor and cooled ceiling in the room. Temperature stratification near the cooled ceiling is more or less present in all rooms with natural convection. The level of stratification depends on the types of heat sources in the room. In the case where heat sources are primarily convective (large portion of energy from source is directly transferred to the air) the stratification is larger, while in the case where heat sources are wall surfaces, the room temperature profile is more uniform (Figure 7.5). Computers and other equipment are primarily convective heat sources, while sun radiation and lighting system are primarily surface (radiative) heat sources.

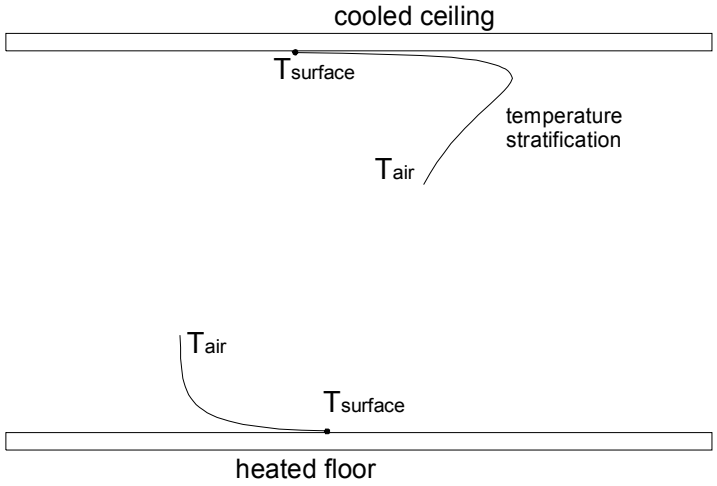

Figure 7.4 Temperature profiles near a cooled ceiling and a heated floor

Experiments with convective and surface heat sources were conducted to evaluate validity of the existing convection correlations for cooled ceilings. With convective heat sources and larger temperature stratification in the vicinity of the cooled ceiling panels, a larger convective heat flux was detected during the measurements. The reason for this is the buoyant plume from convective heat sources, which hits the ceiling and disperses in the vicinity of the ceiling. This creates larger air movement and intensifies convective heat transfer. This effect is not so obvious with the surface heat sources (Figure 7.5). However, the measurements always revealed certain stratification in the vicinity of radiant panel surfaces. This effect of temperature stratification is characteristic of the room airflow-type. Therefore, it was not detected in experiments where the convection correlations were developed based on measurements with isolated surfaces and free edge cooled plates such as Alamdari and Hammond convection correlations (1983). Also, this stratification was not taken into account when the analogy between cooled ceilings and heated floors is used (Awbi and Hatton 1999, Min 1956). Therefore, in this thesis, a new convection correlation was developed based on experimental measurements with radiant cooling panels.

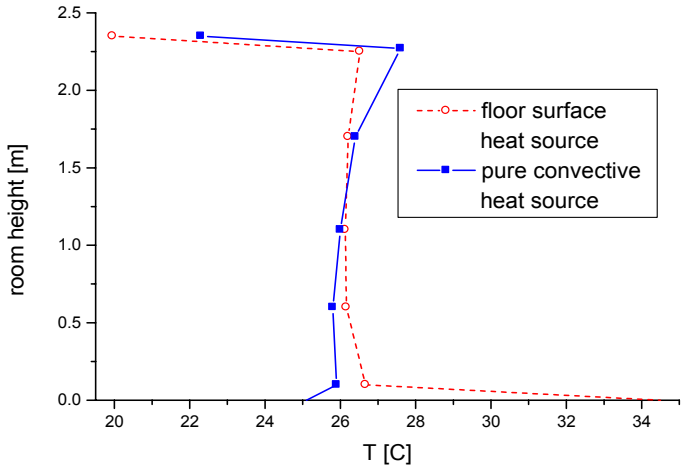

Figure 7.5 Measured air temperature profiles for pure convective and surface heat sources

The air flow in the vicinity of cooled ceiling panels is primarily turbulent. For typical dimensions of cooling panels (hydraulic diameter larger than 1.0 m) and temperature differences between the air and panel surface (most of the time larger than 2°C), Rayleigh number is $Ra>2\cdot10^{8}$, which indicates turbulent air flow for horizontal surfaces (Kakac 1987). Therefore, newly developed convection correlations have the form of equation (7.13). Local temperature of the air layer at a distance of 0.1 m from the cooling panels is used as the reference air temperature for convection correlation development. Figure 7.6 shows the results of the measurements in the

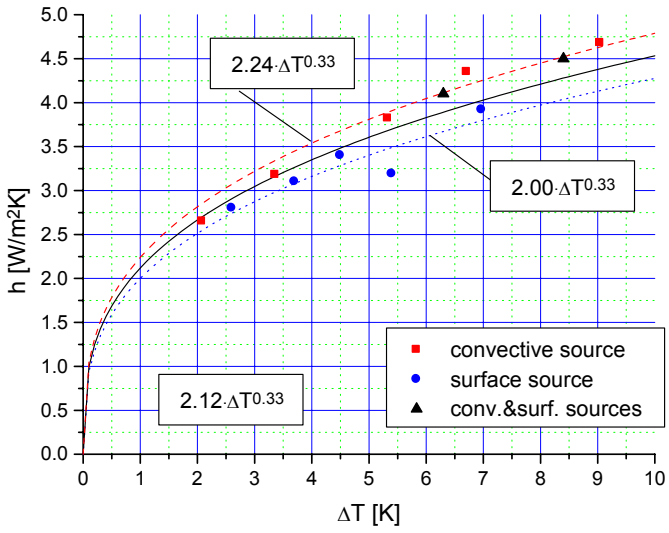

Figure 7.6 Experimental results used for the development of cooled ceiling convection correlations

case with pure convective and surface heat sources. The difference in convective coefficients is more than 10%. In real buildings, heat sources are combinations of convective and surface heat sources. Therefore, additional experiments were conducted with convective and surface heat sources in the experimental chamber. The obtained results "fall" between correlations for pure convective and surface heat sources (Figure 7.6). Using all measured data a final convection correlation for cooled ceiling panels is obtained:

$$h_c = 2.12 \cdot \Delta T^{0.33} \tag{7.14}$$

7.4 Convection Correlations in a Room with High Aspiration Diffuser

A large volume flow rate is common in typical ventilation systems, where standard mixing diffusers are usually used with ventilation volume flow rates resulting in 4 or more air changes per hour (*ACH*). For systems where only fresh air is supplied, such as Dedicated Outdoor Air System -DOAS (Mumma 2001), usual occupancy level requires supply volume flow rate that provide less than 4 *ACH* in the room. With this low volume flow rate, a standard mixing diffuser usually has a problem to produce appropriate mixing (Novoselac and Srebric 2002). Therefore, special high-aspiration diffusers are used with this system. High-aspiration diffusers create larger

mixing with the same primary volume flow rate. Therefore, different correlations are expected for this type of flow when compared to the flow for Fisher and Pedersen's correlations (1995, 1997). In addition, rooms with cooled ceilings have enclosure temperature considerably lower than with other HVAC cooling systems. In these rooms enclosure temperatures are close to the room air temperature (Novoselac and Srebric 2002) and buoyancy at enclosure surfaces is small. Therefore, forced convection can be dominant at the majority of surfaces when high-aspiration diffusers are combined with ceiling cooling panels. To develop convection correlations for rooms with cooled ceiling and high aspiration diffusers, a new set of experiments with high aspiration diffuser was conducted.

In the experimental setup a high aspiration diffuser positioned between the radiant panels supplied the air along the panel's longer sides (Figure 7.1). As a heat source in the room, a pure convective heat source was used. Radiant panels extracted the heat directly by convection and indirectly by radiation. Cooled ceiling panels decreased the temperature of the rest of the surfaces. In these experiments, all room surfaces had lower temperature than the room air temperature because the pure convective heat source (with minor radiation effects) was used to produce cooling load.

To create generalized forced convection correlations, specific volume flow rate represented by *ACH* is used to describe the intensity of air movement near surfaces. Therefore, forced convection correlations have the form of Equation (7.12). As a reference temperature, local air temperature was selected instead of supply air temperature, which was used by Fisher and Pedersen (1995, 1997). The high aspiration diffuser creates large air entrainment and jet temperature becomes close to the room air temperature after a short distance from the diffuser. Hence, with the high aspiration diffuser, a reference temperature difference between supply air and surface temperatures that are distant from diffuser would not be relevant.

A high aspiration diffuser combined with a cooled ceiling system supplies constant volume flow rate. Therefore, during the experiments, air volume flow rate was varied for several different heat loads in order to get a correlation between *ACH* and *h*, while the jet velocity was kept approximately constant at a face velocity of 15 m/s. The high aspiration diffuser supply velocity was kept approximately constant by changing the number of supply diffuser openings. Also, supply temperature was kept constant and approximately equal to the room temperature because supply temperature has a small effect on forced convection correlation with the high

aspiration diffuser. Besides temperature, air velocity was measured in the vicinity of surfaces in order to calculate Reynolds *(Re)* numbers and Grashof *(Gr)* numbers. The ratio Gr/Re^2 was used to determine surfaces with dominant forced convection ($Gr/Re^2<1$) or buoyant convection ($Gr/Re^2>1$) - Schlichting (1968).

The measurement results show that a high aspiration diffuser creates a directional jet, which attaches to a narrow ceiling area between cooling panels (Figure 7.7). As a consequence, only a small area of the room ceiling is directly affected by the high velocity forced convection. The air velocity in the vicinity of the cooling panel surfaces increases with increase of *ACH* because larger jet momentum creates a larger jet entrainment (Figure 7.7). However, an increase of air velocity near the rest of the ceiling is not large. For example, with an increase of *ACH* from 0 to 5, the measured increase of velocity in the vicinity of cooling panels is from 0.2 to 0.4 m/s. For the floor surface, the measured increase of velocity is from 0.05 to 0.2 m/s (for *ACH* from 0 to 5). At zero *ACH* in the room, the velocity in the vicinity of the cooling panels (0.2 m/s) was larger than at the floor surfaces (0.05 m/s) because of larger heat flux and air movement caused by natural convection at these panels.

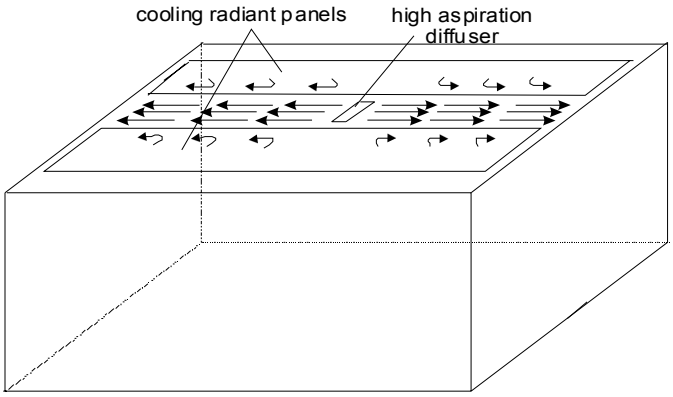

Figure 7.7 High aspiration diffuser providing a narrow jet with high entrainment of room air

For vertical surfaces, a directional jet creates the situation where side walls that were hit by the jet (see Figure 7.7) have larger velocity and forced convection coefficients than wall surfaces parallel to the jet. In fact, forced convection coefficients for walls depend on room geometry and orientation of high aspiration diffuser's jets. To create general correlations that are applicable in practice, convection coefficients for walls with dominant forced convection were averaged and presented as a function of *ACH* (Figure 7.8). Function-fitting was used for determining coefficient 'c' in Equation 7.12 (c=1.31).

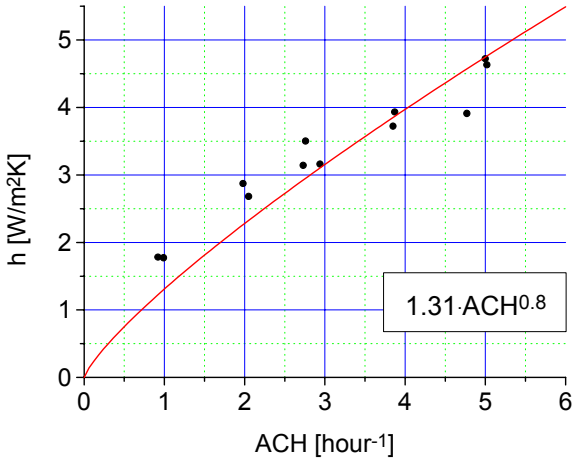

Figure 7.8 Forced convection correlation for walls in a room with the high aspiration diffuser

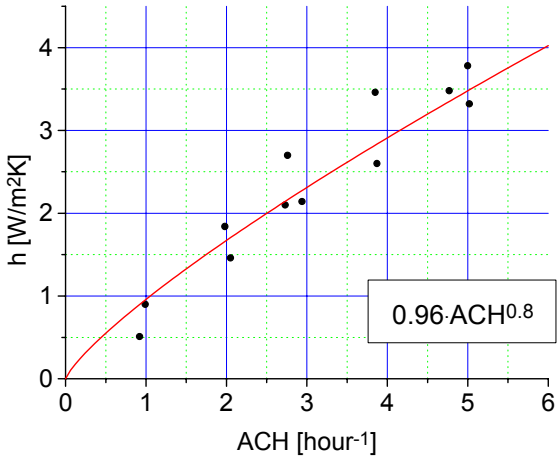

Figure 7.9 Forced convection correlation for a floor in a room with the high aspiration diffuser

Figure 7.9 shows measurement results for floor surfaces. Unlike for walls, measured forced convection coefficients at floor surfaces were rather uniform. An *ACH* function in the form of Equation (7.12) was used to express forced convection coefficient at floor surfaces.

At the ceiling radiant panels, the temperature difference between the surface and local air creates a buoyant effect which is predominant heat transfer mechanism. This was the case for measurements with small *ACH* (=1,2,3), where buoyant (natural) convection was created by ΔT=5-8°C. Therefore, in the ceiling area with the forced convection development, the buoyant effect was taken into account using an equation for combined forced and natural convection

(Equation 7.13). To take into account the natural convection coefficient at cooled ceiling surfaces, the newly developed correlation for cooled ceiling surfaces is used (Equation 7.14). Then, using the data set: h_c, ΔT, ACH, for each experiment and equation:

$$h_c = \left[(2.12 \cdot \Delta T^{0.33})^3 + (c \cdot ACH^{0.8})^3\right]^{1/3} \tag{7.15}$$

the coefficient 'c' is calculated. Resulting forced convection correlation at ceiling panels is presented in Figure 7.10.

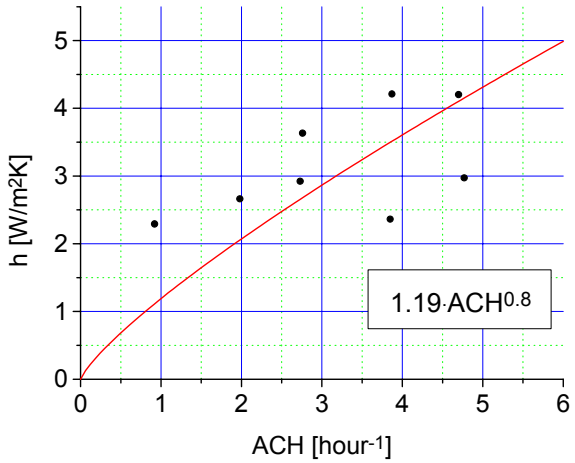

Figure 7.10 Forced convection correlation for a ceiling in a room with the high aspiration diffuser

To create general correlations for rooms with high aspiration diffusers, newly developed correlations, presented in Figures 7.8-7.10, are combined with expressions for natural convection. These general correlations can be used at surfaces where both forced and natural convection are present. There are several existing correlations for natural convection, which all provide different results. To select the most appropriate one, several measurements of convection coefficients were conducted at floor and wall surfaces in the environmental chamber with no air supply. Figures 7.11 and 7.12 show the comparison of these measured convection coefficients with two existing convection correlations. The results are compared for the characteristic height of the chamber walls of 2.35 m (Figure 7.11) and hydraulic diameter of the heating panels at the floor of 2.6 m (Figure 7.12).

Correlations developed by Awbi & Hatton (1999) have better agreement with measured results than correlations developed by Alamdari & Hammond (1983) for both a natural

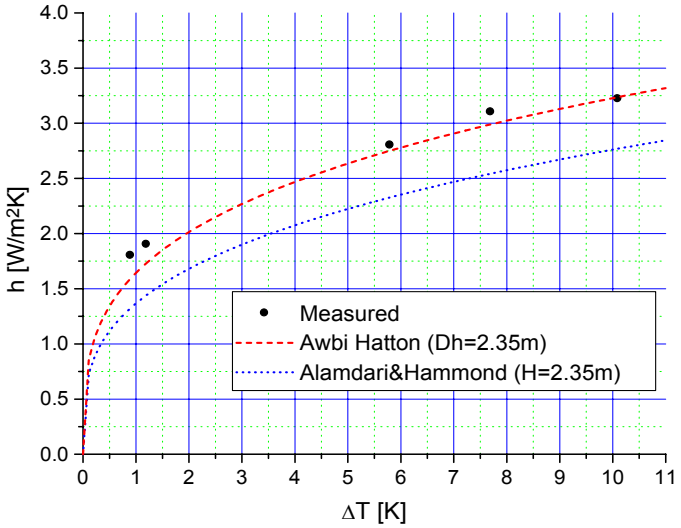

Figure 7.11 Natural convection correlations for vertical surfaces in a room with no ventilation

convection correlation for vertical surfaces and a natural convection correlation for floor when $T_{floor}>T_{air}$. The most likely reason for this better agreement is the similar experimental set-up. Awbi & Hatton's natural convection correlations were developed in a similar environmental chamber using local air temperature as a reference temperature, while Alamdari & Hammond natural convection correlations were developed by a series of experiments which were primarily conducted with isolated surfaces. Therefore, newly developed forced convection correlations for rooms with high aspiration diffusers are combined with Awbi & Hatton's natural convection

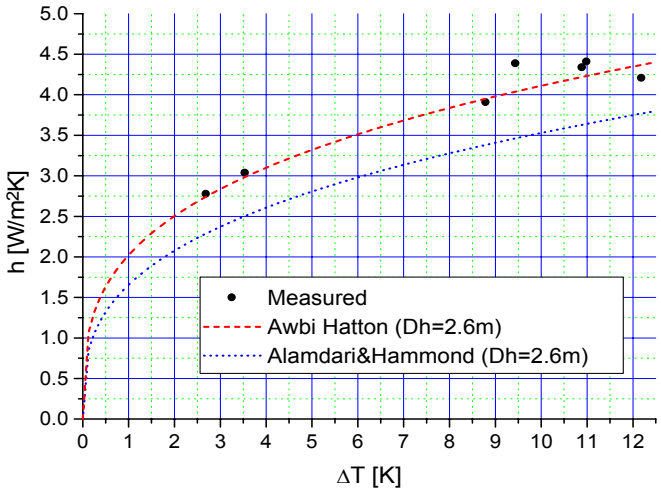

Figure 7.12 Natural convection correlations for a floor surfaces where $T_{floor}>T_{air}$ and there is no ventilation in a room

correlations for all surfaces except for ceiling surfaces. For the ceiling surfaces, where $T_{surface}<T_{air}$, Equation 7.15 is used with c=1.19 (Figure 7.10).

The newly developed general convection correlations for rooms with high aspiration diffusers have the following forms:

Floor $T_s>T_{air}$:

$$h_c = \left[(2.175 \cdot \Delta T^{0.308} / D_h^{0.076})^3 + (0.96 \cdot ACH^{0.8})^3\right]^{1/3} \quad (7.16)$$

Floor $T_s<T_{air}$:

$$h_c = \left[(0.704 \cdot \Delta T^{0.133} / D_h^{0.601})^3 + (0.96 \cdot ACH^{0.8})^3\right]^{1/3} \quad (7.17)$$

Ceiling $T_s>T_{air}$:

$$h_c = \left[(0.704 \cdot \Delta T^{0.133} / D_h^{0.601})^3 + (1.19 \cdot ACH^{0.8})^3\right]^{1/3} \quad (7.18)$$

Ceiling $T_s<T_{air}$:

$$h_c = \left[(2.12 \cdot \Delta T^{0.33})^3 + (1.19 \cdot ACH^{0.8})^3\right]^{1/3} \quad (7.19)$$

Walls:

$$h_c = \left[(1.823 \cdot \Delta T^{0.293} / D_h^{0.121})^3 + (1.31 \cdot ACH^{0.8})^3\right]^{1/3} \quad (7.20)$$

7.5 Convection Correlations in a Room with Displacement Ventilation

With Displacement Ventilation (DV) diffusers, there are specific air flow and temperature profiles, reflecting stratification and jet attachment, in the vicinity of the floor (Figure 7.13). Supply air with a temperature that is lower than the room air temperature creates

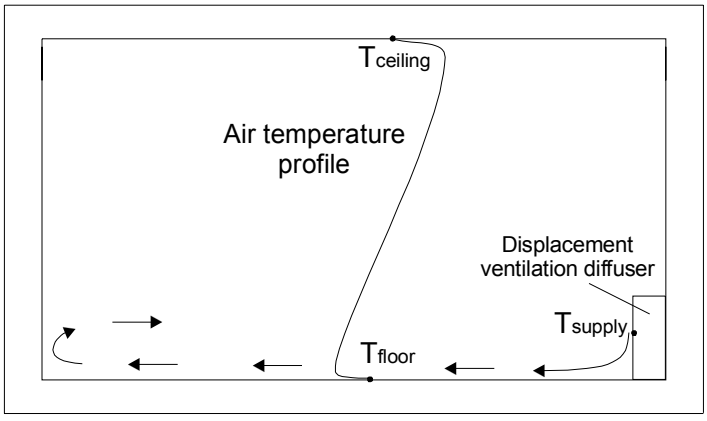

Figure 7.13 Air flow and temperature stratification in a room with displacement ventilation

an air layer in the vicinity of the floor which has lower temperature than the floor surface temperature. Above this layer, the air stratification creates a positive temperature gradient (Figure 7.13). In the vicinity of the ceiling, air temperature stratification very often creates the situation where local air has a higher temperature than most of the ceiling surfaces, except for ceiling lamps. Because of specific air flow near the floor and temperature stratification, use of existing convection correlations for natural convection in the room with displacement diffusers is inappropriate. Therefore, this section presents newly developed correlations for floor surface in the room with DV diffuser.

At the floor level, air flow increases convective heat transfer, and, therefore, the convection coefficient should be calculated by a mixed forced and natural convection correlation. To develop this mixed correlation, a new set of experiments with displacement diffusers were conducted in the climate chamber of the experimental facility (Figure 7.1). The convective heat flux at the floor was measured for different volume flow rate of the supply air. Details about the experimental set up are provided in Chapter 8.

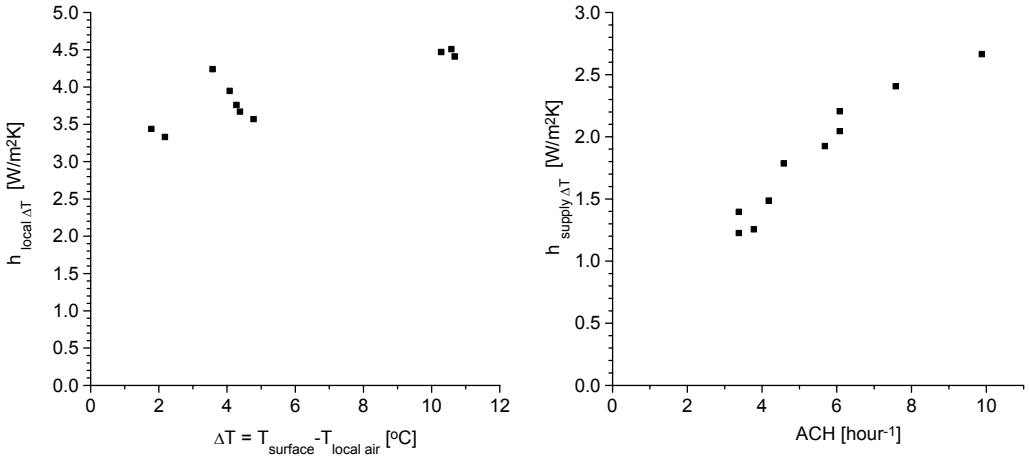

Figure 7.14 Measured convection coefficients for the floor in rooms with displacement ventilation as a function of a local temperature difference *(ΔT)* and the supply flow rate *(ACH)*

During the development of a forced convection correlation at floor surfaces with displacement ventilation, two reference temperatures are considered: local air temperature (T_{local_air} - 0.1m from floor) and supply air temperature *(T_{supply})*. In the case when the reference temperature is the supply air temperature, the convective heat flux is calculated as $q_{surface}=h_{supply}\cdot[T_{surface}-T_{supply}]$ and the convection coefficient *(h_{supply})* is a function of the supply air volume flow rate expressed by the number of Air Changes per Hour *(ACH)*. Figure 7.14 presents

the results of measurements as a function of local temperature difference (ΔT=$|T_{surface}$- $T_{air}|$) and *ACH*. These results indicate that the convection correlation expressed as a function of volume flow rate is stronger than the correlation expressed as a function of a temperature difference of local air and floor surface. Therefore, forced convection correlation at floor surface with displacement ventilation system has the form of Equation (7.12).

Using function-fitting and experimental results, the coefficient '*c*' for the forced convection correlation (Equation 7.12) is determined (*c*=0.48):

$$h_{c\_\mathrm{sup}\,ply} = 0.48 \cdot ACH^{0.8} \tag{7.21}$$

This correlation is based on the supply air temperature and needs to be modified for use with the local air temperature (or the room average temperature):

$$h_{c\_local} = \frac{\left|T_{surface} - T_{supply}\right|}{\Delta T} 0.48 \cdot ACH^{0.8} \tag{7.22}$$

This equation should be used carefully because at some surfaces the local air and surface temperature difference ΔT is very small and close to zero. In these cases, h_{c_local} takes unrealistic values. This is especially the case when this equation is used with automatic iterations such as in the MACA algorithm. To avoid the problem, restrictions are implemented in the MACA algorithm. When $\Delta T < \varepsilon$ instead of $\left|T_{surface} - T_{supply}\right| / \Delta T$, $\left|T_{surface} - T_{supply}\right| / \varepsilon$ is used, where in MACA $\varepsilon = 0.2$°C.

The correlation Equation (7.21) is based on measurements where the whole floor area has the same heat flux. In reality, some parts of the floor may have larger temperature and convective heat flux than the rest of the floor. For example: surfaces heated by direct solar radiation (sun patches) or surfaces heated by local lighting system have a considerably larger temperature than the surfaces in the vicinity of the displacement diffuser. To test the newly developed convection correlations, additional experiments with heat patches were conducted. In these experiments part of the floor was releasing a larger heat flux (convection portion ~38 W/m^2). The results of these experiments are presented in Figure 7.15.

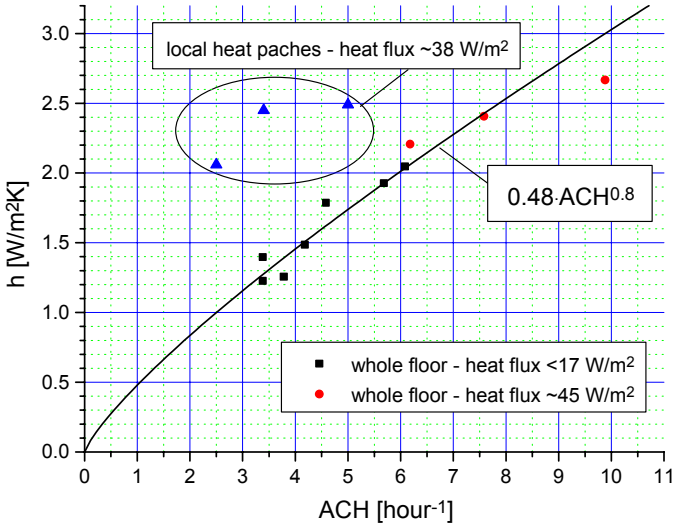

Figure 7.15 Forced convection correlations for the floor in rooms with a DV diffuser including the convection coefficients measured at heat patch surfaces

Figure 7.15 shows that the newly developed correlation for forced convection (Equation 7.21) cannot predict convective heat transfer for local heat patches where buoyant air flow is predominant. The measurements show that Equation (7.21) under-predicts convective heat flux at heat patches from 30 to 50%. To take into account buoyant convective effect of local heat patches, Equation (7.22) is combined with the Awbi & Hatton equation for buoyant flow at floor surfaces (Table 4.6). Equation (7.13) combines the effects of natural and forced convection where exponent coefficient n=6 provides the best results. The largest difference between measured and predicted (by the combined equation) heat flux is below 19%, including heat patches. With these large exponent coefficient n, Equation (7.13) "works" more like a "selector" between the two correlations. The final forms of convection correlations at floor in the room with the displacement ventilation diffuser are given at the end of this section (Equations 7.23 and 7.24).

In rooms with displacement ventilation, air velocities are generally small. In experiments with displacement diffusers at points near wall surfaces, the ratio Gr/Re^2 was above 1. This means that natural convection was dominant at wall surfaces. Therefore, the convection correlation (Awbi & Hatton) for vertical surfaces is proposed for use in rooms with displacement ventilation. For ceiling surfaces, the displacement ventilation temperature stratification often causes higher local air temperatures than ceiling surface temperatures (Figure 7.13). At these

surfaces, the convective heat transfer is similar to the one described for cooled ceiling panels (refer to Figure 7.4). Therefore, the newly developed correlation for cooling ceiling panels (Equation 7.13) is proposed at these surfaces when $T_s<T_{air}$. In the case when $T_s>T_{air}$ (such as lamps surfaces or ceiling surfaces in rooms with large solar heat gains), Awbi & Hatton correlations for heated ceiling surfaces are appropriate (refer to Table 4.6).

The general forms of proposed convection correlations for rooms with displacement ventilation diffusers are:

Floor, $T_s>T_{air}$:

$$\left[\left(2.175 \cdot \Delta T^{\,0.308} / D_h^{0.076} \right)^6 + \left(\frac{\left| T_s - T_{supply} \right|}{\Delta T} 0.48 \cdot ACH^{\,0.8} \right)^6 \right]^{1/6} \tag{7.23}$$

Floor, $T_s<T_{air}$:

$$\left[\left(0.704 \cdot \Delta T^{0.133} / D_h^{0.601} \right)^6 + \left(\frac{\left| T_s - T_{supply} \right|}{\Delta T} 0.48 \cdot ACH^{\,0.8} \right)^6 \right]^{1/6} \tag{7.24}$$

Walls:

$$1.823 \cdot \Delta T^{0.293} / D_h^{0.121} \tag{7.25}$$

Ceiling, $T_s>T_{air}$:

$$0.704 \cdot \Delta T^{0.133} / D_h^{0.601} \tag{7.26}$$

Ceiling, $T_s<T_{air}$:

$$2.12 \cdot \Delta T^{0.33} \tag{7.27}$$

7.6 Discussion and Summary

Figure 7.16 shows the comparison of the newly developed convection correlation for cooled ceiling panels (Equation 7.14) with correlations developed by other researchers. Results are compared for hydraulic diameter of cooling surfaces of D_h=2.0 m because of the cooling panels with these dimensions were used for the new correlation development. The newly developed correlation predicts considerably larger heat flux than the Alamdari & Hammond correlation (Table 4.2), and slightly larger heat flux than the correlation developed by Awbi & Hatton (Table 4.6) or the correlation developed by Min et al. (1956). The newly developed correlation is closer to the correlations of Awbi & Hatton, and to the correlation developed by Min et al. than to the Alamdari & Hammond correlation because these correlations are developed based on measurements in experimental chambers, while the Alamdari & Hammond correlation is based on measurements at isolated surfaces. The new correlation calculates 9% larger convection coefficients than Awbi & Hatton correlation and 5% larger coefficients than correlation developed by Min et al. The most probable reason for this is the fact that convective heat sources were used for the new correlation development (refer to Section 7.3 and Figure 7.6), while for the two existing correlations only surface sources and sinks were used (Awbi and Hatton 1999 and Min et al. 1956).

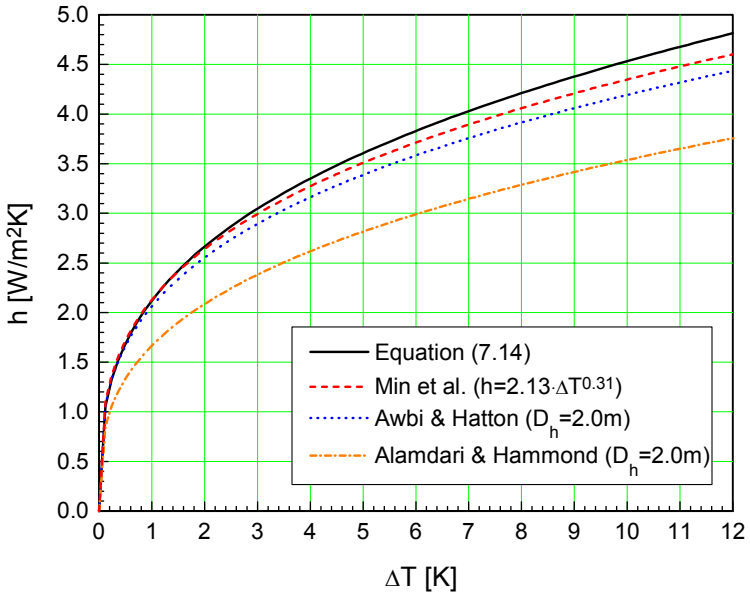

Figure 7.16 Comparison of new developed correlation (Equation 7.14) with other correlations used for convective heat flux calculation on cooled ceiling surfaces

Convection correlations for high aspiration diffusers (Equations 7.16-7.20) were developed for the use in rooms when these diffusers are combined with radiant cooling panels. These rooms have low *ACH* because only fresh air is supplied and the effect of supply temperature on local air temperatures in the vicinity of the surfaces is small. Therefore, these correlations are based on local temperatures. In the cases when high aspiration diffusers are used with all air systems and a considerably larger supply air flow rate, the effect of supply temperature is not negligible. In these rooms, the new convection correlations (7.16-7.20) should not be used because they neglect the effect of supply temperature on the surface heat transfer. Also, these correlations are valid for volume flow rates that provide less than 5 *ACH* in the room.

During the development of the new convection correlations, special attention was dedicated to development of a convection correlation for floor surfaces in rooms with displacement ventilation. Precise calculation of convective heat flux at floor surfaces in room with DV is crucial for room temperature profile calculation (Yang 1993). Heat flux at these surfaces depends on supply air temperature, volume flow rate, and local air temperature. Therefore, new convection correlations (7.23 and 7.24) have a general form, which combines the effects of local temperature (surface and local air temperature difference) and air supply temperature (surface and supply temperature difference).

Considering effects of a high aspiration diffuser on convection at a cooled ceiling, the general equation (7.19) for combined natural and forced convection at cooled ceiling surfaces shows that the effect of forced convection with high aspiration diffusers is not negligible. This is especially the case for large flow rates. For example, for ΔT=8°C and a volume flow rate that provides 4 *ACH*, the increase of the convection coefficient is 18%.

The newly developed convection correlations presented in this chapter were implemented into MACA in order to improve the accuracy of thermal boundary conditions calculations in a CFD simulation domain. Moreover, the use of these correlations is not limited to CFD-type simulations. For example, the correlations for cooled ceiling combined with high aspiration diffuse, Equations (7.16-7.20), can also be used in ES programs or in standard design procedures by assuming perfect mixing ($T_{room}=T_{local\ air}$). Also, Equation (7.21) for the forced convection correlation at a floor with displacement ventilation can be applied in ES or in standard design procedures because it uses supply air temperature as the reference temperature and does not need air temperature distribution.

CHAPTER 8

LABORATORY MEASUREMENTS AND RESULT ANALYSIS

8.1 Introduction

In this thesis, measurements were conducted in a controlled laboratory environment for the following three different purposes:

1) collecting data for development of surface convection correlations,
2) collecting data for validation of new model for thermal boundary conditions in CFD,
3) collecting data for evaluation of CFD models used for air quality and thermal comfort studies.

All these measurements were conducted in The Building Energy and Environmental Systems Testing Facility at the Architectural Engineering department of Penn State University. Activities related to measurements in this facility include not only work on setting-up the experiments and data collection, but also work on design and construction of this facility. In the next section of this chapter (Section 8.2), the experimental facility is described. Sections 8.3, 8.4, and 8.5 provide the experimental set-up and the results for each of the three types of above mentioned measurements. In Section 8.6, an analysis of measurement uncertainty is provided. Finally, Section 8.7 provides a short summary of this chapter.

8.2 Experimental Facility

The Building Energy and Environmental Systems Testing Facility is a state-of-the-art installation designed for full-scale thermal and air quality research. The facility consists of environmental and climate chambers with two separate Heating Ventilating and Air-Conditioning (HVAC) systems (Figure 8.1). An important part of this facility is the sophisticated measuring and data acquisition system used for measurements of: energy, air, and tracer gas concentration in different components of this facility.

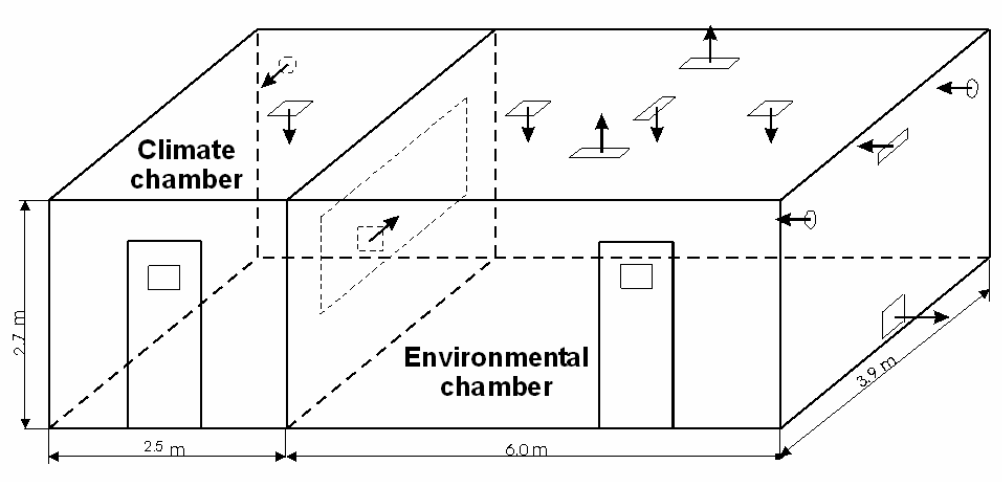

Figure 8.1 A schematic of climate and environmental chambers

8.2.1 Environmental and Climate Chambers

The primary purpose of the environmental chamber is to create various indoor environmental conditions, where certain groups of indoor parameters are controlled and other groups of parameters are measured. For example, for a certain ventilation strategy, a volume flow rate and temperature of supply air are controlled, while distribution of surface temperature, air velocity, air temperature, and tracer gas concentrations are measured. On the other hand, the primary purpose of the climate chamber is to simulate a wide range of outdoor weather conditions, from cold winters to hot summers. The two chambers are separated from each other by a partition wall with a window. To insulate the chambers from external influences, the chambers walls are built from insulating material that provides conduction resistance of R=5.3 W/m^{2}K.

Two separate Air Handling Units (AHUs) provide various environmental conditions in environmental and climate chambers (Figure 8.2). The AHU of the environmental chamber provides up to 20 Air Changes per Hour (ACH), while the AHU of the climate chamber provides up to 40 ACH. Both AHUs have an option to use 100% outdoor air and have the capability to provide a wide range of temperatures and relative humidities in the chambers. Each AHU is connected with its chamber by a duct network that enables several position variations for inlets and outlets (Figure 8.1). Depending on the ventilation strategy, displacement ventilation or mixing ventilations with various diffuser types and positions, an appropriate set of inlet and outlet openings are connected with AHUs.

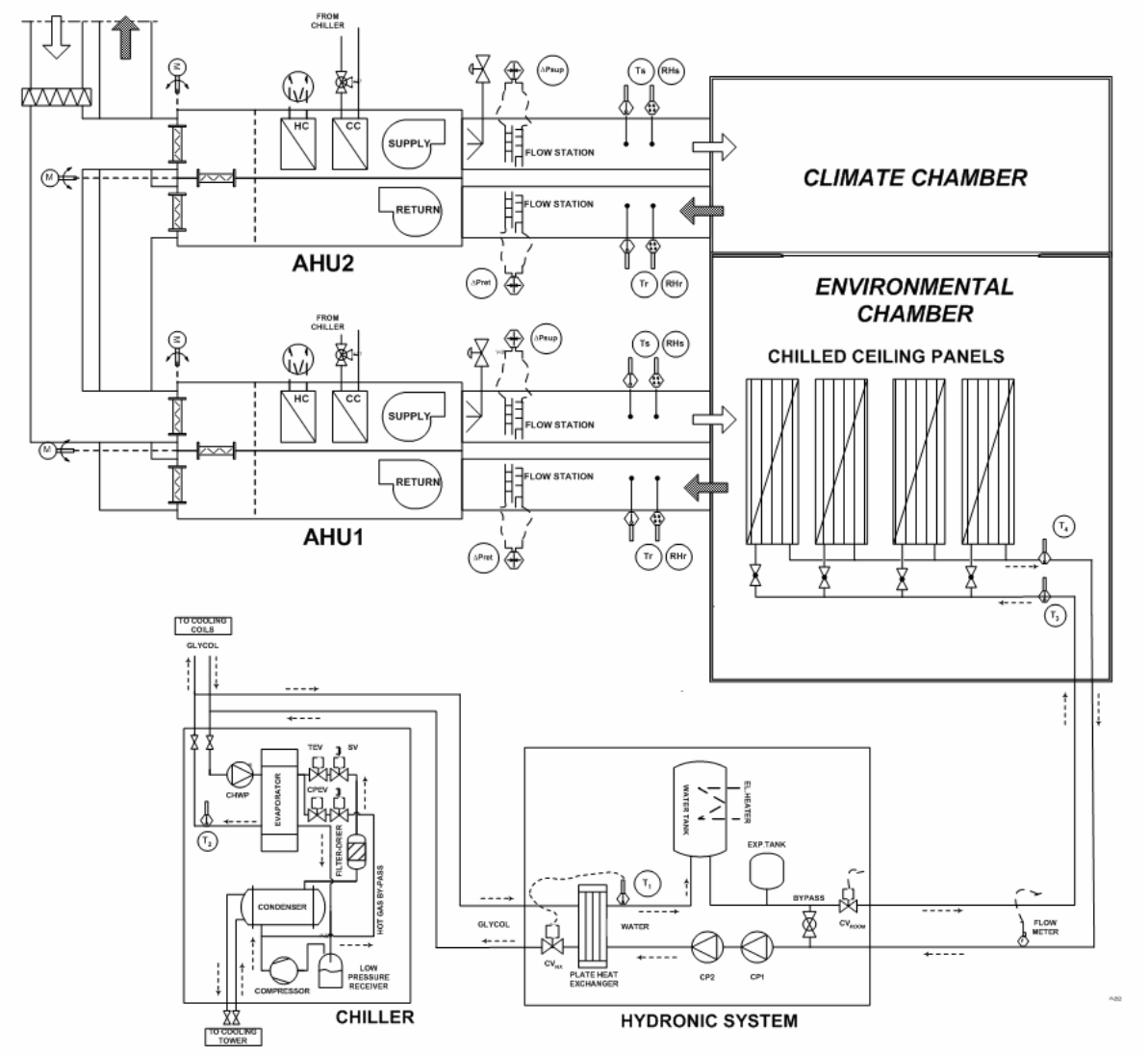

Figure 8.2 A schematic of water-flow and air-flow in climate and environmental chambers

Beside AHUs, a hydronic cooling and heating system is installed to provide hot and chilled water for components of the HVAC system such as radiant heating/cooling panels or fan coil units installed inside of the chambers (Figure 8.2). The chiller, which has 35 kW of cooling capacity, uses glycol solution to provide cooling to the AHUs' coils and the hydronic system. A Direct Digital Control (DDC) system provides control for: the chiller, the AHUs, and the hydronic cooling system (see Figure 8.3). DDC enables precise control of the set-variables for both steady-state and variable heating/cooling loads in chambers. The control system is designed to be flexible and adaptable for various types of experiments. Users can easily switch between different control strategies for different HVAC configurations. For example, a user can select

between (1) Variable Air Volume (VAV) or Constant Air Volume (CAV) system; (2) control of supply or return air temperature; (3) control by the AHU or hydronic system.

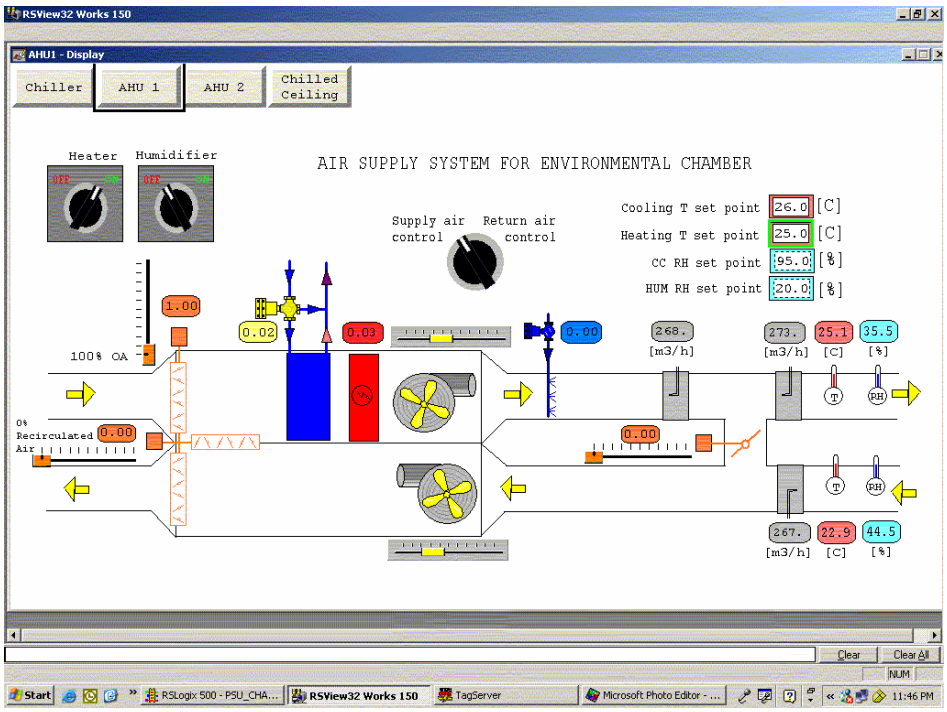

Figure 8.3 Control system of building energy and an environmental systems testing facility

8.2.2 Measuring Equipment

The measuring equipment consists of three major subsystems:

- Air low-velocity and temperature measuring system
- Air and surface temperature measuring system
- Tracer gas measuring system

The air low-velocity and temperature measuring system is based on omnidirectional thermo-anemometer sensors (HT400). The system is used for air temperature and low air velocity measurements in rooms, as well as for measurement of supply air velocities and temperatures. This system consists of 24 omnidirectional probes with transducers connected to 3 data-acquisition modules with 8 channels per module. The measuring velocity range is from 0.05 to 5 m/s with an accuracy of ±0.02 m/s for the range of 0.05 to 1 m/s. The accuracy of the temperature sensors is ±0.2°C. The interface for the air low-velocity measuring system is presented in Figure 8.4.

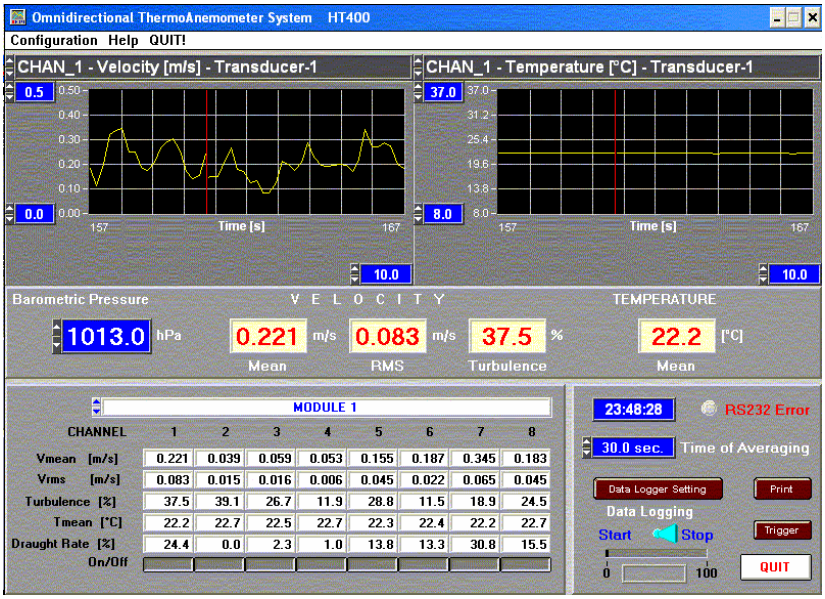

Figure 8.4 Interface of an air-velocity measuring system

Thermistor sensors were used for precise measurements of surface and air temperatures in the chambers. Seventy-two Omega thermistors (series 44033) were connected to 4 modules of an InstruNet data-acquisition system with 8 channels per module. The system enables 32 points of dynamic surface and air temperature measurement (see Figure 8.5) and 72 points of steady state measurements. In addition to the high accuracy of the sensors and transducers, the entire system was additionally calibrated by use of a thermal bath and a high precision thermometer. The accuracy of the temperature system is ±0.1°C for the range 0-45°C.

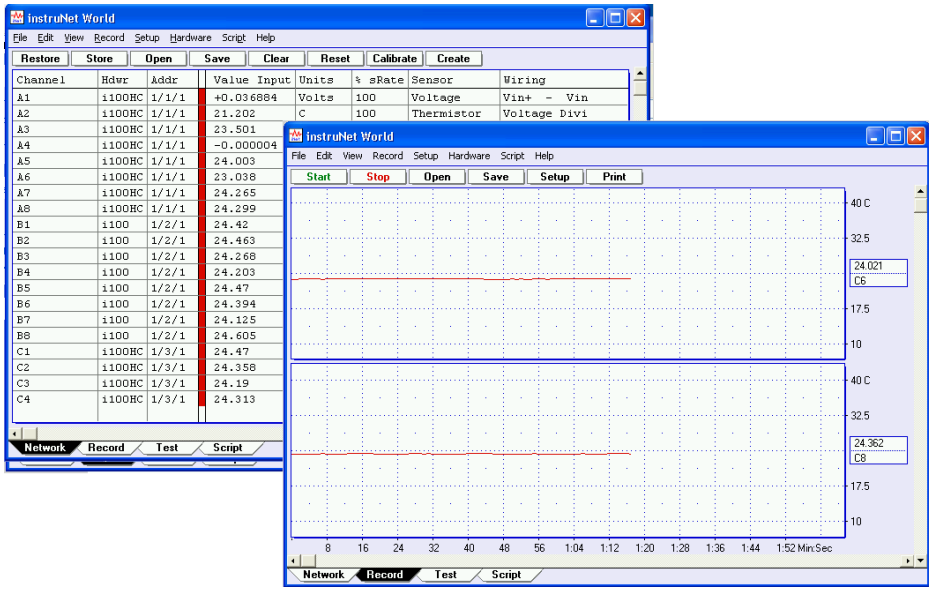

Figure 8.5 Interface of a data acquisition system used for temperature measurements

A tracer gas measuring system was used for monitoring of SF_6 gas concentrations in the environmental and climate chambers. This system was also used for control measurements of supply volume flow rates in the chambers. The tracer gas system encompasses a system for release of tracer gas and a system for tracer gas sample collection and analysis. The system used for sample collection and analysis is an AUTOTRAC automatic sampling module, which uses gas chromatography for measurements of tracer gas concentration in the collected air sample (Figure 8.6). Using a system of valves and connectors, the AUTOTRAC module automatically collects and sequentially analyses samples from up to 27 sampling positions in the facility. As a tracer gas, SF_6 is used because it is easily-detectable, not found in the environment, low in toxicity, odorless, colorless, and non-reactive at the room temperature. In conducted experiments, a system for continuous gas injection was used. This is the system of pressure regulators, valves, and flow meters connected in series. Two flow meters with different flow ranges were used to ensure accuracy in a wide range of SF_6 injections. The precision of the SF_6 injection system is ±1.5%, while the precision of the sample analysis is ±3%.

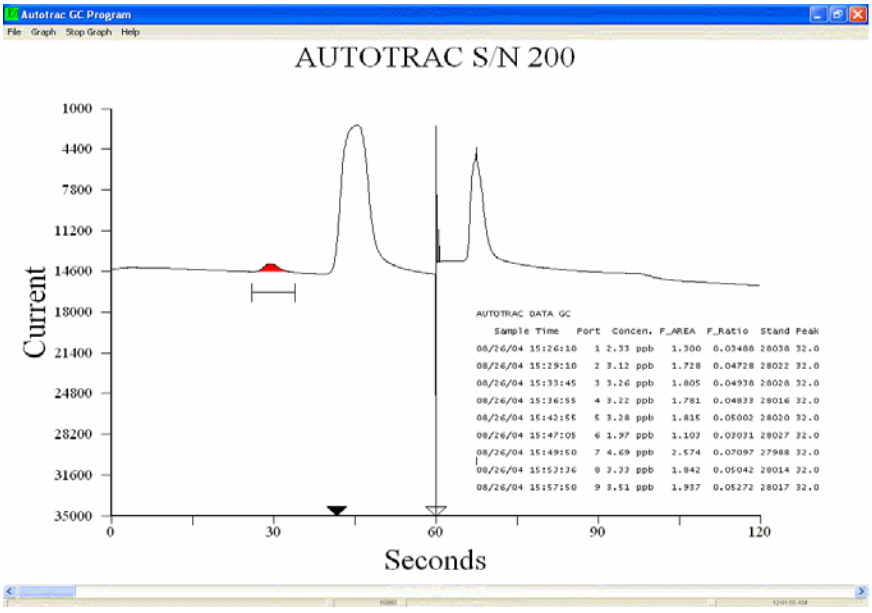

Figure 8.6 Interface of a tracer gas measuring system based on gas chromatography

Beside these three acquisition systems, surface heat flux meters, a hydronic calorimeter, air flow stations, and an electric power meter were used in this experimental facility. Five Thermonetics heat flux meters, with a precision of ±3%, were used for measurements of conductive heat fluxes at different surface. The hydronic calorimeter was used for energy consumption measurements of the chilled ceiling installed in the environmental chamber (Figure 8.2). This device contains two thermistors and a water flow-meter. The thermistors were

calibrated to provide a precision of ±0.1 ^{o}C for temperature differences between supply and return water. Also, the flow-meter was selected and calibrated to provide a precision of ±1.5% in the entire range of meter flow rates (0.7-7 L/min). Five air flow stations were instilled in the duct system to measure supply and return air flows in the chambers. In the supply duct of the environmental chamber, a two stage air flow measuring system was used to ensure accuracy in a wide range of supply flows (Figure 8.3). The flow stations were calibrated with an accuracy of ±5%. For power measurements of different electric devices, used as heat sources in the chambers, an electric multi-meter, an ammeter combined with voltmeter, was used. The accuracy of this device is ±2% Amp and ±1.5% Volt.

8.3 Measurements for Convection Correlations Development

Measurements related to convection correlations development for displacement and high aspiration diffusers with radiant cooling panels were conducted in the climate and environmental chambers. The experimental set-up created environmental conditions that exist in typical rooms of modern buildings. Cooling loads were created by: (1) heat conduction through the window and the partition wall, and (2) internal heat sources (Figure 8.7). Internal heat sources were created by lighting, low temperature heating panels that simulate heat gains from sun radiation, and convective heat sources that simulate occupants and other equipment. The cooling loads were extracted by ventilation system and/or radiant panels, depending on the convection correlations under consideration. In the environmental chamber, a drop ceiling, which holds the chilled ceiling panels and luminaries was used (Figures 8.7b). This reduced the height of the environmental chamber to from 2.70m to 2.35m.

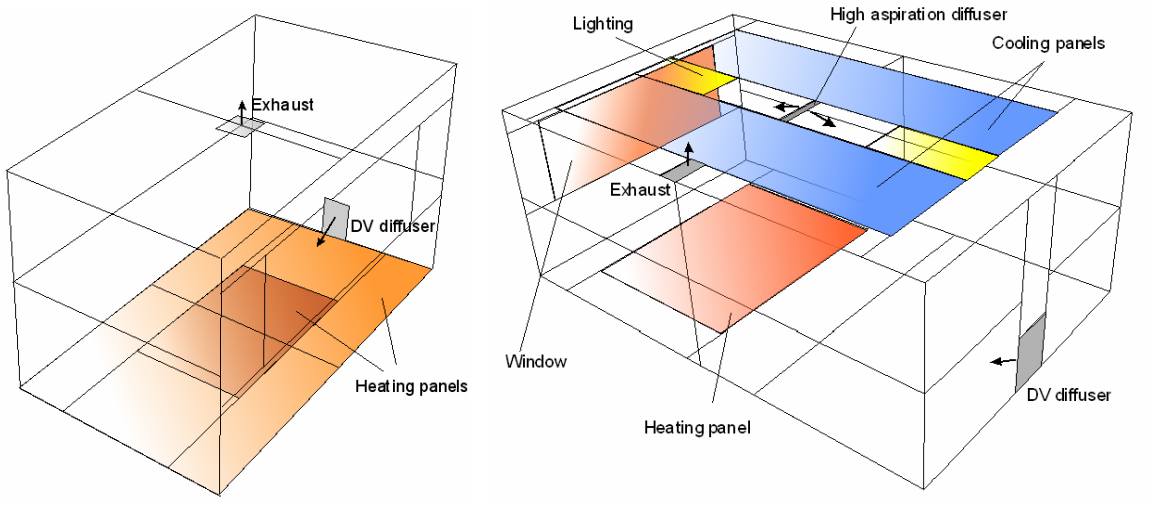

a) b)

Figure 8.7 Experimental set-ups for (a) Climate and (b) Environmental chambers

To accurately calculate convective heat fluxes at different surfaces using the methodology described in Section 7.2, the envelopes of the climate and environmental chambers were divided into a set of surfaces (Figure 8.7). The environmental chamber was divided into 38 and the climate chamber into 21 characteristic surfaces. For surface temperature measurements, various numbers of thermistor sensors were attached to the surfaces, depending on the importance of the surface related to the overall heat flow in the chamber. For example, in the environmental chamber, six thermistors were attached to the cooling panels and four to the heating floor panel since the exact temperature of these surfaces were crucial for the radiative heat flux calculations. By adding more sensors, error related to nonuniform surface temperature is reduced. To account for uneven floor surface temperature in experiments with the displacement ventilation diffuser, the floor surface in climate chamber is divided into 8 sub-surfaces and 10 thermistor sensors were attached.

Using measured surface temperatures and radiative heat exchange fractions (Equation 7.3), the radiative heat flux at each chambers' surface was calculated. The BES program function for internal radiation calculations was modified for this calculation. To simulate effects of thermal plumes from internal objects such as equipment and occupants, pure convective heat sources were used. In these measurements, radiation from internal objects to the surrounding surfaces was avoided to reduce error due to imprecise calculation of the convective/radiative heat flux ratio for internal objects. Internal objects had nonuniform surface temperatures and calculation of radiative heat fluxes from internal objects to each surface of the chamber enclosure would introduce an error. Therefore, in experiments for correlations developments, radiative heat flux from heat

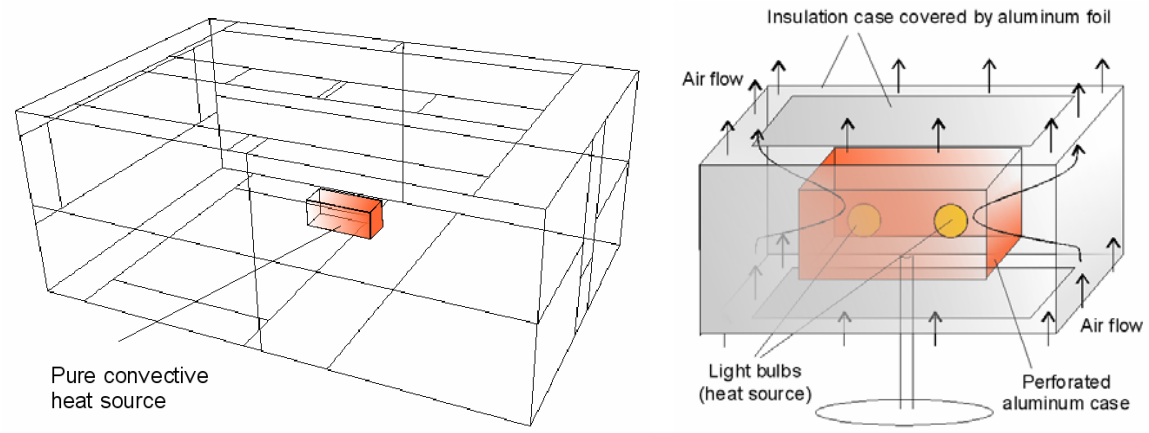

(a) (b)

Figure 8.8 The (a) positioning and (b) constriction of a pure convective heat source used for convection correlation development

sources positioned in the environmental chamber was minimized by use of an object that released energy only by convection. The positioning and structure of this object is shown in Figure 8.8. Two light bulbs were positioned in a perforated aluminum case that was positioned in a semi-closed box built from thermal insulating material covered by aluminum foil (Figure 8.8b). Using a double casing, aluminum materials with low emissivity, and insulation, external surface temperatures of this object were similar to the enclosure surface temperatures. The total radiative heat flux from this object was negligible compared to the total convective flux because of a relatively small temperature differences, a small surface area of object, and the low emissivity of aluminum foil.

In the environmental chamber (Figure 8.7b), air temperatures were measured in the vicinity of surfaces and in the central part of the room. Similar to the surface temperature measurements, the number of sensors positioned in the vicinity of the surface depended on the importance of the surface related to the overall heat flow in the chamber. Temperature sensors of the HT400 measuring system were positioned in the vicinity of the surfaces (0.1m from the surfaces). Furthermore, thermistor sensors were positioned in the central part of the room at different heights (see Figure 8.9). Besides surface and air temperature measurements in the environmental chamber, air velocities in the vicinity of the surfaces were also measured. Velocities at 24 points in the vicinity of the surfaces were measured to determine if the convective regime at a certain surface was predominantly forced or buoyant. When the climate chamber is used for convection correlations development with displacement ventilation diffuser (Figure 8.7a), air temperatures were measured at 8 positions 0.1 m above the floor. In the center of the climate chamber, thermistor sensors were positioned at different heights.

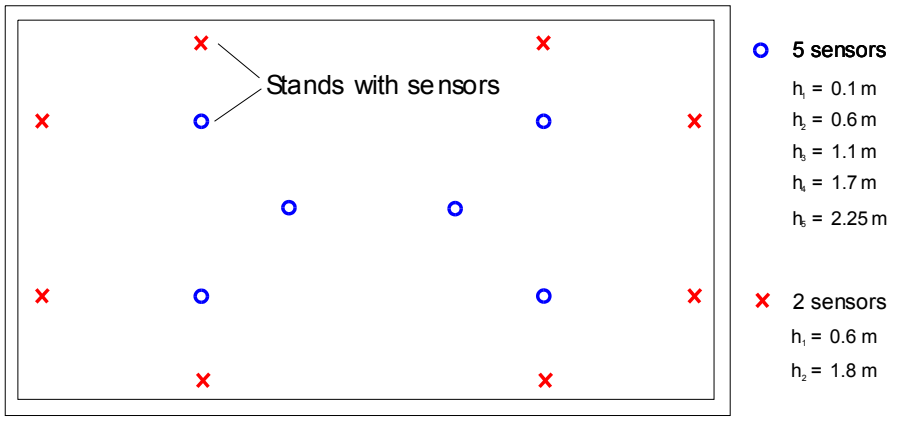

Figure 8.9 Positions of stands with temperature sensors in an environmental chamber

To precisely calculate convective heat fluxes, measurements were conducted for steady state airflow and conductive heat flow in elements of the chamber's structure. For each experiment:

1) the controlled parameters such as the air supply temperature and volume flow rate and/or water flow for radiant panels were adjusted to a set point;
2) surface and air temperatures for 32 reference points were recorded every 50 seconds (Figure 8.10);
3) when steady-state temperature distribution was attained, values for temperature and velocity at all installed sensors were recorded for 2 minutes and then averaged.

To test the validity of measurements, an energy balance check was conducted for each experiment by comparing the heat gains with the energy extracted by the ventilation system and cooling panels.

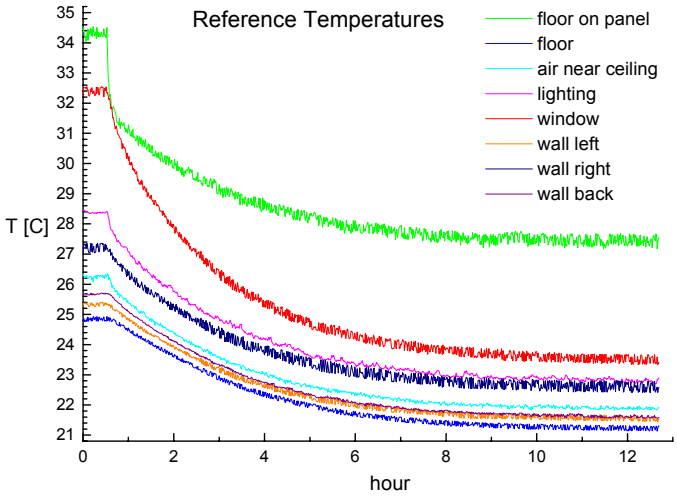

Figure 8.10 A temperature recording to determine steady-state conditions

8.3.1 Measurements of Convection Coefficients at Cooled Ceiling Surfaces

The analysis of the measurement results related to the development of convection correlations for cooled ceiling surfaces is presented in Section 7.3. Each point in Figure 7.6 presents a separate experiment, and the numerical values of results are presented in Table 8.1. In experiments with the convective heat source, the pure convective heat device was positioned in the central part of the environmental chamber (refer to Figure 8.8). In these experiments, the power of the convective heat source was varied to obtain a different cooling loads and

corresponding $\Delta T_{local} = T_{surface} - T_{local\ air}$ at cooling panels (see Table 8.1). In experiments where surface heat sources were used, the power of the floor panel was varied. In experiments where large cooling loads were needed, floor heating panels were combined with lighting and conductive heat gains through the window and the partition wall. This was conducted in such a manner to create large cooling loads without raising surface temperature of the floor panels above temperatures typical in buildings. Also, two experiments were conducted where the pure convective source was combined with surface heat sources. Table 8.1 shows that surface heat sources create considerably larger radiative heat transfer than convective sources. The last column in this table shows the error (difference for developed correlations and measured results).

Table 8.1 Measurement results for cooled ceiling surfaces

Heat source type	**ΔT local** [°C]	**h measured** [W/m^{2}K]	q_panel total [W/m^2]	q convect./q tot. ratio	Equation 7.14 [W/m^{2}K]	Difference [%]
Pure convective heat source	2.1	2.65	11.2	0.49	2.70	1.9
	3.4	3.18	23.4	0.46	3.16	-0.6
	5.3	3.82	40.4	0.50	3.68	-3.6
	6.7	4.35	55.3	0.53	3.97	-8.7
	9.0	4.68	77.0	0.55	4.38	-6.3
Surface heat sources	4.5	3.41	55.0	0.28	3.48	2.4
	5.4	3.21	61.6	0.33	3.70	15.6
	7.0	3.92	83.2	0.33	4.02	2.6
	3.7	3.10	31.4	0.35	3.26	5.3
	2.6	2.80	23.8	0.31	2.91	3.8
Combination	6.3	4.12	65.1	0.40	3.89	-5.1
	8.4	4.53	92.6	0.43	4.28	-4.9

8.3.2 Measurements of Convection Coefficients in Rooms with High Aspiration Diffusers

Experiments related to the developments of convection correlations with high aspiration diffuser combined with cooled ceiling system were conducted in the environmental chamber using the pure convective device as a heat source. The air system supplied an air temperature that was the same as the air temperature in the chamber, and the entire cooling load was extracted by ceiling cooling panels. In these experiments, the cooling panels cooled down (by radiation) the rest of the chamber's envelope, and as a consequence, the air temperature was higher than the envelope surface temperatures. Table 8.2 contains the results of these experiments. Due to low temperature difference between the surface and local air (ΔT_{local}), a forced convection was dominant at all surfaces except at the surfaces of the cooling panels, which had large ΔT_{local}. To develop the correlations between volume flow rates and convection coefficients, volume flow rates were varied from 1 to 5 ACH. For each volume flow rate, several measurements were

conducted with different cooling loads. For cooing panels, ΔT_{local} were measured to get a total convection coefficient at these panels ($h_{total\_measured}$ in Table 8.2). Using these total convection coefficients and corresponding natural convection coefficients for measured ΔT_{local}, forced convection coefficients (h_{forced}) were calculated by Equation (7.13). For the wall and floor surfaces, average values of ΔT_{local} and corresponding h_{forced} were calculated to obtain general convection coefficients at these surfaces. These averaged convection coefficients at walls and the floor are presented in Table 8.2. Using these h_{forced} and ACH, the correlations presented in Figures 7.8-7.10 were developed. The comparison of measured convection coefficients ($h_{total\ measured}$) and convection coefficients obtained by final forms of correlations (Equations 7.16-7.20) is presented in the last column of Table 8.2.

Table 8.2 Measurement results for the room with a high aspiration diffuser and cooled ceiling

Surface	**ACH** [h^{-1}]	**h forced** [W/m^2K]	ΔT local [°C]	h total measured [W/m^2K]	Equations 7.16-7.20 [W/m^2K]	Difference [%]
Walls	0.93	1.77	1.1	2.23	1.89	15.1
	1.00	1.76	1.5	2.33	2.04	12.5
	1.99	2.86	0.9	3.01	2.49	17.2
	2.06	2.67	1.4	3.09	2.63	15.0
	2.74	3.13	1.3	3.44	3.10	9.9
	2.77	3.49	0.8	3.65	3.05	16.5
	2.95	3.15	0.6	3.30	3.16	4.1
	3.86	3.71	1.1	3.91	3.91	-0.1
	3.88	3.92	0.7	4.04	3.89	3.8
	4.78	3.90	0.6	4.07	4.55	-11.8
	5.01	4.71	0.6	4.79	4.73	1.3
	5.03	4.62	1.0	4.74	4.76	-0.4
Floor	0.93	0.50	0.8	0.87	0.93	-6.1
	1.00	0.89	0.7	1.02	0.98	3.9
	1.99	1.83	1.1	1.86	1.67	10.1
	2.06	1.45	0.9	1.51	1.72	-14.1
	2.74	2.09	1.0	2.12	2.15	-1.7
	2.77	2.69	1.1	2.61	2.17	16.6
	2.95	2.13	0.8	2.13	2.28	-7.0
	3.86	3.45	0.9	3.36	2.83	15.8
	3.88	2.59	1.3	2.60	2.84	-9.2
	4.78	3.47	0.9	3.48	3.36	3.6
	5.01	3.77	1.3	3.78	3.49	7.7
	5.03	3.31	0.7	3.31	3.50	-5.8
Cooled ceiling panels	0.93	2.28	4.8	3.85	3.60	6.5
	1.99	2.65	4.4	3.92	3.69	5.8
	2.74	2.91	4.2	3.99	3.87	3.0
	2.77	3.62	7.7	4.93	4.51	8.6
	3.86	2.35	4.2	3.73	4.35	-16.5
	3.88	4.20	7.0	5.18	4.77	7.9
	4.71	4.19	7.1	5.19	5.14	1.0
	4.78	2.96	4.2	4.22	4.81	-13.9

8.3.3 Measurements of Convection Coefficients in Rooms with Displacement Ventilation

Experiments related to convection correlations in rooms with displacement ventilation (DV) diffusers were conducted in the climate and environmental chambers. The experiments related to the development of new correlations at floor surfaces, presented in Figure 7.15, were conducted in the climate chamber. The experiments related to validation of existing natural convection correlation for vertical surfaces (measurements of ratio Gr/Re^2) were conducted in the environmental chamber. For the development of the convection correlation at floor surfaces, the floor in the climate chamber was covered by heating panels and divided into 8 surfaces (see Figure 8.7). The supply flow rate was varied form 2.5 to 10 ACH by different power adjustments of the heat flux panels. Because of the non-uniform floor surface temperature and non-uniform temperature distribution of the air layer above the floor, the convection correlations were developed for average surface and average local air temperatures. Table 8.3 presents the difference between averaged surface and local air temperatures (ΔT_{local}) and averaged surface and supply air temperatures (ΔT_{supply}) for each of experiments. It also contains the convection coefficients based on ΔT_{local} $(h_{\ total\ measured})$ and $\Delta T_{\ supply}$ (h_{supply}). As it was pointed out in Section 7.5, the convection correlation expressed as a function of volume flow rate is stronger than the correlation expressed as a function of a difference between local air and surface temperature. The first group of results in Table 8.3 presents the experimental results where the whole floor was heated. The last three rows show the results where only heating panels in the central part of the chamber were used to test the effect of heat patches (see Figure 8.7). The last column of this table contains the comparison of the measured convection coefficients ($h_{\ total\ measured}$) and convection coefficients obtained by Equations 7.23, which combine the effect of forced and natural convection.

Table 8.3 Measurement results for the floor surface in a room with displacement ventilation

	ACH [h^{-1}]	q convective [W/m^2K]	ΔT local [°C]	ΔT supply [°C]	**h supply** [W/m^2K]	h total measured [W/m^2K]	Equation 7.23 [W/m^2K]	Difference [%]
All floor surfaces heated	6.1	45.9	10.3	20.9	2.20	4.46	4.67	4.7
	7.6	47.7	10.6	19.9	2.40	4.50	4.95	9.9
	9.9	47.1	10.7	17.7	2.66	4.40	5.24	19.1
	3.4	16.1	4.1	11.6	1.39	3.94	3.84	-2.4
	3.8	15.3	3.6	12.2	1.25	4.23	4.76	12.6
	4.6	16.2	4.4	9.1	1.78	3.66	3.69	0.9
	5.7	16.0	4.3	8.4	1.92	3.75	3.98	6.1
	6.1	16.9	4.8	8.3	2.04	3.56	3.86	8.4
	4.2	6.1	1.8	4.1	1.48	3.43	3.56	4.0
	3.4	7.2	2.2	5.9	1.22	3.32	3.57	7.6
Patch	5.0	35.3	10.0	14.2	2.49	3.53	4.17	18.0
	3.4	40.4	9.2	16.5	2.45	4.38	4.06	-7.3
	2.5	38.1	9.8	18.5	2.06	3.90	4.11	5.3

8.4 Measurements for MACA Validation

To provide experimental data for validation of the Modified Adaptive Convection Algorithm (MACA), presented in Section 4.4, measurements for three experimental set-ups in the environmental chamber were conducted. In these experiments, the focus was on strict energy balance in the chamber, accurate measurements of air temperature distribution, and precise measurements and calculations of convective heat fluxes at surfaces with a large temperature differences (ΔT_{local}). To create a non-uniform temperature distribution for CFD simulations in all three validation experiments, the Displacement Ventilation (DV) system was used. This system created evident temperature stratification.

The measurements were conducted at steady state energy flow in the environmental chamber, which was obtained by the method described in Section 8.2 (Figure 8.10). The supply air flow rate was measured by flow stations and the tracer gas measuring system. The surface temperatures of the environmental chamber were measured by thermistors with similar surface discretization such as for the convection correlation development (see Figure 8.11). The air temperature distribution was measured at different positions in the room (see Figure 8.9). For each measurement, the energy balance was checked by comparing energy released in the chamber and energy extracted from the chamber.

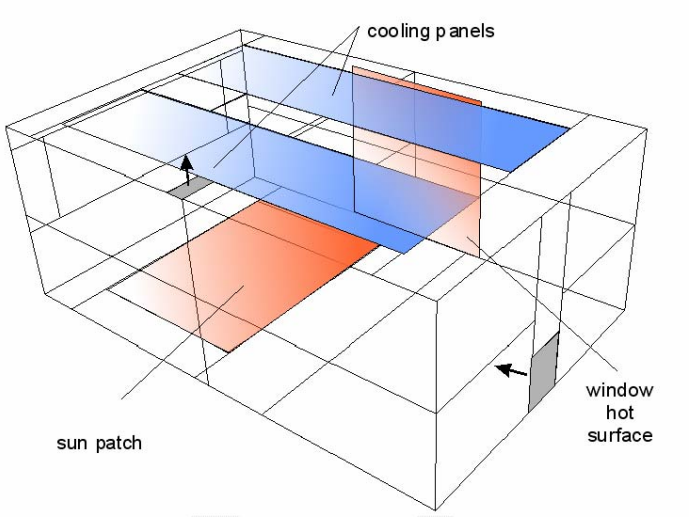

Figure 8.11 Distribution of surface heating/cooling devices in experiments for MACA validations

The first of three experimental set-ups was adjusted to test MACA for convective heat fluxes at the floor. The heating panel with major heat flux was attached to the part of the floor simulating effect of a sun patch (Figure 8.11). The second experimental set-up was for testing convective heat transfer at the cooled ceiling surfaces (Figure 8.11). The cooling load was created by the pure convective heat source described in Section 8.2. The third experimental set-up was related to data collection for validation of MACA when the major heat source was at vertical surfaces. With this set-up, the heating panels were attached to the wall to simulate window surfaces (Figure 8.11). Table 8.4 contains characteristic data for these three experimental measurements (cases). The important results of the measurements related to validation are presented in Section 4.4 (Table 4.11).

Table 8.4 Characteristic data of cases used for experimental validation of MACA

Convective and radiative heat sources	Q_{total} [W/m^2]	$\Delta T_{at\_surface}$ [°C]	$V_{air\ supply}$ [m^3/h]	$T_{air\ supply}$ [°C]	Specific details
Case 1: Sun patch at floor, displacement ventilation only					
Heating panel on floor Heating panels on ceiling	752 179	11.6 1.3	208	17.2	$Q_{convection}/Q_{total}$ at floor heating panel was 57% and at ceiling 24 %
Case 2: Convective heat, displacement ventilation system combined with cooled ceiling (CC)					
Pure convective source	814	-	92	17.7	At all surfaces except floor $T_{local\ air} > T_{surface}$. At CC $\Delta T_{at\ surface}$ was 6.5 °C
Case 3: Hot window surface, displacement ventilation only					
Heating panel on wall	491	10.0	97	18.9	T_{floor} was 1.5-2 °C higher than $T_{local\ air}$

8.5 Measurements for Evaluation of CFD Models for IAQ and Thermal Comfort Study

To obtain data for an overall validation of CFD application in building analyses, which includes evaluation of velocity and concentration prediction, additional set of experiments were preformed. This experimental data will be used primarily in future work for validation of concentration distribution prediction by a zero-equation turbulence model implemented into the CFD0 program (refer to Chapter 4).

Eight additional experiments were conducted in the climate chamber. Set-ups for these experiments were similar to the set-ups for the three experiments described in the previous section. The major difference was in the distribution of the heat sources. To create air and heat

flow typical for offices, human dummies and heat source that simulate equipment were used in these experiments. Besides these sources, floor heating panels were used for simulation of sun patches. Heat and concentration sources were positioned asymmetrically to create more challenging air flow for CFD simulations. DV and mixing ventilation diffusers were used for air supply. In five experiments, air ventilation systems were combined with the ceiling cooling panels. The general set-up data for these 8 experiments is provided in Table 8.5.

Similarly to the previous two types of experiments, described in Sections 8.2 and 8.3, conductive heat fluxes and temperatures were measured at each surface for a steady state condition, while radiative and conductive heat fluxes were calculated. Besides air velocities and temperatures, the distribution of tracer gas was measured at 27 positions in the chamber, including the supply and exhaust. Depending on the experiment, the source of tracer gas was positioned at different places in the chamber such as at occupants, the floor near the heat patch, and the floor away form the heat sources (refer to Table 8.5).

Table 8.5 The cases for experimental validation of CFD models

Case	Venation system	Cooling panels	ACH [h^{-1}]	Heat source type and intensity [W]			Tracer gas source position
				Occupants	Heat. panels	Convective	
1	DV	ON	1.7	2x102	760	0	Source on occupants
2	DV	ON	1.7	1x70	0	779	Source on occupant
3	DV	ON	1.7	1x70	546	212	Source on floor
4	DV	OFF	3.8	1x70	546	152	Source on occupant
5	DV	OFF	3.8	0	752	0	Source at floor
6	DV	OFF	3.8	0	491	0	Source at floor away from heat sour.
7	MV	ON	1.4	2x35	781	391	Source at heated panel
8	MV	ON	1.4	2x35	781	391	Source at floor

The results for each of these 8 experiments were organized in electronic files which contain:

1) information about experimental set up such as: (a) room geometry, positions of dummies and other heat sources, (b) positions of the surface and air temperature sensors, and (c) basic airflow, concentration, and heat source data.
2) surface and air temperatures, velocities, and calculated convective heat fluxes for each surface.
3) data for tracer gas concentration distribution.

A printout for one experimental case (Case 6 in Table 8.5) is provided in Appendix H.

8.6 Uncertainties of the Measurements

In all the experiments described in the previous sections, the measurement system consists of a chain of a individual measurement. For example, the system for measurement of extracted energy by cooling panels ($Q_{panels\ total}$) encompasses measurements of the water flow and the temperature difference between supply and return water. On the other hand, the measurement of $Q_{panels\ total}$ is part of the other measurement system for determination of surface convective heat fluxes (Section 7.2). Each component's measurement has an uncertainty, which is the uncertainty of the measuring instrumentation. These uncertainties are given in Section 8.2.2, while this section contains analyses of overall measuring-system accuracy.

When the considered quantity (Q) is a function of *'n'* independent variables:

$$Q = f(u_1, u_2, u_3, ..., u_n) \tag{8.1}$$

the uncertainty of a function can be computed by the following equation (Young 1962):

$$\delta Q = \sqrt{(\delta u_1 \frac{\partial Q}{\partial u_1})^2 + (\delta u_2 \frac{\partial Q}{\partial u_2})^2 + ... + (\delta u_n \frac{\partial Q}{\partial u_n})^2} \tag{8.2}$$

where variables (u_i) have associated uncertainties $\pm\delta u_i$.

Using Equations (8.2) and (7.1) uncertainty for convection coefficients is:

$$\delta h = h\sqrt{\left(\frac{\delta q_{panels\_convective}}{q_{panels\_convective}}\right)^2 + \left(\frac{\delta \Delta T}{\Delta T}\right)^2} \tag{8.3}$$

where the temperature difference $\Delta T = T_{surface} - T_{air}$. The uncertainty of the temperature difference is:

$$\delta \Delta T = \sqrt{(\delta T_{surface})^2 + (\delta T_{air})^2} \tag{8.4}$$

Convective heat flux for cooling panels is calculated as:

$$q_{panels\_convective} = q_{panels\_total} - q_{panels\_radiative} - q_{above\_panels} \tag{8.5}$$

where q_{panels_total} is the total extracted energy per unit of area, $q_{panels\_radiative}$ is the radiative flux, q_{above_panels} is heat flux on a top side of cooling panels which is directly measured by heat flux meters. The uncertainty for this system is:

$$\delta q_{panels\_convective} = \sqrt{\left(\delta q_{panels\_total}\right)^2 + \left(\delta q_{panels\_radiative}\right)^2 + \left(\delta q_{above\_panels}\right)^2} \tag{8.6}$$

Using the error of the heat flux meter, the uncertainty for heat flux on the top side of the panels is $\delta q_{above\_panels} = 0.03 \cdot q_{above\_panels}$. Considering Equation (7.3), the accuracy of thermistors attached to the surfaces (±0.1 K), and the range of surfaces temperatures from 288 K to 308 K, the maximum absolute value of uncertainty for radiative flux ($\delta q_{panels\_radiative}$) is below 0.8 W/m^{2}K. The uncertainty of the total extracted energy by the cooling panels is:

$$\delta q_{panels\_total} = q_{panels\_total} \sqrt{\left(\frac{\delta \Delta T_{water}}{\Delta T_{water}}\right)^2 + \left(\frac{\delta m}{m}\right)^2} \tag{8.7}$$

where 'm' is the measured water flow rate and ΔT_{water} is the measured temperature difference between supply and return water.

At surfaces that are not cooling panels, uncertainties for convection coefficients are determined by:

$$\delta q_{surface\_convective} = \sqrt{\left(\delta q_{conductive}\right)^2 + \left(\delta q_{surface\_radiative}\right)^2} \tag{8.8}$$

where $\delta q_{surface\_radiative}$ is calculated in the same way as with cooling panels. The value for $\delta q_{conductive}$ is determined by the error of heat flux meters attached to the window and partition wall surfaces. In the case of external walls of the chamber, $\delta q_{conductive}$ is negligible compared to $\delta q_{surface\_radiative}$ because of thick insulation that creates small values of $q_{conductive}$. At internal surfaces, where heating panels are attached, conductive sources are electric heat panels and uncertainty of these sources is:

$$\delta q_{heating\_panel} = q_{heating\_panel} \sqrt{\left(\frac{\delta U}{U}\right)^2 + \left(\frac{\delta I}{\Delta I}\right)^2} \tag{8.9}$$

where *'I'* is the measured electric current, and *'U'* is the measured voltage.

In experiments where the volume flow rate *(V)* is measured by the tracer gas measuring system, using $V = N / \Delta C$,where N is the traces gas volume flow rate and ΔC is the difference of measured concentrations at the outlet and inlet ($\Delta C = C_{out} - C_{in}$), the uncertainty of the volume flow rate is:

$$\delta V = V \sqrt{\left(\frac{\delta \Delta C}{\Delta C}\right)^2 + \left(\frac{\delta N}{N}\right)^2} \tag{8.10}$$

The uncertainty of the concentration difference is:

$$\delta \Delta C = \sqrt{(\delta C_{out})^2 + (\delta C_{in})^2} \tag{8.11}$$

When the tracer gas system is used in experiments for contaminant distribution, the uncertainty of the local concentration measurements is a combination of the uncertainty for the tracer gas distribution and the uncertainty of the tracer gas analyzing system. The total uncertainty for the tracer gas distribution is:

$$\delta C_{distribution} = C_{distribution} \sqrt{\left(\frac{\delta V}{V}\right)^2 + \left(\frac{\delta N}{N}\right)^2} \tag{8.12}$$

The uncertainty of the local concentration measurements is:

$$\delta C_{overall} = \sqrt{(\delta C_{distribution})^2 + (\delta C_{gas\_analyser})^2} \tag{8.13}$$

Uncertainty of convection coefficients

The uncertainty for convection coefficients measured at cooled ceilings were calculated by use of equations (8.1-8.13), measured data, and the equipment's measuring error. Results are presented in Figure 8.12. The largest uncertainty (21%) is for the smallest cooling load and

temperature difference, while the smallest uncertainty (10%) is for the largest load and temperature difference.

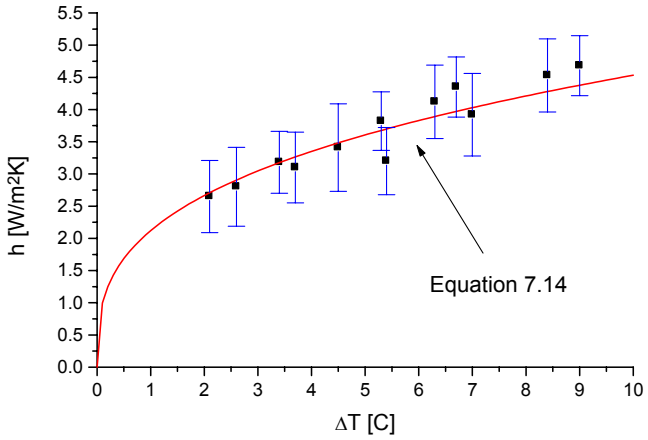

Figure 8.12 Uncertainty for a measured convection coefficient at cooling panels

The uncertainty of the forced convection coefficient at walls and floor, measured in experiments related to high aspiration diffuser combined with cooled ceilings, is large (up to 38%). The reason for this is a relatively small temperature differences (see ΔT_{local} in Table 8.2), which were needed to get primarily forced convection at these surfaces. The uncertainty of convection coefficients at these surfaces mainly depends on the uncertainty of the temperature measurements (term $\delta \Delta T / \Delta T$ in Equation 8.3). The uncertainty of measured forced convection coefficients at walls is in the range of 15-33%, while at floor in the range of 17-31%. The low uncertainty is for measurements with large ΔT. At the cooling panels, the temperature difference (ΔT_{local}) is larger and the uncertainty for measured convection coefficients is in the range of 6-9%. However, at these surfaces convection due to buoyant forces was dominant and forced convection coefficients were recalculated using Equation (7.15). This recalculation and use of convection correlations for buoyant flow (which also has uncertainty) further increases the uncertainty of the forced convection coefficients presented in Figure 7.10, up to 38%.

Measurements of convection coefficients at the floor surface in the room with displacement ventilation, presented in Table 8.3, were conducted with large temperature differences (ΔT_{supply}). Therefore, the uncertainty of these convection coefficients is created by the error in measurements of electric power of the heating panels and by the uncertainty of the measurements of radiative heat fluxes (refer to Equations 8.8 and 8.9). Uncertainties are in the a range from 6% to 15% and Figure 8.13 show the uncertainty bar for each experiment.

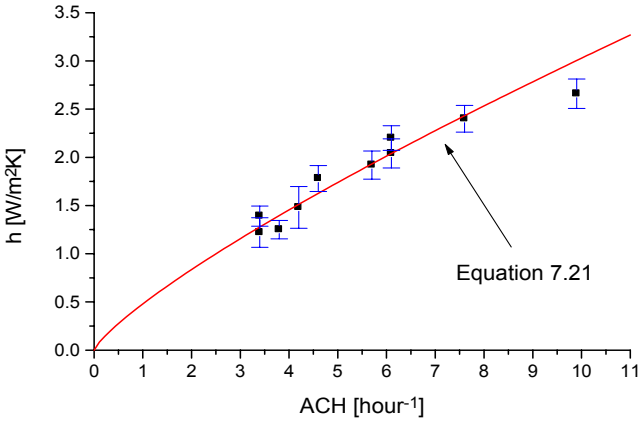

Figure 8.13 Uncertainty for a measured convection coefficient on floors in a room with displacement ventilation diffuser

Uncertainty of data collected for validation of MACA

For validation of MACA, temperature and heat fluxes at all surfaces were measured to calculate the overall heat transfer. However, in Section 4.4 experimental and simulation results (heat fluxes) were compared primarily for surfaces which have a large temperature difference (ΔT_{local}) because this gives the smallest uncertainty in measurements. The uncertainties of convective heat fluxes at the heating panels are 7% and 8% for experiment 1 and 3 respectively (see Section 3). For experiment 2, the uncertainty of measured heat fluxes at the cooled ceiling panel is 13%. The uncertainty of the supply airflow rate is 5%. The uncertainty of the temperature measurements is ±0.2°C for air and ±0.1°C for surface temperatures.

Uncertainty of concentration distribution

In experiments related to concentration distribution, presented in Section 8.4, the tracer gas concentrations were measured with an uncertainty of 7%, considering measuring equipment. However, repeatability, defined as a difference of concentrations for two consecutive measurements at the same point, was larger. The most probable reason for this is the imperfect steady-state airflow, even when measured temperatures and total (ominidirectional) velocities indicate steady state airflow. A small change in the velocity direction in the vicinity of the tracer gas source may considerably affect the concentration distribution. The repeatability of concentration measurements at locations in the room was in the range 5-14%, depending on the type of airflow. The repeatability of measurements in supply and exhaust air was below 5%. The uncertainty of temperature measurements is similar to the experiments related to the MACA

validation, while the uncertainty of convective heat fluxes at heating and cooling surfaces is in the range of 7-15%. For other surfaces, the uncertainty is approximately equal to the uncertainty of the radiative heat flux calculation (0.8 W/m^2K).

Generally, the measurements presented in Sections 8.2-8.4 were conducted for an experimental set-up that provided an environment similar to real buildings. As a consequence, the ranges of environmental parameters such as the range of temperature differences, flow rates, and velocities were relatively small. On the other hand, many parameters can be measured only by measurements of several other parameters (components). Considering small velocities and temperature differences and the complexity of experiments, the uncertainty of the conducted measurements is relatively good for all measurements except for the forced convection coefficients developed for use in the room with high aspiration diffuser.

The large uncertainty of forced convection coefficients with high aspiration diffusers (15-38%) is difficult to avoid because a low temperature difference is needed to measure the heat transfer caused by forced convection at room surfaces. However, these forced convection correlations are developed primarily for correction of buoyant convection when high aspiration diffuser is used with cooling panels (Equations 716-7.20). With a large temperature difference (ΔT), the buoyant term in Equations 716-7.20 is dominant and the effect of the uncertainty of forced convection on the overall convention coefficient is small. When ΔT is small, convective heat flux is also small and the uncertainty of heat flux calculated by dominant forced convection term has no large effect on the overall heat flux in the room.

8.7 Summary

This chapter has presented the major details of the conducted measurements. As a result of these measurements, significant amount of experimental data were collected and processed. Part of these measuring results was used in this thesis for convection correlation development and validation of the new models for thermal boundary condition calculations in CFD programs. The other data was processed and prepared for future use in validation of CFD models applied for building airflow calculation. In all the experiments, a large amount of environmental data and data about properties of cooling panels, displacement ventilation, and high aspiration diffusers were collected. Therefore, this data can be used in other types of analyses such as analysis of air quality and thermal comfort with different ventilation systems or validation of the cooling panel models.

CHAPTER 9

APPLICATION OF THE COUPLED PROGRAM

9.1 Introduction

This chapter contains two studies in which coupling between BES and CFD programs is used to analyze indoor air quality and thermal comfort parameters in buildings. The first study is related to an analysis of indoor quality indicators, and the second is related to energy consumption and thermal comfort with different ventilation systems. In the study related to indoor quality indicators, the CFD program is used to calculate concentration distributions. Therefore, in the following section, the effect of thermal boundary conditions on concentration distribution is described to demonstrate the importance of accurate thermal boundary conditions.

9.1.1 The Effect of Thermal Boundary Conditions on Concentration Distribution

While the analysis in Section 4.4 showed the influence of boundary conditions on temperature distribution, this section demonstrates the influence of boundary conditions on concentration distribution. Measured concentration distribution is compared with distributions obtained by CFD simulations that use different methods for boundary condition calculations. Two CFD analyses were performed for a model room which has the same geometry, volume flow rate, heat sources, and contaminant position as the experimental set-up which was presented in Section 8.5 (Case 6 in Table 8.5). In the first CFD analysis, the measured surface temperatures were used as input data while the CFD program calculated thermal boundary conditions by wall functions. In the second analysis, the measured heat fluxes were directly used as thermal boundary conditions. Both CFD analyses were performed by the PHOENICS program package.

Figure 9.1 presents the results of this analysis. The figure shows the tracer gas (SF_6) concentration profile at five positions in the room. The concentration is presented in a normalized form $(C - C_s)/(C_e - C_s)$ where C_s and C_e are concentrations in supply and exhaust air respectively. At positions close to the SF_6 source (positions 1, 4, and 5), the concentration profile obtained by wall functions indicate considerably larger concentration than the measured profile. The major reasons for this are log-law wall functions which predict lower heat flux at heat-source surface (see Figure 9.1). Lower heat flux creates lower air mixing in the room which, as a consequence, creates higher local concentration in the vicinity of the SF_6 source. When exact heat

fluxes are used as thermal boundary conditions (measured heat fluxes), the CFD program more accurately predicts the concentration distribution (refer to Figure 9.1). This indicates that thermal boundary conditions can have large influences on contaminant distribution, especially in rooms where major air motion is driven by surface buoyancy.

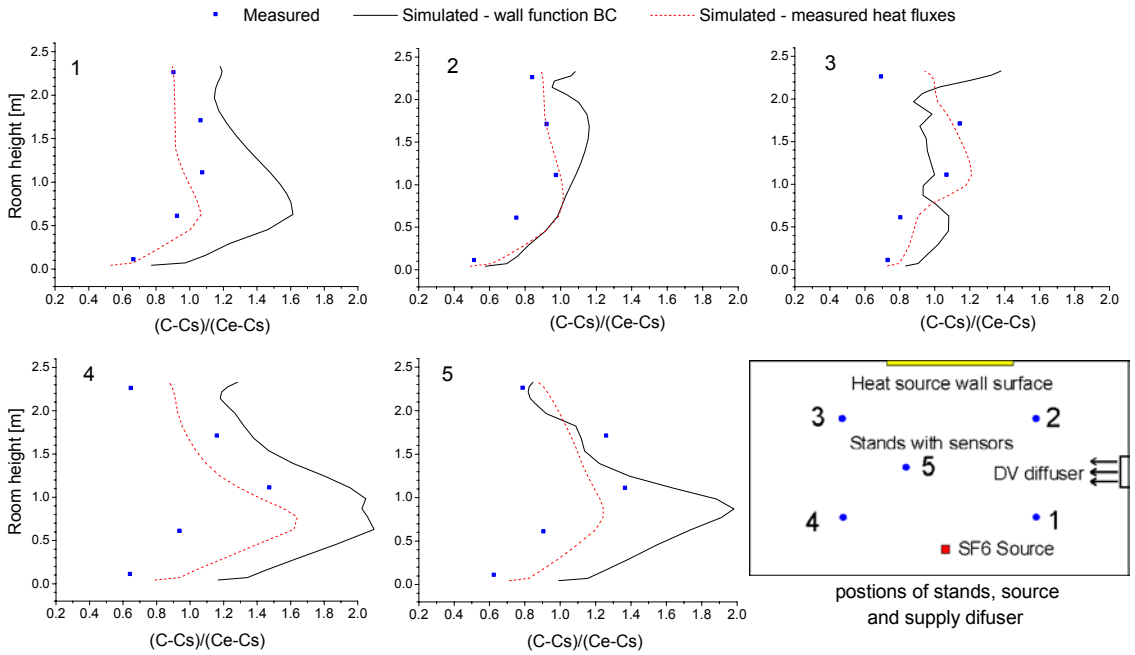

Figure 9.1 A comparison of the measured concentrations with CFD results when (1) wall functions are used for heat flux calculation and (2) measured heat fluxes are used as boundaries

9.1.2 Chapter outline

The previous section shows that thermal boundary conditions at walls may have a considerable influence on concentration distribution. Therefore, for the IAQ study presented in Section 9.2, thermal boundary conditions for CFD models were calculated in collaboration with the BES. This study is a comparative analysis of contaminant removal effectiveness and air exchange efficiency based on a large number of numerical experiments. This study is also an example of how a coupled program can be used for research studies. Section 9.3 provides a second example of the use of coupling. This example is directly related to the use of the newly developed coupled program and it shows the advantages of this program. In this study, energy consumption and thermal comfort are analyzed in a room with a Displacement Ventilation (DV) system combined with Cooled Ceiling (CC) panels. At the end of this chapter, Section 9.4 provides a short summary and discussion about the possible use of the coupled program.

9.2 Comparison of Contaminant Removal Effectiveness and Air Exchange Efficiency

This section focuses on a study of air exchange efficiency (ε_a) and contaminant removal effectiveness (ε) as indicators that are suitable for evaluating Indoor Air Quality (IAQ) in buildings. These two IAQ indicators were numerically studied and compared in four typical indoor spaces with different ventilation strategies and contaminant sources. Overall, more than fifty different simulations cases were performed with the PHOENICS CFD program code where the thermal boundary conditions were defined by use of the BES program described in Chapter 3. Since, a commercial CFD program package is used in these simulations, one-directional coupling is applied (refer to Section 5.2). Based on these numerical experiments, the next section provides properties of this two IAQ parameters and relations between them.

9.2.1 Properties of Air Exchange Efficiency and Contaminant Removal Effectiveness

Contaminant removal effectiveness (ε) is one of the oldest indicators that define a perceived air quality in the space (Yaglou and Witheridge 1937). This indicator is based on the room average contaminant concentration ($\langle C \rangle$), the contaminant concentration at supply (C_s), and the contaminant concentration at exhaust (C_e):

$$\varepsilon = \frac{C_e - C_s}{\langle C \rangle - C_s} \tag{9.1}$$

While the contaminant removal effectiveness is based on contaminant distribution, air exchange efficiency (ε_a) is based on a local value of age of air (τ). Experimental and theoretical background of this IAQ indicator is provided by Etheridge and Sandberg (1996). Air exchange efficiency (ε_a) represents the ratio between the shortest possible time needed for replacing the air in the room (τ_n) and the average time for air exchange (τ_{exe}):

$$\varepsilon_a = \frac{\tau_n}{\tau_{exe}} = \frac{\tau_n}{2\langle \tau \rangle} \tag{9.2}$$

The average time for air exchange may be calculated as $\tau_{exe}=2\cdot\langle\tau\rangle$, where $\langle\tau\rangle$ represents the average local values of age of air. The shortest possible time needed for replacing the air in the room (τ_n) is the reciprocal of the number of air changes in the room (τ_n=1/ACH). Table 9.1 presents the air exchange efficiency values for characteristic flow types.

Table 9.1 Air exchange efficiency for characteristic ventilation flow types

Flow pattern	Air exchange efficiency	Comparison with the average time of exchange
Unidirectional flow	0.5 - 1.0	$\tau_n < \tau_{exc} < 2\tau_n$
Perfect mixing	0.5	$\tau_{exc} = 2\tau_n$
Short Circuiting	0 - 0.5	$\tau_{exc} > 2\tau_n$

Comparison of contaminant removal effectiveness (ε) and the air exchange efficiency (ε_a) should provide an answer to the question: which one of these two perceived air quality indicators is more appropriate for general use, such as for design and standards? This is especially so because these perceived air quality indicators may show conflicting values for indoor air quality in the same room, as illustrated in Figure 9.2. Figure 9.2a presents two dimensional airflow velocities with a bypass flow in upper zone and a recirculation in the occupied zone. Figure 9.2b shows the corresponding age of air normalized by the shortest time needed for the replacement of air ($\varepsilon/\varepsilon_n$). Figures 9.2c and 9.2d represent contaminant concentration normalized with the contaminant concentration at the exhaust (C/C_n) for two different positions of a contaminant source: (1) in the room center (Figure 9.2c) and (2) within the bypass flow (Figure 9.2d). The comparison of Figure 9.2b with 9.2c and 9.2d show that, depending on the position of the contaminant source, the age of air and the contaminant concentration field may have a similar or completely different distribution. Consequently, the air exchange efficiency (ε_a) and the contaminant removal effectiveness (ε) may have the same or conflicting values for perceived indoor air quality in the same space.

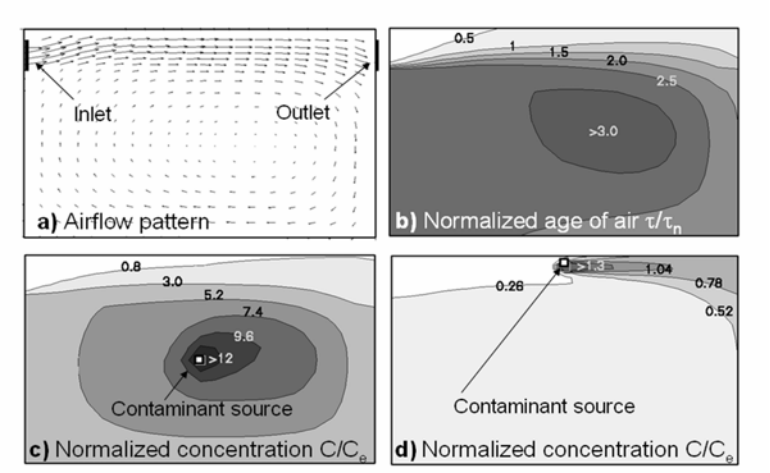

Figure 9.2 Normalized local age of air and contaminant concentration distributions for similar airflow field and different positions of the contaminant source

(a) airflow pattern, (b) $\varepsilon_a = 0.21$ for this airflow pattern, (c) $\varepsilon_a = 0.21$ and $\varepsilon = 0.19$ for contaminant source at room centre, (d) $\varepsilon_a = 0.21$ and $\varepsilon = 2.20$ for contaminant source in the supply air jet

The discrepancies in the concentration and age of air distribution patterns result in conflicting values of ε_a and ε with different positions of the contaminant source (refer to Figure 9.2). The differences in values of ε_a and ε are due to the different "nature" of these two indicators. The air exchange efficiency is an indicator of air distribution quality because it quantifies how good the air flow pattern is. This efficiency indicator accounts for the size and intensity of the recirculation in the room by comparing the room airflow pattern with the airflow pattern of the ideal piston flow. On the other hand, the contaminant removal effectiveness is the indicator of contamination level in a room. The effectiveness indicator depends not only on the airflow pattern, but also on the intensity, area, and positions of contaminant sources relative to this airflow pattern.

Equations (9.1) and (9.2) also demonstrate the different physical meaning of the contaminant removal effectiveness and the air exchange efficiency, thus rendering a direct comparison meaningless. The air exchange efficiency has values from 0 to 1, while the contaminants removal effectiveness takes values from 0 to infinity. Table 9.2 shows ventilation cases for which ε and ε_a values approach their lower and upper limits.

Table 9.2 Limits for air exchange efficiency and contaminants removal effectiveness

Air exchange efficiency	Upper limit	$\varepsilon_a = 1$	Ideal piston flow
	Perfect mixing	$\varepsilon_a = 0.5$	Complete and instantaneous mixing
	Lower limit	$\varepsilon_a \to 0$	Bypass area and recirculation area are completely separated
Contaminant removal effectiveness	Upper limit	$\varepsilon \to \infty$	Contaminant source at the outlet Flow field does not have influence
	Perfect mixing	$\varepsilon = 1$	Complete and instantaneous mixing Position of contaminant does not have influence
	Lower limit	$\varepsilon \to 0$	Contaminant source is in the recirculation area which is completely separated from the bypass area

The contaminant removal effectiveness depends not only on the position of the contaminant relative to the airflow pattern, but also on the area of the source region. For example, a contaminant may be released from a point source such as tobacco smoke or from a large area source such as pollutants from a floor finish. Furthermore, contaminant removal effectiveness depends on source properties such as contaminant density. Consequently, it is hard to expect a relationship between ε and ε_a (Sandberg and Sjoberg 1984, and Skaret 1984) because the number of combinations of flow patterns and type and positions of the contaminant sources are unlimited. However, for typical spaces usually found in buildings, there are a limited number of ventilation strategies with common types of contaminants and their positions. Therefore, the number of

combinations in typical buildings is limited and certain correlations between the air exchange efficiency and the contaminant removal effectiveness may exist. The following sections establish the room types and ventilation strategies in which those correlations exist, quantify them and detect the most important parameters that influence the intensity of the correlations.

9.2.2 Analyzed Cases

The relationship between contaminant removal effectiveness (ε) and air exchange efficiency (ε_a) was analyzed for several different spaces in typical buildings wit h typical ventilation strategies. The following space layouts were analyzed:

- A personal office, which is usually located in the perimeter zone in office buildings,
- A large cubicle office, which is typical for internal zones in office buildings,
- A classroom, which may also be equivalent to a small conference room, and
- A residential space with a typical layout for a residential house or an apartment room.

Figure 9.3 shows space layouts with supply and exhaust positions for the studied spaces. Each of these four space types has its own characteristics related to room size, number occupants per unit of floor, fresh air requirement, cooling or heating loads, and typical ventilation systems.

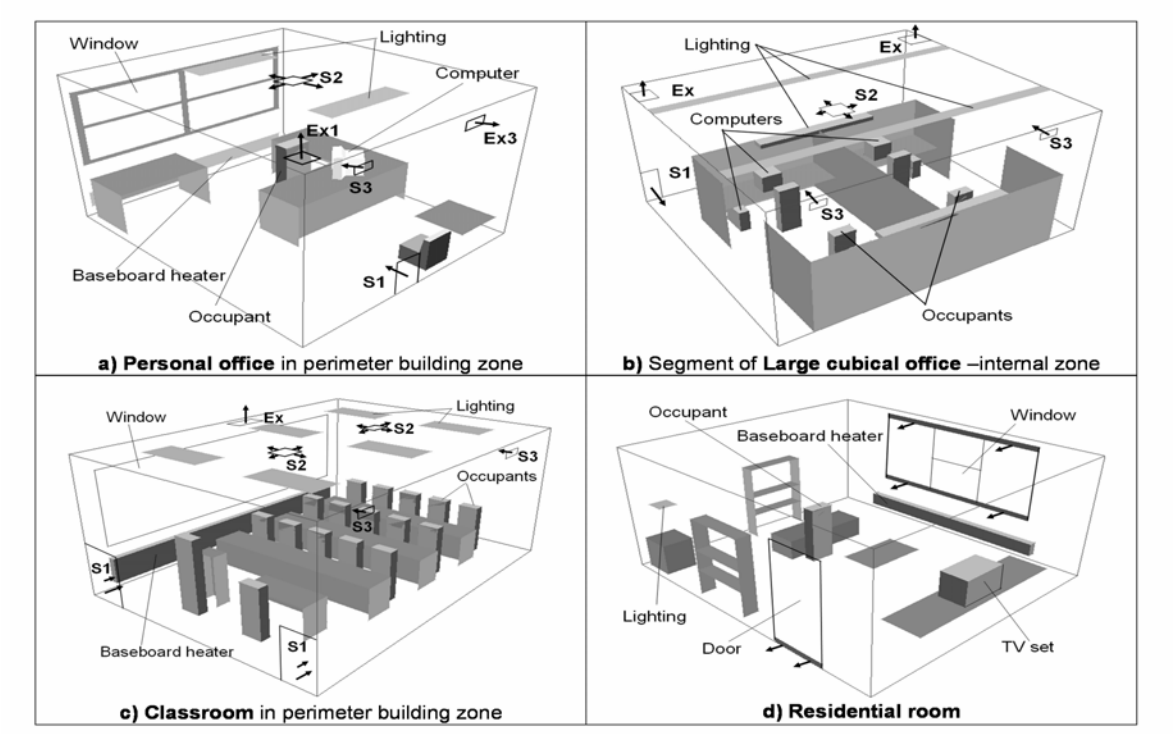

Figure 9.3 Space layouts with supply and exhaust positions for the analyzed cases
(S1 -Displacement ventilation diffuser, S2 -Ceiling mixing diffuser, S3 -Grill diffuser, Ex -Exhaust)

The number of occupants determines the required amount of fresh air, which together with heating/cooling loads, has a considerable influence on the selection of a ventilation system. For example, the personal office has a small occupancy rate and relatively high cooling load per unit of area, which results in small flow rates of fresh air and large total supply air flow rates for all-air systems. On the other hand, in cases where heating/cooling loads are treated with a perimeter heater, fan coil or chilled ceiling, only fresh air is supplied to save fan energy. The large cubicle office has a large occupancy per unit of floor, but also very large cooling loads. Therefore, for this type of room and all-air systems, the amount of supply air is usually determined by cooling loads. In classrooms or small conference rooms, the number of occupants per unit of floor area is large and the amount of supply air is determined by the required amount of fresh air per occupant. Consequently, this type of spaces usually does not have recirculation. Finally, in the case of residential rooms, the occupancy is typically low and ventilation is usually accomplished by infiltration when the outdoor temperature is low or by an open window where the outdoor climate and noise conditions are acceptable.

Based on the cooling or heating loads and the amount of supply air, several ventilation strategies were selected for each of the analyzed spaces. These ventilation strategies determined the position and type of supplies and exhausts (S1, S2, S3, and Ex in Figure 9.3). The analyzed ventilation strategies are displacement ventilation, displacement ventilation combined with cooled ceiling, mixing ventilation with ceiling diffuser, mixing ventilation with grill diffusers, displacement diffuse combined with baseboard heater, ceiling diffuser combined with baseboard heater, ceiling diffuser for all air heating, natural ventilation with open window, natural ventilation with infiltration and heating by baseboard heater, and natural ventilation with infiltration and air heating supply below window. Table 9.3 contains the important parameters for all these cases. In some cases, the total convective loads differ from air loads due to the installed chilled ceiling or baseboard heater or in cases with an all-air heating system due to internal heat sources. In the Table 9.3, the “Total convective load” indicates the intensity of buoyancy driven flow in the room, while the “Air load” indicates a fraction of the total convective load removed by air. A negative value for total convective loads indicates that heating in the room is needed, while a negative value for air loads shows that the supply air has larger temperature than the exhaust air. The level of thermal comfort in each analyzed case was approximately the same. The last column in Table 9.3 shows the difference between the supply air and average room temperatures.

Table 9.3 Simulation parameters for the studied cases of four room types

Room Type	Case	Ventilation strategy	Air changes [h^{-1}]	Recirculation rate [-]	Total convective load [W/m2]	Air load [W/m2]	T_{room}-T_{supply} [^oC]
A) Personal office Space area: A = 14 m^2 Space volume: V = 33.6 m^3 Outdoor Air per person: OA=10 L/s	A1	DV	4.4	0.75	35	35	6
	A2	DV/CC	1.1	0	21	6	7
	A3	CD	4.4	0.75	35	35	10
	A4	CD-lo	4.4	0.75	35	35	10
	A5	GD	4.4	0.75	35	35	10
	A6	DV/BH	1.1	0	-45	4	3
	A7	CD/BH	2.2	0.5	-45	7	4
	A8	CD-w	4.4	0.75	-45	-30	-11
B) Large cubicle office A = 31.2 m^2, V = 93.6 m^3, OA=10 L/s	B1	DV	6.4	0.75	65	65	6
	B2	DV/CC	1.6	0	36	7	7
	B3	CD	6.4	0.75	65	65	10
	B4	GD	6.4	0.75	65	65	10
	B5	GD-s	6.4	0.75	65	65	10
C) Classroom A = 34 m^2 , V = 102 m^3 , OA=7.5 L/s	C1	DV	6	0	50	50	4
	C2	CD	6	0	50	50	9
	C3	GD	6	0	50	50	9
	C4	DV/BH	6	0	-30	18	2
	C5	CD/BH	6	0	-30	18	3
D) Residential room A = 22.5 m^2, V = 54 m^3, OA=7.5 L/s *	D1	OW	4	0	15	15	5
	D2	INF/BH	0.5	0	-38	5	30
	D3	INF/AH	3	0.83	-38	5	30

DV – displacement ventilation, DV/CC – displacement ventilation combined with cold ceiling, CD – ceiling diffuser, CD-lo – ceiling diffuser with low outlet, GD – grill diffuser, GD-s – grill diffuser with outlet on same side of room, DV/BH – displacement ventilation combined with baseboard heater, CD/BH – ceiling diffuser combined with baseboard heater, OW – open window, INF/BH – infiltration combined with baseboard heater, INF/AH – infiltration combined with air heating, * – for case D1 with open window Outdoor Air per person (OA) is 60 L/s

Values ε and ε_a for active and passive contaminant sources were calculated for all cases. To study active types of pollutants that are associated with heat sources, the distribution of contaminant released in the vicinity of an occupant's head was analyzed. This contaminant may represent tobacco smoke, CO_2, or any human bioeffluent. On the other hand, passive pollutants are not directly moved with thermal plumes of heat sources because of their position relative to the heat sources or size of the source area. To evaluate the transport of passive pollutants the distribution of contaminants released from a carpet was analyzed. Moreover, carpets often present a main source of Volatile Organic Compounds (VOC) and other types of pollutants such as dust

and bio-organisms. Details on passive pollutants distribution with different contaminant positions was obtained by analyzing the concentration distribution when the contaminants were released from the floor, walls, and partition dividers in the cubicle office.

To calculate values of air exchange efficiency (ε_a) and contaminant removal effectiveness (ε) for different contaminant sources, spatial distributions of age of air (τ) and different contaminants (C) were calculated for each case. Figure 9.4 shows the example distributions of these values in segment of large cubicle office with displacement ventilation (case B1 in Table 9.3). Values of ε and ε_a were calculated by Equations (9.1) and (9.2) based on spatial distributions of age of air (τ) and different contaminants (C). Depending on the spatial values that are used to calculate average values $\langle C \rangle$ and $\langle \tau \rangle$ in Equations (9.1) and (9.2), ε_a and ε can be defined for a whole space, occupied zone, and breathing plane.

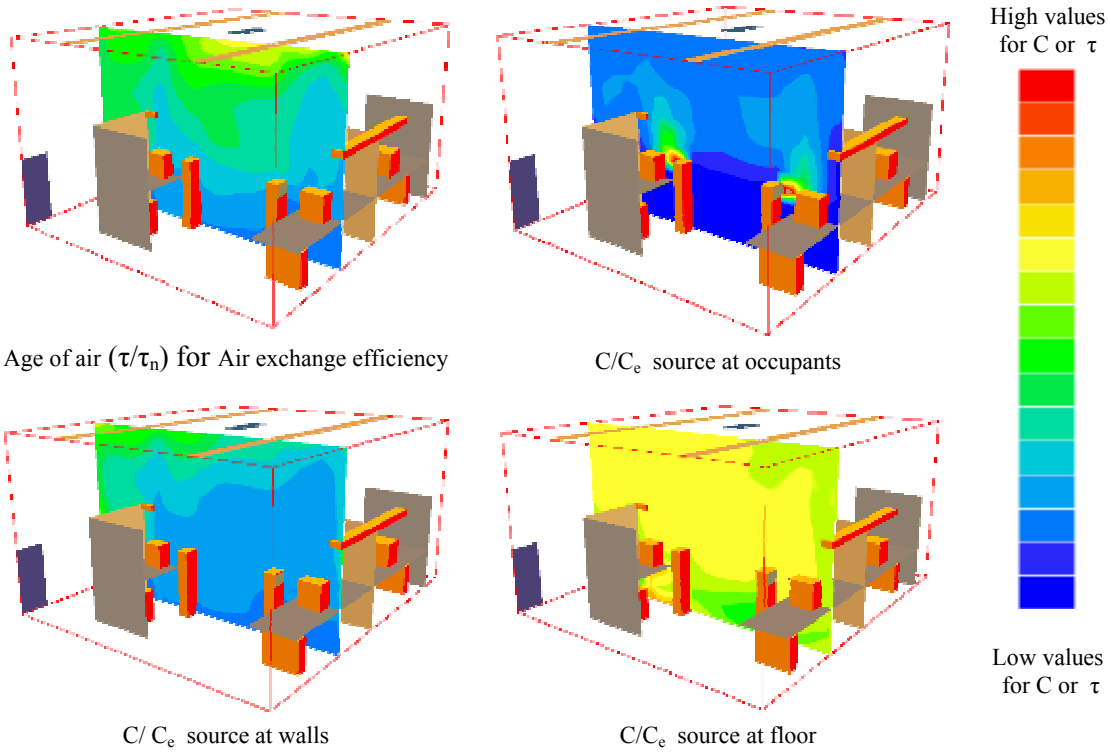

Figure 9.4 Spatial distribution of the age of air (τ) and different contaminants (C) in a segment of a large cubicle office

9.2.3 Results and analysis

Difference in ε_a and ε defined for whole space, occupied zone, and breathing plane

Because the comfort of occupants is the focus of ventilation design, it is important to evaluate ε_a and ε in the occupied zone. Figure 9.5 shows the occupied zone definition available in ASHRAE Standard 62 (2001). For all analyzed cases, ε_a and ε were calculated for a whole space, occupied zone and breathing plane. The difference between the calculated ε_a or ε for the whole space, occupied zone and breathing plane depends on the space type, ventilation strategy, and position of contaminant sources.

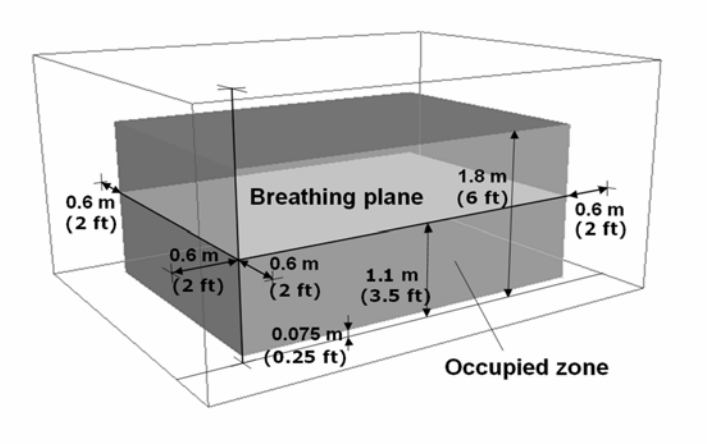

Figure 9.5 Positions of the occupied zone and breathing plane

With a displacement ventilation system, air quality indicators calculated for the occupied zone generally suggest better air quality than indicators calculated for the whole space. On the other hand, with a mixed ventilation system, air quality indicators calculated for the occupied zone usually suggest similar or worse IAQ than indicators calculated for the whole space. Also, results show that perceived air quality indicators defined for the occupied zone and breathing plane have very similar values. This overlapping of quality indicators for the occupied zone and breathing plane reduces the number of necessary measuring points with the experimental evaluation of air quality, which is very important for on-site measurements where the number of measuring points is limited.

Correlations between ε_a and ε

Figure 9.6 presents correlations between ε_a and ε for different ventilation strategies. For studied cases where cooling is provided by mixing ventilation (GD and CD cases in Table 9.3), ε_a

is between 0.42 and 0.53. For these cases the correlation between ε_a and ε is strong for all of the analyzed types of sources (refer to Figure 9.6). Generally, with ceiling diffusers, ε_a and ε have smaller values compared to their corresponding values for the perfect mixing ventilation system because of the bypass flow in the upper part of a room. The bypass flow with mixing ventilation increases in the cubicle office where partition walls prevent appropriate mixing. In the case where the outlet is moved to the lower part of the room, bypassing is reduced and values for both ε_a and ε became slightly closer to the values for the cases with perfect mixing (cases A3 and A4 in Table 9.3).

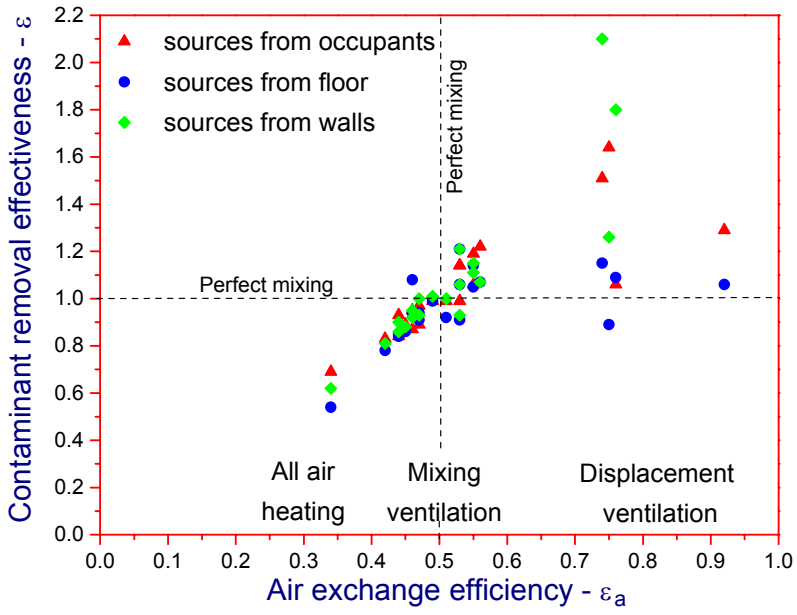

Figure 9.6 The correlation between air exchange efficiency and contaminant removal effectiveness

In the cases where heating is present and the ceiling air jet has a higher supply temperature than the room average such as one with an all-air heating system with exhaust at the ceiling level, a short circuiting occurs (case A8 in Table 9.3). In this case, ε_a and ε for all of the analyzed types of contaminants have considerably lower values compared to the case with perfect mixing (refer to Figure 9.6). Fortunately, this type of bypassing is always followed by temperature stratification, and therefore it is easy to detect it.

In cases where displacement ventilation is used, ε_a is in the range of 0.55-0.92. Lower values are obtained for cases of combined displacement ventilation with cooled ceiling or baseboard heater. These additional water systems eliminate a major part of the sensible cooling or

heating loads causing larger air mixing than with air displacement ventilation alone. For cases where displacement ventilation provides large amount of supply air, the airflow pattern is more similar to the unidirectional flow and ε_a have values above 0.7 (refer to Figure 9.6). Correlations between ε_a and ε for cases with displacement ventilation are weaker than for the cases with mixing ventilation because the influence of the contaminant source position on ε is significant for displacement ventilation. When sources are positioned at floor, values for ε with displacement ventilation are similar to values with mixing ventilation. This is not the case when sources are in the vicinity of the occupants or walls (refer to Figure 9.6).

9.2.4 Summary of Analysis of ε_a and ε

A comparison of air exchange efficiency (ε_a) and contaminant removal effectiveness (ε) for typical ventilation systems and contaminant sources showed that certain correlations exist between these two perceived air quality indicators. The intensity of these correlations depends largely on the ventilation strategy. With mixing ventilation systems, the correlation is strong and it does not depend on contaminant sources. With displacement ventilation, the correlation is weaker because of the significant influence of the contaminant source position. For contaminants released by occupants, the correlation between ε_a and ε still exists, while for the contaminants released from a floor finish, the correlation is considerably weaker.

Considering a whole building, it is easier to measure ε_a than ε (Persily 1994) and therefore ε_a is more suitable for practical on-site applications. Furthermore, the existence of correlations between ε_a and ε justify the use of air-change efficiency ($E=2\cdot\varepsilon_a$) to calculate the average contaminant concentration. This average value can be calculated based on the equations in Appendix D of ASHRAE Standard 62 (2001) for the spaces with known contaminant generation rates. However, in the spaces where a particular contaminant with a known position is investigated, ε should be used because it provides more informative results.

9.3 Energy and Thermal Comfort Analysis of DV System Combined with CC Panels

The combined Displacement Ventilation and Cooled Ceiling (DV/CC) system can successfully combine advantages of DV related to improvement of air quality in the breathing zone of the room with advantages of CC related to increase of cooling capacity. However, this system is very sensitive because the stratified boundary layer with high pollutant concentration which is in the upper zone of a room can be easily suppressed into the breathing zone. To avoid this, a certain temperature gradient has to be maintained to provide effective contaminant removal (Novoselac and Srebric 2001). Furthermore, the portion of cooling load removed by the cooled ceiling system is a key parameter for the temperature gradient and air quality. With the increase of the portion of the cooling load removed by CC, the vertical temperature gradient becomes lower. This suggests a higher degree of pollutant dispersion by air mixing. On the other hand, a large temperature gradient can create temperature discomfort. The design of DV/CC system is very challenging since it includes many parameters that can be analyzed in details by a coupled energy and airflow simulation program. Therefore, this section presents the application of the coupled program for analyses of the DV/CC system, with considerations given to thermal comfort and energy consumption.

9.3.1 Model Room

For a model room, which is a part of large building, the thermal comfort and cooling load for installed DV/CC system are analyzed considering different levels of analysis such as analysis

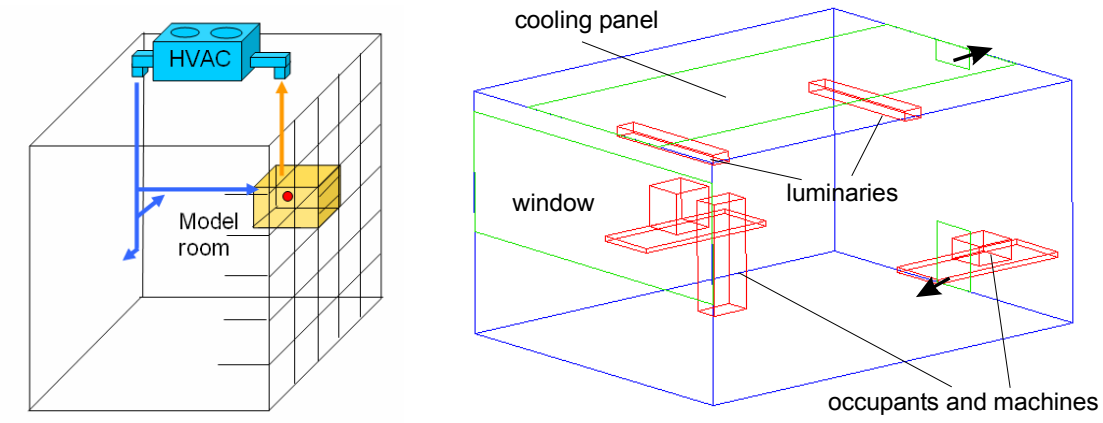

(a) (b)

Figure 9.7 Position of model room in the building (Figure a) with geometry and positions internal heat sources (Figure b)

by the BES program alone or by the coupled BES and CFD0 program. The model room is a typical office space with a size of 3.5× 4.5×2.4 m and small thermal mass. The geometry for this room is presented in Figure 9.7. The room is positioned in the central part of the building, which is assumed to be in Chicago. Furthermore, the considered room is surrounded by other similar rooms. This means that the effect of surrounding rooms on heat transfer in the considered room is negligible. Details about heat sources of the model room are provided in Table 9.4.

Table 9.4 Properties of heat sources for the model room

Object	Q_{total} [W]	Q_{conv}/Q_{total}	Active period
Occupant	75	0.3	9am - 7pm
Computer	150	0.5	continuous
Printer	75	0.5	continuous
Luminaries	2x100	0.3	9pm - 7pm
Solar gain though south shaded window	max ~500	- depends on whether condition	
External conduction	max ~150	- depends on whether condition	
Max cooling load	~1000		

Several HVAC system configurations were considered in three different analyses:

1) In the first analysis performance of an all-air mixing ventilation system are compared with performance of a system that extracts all cooling load by radiant panels. Cooling load and characteristic room temperatures are considered.
2) The second analysis is related to cooling load calculation for a DV/CC system. Also, effects of limitations of HVAC system on thermal comfort and energy consumption are considered.
3) The third analysis compares the results of the BES program with results obtained by coupled program. Thermal comfort and energy consumptions are compared.

9.3.2 Results and Discussion

Comparison of all-air HVAC system with cooled ceiling system

The scope of this analysis is to demonstrate the advantages of the BES program, which implemented models for HVAC system that exchange energy by radiation (refer to Section 3.4.2), compared to energy simulation programs that cannot simulate radiative effects and always assume all-air HVAC system in cooling load calculations. Figure 9.8 shows how the characteristic temperatures and cooling loads change during a period of one week when all-air ventilation system or cooled ceiling panel (CC) is used as HVAC system. Both systems work all day and air set point temperature is 25 °C. Comparison of Mean Radiant Temperatures (MRT) of room surfaces with these two HVAC systems shows that the CC panels provide 1-2 °C lower

temperature than an all air system. On the other hand, the total energy requirement (sum of cooling loads for analyzed period) with the CC system is 6% larger than with the all-air system while the peak cooling loads are slightly smaller. The reason for the larger energy requirement with the CC system rather than with the all-air system is larger conductive heat gain. This heat gain is larger with CC because of the lower temperature of external wall. On the other hand, the CC panel cools down the building structure which increases the energy accumulation during the peak heat gains (refer to Figure 9.8). As consequence, peak cooling load is smaller with the CC system than with the all air system.

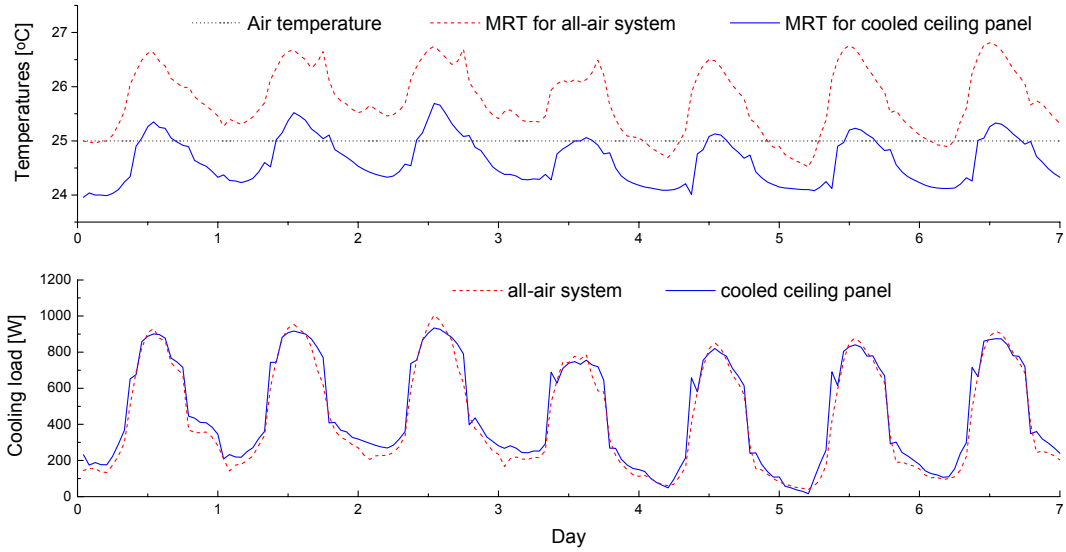

Figure 9.8 Characteristic temperatures and extracted energy for the model room with DV/CC system for a period of 7 days as calculated by the BES program

These two systems do not provide the same level of thermal comfort because the operative temperature ($T_o \approx 0.4 \cdot T_{air} + 0.6 \cdot MRT$) with the CC system is lower (Figure 9.8). In order to provide similar thermal comfort defined by operative temperature, air temperature with the all-air system needs to be 1-1.5 degree smaller for the analyzed case. When the air temperature set point for all air system is 23.5 °C and for CC system is 25 °C, the energy requirement with CC is only slightly larger (3%) than with the all air system. The reason for this is still lower temperature of building envelope with the CC system. This analysis considers only cooling load. For an appropriate comparison of total energy consumption in these two systems: (1) complete HVAC configurations for both systems should be defined; (2) the entire systems should be simulated for whole year and several locations. However, this analysis is not provided as it lies beyond the scope of this example.

Cooling load calculation by DV/CC system and effect of limitation related to HVAC systems

The scope of this analysis is to show realistic change of room temperatures, calculated by BES, in a complex ventilation system such as a DV/CC system, considering the effect of HVAC limitations. Figure 9.9 shows the cooling load and characteristic temperatures for the model room with the DV/CC system. The period of 7 days is considered, same as in the previous analysis. The air system, which is a displacement ventilation system, delivers a constant volume flow rate of 20 l/s with supply temperature of 18°C. Cooling load removed by the air system is presented together with cooling load removed by the CC panel (refer to Figure 9.9). The CC panel, with area of 8.5 m^2, controls the temperature in the room. When the air temperature is below the set point value (25 °C), the cooling panel is OFF and the room temperature freely floats. Evolution of the CC surface temperature and MRT are also plotted in Figure 9.9. In this case there is neither limitation related to cooling capacity nor limitation related to the minimum CC surface temperature. Therefore, air temperature in the room never exceeds the set point value.

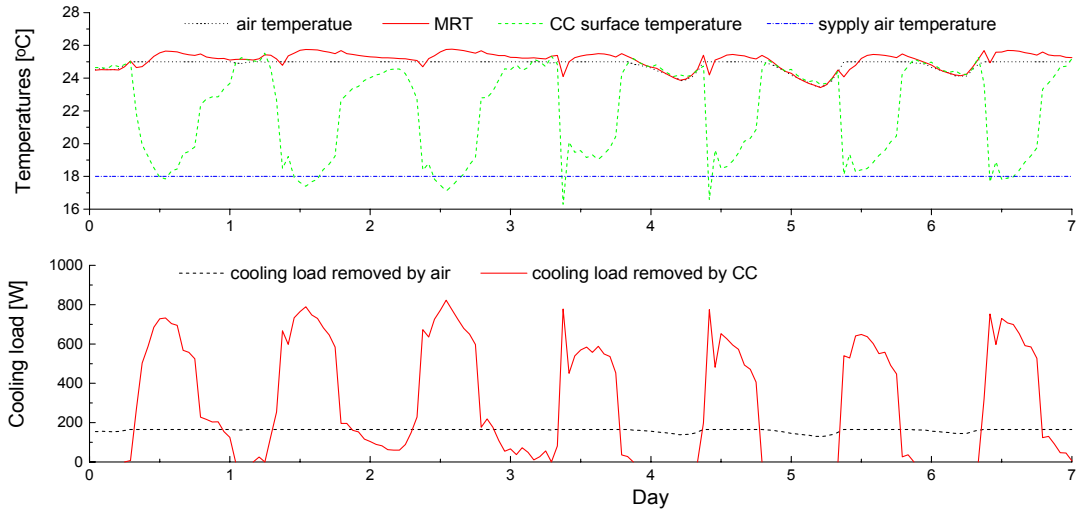

Figure 9.9 Cooling load and temperatures in the model room with a DV/CC system for a period of 7 days as calculated by the BES program

In order to demonstrate effects of constraints in HVAC systems on energy and thermal comfort parameters, Figure 9.10 shows the daily change of air temperature and energy consumption when minimum values of cooled ceiling surface temperature are 16, 18, and 20 °C. The model room is the same as in previous analyses except that the air system is off in order to create a larger cooling load for the CC system. Results show that these limitations can have large effect on temperature and cooling load and demonstrate a need for implementation of Constraints Control Algorithm (refer to Section 3.4.3) into the BES program.

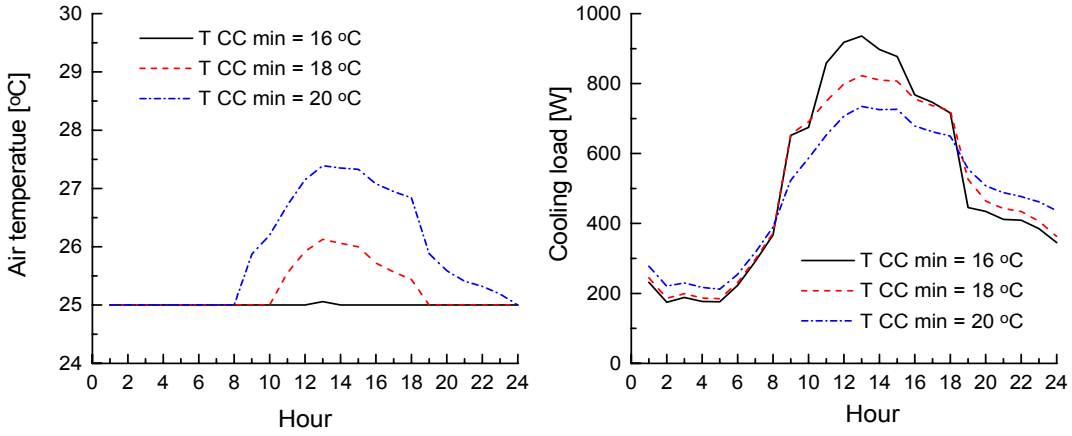

Figure 9.10 The effect of the minimum CC surface temperature on air temperature and cooling load in a model room

Comparison of results obtained by the BES program with results obtained by coupled program

The scope of these analyses is to show the advantages of the coupled program compared to the BES program alone. BES assumes uniform temperature distribution in the room. This is not the case with the DV/CC system. Therefore, energy and thermal comfort analyses were performed for the same model room by using the coupled program. Exhaust air temperature is used as variable that is controlled to be equal to the set point. The analyzed period is one day with calculation time step of 30 minutes. For coupling of the BES and CFD0 programs fully dynamic coupling method is used (refer to Section 5.2). Figure 9.11 compares the results of this analysis with results of an analysis where only the BES program is used. It shows daily change of air temperature in occupied zone of the room and cooling load extracted by the CC system.

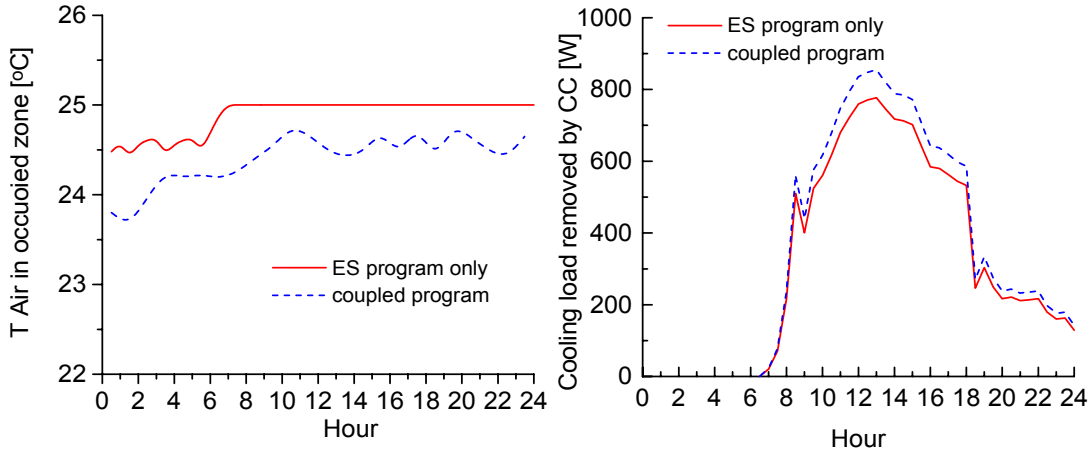

Figure 9.11 Air temperature and cooling load in the model room with a DV/CC system as calculated by the BES program and by the coupled program

Temperature stratification with DV/CC system leads to lower air temperature in occupied zone than in exhaust air. Therefore, for analyzed case air temperature in occupied zone, calculated by the coupled program, is 0.4-0.8°C lower than with the BES program alone, which assumes perfect mixing (refer to Figure 9.11). Energy extracted by CC is higher with the calculation by the coupled program than by BES alone because of the lower calculated temperature of building structure due to temperature stratification.

Temperature stratification is a parameter which affects thermal comfort and air quality in the room. The daily change of this gradient in the occupied zone (0.1 - 1.1 m from the floor) is presented in Figure 9.12. Temperature stratification is not larger because of low air flow rate with DV system and larger air mixing created by buoyant downward air flow at the CC panel. Figure 9.12 shows a decrease of temperature stratification around noon. The reason for this is large solar radiation and increased air mixing due to increased convective heat transfer at the CC surface.

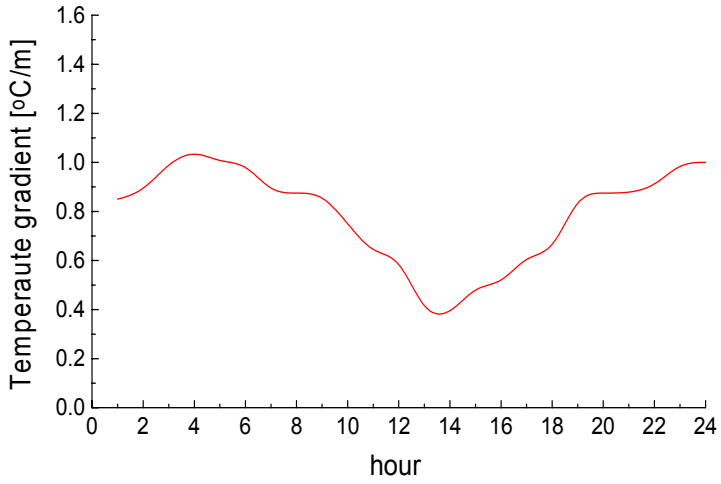

Figure 9.12 Daily change of the temperature gradient in the model room with a CC/DV system

The CFD0 program has implemented a model for thermal comfort index calculation. This index is the Predicted Percentage of Dissatisfied occupants -PPD, and it combines several thermal comfort parameters (ASHRAE Fundamentals 2001). For analysis performed by the coupled program, the spatial distribution of this index is calculated for each time step. Figure 9.13 shows the spatial distribution of this parameter in central plane at 5 pm (17^{th} hour). The figure shows that PPD is very low (below 15%) in the whole room for considered time. Figure 9.14 shows the daily change of PPD in the vicinity of the occupant. Values around noon are higher due to larger cooling load and higher mean radiant temperature. The Figure 9.14 shows that overall thermal

comfort with the CC/DV system change during the day. In the analyzed case this change is small and does not affect considerably the thermal comfort. However it can be more dramatic with other ventilation systems.

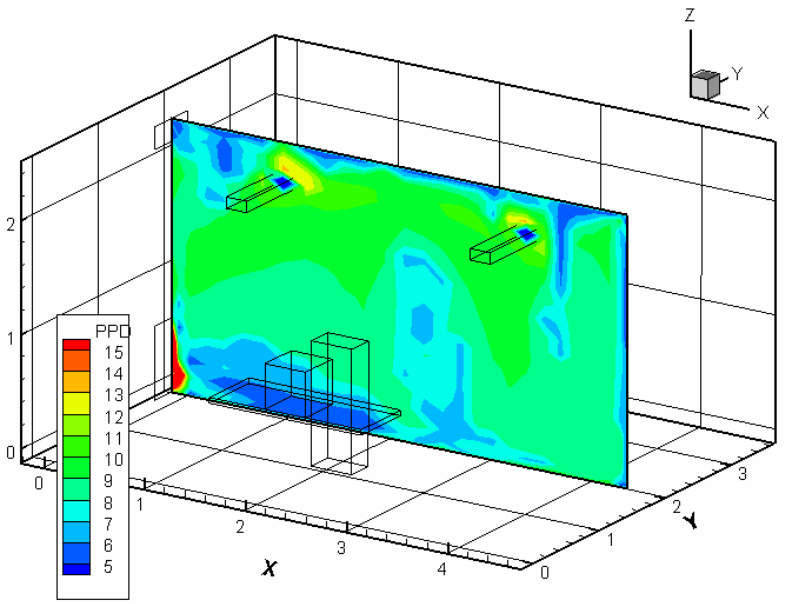

Figure 9.13 Spatial distribution of thermal comfort index PPD in the model room with the DV/CC system

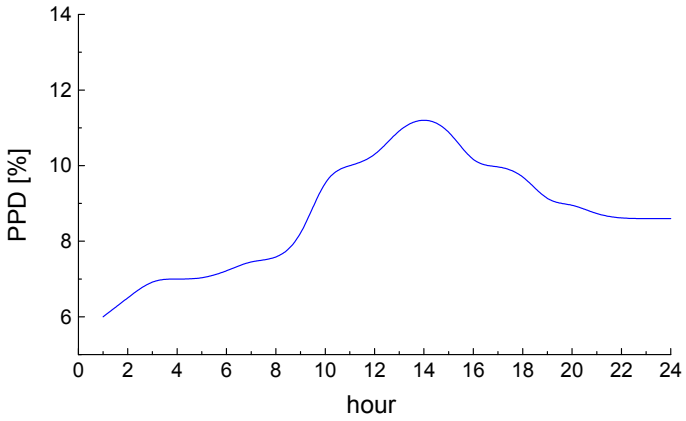

Figure 9.14 Daily change of thermal comfort index PPD in the model room with DV/CC system

In summary, studied cases in this section show that integrated models for load calculation and HVAC performance should be used for the simulation of any system which has a considerable portion of radiative heat exchange. Furthermore, the coupling of the BES and CFD0 program increases the accuracy of energy consumption calculation and enables a detailed thermal comfort analysis which is not possible if the ES program is used alone.

9.4 Discussion and Summary

The newly developed coupled BES and CFD0 program is primarily a research tool. Section 9.2 demonstrates how this program can be used for research which is not directly related to energy or air quality performance of a certain building or HVAC system. However, this program can also be used as an advanced design tool, as described in Section 9.3. For a certain room within considered building, energy consumption, thermal comfort, an IAQ can be evaluated with different ventilation systems which enables the selection of appropriate system and improvement in design.

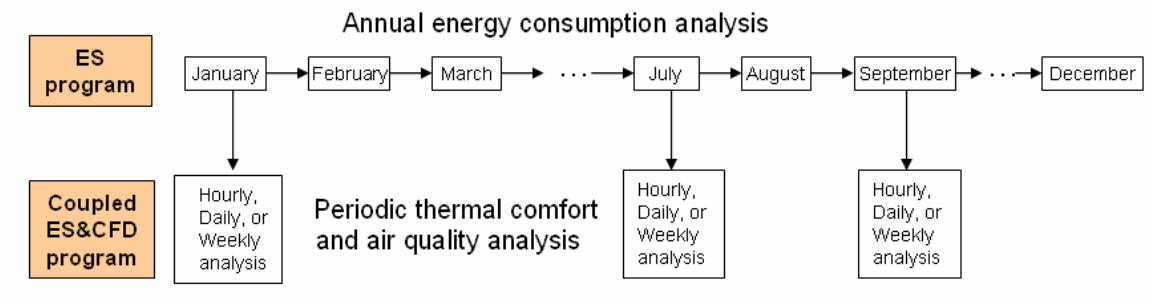

Figure 9.15 Use of the coupled program for periodic thermal comfort and air quality analysis

Considering computation time, a coupled analysis is still impractical for an annual calculation of energy consumption and indoor airflow distribution in each time step (usually an hour or less). Instead of this, the user of the coupled program can perform an energy analysis for a whole year and the coupled energy and airflow analysis for smaller periods of time. Figure 9.15 illustrates this. The selection of entry points for the coupling of the BES with CFD0 program and duration of analyzed period (hour, day or week) is left entirely up to the user and the criteria may be different. For example, a user can select: several hours in each first day of the moth, days with maximum cooling and heating load, or week in transition period of the year (period when heating and cooling is needed in a same day).

CHAPTER 10

CONCLUSIONS AND RECOMMENDATIONS FOR FUTURE RESEARCH

10.1 Conclusions

This section summarizes the main results and conclusions from the research presented in this thesis. The thesis objective was to enhance the accuracy of indoor air flow and thermal modeling within the context of a whole-building simulation. The accomplishments of this research are the following:

(1) new models for air flow and energy simulation in buildings were developed and existing models were improved,

(2) large amount of experimental data were collected and used for the validation of new and existing models, and

(3) new software for combined air and energy flow analyses in buildings was developed and validated.

For the coupling of Energy Simulation (ES) and Computational Fluid Dynamics (CFD) programs, a new building energy simulation program (BES) was developed. This program encompasses existing and newly developed models for heat transfer in building components. With these models, the BES program accurately calculates internal surface temperatures that are necessary for coupling with the CFD program. Also, a new method for simultaneous load calculation and HVAC system simulation was developed and implemented in the BES program. The method enables a modular organization of HVAC system models because HVAC equations are not integrated into the zone matrix for heat transfer through building envelope. For coupling of HVAC modules and the zone matrix, a new Constraint Control Algorithm (CCA) was developed. This algorithm introduces the effect of the HVAC system on building elements by correcting all temperatures in the calculation domain of the BES program. As result, CCA enables a better prediction of thermal comfort and HVAC system performance, especially in buildings where fabric thermal storage has a large influence on energy flow. This includes heating/cooling slabs and systems with radiant panels. The BES program was extensively validated by several validation procedures that include energy balance tests and BESTEST procedures. Good validation results showed that the BES program can be successfully coupled with the airflow program.

An existing CFD program (CFD0 Srebric 2000) was modified for coupling purposes and further developed by adding improved models for thermal boundary conditions calculations. Experiment-based correlations were implemented into CFD0 through the Modified Adaptive Convection Algorithm (MACA). MACA is a modification of the Adaptive Convection Algorithm - ACA (Beausoleil 2000). ACA was extended by addition of new convection correlations and further developed for use as a part of CFD0. Experimental validation of MACA showed that this algorithm and experiment-based correlations provide considerably better accuracy than log-law wall functions for surface heat flux calculation and air temperature distribution. Thermal boundary conditions calculated by MACA are still grid-dependent and a variation of 10% in heat flux may occur. This result is encouraging because 10% variation is much smaller that the variation of heat fluxes resulting from log-law wall functions grid dependency.

In the analyses related to coupling procedures for ES and CFD programs, issues such as data transfer methods, difference of the numerical solutions between various coupling methods, numerical stability, and computation time were considered. Three two-directional coupling methods with different techniques and dynamics of information exchange between the energy and airflow programs were analyzed. When appropriate numerical criteria were satisfied, the difference between numerical solutions calculated by all considered method is insignificant. The quasi-dynamic coupling is the simplest method, which does not have any problems related to numerical stability, but it requires small time steps to provide the same numerical solution as the other methods. The fully dynamic coupling provides numerical solutions that satisfy the energy balance at surfaces in the ES and CFD domains regardless of time step, but it can be computationally expensive since it needs many consecutive runs of the CFD program for a single time step. The integrated coupling method is the most efficient, considering computation time. However, this method uses CFD results that are not fully converged for data exchange between the two programs and this can create numerical instability. Generally, quasi-dynamic coupling should be used for analyses which consider small time periods. Fully dynamic coupling is suitable for occasional coupled analysis that include coupling for only a few time steps, while for other time steps just an energy analysis is considered. Integrated coupling can be used in both types of analyses; however it requires careful selection of calculation step when data in-between programs are exchanged in order to prevent divergence.

In the course of this thesis, several new convection correlations were developed. These are convection correlations for rooms with relatively new ventilation systems such as

displacement ventilation or mixing ventilation with high aspiration diffusers combined with radiant cooling panels. These correlations are developed using state-of-the-art experimental facilities, which enable measurements in environments such as a representative room in the building. The measurements of convection coefficients in rooms with analyzed ventilation systems show that for certain surfaces the existing correlation can be used while for others, the newly developed correlation should be used. The newly developed convection correlations are implemented into the MACA algorithm to improve the accuracy of thermal boundary condition calculations in CFD analyses for rooms with these relatively new ventilation systems.

Another set of experimental measurements was conducted to validate MACA, together with eight additional measurements that include experiments with a tracer gas. Experiments were conducted in a chamber with displacement ventilation, high aspiration diffuser, and heating and cooling panes. These experimental set-ups emphasized air stratification, air motion due to surface convection, or mixing by jet with large entrainment of room air. The measured data were processed and prepared for future use in validation of CFD applications in building analyses.

In this thesis, the coupled program was developed as a tool for accurate energy and thermal comfort analyses. This is a user-friendly software, which has a newly developed Graphical User Interface (GUI) and 3D visualization tool for presenting CFD results. The developed GUI is specialized to provide input data for both BES and CFD0 when they are used for buildings simulations. Combined with the new 3D visualization tool, GUI enables easy application of the coupled program for different energy consumption, air quality, and thermal quality analyses.

Finally, the coupled program was applied to two studies, which demonstrate the capabilities of this program for use in research and advanced design. The first example is a comparative analysis of contaminant removal effectiveness and air exchange efficiency based on a large number of numerical experiments. Based on this analysis, designers can select an appropriate air quality indicator for their application. The second example shows the advantages of the couple program for analysis of energy consumption and air quality in a room with displacement ventilation and cooled ceiling panel. This is the system which includes many parameters that can be analyzed by the coupled energy and airflow simulation program. The results of this example show that, by using the coupled program, the accuracy of energy calculation is increased and the quality of thermal comfort and indoor air quality analysis are considerably improved.

10.2 Recommendations for Future work

This research was focused on developing new and advanced models and tools to simulate an entire building, accompanied with extensive validation. However, there is much space for further improvement and validations in this relatively new research area. A few areas identified for further research are given in the following paragraphs.

Further development of MACA

The performance of MACA in CFD is highly dependent on the implemented convection correlations. Since new ventilation systems are regularly developed, additional convection correlations for specific air flow are always useful. Also, improvements made to models for convection correlation selection, based on velocity distribution in near-wall regions, could improve the applicability of MACA in wide range of airflow regimes in a room.

Improvements in coupling methods

The analysis of the integrated coupling method shows that numerical stability of the solution procedure depends on the frequency (time steps) of information exchange between the ES and CFD programs. Additional analyses related to the selection of optimal iteration step for information exchange could enable faster convergence without problems with numerical instability. Also, there is a need for algorithm which combines different coupling methods to obtain optimal compromise between accuracy and computation time.

Further validation and development of the BES program

The current version of the BES program can be used in analyses of single rooms with or without plenum space. This version of the program can be further developed by advancing and adding procedures that enable multizone energy simulation. With this improvement the coupled program would be capable for the analyses that require whole-building simulation.

Implementation and validation of concentration models in CFD0

The current version of CFD0 does not include models for concentration calculation. With these models, the coupled program would be fully equipped for indoor air quality studies. Using concentration models, the coupled program would be able to calculate contaminant removal effectiveness and air exchange efficiency in a whole room, occupied zone, or breathing plane and provide these data as output. To validate the concentration calculation with the zero equation turbulence model, the measured data collected as part of this thesis can be used.

REFERENCES

Alamdari F. and Hammond G.P. 1983. "Improved Data Correlations for Buoyancy-Driven Convection in Rooms", *Building Services Engineering Research and Technology*, 4 (3): 106-112.

ASHRAE, 1985. "1985 ASHRAE Handbook Fundamentals," ASHRAE, Atlanta. Ch 28.

ASHRAE, 2001. "2001 ASHRAE Handbook Fundamentals," ASHRAE, Atlanta.

ASHRAE. 2001. *ASHRAE Standard 62–2001. Ventilation for acceptable indoor air quality*. Atlanta: American Society of Heating, Refrigerating and Air-Conditioning Engineers, Inc.

Awbi H.B. 1998. "Calculation of Convective Heat Transfer Coefficients of Room Surfaces for Natural Convection", *Energy and Buildings*, 28: 219-227.

Awbi H.B. 1998. "Calculation of convective heat transfer coefficients of room surfaces for natural convection," Energy and Buildings, 28: 219-227.

Awbi H.B. and Hatton A.. 1999. "Natural Convection from Heated Room Surfaces", *Energy and Buildings*, 30: 233-244.

Beausoleil-Morrison I. 2000. "The adaptive coupling of heat and air flow modeling within dynamic whole-building simulation", *PhD Thesis, University of Strathclyde, Glasgow, UK*.

Beausoleil-Morrison I. and Clarke J. 2003. "An Adaptive Conflation Between CFD and Thermal Simulation for Modeling Indoor Airflow and Convective Heat Transfer at Internal Building Surfaces", *ASHRAE Transactions*, KC-03-10-1.

Beausoleil-Morrison I. et al. 2001. "Further developments in the conflation of CFD and building simulation", *Seventh International IBPSA Conference (BS2001), Rio de Janeiro, Brazil, August 13-15*, 2: 1265-1274.

Bejan A. 1995. "Convection heat transfer," 2nd Ed., *John Wiley and Sons Inc.*

Birdsall B.E., et al. 1985. "The DOE-2 computer program for thermal simulation of buildings", *Energy Sources: Conservation and Renewable, American Institute of Physics*, Ed. David Hafmeister.

CHAM, 2004. "The Phoenics Encyclopedia" http://www.cham.co.uk/website/new/phoenic2.htm

Chen Q. 1995. "Comparison of different k-ε models for indoor airflow computations", *Numerical Heat Transfer, Part B: Fundamentals*, 28: 353-369.

Chen Q. 1996. "Prediction of room air motion by Reynolds-stress models", *Building and Environment*, 31(3): 233-244

Chen Q. 1996. "Prediction of room air motion by Reynolds-stress models", *Building and Environmen*t, 31(3): 233-244

Chen Q. and Jiang Z. 1992. “Significant questions in predicting room air motion”, *ASHRAE Transactions,* 98(l): 929-939.

Chen Q. and Van der Kooi J. 1988. “ACCURACY — A computer program for combined problems of energy analysis, indoor airflow, and air quality,” *ASHRAE Transactions*, 94(2): 196-214.

Chen Q. and Xu W. 1998. “A zero-equation turbulence model for indoor airflow simulation",*Energy and Buildings,* 28: 137-144.

Chen Q., Moser A., and Huber A. 1990. “Prediction of Buoyant, Turbulent Flow by a Low-Reynolds-Number $k-\varepsilon$ Model”, *ASHRAE Transactions*, 96(1): 564-573.

Chen Q., Peng X., and van Paassen A.H.C. 1995. “Prediction of room thermal response by CFD technique with conjugate heat transfer and radiation models”, *ASHRAE Transactions*, 3884: 50-60.

Chen Q., Zhai Z., 2002. “Coupling Energy Simulation and Computational Fluid Dynamic Programs”, *Final report submitted to Lawrence Berkley National Laboratory Berkley, CA 94729.*

Churchill, S.W. and R. Usagi. 1972. "A general expression for the correlation of rates of transfer and other phenomena", *AIChE Journal* 18(6): 1121-1128.

Clarke J.A. 1985. "Energy Simulation in Building Design", *Adam Hilger Ltd, Bristol and Boston*.

Clarke J.A. 2001. "Energy Simulation in Building Design", *Butterworth-Heinemann, Oxford.*

Clarke J.A., Hensen J.L.M. and Negrao C.O.R. 1995. "Predicting Indoor Air Flow by Combining Network Approach, CFD and Thermal Simulation", *Proc. 16th AIVC Conf.*, 145-53.

Crawley D.B. et al. 2001. “EnergyPlus: new capabilities in a whole-building energy simulation program,” *Seventh International IBPSA Conference (BS2001), Rio de Janeiro, Brazil,* 1: 51-58.

Crawley D.B., Lawrie L.K., Pedersen C.O., and Winkelmann F.C. 2000. “EnergyPlus: Energy simulation program”, *ASHRAE Journal,* 42(4): 49-56.

Curcija, D. 1992. *“*Three-Dimensional Finite Element Model of Overall, Night Time Heat Transfer Through Fenestration Systems*”, Ph.D. Dissertation, Department of Mechanical Engineering, University of Massachusetts, Amherst, 1992*

Davidson L. and Nielsen P.V. 1996. “Large eddy simulations of the flow in a three dimensional ventilated room”, *Proc. Roomvent ’96,* 2: 161-168.

Deardorff J.W. 1970. “A numerical study of three-dimensional turbulent channel flow at large Reynolds numbers”, *J. Fluid Mech.,* 42: 453-480.

Diamond S.C., Horak H.L., Hunn B.D., Peterson J.L., Roschke M.A., and Tucker E.F. 1977. “DOE-1 program manual”, *Report ANL/ENG-77-04. Los Alamos Scientific Laboratory*.

DOE. 2004. **“**Annual Energy Outlook 2004 with Projections to 2025**”,** *DOE/EIA-0383(2004)* http://www.eia.doe.gov/oiaf/aeo/download.html

Dols, W. S. and Walton G. N. 2003. “CONTAMW 2.0 User Manual” http://www.bfrl.nist.gov/IAQanalysis/docs/NISTIR6921.pdf

Duffie J. A. and Beckman W. A. 1991. “Solar Engineering of Thermal Processes”, *Wiley, John & Sons, Inc.*

Emmerich S. and McGrattan K. 1998. “Application of a large eddy simulation model to study room airflow,” *ASHRAE Transactions.,* 104(1).

Emmerich S.J. 1997. "Use of Computational Fluid Dynamics to Analyze Indoor Air Quality Issues", *National Institute of Standards and Technology report NISTIR 5997, USA.*

EnergyPlus 2001. “EnergyPlus engineering document”, *The reference to EnergyPlus calculation*, http://www.eere.energy.gov/buildings/energyplus/pdfs/engineeringdoc.pdf

Etheridge, D. and Sandberg, 1996. "Building ventilation – theory and measurement", *West Sussex, England: John Wiley & Sons.*

Feustel H.E. 1998. “COMIS – an international multizone air-flow and contaminant transport model”, *Lawrence Berkeley National Laboratory, USA, Report LBNL-42182.*

Fisher D.E. 1995. "An Experimental Investigation of Mixed Convection Heat Transfer in a Rectangular Enclosure", *PhD Thesis, University of Illinois, Urbana USA.*

Fisher D.E. and Pedersen C.O. 1997. “Convective Heat Transfer in Building Energy and Thermal Load Calculations”, *ASHRAE Transactions*, 103 (2): 137-148.

Fluent News. 2004. “Is my Simulation Converged ?”, *Fluent Newsletters*, *Winter01, Article# 20* http://www.fluent.com/about/news/newsletters/01v10i2/a20.htm

Gautier B., Rongere F.X., and Bonneau D. 1991. “CLIM 2000: the building energy simulation tool and the modelling method”, *Proc. Building Simulation ’91, Sophia-Antipolis, Nice.*

Harris, D.J. and Elliot, C.J. 1997. “Energy Accounting for Recycled Buildings Components”, *Proceeding of 2nd Int. Conference on Building end Environment*, *CIB TG8, Paris*

Hensen J. 1999. "A comparison of coupled and de-coupled solutions for temperature and air flow in a building", *ASHRAE Transactions,* 105(2): 962-969

Hittle D.C. 1979. “Building loads analysis and system thermodynamics (BLAST) users manual (Version 2.0),” *Technical Report E-153, Vol. 1 and 2, U.S. Army Construction Engineering Research Laboratory (USA-CERL), Champaign, IL.*

Holmes M.J., Lam J.K.-W., Ruddick K.G., and Whittle G.E. 1990. “Computation of conduction, convection, and radiation in the perimeter zone of an office space”, *Proc. Roomvent ’90, Oslo, Norway.*

Hoornstra, T. G. 1986. “Capaciteitsberekening voor Stralingssverwarming”, *Reports no. ST256, Lab of Refrigeration and Indoor Climate Technology, Delft University of Technology, Delft.*

Howell J., 2002. “A Catalog of Radiation Heat Transfer Configuration Factors”, *Taylor & Francis 2002.*

Inard C., Bouia H., and Dalicieux P. 1996. “Prediction of air temperature distribution in buildings with a zonal model”, *Energy and Buildings,* 24: 125-132.

Jackman P.J. 1970. “A Study of Natural Ventilation of Tall Office Buildings”, *J. Inst. Heat. Vent. Eng.*, 38.

Jiang Y. and Chen Q. 2001. “Study of natural ventilation in buildings by large eddy simulation”, *Journal of Wind Engineering and Industrial Aerodynamics*, 89(13): 1155-1178.

Jiang Y. and Chen Q. 2002. “Study of particle dispersion in buildings with large eddy simulation,” *Proceedings of Indoor Air 2002, The 9th International Conference on Indoor Air Quality and Climate, Monterey, California.*

Jiang, Y., Su., M., and Chen, Q. 2003. “Using large eddy simulation to study airflows in and around buildings,” *ASHRAE Transactions,* 109(2).

Jones P.J. and Whittle G.E. 1992. “Computational fluid dynamics for building air flow prediction—current status and capabilities,” *Building and Environment,* 27(3): 321-328.

Judkoff R. and Neymark J. 1995. "International Energy Agency Building Energy Simulation Test (BESTEST) and Diagnostic Method", *IEA Energy Conservation in Buildings and Community Systems Programme Annex 21 Subtask C and IEA Solar Heating and Cooling Programme Task 12 Subtask B.*

Kakac. S., Ramesh K.S., and Win A.1987. "Handbook of Single-Phase Convective Heat Transfer", *John Wiley & Sons, 1987, New York.*

Khalifa A.J.N. and Marshall R.H. 1990. ‘Validation of Heat Transfer Coefficients on Interior Building Surfaces Using a Real-Sized Indoor Test Cell’, *Int. J. Heat Mass Transfer*, 33(10): 2219-2236

Kimura, K. 1977. “Scientific Basis of Air Conditioning”, *Applied Science Publisher LTD, London*

Klein S.A., Beckman W.A., et al. 1994. “TRNSYS: A transient simulation program”, *Engineering Experiment Station Report 38-12, University of Wisconsin: Madison.*

Kusuda T. 1978. “NBSLD, the computer program for heating and cooling loads in buildings”, *NBS Building Science Series No. 69-R, Washington, DC.*

Launder B.E. and Spalding D.B. 1974. “The numerical computation of turbulent flows,” *Computer Methods in Applied Mechanics and Energy*, 3: 269-289.

Lebrun J. 1970. “Physiological requirements and physical conditions for air conditioning by concentrated static source”, *Ph.D. Thesis, Universite de Liege*.

Loomans M. 1995. “Comments on and Simulations with the Domain Flow Solver”, *FAGO Report 95.45.W, Eindhoven University of Technology, The Netherlands.*

Luikov, A. 1980. "Heat and Mass Transfer", *Mir Publishers, Moscow 1980.*

Marion W. and Urban K., 1995. “User's Manual for TMY2s”, *NREL, Colorado*

Min, T.C., L.F. Schutrum, G.V. Parmelee, and J.D. Vouris. 1956. "Natural convection and radiation in a panel heated room", *Heating Piping and Air Conditioning (HPAC), May*, 153-160.

Moser A., Schalin A., Off F., and Yuan X. 1995. “Numerical modeling of heat transfer by radiation and convection ina an atrium with thermal interia”, *ASHRAE Transaction, 92(2).*

Mumma, S. A. 2001. “Overview Of Integrating Dedicated Outdoor Air Systems With Parallel Terminal Systems”, *ASHRAE Transactions,* 104 (1): 168-175.

Murakami S., Mochida A., Ooka R., Kato S., and Izuka, S. 1996. “Numerical prediction of flow around a building with various turbulence models: comparison of k-ε,.EVM, ASM, DSM, and LES with wind tunnel tests”, *ASHRAE Trans.,* 102(1).

Musy M., Wurtz E., and Sergent A. 2001. “Buildings air-flow simulations: automatically generated zonal models”, *Seventh International IBPSA Conference (BS2001), Rio de Janeiro, Brazil, August 13-15,* 1: 593-600.

NASA. 1975. “NECAP: NASA energy/cost analysis program”, Vol. I-User's manual and Vol II-Engineering manual. *NASA Report CR-2590. Houston.*

Negrao C.O.R. 1995. "Conflation of Computational Fluid Dynamics and Building Thermal Simulation", *PhD Thesis, University of Strathclyde, Glasgow UK.*

Neymark J.and Judkoff R. 2002. "International Energy Agency Building Energy Simulation Test and Diagnostic Method for Heating, Ventilating, and Air-Conditioning Equipment Modules (HVAC BESTEST)", *IEA Energy Conservation in Buildings and Community Systems Programme Annex 21 Subtask C and IEA Solar Heating and Cooling Programme Task 12 Subtask B.*

Nielsen P.V. 1989. "Airflow Simulation Techniques —Progress and Trends", *Proc. 10th AIVC Conf.*, (1): 203-223.

Nielsen P.V. 1989. “Progress and trends in air infiltration and ventilation research,” *Proc. 10th AIVC Conf., Convetry: Air Infiltration and Ventilation Centre.*

Nielsen P.V. 1998. “The selection of turbulence models for prediction of room airflow,” ASHRAE Transactions, SF-98-10-1.

Nielsen P.V. and Tryggvason T. 1998. “Computational fluid dynamics and building energy performance simulation,” *Proc. Roomvent ’98,, Stockholm Sweden,* (1): 101-107.

NIOSH. 2004. *The National Institute for Occupational Safety and Health,* http://www.cdc.gov/niosh/homepage.html

Novoselac, A. and Srebric, J. 2002. "A Critical Review on the Performance and Design of Combined Cooled Ceiling and Displacement Ventilation Systems," *Energy and Buildings*, 34(5): 497-509.

Niu J. and van der Kooi J. 1992. "Grid-Optimization for k -ε Turbulence Model Simulation of Natural Convection in Rooms", *Proc. ROOMVENT '92 Aalborg Denmark*, 1: 207-223.

Novoselac, A. and Srebric, J. 2002. "A Critical Review on the Performance and Design of Combined Cooled Ceiling and Displacement Ventilation Systems", *Energy and Buildings*, 34(5): 497-509.

Novoselac, A. and Srebric, J. 2002. "Influence of Different Pollutant Sources on Selection of Ventilation System in Offices with Cooled Ceiling", *Proceedings of Indoor Air 2002*, Monterey, California.

Paassen A.H.C. 1986. "Design of low energy HVAC-systems with a computerized psychrometric chart", *The 2nd International Conference on System Simulation in Buildings, Liege, Belgium.*

Patankar S.V. 1980. "Numerical heat transfer and fluid flow", *New York: Hemisphere/ McGraw-Hill.*

Patankar S.V., and Spalding, D.B. 1972. "A calculation procedure for heat, mass and momentum transport in three-dimensional parabolic flows", *Int. J. of Heat and Mass Transfer*,Vol 15.

Persily, A. K., Dols, W.S. and Nabinger, S.J 1994. "Air Change Effectiveness Measurement in Two Modern Office Buildings", *Indoor Air journal*, 4: 40-55.

Renz U. and Terhaag U. 1990. "Predictions of air flow pattern in a room ventilated by an air jet, the effect of turbulence model and wall function formulation," *Proc. Roomvent '90, Oslo*, 18.1-18.15.

Rodi W. 1993, "Turbulence Models and their Applications in Hydraulics—A State of the Art Review", *International Association for Hydraulic Research, A.A.. Balkema 1993.*

Sandberg, M. and Sojeberg, M. 1984. "A comparative study of the performance of general ventilation system in evacuating contaminants", *Indoor Air, Proc of 3rd International Conference on Indoor Air Quality and Climate, Stockholm, Sweden,* Vol. 5

Sander D.M. 1974. "FORTRAN IV Program to Calculate Air Infiltration in Buildings, DBR Computer Program No. 37", *National Research Council Canada, Ottawa.*

Schlichting H. 1968. "Boundary Layer Theory", *6th Edition, McGraw-Hill.*

Skaret, E. 1984. "Contaminant removal performance in terms of ventilation effectiveness", *Indoor Air, Proc of 3rd International Conference on Indoor Air Quality and Climate, Stockholm, Sweden,* Vol. 5.

Srebric J. 2000. "Symplified Methodology for Idoor Environmetal Design," PhD Thesis, Massachusetts Institute of Technology

Srebric J., Chen Q., and Glicksman L.G. 2000. "A coupled airflow-and-energy simulation program for indoor thermal environmental studies," ASHRAE Transactions, 106(1): 465-476.

Srebric, J., Chen, Q., and Glicksman, L.R. 1999. "Validation of a zero-equation turbulence model for complex indoor airflows", *ASHRAE Transactions,* 105(2): 414-427.

Tennekes H. and Lumley J.L. 1972. “A first course in turbulence”, *London: MIT Press.*

Thompson C.P. and Leaf G.K. 1988. “Application of a multigrid method to a buoyancyinduced flow problem”, *Multigrid Methods--Theory, Applications and Supercomputing. S.F. McCormick. New York: arcel Dekker Inc.*

Versteeg and Malalaskera. *1995.* "An Introduction to Computational Fluid Dynamics - The Finite Volume Method", *Longman Group 1999, London*

Visual DOE 3.1. “A New Tool for Green Building Design”, http://www.eley.com/gdt/visualdoe/index.htm

Voke P.R. and Gao S. 1993. “Large-eddy simulation of heat transfer from an impinging plane jet,” *ASME: FED-Engineering Applications of Large Eddy Simulations*, 162: 29-35.

Wilcox, D. C. 2000. “Turbulence Modeling for CFD”, *DCW Industries, Inc 2000.*

Xu W. and Chen Q. 1998. “Numerical simulation of air flow in a room with differentially heated vertical walls,” *ASHRAE Transactions,* 104 (1): 168-175.

Yaglou, C. P. and Witheridge, W. N. 1937. "Ventilation requirements, Part 2", *ASHRAE Transaction*, 42: 423-436.

Yang, X. 1993. “Study of Building Material Emissions and Indoor Air Quality,” *PhD Thesis, Massachusetts Institute of Technology*

Young, H. D. 1962. “Statistical treatment of experimental data”, *New York: McGraw-Hill*

Yuan X., Moser A. and Suter P. 1993. "Wall Functions for Numerical Simulation of Turbulent Natural Convection Along Vertical Plates", *Int. J. Heat Mass Transfer*, 36 (18): 4477-4485.

Zhai Z, Chen Q, Haves P and Klems J.H. 2001. "Strategies for Coupling Energy Simulation Programs and Computational Fluid Dynamics Programs", *Proceedings of Building Simulation Conference 2001, Rio de Janeiro, Brazil.*

APPENDIX A

ANGLES OF SOLAR RADIATION

BES program calculates solar angles (Figure A1), need in computation of solar radiation on external and internal building surfaces (Duffie and Beckman 1991).

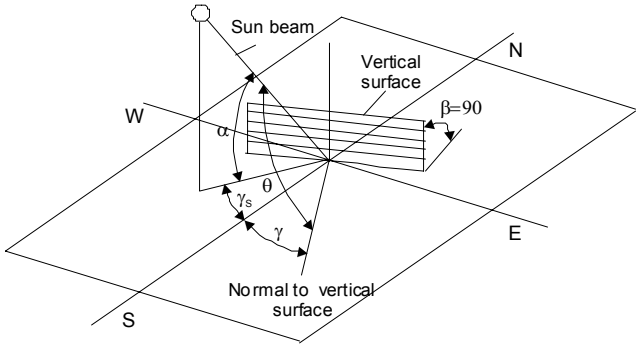

Figure A.1 Solar angles for vertical and horizontal surfaces

Based on input data such as:

- Time - Month, Day, Hour,
- Longitude L, Latitude ϕ,
- Surface orientation –such as horizontal surface or vertical surfaces with azimuth γ

ES program calculates:

1) Declination:

$$\delta = 23.45 \sin[360 \cdot (284 + n) / 365] \quad \text{(A1)}$$

where n is the day in the year.

2) Location solar time:

$$\text{LST} = \text{Standard time} + 4 \cdot (\text{L}_{\text{time zone}} - \text{L}_{\text{location}}) + E \quad \text{(A2)}$$

where E is correction for variable distance of Earth from Sun during the year.

3) Hour angle:

$$\omega = 15 \cdot (\text{LST in hours} - 12) \tag{A3}$$

4) Angle of incidence (θ):

$$\cos\theta = \cos(\phi \pm \beta)\cos\delta\cos\omega + \sin(\phi \pm \beta)\sin\delta \tag{A4}$$

where β is the surface slope.

5) Solar altitude (α):

$$\sin\alpha = \cos\phi\cos\delta\cos\omega + \sin\phi\sin\delta \tag{A5}$$

6) Solar azimuth angle (γ_s):

$$\cos\gamma_s = C_1 C_2 \arctan(\sin\omega/(\sin\phi\cos\omega - \cos\phi\tan\delta)) + C_3(1 - C_1 C_2)\cdot 180/2 \tag{A6}$$

where

$$C_1 = \begin{cases} 1 & for \quad \omega < \arccos(\tan\delta/\tan\phi) \\ -1 & otherwise \end{cases}, \quad C_2 = \begin{cases} 1 & for \quad \phi(\phi - \delta) \geq 0 \\ -1 & otherwise \end{cases}, \quad C_3 = \begin{cases} 1 & for \quad \omega > 0 \\ -1 & otherwise \end{cases} \tag{A7}$$

APPENDIX B

VIEW FACTOR CALCULATION

Elements that form the room enclosure, in BES program, are surfaces which can be parallel or orthogonal to each other. Therefore, there is a need for only two general solutions of integral (3.23). These are solutions for parallel surfaces and orthogonal surfaces (Howell 2002):

Paralel surfaces:

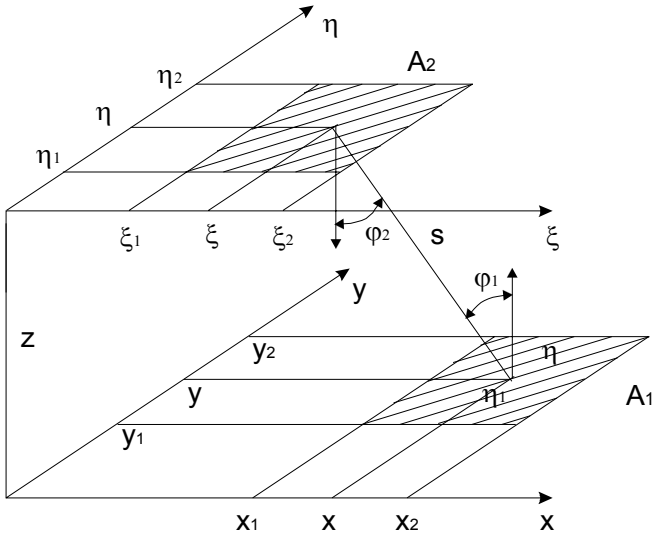

Figure B.1 View factor for parallel surfaces

$$F_{12} = \frac{1}{(X_2 - X_1)(Y_2 - Y_1)} \sum_{l=1}^{2} \sum_{k=1}^{2} \sum_{j=1}^{2} \sum_{i=1}^{2} \left[(-1)^{(l+k+j+i)} G(Z_{li}, P_{kj}) \right] \tag{B1}$$

where:

$$X = x/z\,, \quad Y = y/z\,, \quad N = \eta/z\,, \quad S = \xi/z\,, \quad Z_{li} = S_l - X_i\,, \quad P_{jk} = N_k - Y_j \tag{B2}$$

$$G(Z_{li}, P_{kj}) = \frac{1}{2\pi} \left\{ \begin{array}{l} Z_{li}\left(1 + P_{kj}^2\right)^{1/2} \tan^{-1}\left[Z_{li} / \left(1 + P_{kj}^2\right)^{1/2} \right] - P_{kj} \tan^{-1} P_{kj} + \left(1 + Z_{li}^2\right)^{1/2} P_{kj} \tan^{-1}\left[P_{kj} / \left(1 + Z_{li}^2\right)^{1/2} \right] - \\ Z_{li}^2 \ln Z_{li} + 0.5 \ln\left(1 + P_{kj}^2\right) - 0.5 \ln\left[1 + Z_{li}^2 + P_{kj}^2 \right] \end{array} \right\} \tag{B3}$$

Ortogonal surfaces:

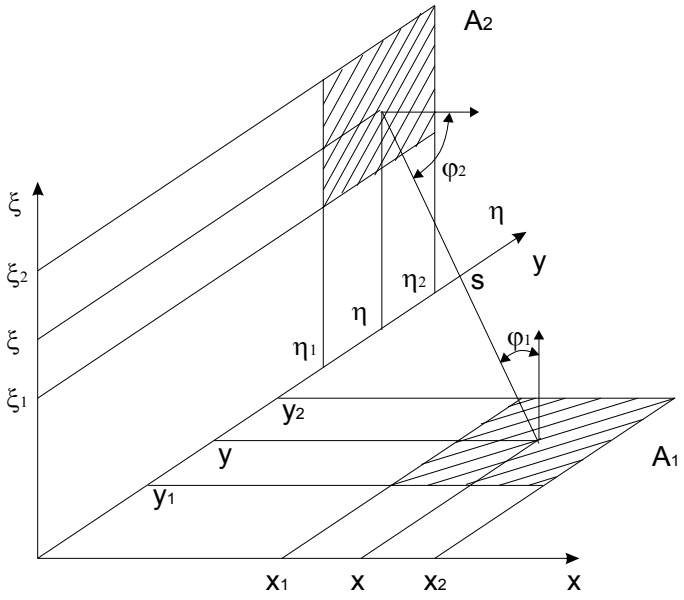

Figure B.2 View factor for orthogonal surfaces

$$F_{12} = \frac{1}{(X_2 - X_1)(Y_2 - Y_1)} \sum_{l=1}^{2}\sum_{k=1}^{2}\sum_{j=1}^{2}\sum_{i=1}^{2}\left[(-1)^{(l+k+j+i)} G(Z_{li}, P_{jk})\right] \tag{B4}$$

where:

$$Z_{li} = \left(\xi_l^2 - x_i^2\right)^{1/2}, \qquad P_{jk} = y_j - \eta_k \tag{B5}$$

$$G(Z_{li}, P_{jk}) = \frac{1}{2\pi}\left[P_{jk} Z_{li} \tan^{-1}\left(P_{jk} / Z_{li}\right) - \frac{1}{2}\left(Z_{li}^2 - P_{jk}^2\right)\ln\left(Z_{li}^2 + P_{jk}^2\right)^{1/2} + \frac{1}{4} P_{jk}^2 \left(1 - 4\ln P_{jk}\right) + \frac{1}{2} Z_{li}^2 \ln Z_{li}\right] \tag{B6}$$

APPENDIX C

COEFFICIENTS OF ZONE-MATRIX EQUATIONS

Discretization of BES program domain (Figure 3.12) creates 4 characteristic nodes with their energy balance equations. This appendix gives these equations and their coefficients.

Element-inner node

$$A \cdot T_{I-1}^{\tau+\Delta\tau} + B \cdot T_{I}^{\tau+\Delta\tau} + C \cdot T_{I+1}^{\tau+\Delta\tau} = F \tag{C1}$$

$$A = -f \frac{k_{I-1}}{(\delta x)_{I-1} \Delta x_I} \tag{C2}$$

$$B = \frac{\rho_I c_I}{\Delta\tau} + f \frac{k_{I-1}}{(\delta x)_{I-1} \Delta x_I} + f \frac{k_I}{(\delta x)_I \Delta x_I} \tag{C3}$$

$$C = -f \frac{k_{I+1}}{(\delta x)_{I+1} \Delta x_I} \tag{C4}$$

$$F = T_I^{\tau}\left[\frac{\rho_I c_I}{\Delta\tau} - (1-f)\frac{k_{I-1}}{(\delta x)_{I-1}\Delta x_I} - (1-f)\frac{k_I}{(\delta x)_I \Delta x_I}\right] + T_{I-1}^{\tau}\left[(1-f)\frac{k_{I-1}}{(\delta x)_{I-1}\Delta x_I}\right] + T_{I+1}^{\tau}\left[(1-f)\frac{k_{I+1}}{(\delta x)_{I+1}\Delta x_I}\right] + (1-f)q^{\tau} + f\, q^{\tau+\Delta\tau} \tag{C5}$$

δx is distance to the surrounding node , Δx is size of control volume, ρ is density, c is specific capacity, k is conductivity, q is source, f is coefficient which determines type of numerical scheme (1- fully implicit, 0.5 - Crank-Nicolson, 0 - implicit).

Internal surface node

$$A \cdot T_{I-1}^{\tau+\Delta\tau} + B \cdot T_{I}^{\tau+\Delta\tau} + R \cdot T_{A}^{\tau+\Delta\tau} + \sum_{i=1}^{n} S \cdot T_{S,i}^{\tau+\Delta\tau} = F \tag{C6}$$

$$A = -f \frac{k_{I-1}}{(\delta x)_{I-1} \Delta x_I} \tag{C7}$$

$$B = \frac{\rho_I c_I}{\Delta\tau} + f\frac{k_{I-1}}{(\delta x)_{I-1}\Delta x_I} + f\frac{h_C^{\tau+\Delta\tau}}{\Delta x_I} + f\frac{\sum_{i=1}^{n} h_{R,i}^{\tau+\Delta\tau}}{\Delta x_I} \tag{C8}$$

$$R = -f\frac{h_C^{\tau+\Delta\tau}}{\Delta x_I} \tag{C9}$$

$$S = -f\frac{h_{R,i}^{\tau+\Delta\tau}}{\Delta x_I} \tag{C10}$$

$$F = T_I^{\tau}\left[\frac{\rho_I c_I}{\Delta\tau} - (1-f)\frac{k_{I-1}}{(\delta x)_{I-1}\Delta x_I} - (1-f)\frac{h_C^{\tau}}{\Delta x_I} - (1-f)\frac{\sum_{i=1}^{n} h_{R,i}^{\tau}}{\Delta x_I}\right] + T_{I-1}^{\tau}\left[(1-f)\frac{k_{I-1}}{(\delta x)_{I-1}\Delta x_I}\right] + T_A^{\tau}\left[(1-f)\frac{h_C^{\tau}}{\Delta x_I}\right] + (1-f)\frac{\sum_{i=1}^{n} h_{R,i}^{\tau}\cdot T_{S,i}^{\tau}}{\Delta x_I} + (1-f)q^{\tau} + f\,q^{\tau+\Delta\tau} \tag{C11}$$

h_C is convection coefficient at considered surface, $h_{R,i}$ is radiative heat exchange coefficient of considered surface to surface 'i', q_{or} is sum of all other radiative heat fluxes that are absorbed by considered surface, $T_{S,i}$ is temperature of surrounding surfaces, and T_A is temperature of air node.

External Surface node

$$B\cdot T_I^{\tau+\Delta\tau} + C\cdot T_{I+1}^{\tau+\Delta\tau} = F \tag{C12}$$

$$B = \frac{\rho_I c_I}{\Delta\tau} + f\frac{k_{I-1}}{(\delta x)_{I-1}\Delta x_I} + f\frac{h_C^{\tau+\Delta\tau}}{\Delta x_I} + f\frac{\sum_{i=1}^{n} h_{ER,i}^{\tau+\Delta\tau}}{\Delta x_I} \tag{C13}$$

$$C = -f\frac{k_{I+1}}{(\delta x)_{I+1}\Delta x_I} \tag{C14}$$

$$F = T_I^{\tau}\left[\frac{\rho_I c_I}{\Delta\tau} - (1-f)\frac{k_{I-1}}{(\delta x)_{I-1}\Delta x_I} - (1-f)\frac{h_C^{\tau}}{\Delta x_I} - (1-f)\frac{\sum_{i=1}^{n} h_{ER,i}^{\tau}}{\Delta x_I}\right] + T_{I+1}^{\tau}\left[(1-f)\frac{k_{I-1}}{(\delta x)_{I-1}\Delta x_I}\right] + T_{EA}^{\tau+\Delta\tau}\left[f\frac{h_C^{\tau+\Delta\tau}}{\Delta x_I}\right] + T_{EA}^{\tau}\left[(1-f)\frac{h_C^{\tau}}{\Delta x_I}\right] + f\frac{\sum_{i=1}^{n} h_{ER,i}^{\tau+\Delta\tau}\cdot T_{ES,i}^{\tau+\Delta\tau}}{\Delta x_I} + (1-f)\frac{\sum_{i=1}^{n} h_{ER,i}^{\tau}\cdot T_{ES,i}^{\tau}}{\Delta x_I} + (1-f)q_{or}^{\tau} + f\,q_{or}^{\tau+\Delta\tau} \tag{C15}$$

h_C is external convection coefficient at considered surface, $h_{ER,i}$ are radiative heat exchange coefficients of considered external surface to ground and sky, q_{or} is sum of all other radiative heat fluxes that are absorbed by considered external surface, T_{EA} is temperature of external node, and $T_{ES,i}$ *(i=1,2)* represents ground and sky temperatures.

Air node

$$D \cdot T_A^{\tau+\Delta\tau} + \sum_{i=1}^{n} E \cdot T_{S,i}^{\tau+\Delta\tau} + \sum_{j=1}^{m} I \cdot T_{E,j}^{\tau+\Delta\tau} = F \tag{C16}$$

$$D = \frac{\rho_I c_{p,I}}{\Delta\tau} + f \frac{\sum_{i=1}^{n} (h_C^{\tau+\Delta\tau} A_i)}{V_{room}} + f \frac{\sum_{j=1}^{m} mc_{p,j}^{\tau+\Delta\tau}}{V_{room}} \tag{C17}$$

$$E = -f \frac{h_C^{\tau+\Delta\tau} A_i}{V_{room}} \tag{C18}$$

$$I = -f \frac{mc_{p,j}^{\tau+\Delta\tau}}{V_{room}} \tag{C19}$$

$$F = T_A^{\tau} \left[\frac{\rho_I c_{p,I}}{\Delta\tau} - (1-f) \frac{\sum_{i=1}^{n} (h_C^{\tau} A_i)}{V_{room}} - (1-f) \frac{\sum_{j=1}^{m} mc_{p,j}^{\tau}}{V_{room}} \right] + (1-f) \frac{\sum_{i=1}^{n} (h_C^{\tau} A_i \cdot T_{S,i}^{\tau})}{V_{room}} + (1-f) \frac{\sum_{j=1}^{m} (mc_{p,i}^{\tau} \cdot T_{E,j}^{\tau})}{V_{room}} + (1-f) \frac{Q_{is}^{\tau}}{V_{room}} + f \frac{Q_{is}^{\tau+\Delta\tau}}{V_{room}} \tag{C20}$$

V_{room} is the volume of the room, A_i is surface area, m is mass flow rate of HVAC supply air and/or infiltration air, and/or inter-zone flow, $T_{E,i}$ is supply air temperature, and/or external air temperature, and/or surrounding-zone air temperature, T_i is temperature of surrounding surfaces, and Q_{is} is internal convective heat source.

APENDIX D

SPARSE MATRIX SOLVER

This appendix describes the sparse matrix solver for heat balance equations used in the BES program (Clarke 2001). The formation of the sparse zone matrix is described in Section 3.3.2. The zone matrix solution from Figure 3.19 is presented in Figure B1 with a rearranged matrix-element numeration. The numeration in Figure 3.19 is more suitable for describing the matrix formation, while the numeration and indexing in Figure D.1 is more suitable for explaining the solving procedure. A vector form of the equation of Figure D.1 is A×T=F where A presents the sparse matrix, T the temperature vector, and F the solution vector.

$$
\begin{vmatrix}
a_{1,1} & a_{1,2} & & & & & & & & & & & & \\
a_{2,1} & a_{2,2} & a_{2,3} & & & & & & & & & & a_{2,14} & \\
 & a_{3,2} & a_{3,3} & & & a_{3,6} & & & a_{3,9} & & & a_{3,12} & a_{3,13} & \\
 & & & a_{4,4} & a_{4,5} & & & & & & & & & \\
 & & & a_{5,4} & a_{5,5} & a_{5,6} & & & & & & & & \\
 & & a_{6,3} & & a_{6,5} & a_{6,6} & & & a_{6,9} & & & a_{6,12} & a_{6,13} & \\
 & & & & & & a_{7,7} & a_{7,8} & & & & & & \\
 & & & & & & a_{8,7} & a_{8,8} & a_{8,9} & & & & & \\
 & & a_{9,3} & & & a_{9,6} & & a_{9,8} & a_{9,9} & & & a_{9,12} & a_{9,13} & \\
 & & & & & & & & & a_{10,10} & a_{10,11} & & & \\
 & & & & & & & & & a_{11,10} & a_{11,11} & a_{11,12} & & \\
 & & a_{12,3} & & & a_{12,6} & & & a_{12,3} & & a_{12,11} & a_{12,12} & a_{12,13} & \\
 & & a_{13,3} & & & a_{13,6} & & & a_{13,3} & & & a_{13,12} & a_{13,13} &
\end{vmatrix}
\times
\begin{vmatrix}
T_{C1} \\ T_{C2} \\ T_{C3} \\ T_{F1} \\ T_{F2} \\ T_{F3} \\ T_{L1} \\ T_{L2} \\ T_{L3} \\ T_{R1} \\ T_{R2} \\ T_{R3} \\ T_{A} \\ q_{plant}
\end{vmatrix}
=
\begin{vmatrix}
f_1 \\ f_2 \\ f_3 \\ f_4 \\ f_5 \\ f_6 \\ f_7 \\ f_8 \\ f_9 \\ f_{10} \\ f_{11} \\ f_{12} \\ f_{13}
\end{vmatrix}
$$

Figure D.1 A zone matrix of energy equations

The sparse matrix in Figure D.1 contains four three-diagonal matrixes. Therefore, the first step in solving this sparse matrix is to partition it. A sub-matrix is created for each element of the zone by extracting the elements that form these three diagonal matrices. In this example, each of the three diagonal matrixes has three elements on diagonal, but in reality, this number is larger and varies with number of nodes in zone elements. The extracted sub-matrixes are presented in Figure D.2. The last rows in these three-diagonal matrices are not extracted since they are connected with the other three-diagonal matrices. The remaining equations from the zone matrix form the second matrix presented in Figure D.3. The term $a_{2,14}$ is the plant interaction term and it has a function in the case when temperature T_a is known and q_{plant} is unknown.

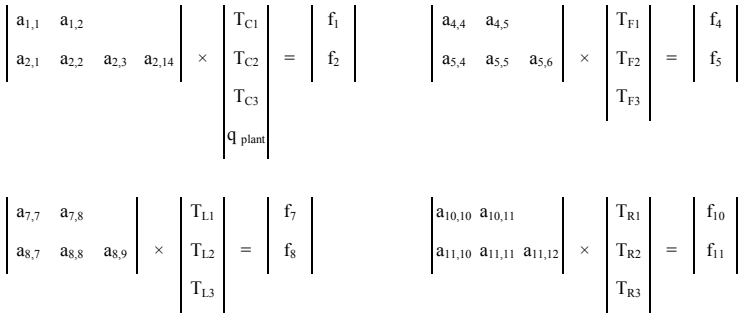

Figure D.2 Sub-matrices for four zone elements

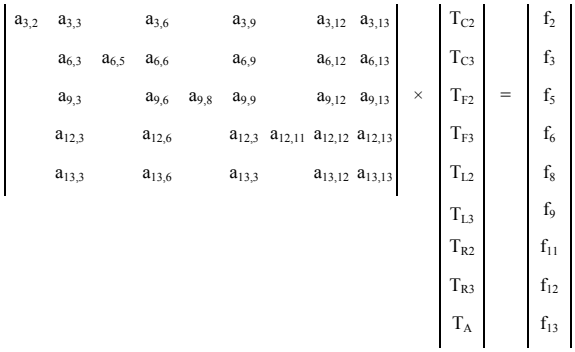

Figure D.3 The second matrix

Equations that describe heat balances at nodes on internal surfaces (equations in the zone matrix in Figure D1: T_{C3}, T_{F3}, T_{L3}, and T_{R3}) are included in the second matrix in Figure D3 and in the sub-matrices in Figure D.2. The same applies to the equation of heat balance next to surface nodes (nodes for T_{C2}, T_{F2}, T_{L2}, and T_{R2}). These equations are the ones that connect the sub-matrices with the second matrix. The linking elements are coefficients: $a_{2,3}$, $a_{5,6}$, $a_{8,9}$, and $a_{11,12}$ in the sub-matrices matrices and matrix elements: $a_{3,2}$, $a_{6,5}$, $a_{9,8}$, and $a_{12,11}$ in the second matrix.

The solution of partitioned matrices occurs in six stages:

1) Gaussian elimination for each sub-matrix

Starting from the top of the matrix, each row of each sub-matrix is treated in a way that eliminates the coefficients below the main diagonal. The resulting sub-matrices are presented in Figure D.4. Coefficients, which are modified by this treatment, have prime symbols (refer to Figure D.4).

To completely solve these modified sub-matrices, surface temperatures (T_{C3}, T_{F3}, T_{L3}, and Tt_{R3}) are necessary. These temperatures are calculated by using the second matrix.

$$\begin{vmatrix} a_{1,1} & a_{1,2} & & \\ & a_{2,2}' & a_{2,3} & a_{2,14} \end{vmatrix} \times \begin{vmatrix} T_{C1} \\ T_{C2} \\ T_{C3} \\ q_{plant} \end{vmatrix} = \begin{vmatrix} f_1 \\ f_2' \end{vmatrix} \qquad \begin{vmatrix} a_{4,4} & a_{4,5} & \\ & a_{5,5}' & a_{5,6} \end{vmatrix} \times \begin{vmatrix} T_{F1} \\ T_{F2} \\ T_{F3} \end{vmatrix} = \begin{vmatrix} f_4 \\ f_5' \end{vmatrix}$$

$$\begin{vmatrix} a_{7,7} & a_{7,8} & \\ & a_{8,8}' & a_{8,9} \end{vmatrix} \times \begin{vmatrix} T_{L1} \\ T_{L2} \\ T_{L3} \end{vmatrix} = \begin{vmatrix} f_7 \\ f_8' \end{vmatrix} \qquad \begin{vmatrix} a_{10,10} & a_{10,11} & \\ & a_{11,11}' & a_{11,12} \end{vmatrix} \times \begin{vmatrix} T_{R1} \\ T_{R2} \\ T_{R3} \end{vmatrix} = \begin{vmatrix} f_{10} \\ f_{11}' \end{vmatrix}$$

Figure D.4 Modified sub-matrices

2) Modification of the second matrix

In this step, the modified sub-matrices (from Figure D.4) are used to eliminate the next-to-surface nodal temperatures from the second matrix (temperatures T_{C2}, Tt_{F2}, T_{L2}, T_{R2} and elements $a_{3,2}$, $a_{6,5}$, $a_{9,8}$, $a_{12,11}$ in Figure D.3). Adding each sub-matrix multiplied by an appropriate constant to the second matrix row equations that operate on the same zone elements, next-to-surface nodal temperatures are eliminated. For example, $T_{C,2}$ is eliminated from the second matrix by multiplying the modified sub-matrices (upper left in Figure D.4) by $-a_{3,2}/a'_{2,2}$ and adding this to the first row of the second matrix in Figure D.3. This resulting modified second matrix is presented in Figure D.5. The new plant interaction term $a_{2,14}'$ has a value of $-a_{3,2}/a'_{2,2} \cdot a_{2,14}$.

$$\begin{vmatrix} a_{3,3}' & a_{3,6} & a_{3,9} & a_{3,12} & a_{3,13} & a_{2,14}' \\ a_{6,3} & a_{6,6}' & a_{6,9} & a_{6,12} & a_{6,13} & \\ a_{9,3} & a_{9,6} & a_{9,9}' & a_{9,12} & a_{9,13} & \\ a_{12,3} & a_{12,6} & a_{12,3} & a_{12,12}' & a_{12,13} & \\ a_{13,3} & a_{13,6} & a_{13,3} & a_{13,12} & a_{13,13} & \end{vmatrix} \times \begin{vmatrix} T_{C3} \\ T_{F3} \\ T_{L3} \\ T_{R3} \\ T_A \\ q_{plant} \end{vmatrix} = \begin{vmatrix} f_3' \\ f_6' \\ f_9' \\ f_{12}' \\ f_{13}' \end{vmatrix}$$

Figure D.5 Modified second matrix

3) Gaussian elimination for modified second matrix

Using Gaussian elimination, which starts from second row, the matrix form in Figure D.6 is obtained. Coefficients that are modified twice have double primes.

4) Major unknown calculation - T_A or q_{plant}

If the set point for air temperature (t_A) is given, the required plant-energy (q_{plant}) is calculated from the first equation of the matrix in Figure D.6: $q_{plant} = -(a_{3,13} / a_{2,14}) \cdot T_A$. If the set point for air temperature is unknown, but given plant-energy is known, the next equation is used: $T_A = -(a_{2,14} / a_{3,13}) \cdot q_{plant}$.

$$\begin{vmatrix} & & & & a_{3,13}' & a_{2,14}'' \\ a_{6,3} & a_{6,6}' & a_{6,9} & a_{6,12} & a_{6,13} & \\ & a_{9,6}' & a_{9,9}'' & a_{9,12}' & a_{9,13}' & \\ & & a_{12,3}' & a_{12,12}'' & a_{12,13}' & \\ & & & a_{13,12}' & a_{13,13}'' & \end{vmatrix} \times \begin{vmatrix} T_{C3} \\ T_{F3} \\ T_{L3} \\ T_{R3} \\ T_A \\ q_{plant} \end{vmatrix} = \begin{vmatrix} f_3'' \\ f_6'' \\ f_9'' \\ f_{12}'' \\ f_{13}' \end{vmatrix}$$

Figure D.6 Modified second matrix after Gaussian elimination

5) Back-substitution process on second matrix

Knowing T_A and q_{plant} and using a back-substitution process on the second matrix in Figure D.6, temperatures of surface nodes (T_{C3}, T_{F3}, T_{L3}, T_{R3}) are calculated. First, the t_{R3} is solved using last row of the second matrix and calculated using values for T_A and q_{plant}.

6) Back-substitution process in modified sub-matrices

Using the calculated temperatures of internal surface nodes (T_{R3}, T_{F3}, Tt_{L3}, T_{R3}) and modified sub-matrices in Figure B4, the remaining temperatures of internal nodes are calculated. Surface temperatures are substituted into the sub-matrices. Then, additional back substitution processes are performed for each sub-matrix in order to calculate temperatures at these internal nodes.

APPENDIX E

VIEW FACTORS AND DIFFUSE AND DIRECT SOLAR RADIATION DISTRIBUTION

Building geometry and orientation used for testing of newly developed energy simulation (ES) program is presented in Figure E1. Table E1 shows the calculated view factors for internal surface of the test building (Figure E1) by view factor model implements in BES program.

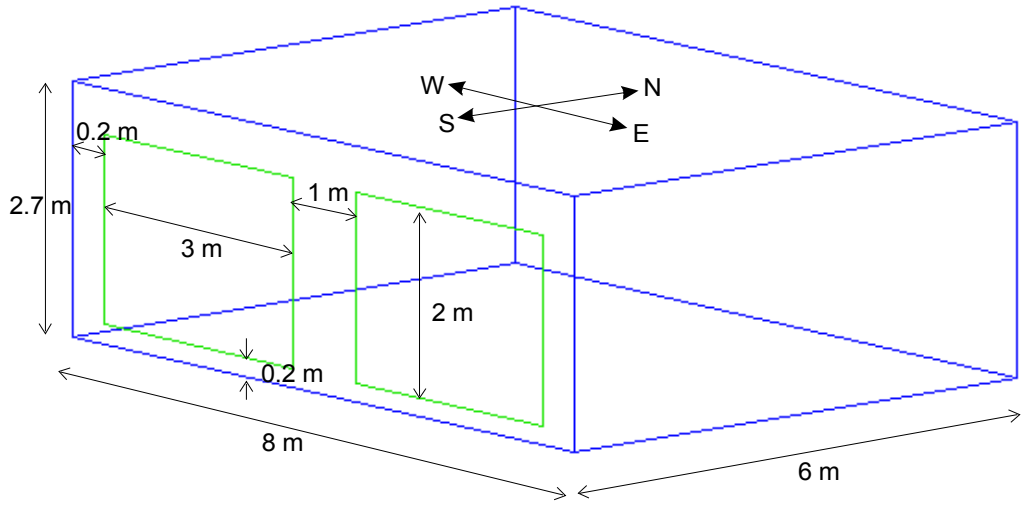

Figure E.1 Test building geometry

Table E.1 View factors for the test building (room)

	floor	ceiling	W wall	E wall	N wall	window 1	window 2	S wall	sum
floor	0.0000	0.4942	0.1068	0.1068	0.1461	0.0430	0.0430	0.0600	1.0000
ceiling	0.4942	0.0000	0.1068	0.1068	0.1461	0.0391	0.0391	0.0679	1.0000
W wall	0.3166	0.3166	0.0000	0.0668	0.1500	0.0661	0.0134	0.0705	1.0000
E wall	0.3166	0.3166	0.0668	0.0000	0.1500	0.0134	0.0661	0.0705	1.0000
N wall	0.3246	0.3246	0.1125	0.1125	0.0000	0.0357	0.0357	0.0543	1.0000
window 1	0.3441	0.3126	0.1785	0.0362	0.1286	0.0000	0.0000	0.0000	1.0000
window 2	0.3441	0.3126	0.0362	0.1785	0.1286	0.0000	0.0000	0.0000	1.0000
S wall	0.3002	0.3397	0.1190	0.1190	0.1221	0.0000	0.0000	0.0000	1.0000

Based on view factors and surfaces absorptance, BES program calculates distribution of transmitted direct and diffuse radiation using short wave radiation models presented in Section 3.2.2. Table E2 presents the solar fractions of direct solar radiation for building geometry presented in Figure E1. Tables E3 and E4 present the solar fractions for transmitted diffuse radiation through window1 1 and 2 respectively.

Table E.2 Direct solar radiation distribution for test building (room) and ε = 0.6

	first strike (A1)	second strike (A2)	third strike (A3)	remaining (AR)	Total for surface
floor	0.6	0	0.0254	0.0157	0.6411
ceiling	0	0.1186	0.0254	0.0157	0.1597
W wall	0	0.0256	0.0086	0.0053	0.0395
E wall	0	0.0256	0.0086	0.0053	0.0395
N wall	0	0.0351	0.0114	0.0071	0.0536
window 1	0	0.0146	0.0045	0.0028	0.0219
window 2	0	0.0146	0.0045	0.0028	0.0219
S wall	0	0.0144	0.0051	0.0031	0.0226
				Total for room	1.0

Table E.3 Diffuse solar radiation distribution from Window 1 (ε = 0.6)

	first strike (A1)	second strike (A2)	third strike (A3)	remaining (AR)	Total for surface
floor	0.2065	0.0634	0.0255	0.0158	0.3112
ceiling	0.1875	0.0671	0.0255	0.0158	0.2960
W wall	0.1071	0.0209	0.0086	0.0053	0.1420
E wall	0.0217	0.0232	0.0086	0.0053	0.0588
N wall	0.0772	0.0308	0.0115	0.0071	0.1265
window 1	0	0.0149	0.0045	0.0028	0.0222
window 2	0	0.0124	0.0045	0.0028	0.0197
S wall	0	0.0154	0.0051	0.0032	0.0236
				Total for room	1.0

Table E.4 Diffuse solar radiation distribution from Window 2 (ε = 0.6)

	first strike (A1)	second strike (A2)	third strike (A3)	remaining (AR)	Total for surface
floor	0.2065	0.0634	0.0255	0.0158	0.3112
ceiling	0.1875	0.0671	0.0255	0.0158	0.2960
W wall	0.0217	0.0232	0.0086	0.0053	0.0588
E wall	0.1071	0.0209	0.0086	0.0053	0.1420
N wall	0.0772	0.0308	0.0115	0.0071	0.1265
window 1	0	0.0124	0.0045	0.0028	0.0197
window 2	0	0.0149	0.0045	0.0028	0.0222
S wall	0	0.0154	0.0051	0.0032	0.0236
				Total for room	1.0

APPENDIX F

MATERIAL SPECIFICATION FOR TEST BUILDING

Material properties of BESTEST building presented in Figure E.1 for lightweight and heavyweight test cases are presented in Tables F.1 and F.2.

Table F.1 Material specifications for lightweight BESTEST cases (Judkoff and Neymark 1995)

Lightweight Case Exterior wall (inside to outside)						
Element	k [W/mK]	thickness [m]	U [W/m^{2}K]	R [m^{2}K/W]	density [kg/m^3]	cp [J/kgK]
Int. Surf. Coef. (see note 2)			8.290	0.121		
Plasterboard	0.16	0.1200	13.333	0.075	950	840
Fiberglass quilt	0.04	0.0660	0.606	1.650	10	840
Wood Siding	0.14	0.0090	15.556	0.064	530	900
Ext. Surf. Coef.			29.300	0.034		
Total air-air			0.514	1.944		
Total surf-surf			0.559	1.789		
Lightweight Case Floor (inside to outside)						
Element	k [W/mK]	thickness [m]	U [W/m^{2}K]	R [m^{2}K/W]	density [kg/m^3]	cp [J/kgK]
Int. Surf. Coef.			8.290	0.121		
Timber flooring	0.14	0.0250	5.600	0.179	650	1200
Insulation	0.04	1.0030	0.040	25.075		
Total air-air			0.039	25.374		
Total surf-surf			0.040	25.254		
Lightweight Case Roof (inside to outside)						
Element	k [W/mK]	thickness [m]	U [W/m^{2}K]	R [m^{2}K/W]	density [kg/m^3]	cp [J/kgK]
Int. Surf. Coef.			8.290	0.121		
Plasterboard	0.16	0.0100	16.000	0.063	950	840
Fiberglas quit	0.04	0.1118	0.358	2.794	12	840
Roof deck	0.14	0.0190	7.368	0.136	530	900
Ext. Surf. Coef.			29.300	0.034		
Total air-air			0.318	3.147		
Total surf-surf			0.334	2.992		
Lightweight Case Summary						
Element	Area [m^2]		UA [W/K]			
Wall	63.6		32.580			
Floor	48.0		1.892			
Roof	48.0		15.253			
S. window	12.0		36.000			
Infiltration			18.440	(see note 1)		
Total UA (wf S. Glass)			104.300			
Total UA (No S. Glass)			68.300			
		ACH	Volume [m^3]	Altitude [m]		
		0.5	129.6	1609		

Note 1: Infiltration = ACH × Volume × cp × density (at specific altitude)
Note 2: The interior film coefficient for floors and ceilings is average value for upward and downward heat flow at summer and winter

Table F.2 Material specifications for heavyweight BESTEST cases (Judkoff and Neymark 1995)

Heavyweight Case Exterior wall (inside to outside)						
	k	thickness	U	R	density	cp
Element	[W/mK]	[m]	[W/m^{2}K]	[m^{2}K/W]	[kg/m^3]	[J/kgK]
Int. Surf. Coef. (see note 2)			8.290	0.121		
Concrete Block	0.51	0.1000	5.100	0.196	1400	1000
Foam Insulation	0.04	0.0615	0.651	1.537	10	1400
Wood Siding	0.14	0.0090	15.556	0.064	530	900
Ext. Surf. Coef.			29.300	0.034		
Total air-air			0.512	1.952		
Total surf-surf			0.556	1.797		
Heavyweight Case Floor (inside to outside)						
	k	thickness	U	R	density	cp
Element	[W/mK]	[m]	[W/m^{2}K]	[m^{2}K/W]	[kg/m^3]	[J/kgK]
Int. Surf. Coef.			8.290	0.121		
Concrete Slab	1.13	0.0800	14.125	0.071	1400	1000
Insulation	0.04	1.0070	0.040	25.175		
Total air-air			0.039	25.366		
Total surf-surf			0.040	25.243		
Heavyweight Case Roof (inside to outside)						
	k	thickness	U	R	density	cp
Element	[W/mK]	[m]	[W/m^{2}K]	[m^{2}K/W]	[kg/m^3]	[J/kgK]
Int. Surf. Coef.			8.290	0.121		
Plasterboard	0.15	0.0100	16.000	0.063	950	840
Fiberglas quit	0.04	0.1118	0.358	2.794	12	840
Roof deck	0.14	0.0190	7.368	0.136	530	900
Ext. Surf. Coef.			29.300	0.034		
Total air-air			0.318	3.147		
Total surf-surf			0.334	2.992		
Heavyweight Case Summary						
Element	Area [m^2]		UA [W/K]			
Wall	63.6		32.580			
Floor	48.0		1.892			
Roof	48.0		15.253			
S. window	12.0		36.000			
Infiltration			18.440	See note 1		
Total UA (wf S. Glass)			104.165			
Total UA (No S. Glass)			68.165			
		ACH	Volume [m^3]	Altitude [m]		
		0.5	129.6	1609		

Note 1: Infiltration = ACH × Volume × cp × density (at specific altitude)
Note 2: The interior film coefficient for floors and ceilings is average value for upward and downward heat flow at summer and winter

APPENDIX G

CFD COEFFICIENTS

Equation (4.32) presents the discretized form of general transport equation. Table G.1 contains the coefficients for equation (4.32). These confidents are calculated for hybrid differencing scheme which is used for analyses in this thesis. Table G.2 contains convection and diffusion coefficients which are used for calculation in table G.1.

Table G.1 Coefficients for hybrid differencing schemes

Coefficient	Hybrid scheme
a_e	$\max\left[-F_e,\ (D_e - F_e/2)\ ,\ 0\right]$
a_w	$\max\left[F_w,\ (D_w + F_w/2)\ ,\ 0\right]$
a_n	$\max\left[-F_n,\ (D_n - F_n/2)\ ,\ 0\right]$
a_s	$\max\left[F_s,\ (D_s + F_s/2)\ ,\ 0\right]$
a_h	$\max\left[-F_h,\ (D_h - F_h/2)\ ,\ 0\right]$
a_l	$\max\left[F_l,\ (D_l + F_l/2)\ ,\ 0\right]$
a_τ	F_τ

Table G.2 Convection and diffusion coefficients

Cell face	Convective mass flux F	Diffusion coefficient Γ	Diffusive coefficient D
e	$\rho \cdot u_e A_e$	$(\Gamma_E + \Gamma_P)/2$	$\Gamma_e A_e /(x_E - x_P)$
w	$\rho \cdot u_w A_w$	$(\Gamma_W + \Gamma_P)/2$	$\Gamma_w A_w /(x_W - x_P)$
n	$\rho \cdot u_n A_n$	$(\Gamma_N + \Gamma_P)/2$	$\Gamma_n A_n /(y_N - y_P)$
s	$\rho \cdot u_s A_s$	$(\Gamma_S + \Gamma_P)/2$	$\Gamma_s A_s /(y_S - y_P)$
h	$\rho \cdot u_h A_h$	$(\Gamma_H + \Gamma_P)/2$	$\Gamma_h A_h /(z_H - z_P)$
l	$\rho \cdot u_l A_l$	$(\Gamma_L + \Gamma_P)/2$	$\Gamma_l A_l /(z_L - z_P)$
time	$\rho \cdot Vol/\Delta\tau$	-	-

Values for Γ_ϕ are given in Table 4.1. 'A' is the cell surface area and x, y, and z are coordinates of the cell.

APPENDIX H

EXAMPLE OF RESULTS FOR EXPERIMENTAL VALIDATION OF CFD MODELS

Position of probes and wall surfaces with basic airflow and heat source data

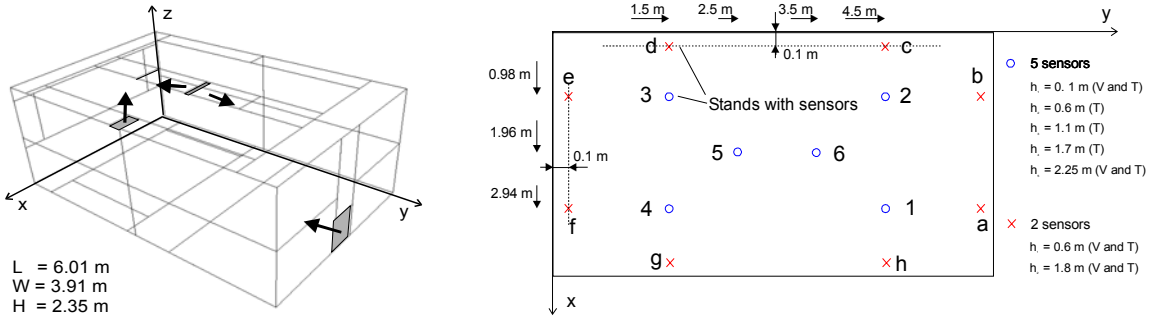

Figure H.1 Geometry of the room and positions of air temperature sensors

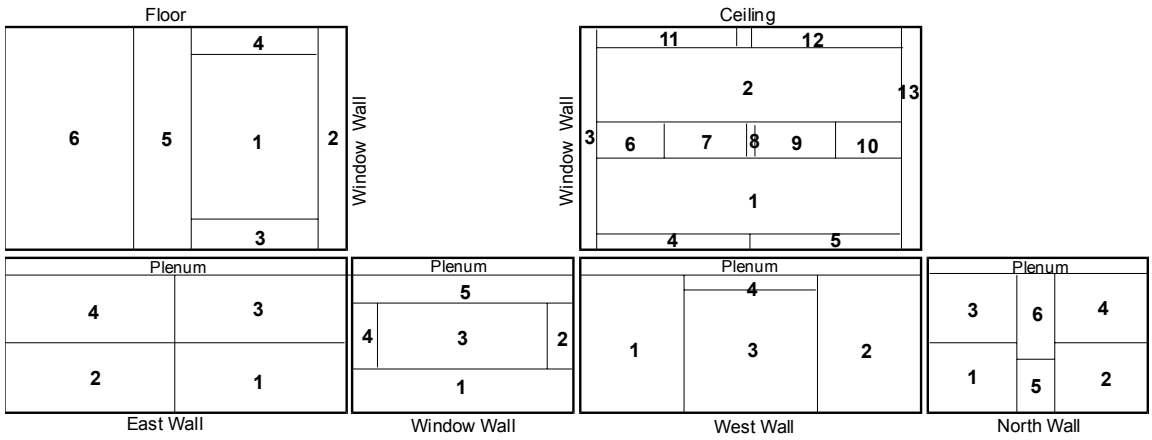

Figure H.2 Positions of characteristic surfaces with surface temperature sensors

Air is supplied by displacement diffuser (surface 5) on North wall:

Dimension D = 0.5 m, H = 0.72 m. Volume supply flow rate V = 97 m^3/hr.

Supply temperature T=18.9 C, Exhaust air temperature T=32.1 C.

Heat source is panel (surface 3) on West wall:

Dimension L= 2.22 m H = 2.2 m, position: y = 1.95 m, z = 0.0 m.

Total heat flux by measure current and voltage: I = 3.89 A, U = 128.8 V.

Tracer gas (SF6) source is at floor surface:

It is a point source at position: x = 3.45 m, y = 3.0 m.

Temperatures, velocities, and heat flux measurement results

Table H1 Surface temperatures and heat fluxes

Surface position	Surface number	Area [m2]	Temperature [°C]	Heat flux [W]
Floor	1	6.26	29.9	52.6
	2	2.19	29.7	3.1
	3	1.21	29.7	2.8
	4	1.21	29.7	4.3
	5	4.03	29.2	65.5
	6	8.6	28.9	95.3
Ceiling	1	5.94	31.10	-4.8
	2	5.94	31.10	-9.0
	3	1.88	31.0	-0.3
	4	1.09	31.0	0.5
	5	1.01	30.6	1.7
	6	0.74	31.1	-0.3
	7	0.74	31.2	0.7
	8	0.06	31.2	0.1
	9	0.68	31.2	0.0
	10	0.74	31.1	-1.8
	11	1.09	31.0	3.4
	12	1.01	30.6	2.5
	13	2.58	30.6	0.8
Window Wall	1	3.60	30.7	-1.8
	2	0.51	30.2	1.8
	3	3.36	30.2	12.1
	4	0.51	30.8	-0.9
	5	1.21	30.9	-0.4
North Wall	1	1.97	29.5	9.2
	2	1.97	29.6	7.9
	3	1.97	30.8	-1.3
	4	1.97	30.9	-4.1
	5	0.40	30.8	-0.9
	6	0.91	29.6	5.7
West Wall	1	4.43	30.6	-6.2
	2	4.43	30.2	-4.7
	4	0.26	30.4	-0.1
	3	4.90	41.6	164.9
East Wall	1	3.53	30.2	14.9
	2	3.53	30.0	12.0
	3	3.53	31.2	-2.3
	4	3.53	31.1	-3.7

Table H2 Air temperatures measured in an occupied zone [°C]

Height [m]	Stand 1	Stand 2	Stand 3	Stand 4	Stand 5	Stand 6
2.25	32.7	32.6	32.9	32.7	32.6	32.6
1.7	31.0	31.2	31.2	31.1	31.3	31.2
1.1	30.3	30.4	30.3	30.4	30.6	30.5
0.6	29.5	29.6	29.4	29.6	29.9	29.6
0.1	26.7	27.4	29.1	28.2	28.0	25.8

Table H3 Air temperatures and velocities measured in the vicinity of surfaces

Height [m]	Stand a	Stand b	Stand c	Stand d	Stand e	Stand f	Stand g	Stand h	**Height [m]**	Stand 1	Stand 2	Stand 3	Stand 4
Temperatures [°C]													
1.8	31.8	31.7	32.3	32.3	31.7	32.3	31.9	31.8	**2.25**	32.7	32.6	32.9	32.7
0.6	30.1	30.1	30.7	30.9	29.8	31.5	30.4	30.2	**0.1**	26.7	27.4	29.1	28.2
Velocities [m/s]													
1.8	0.04	0.03	0.09	0.07	0.03	0.02	0.02	0.03	**2.25**	0.04	0.04	0.05	0.06
0.6	0.02	0.03	0.04	0.04	0.03	0.03	0.02	0.02	**0.1**	0.07	0.04	0.05	0.07

Tracer gas measurements

SF6 source intensity: N = 4.0 ml/min of 1% SF6 solution in nitrogen.

Concentration in inlet air C_{in}=0.64 ppb

Concentration in outlet air C_{out}=3.11 ppb

Table H4 Tracer gas concentration in occupied zone -represented as $(C-C_{in})/(C_{out}-C_{in})$

Height [m]	Stand 1	Stand 2	Stand 3	Stand 4	Stand 5
2.25	0.60	0.91	0.85	0.45	0.79
1.7	1.15	1.27	0.93	1.17	1.17
1.1	1.07	1.08	0.98	1.48	1.37
0.6	1.00	0.93	0.76	0.94	0.91
0.1	0.74	0.67	0.52	0.65	0.63

Vita - Atila Novoselac

Education

- Ph.D. in Architectural Eng, 2005
  Architectural Engineering Department, The Pennsylvania State University
- M.S. in Mechanical Eng 2000
  Department of Mechanical Engineering, University of Belgrade, Serbia
- B.S. in Mechanical Eng 1994
  Department of Mechanical Engineering, University of Belgrade, Serbia

Work Experience

- Graduate Student Researcher, 2000 – 2004
  Department of Architectural Engineering, The Pennsylvania State University
- Research and Teaching Assistant, 1997 – 2000
  Thermal Sciences Group, Dept. of Mechanical Engineering, University of Belgrade, Serbia
- Project Designer, 1995 – 2000 (2 days/week)
  Energy Institute, Dept. of Mechanical Engineering, University of Belgrade, Serbia
- Research Assistant, 1995 - 1997
  Energy Institute, Dept. of Mechanical Engineering, University of Belgrade, Serbia

Academic Honors and Awards

- Jack and Laraine Beiter Excellence Endowment in Architectural Engineering, Penn State University, 2004
- Gordon D. Kissinger Graduate Fellowship, Penn State University, 2003
- Dean's Fellowship for Graduate Students, Penn State University, 2001-2004
- Grant in Aid Fellowship for Graduate Students, ASHRAE, 2001
- Government Fellowship for Young Investigators, Yugoslavia, March 1995 - May 1997

Activities and Associations

- American Society of Heating, Refrigerating and Air-Conditioning Engineers (ASHRAE)
- Member of ASHRAE TC5.3 (Room Air Distribution)
- Penn State Architectural Engineering Graduate Student Association

Publications

- Novoselac, A. and Srebric, J. 2003. "Comparison of Air Exchange Efficiency and Contaminant Removal Effectiveness as IAQ Indices", *ASHRAE Transactions,* paper KC-03-4-5.
- Novoselac, A. and Srebric, J. 2002. "A Critical Review on the Performance and Design of Combined Cooled Ceiling and Displacement Ventilation Systems," *Energy and Buildings*, 34 (5): 497-509.
- Novoselac, A. and Srebric, J. 2003. “Sensitivity Study of Parameters Influencing IAQ indices”, *Proceedings of Ventilation 2003*, Sapporo, Japan.
- Srebric, J. and Novoselac, A. 2002. . “Design of Low-Energy Cooling System by Using Coupled Energy Simulation and Computational Fluid Dynamics”, *Proceedings of Roomvent 2002*, Copenhagen, Denmark.
- Novoselac, A. and Srebric, J. 2002. “Influence of Different Pollutant Sources on Selection of Ventilation System in Offices with Cooled Ceiling”, *Proceedings of Indoor Air 2002,* Monterey, California, USA.
- Marjanovic, L. Novoselac, A. 1997. “Radiator Valve's Influence on Hydrodynamic Performance of a Water Heating System”, *Proceedings of Congress CLIMA 2000,* Brussels.